Universidade de Aveiro Departamento de Engenharia Mecânica
2013

Branca Rosa Ribeiro Leite de Sousa Sher

OTIMIZAÇÃO DE TRATAMENTOS VISCOELÁSTICOS COM ALGORITMOS GENÉTICOS

OPTIMISATION OF VISCOELASTIC TREATMENTS USING GENETIC ALGORITHMS

Universidade de Aveiro Departamento de Engenharia Mecânica
2013

Branca Rosa Ribeiro Leite de Sousa Sher

OTIMIZAÇÃO DE TRATAMENTOS VISCOELÁSTICOS COM ALGORITMOS GENÉTICOS

OPTIMISATION OF VISCOELASTIC TREATMENTS USING GENETIC ALGORITHMS

Tese apresentada à Universidade de Aveiro para cumprimento dos requisitos necessários à obtenção do grau de Doutor em Engenharia Mecânica, realizada sob a orientação científica do Doutor Rui António da Silva Moreira, Professor Auxiliar do Departamento de Engenharia Mecânica da Universidade de Aveiro.

I dedicate this work to my family and to the loving memory of my mother and brother.

“If you want to find the secrets of the universe, think in terms of energy, frequency and vibration.”

(Nikola Tesla – Serbian-American inventor)

o júri / the jury

presidente / president

Prof. Doutor Manuel João Senos Matias
professor catedrático da Universidade de Aveiro

Prof. Doutor José Fernando Dias Rodrigues
professor associado da Faculdade de Engenharia da Universidade do Porto

Prof. Doutor Miguel de Matos Neves
professor auxiliar do Instituto Superior Técnico da Universidade de Lisboa

Prof. Doutor Alfredo Manuel Balacó de Morais
professor associado do Departamento de Engenharia Mecânica da Universidade de Aveiro

Prof. Doutor António João Pina da Costa Feliciano Abreu
professor adjunto do Departamento de Engenharia Mecânica do Instituto Superior de Engenharia de Lisboa

Prof. Doutor Rui António da Silva Moreira
professor auxiliar do Departamento de Engenharia Mecânica da Universidade de Aveiro

acknowledgements

Although the development of a PhD is a very personal work, it would have not been easily attainable without the help of my PhD advisor, Dr. Rui Moreira to whom I would most sincerely like to express my gratitude, first and foremost, for accepting to be my mentor. I appreciate his expertise, guidance and patience throughout the entire development of this dissertation. His encouragement and, above all, optimism rejuvenated me at times of momentary disheartening.

I am also thankful to the engineering institute where I have been a lecturer for over twenty years “Instituto Superior de Engenharia de Lisboa”, not only for the monetary contribution provided for fees but also for reducing my lecturing hours considerably.

I would also like to thank Dr. João Quaresma Dias from the same institute (ISEL) for showing a real interest in this project right from the start, against all the odds, and for being very understanding during this trying period.

A very special thanks goes out to Dr. António Abreu, also from ISEL for his kindness, reassurance and enthusiasm in participating as a member of the defence jury.

A final word to the understanding demonstrated by my aging Dad who, due to this absorbing endeavour, has not been given the attention he deserves.

palavras-chave

amortecimento passivo de vibrações, tratamentos viscoelásticos, energia de deformação modal, algoritmos genéticos, camadas finas, otimização da espessura.

resumo

Os tratamentos viscoelásticos permitem amortecer estruturas finas e leves de uma forma bastante eficiente. Neste tipo de amortecimento passivo, parte da energia de deformação é dissipada pelo material viscoelástico sob a forma de calor. O material viscoelástico é aplicado à superfície de uma estrutura e pode ser, ou não, restringido por uma camada de restrição. Dentro destas duas possibilidades, o tratamento com restrição é o que apresenta maior eficiência. Isto deve-se ao facto de que o movimento relativo das camadas adjacentes impõe uma elevada deformação de corte ao material viscoelástico.

De um modo geral, a minimização da extensão da aplicação do material viscoelástico sob a forma de tratamentos parciais localizados torna-se benéfico em termos de custo, quer económico, quer qualquer outra forma de custo associado à aplicação do tratamento. A aplicação de pequenas porções de material sobre áreas específicas e selecionadas torna o tratamento igualmente eficiente, segundo estudos e resultados apresentados por vários autores.

Como mencionado anteriormente, o mecanismo de amortecimento do material viscoelástico baseia-se na dissipação de parte da energia de deformação. Este facto permite relacionar a eficiência do tratamento parcial com a energia de deformação modal da estrutura para cada um dos modos naturais. Não obstante os bons resultados obtidos na abordagem desta técnica, este método requer a aplicação de um processo de otimização que conduza a uma solução ótima. Todavia, a simulação numérica deste processo de otimização, exige um elevado custo computacional pois é baseado num processo evolutivo de redesenho da geometria e cálculo do amortecimento modal por forma a utilizar o mínimo de material possível.

Baseado nestes pressupostos, este estudo utiliza elementos finitos de camada discreta adaptativos associados a um processo de otimização com base em Algoritmos Genéticos. Este procedimento permite desenvolver um método de otimização de baixo custo computacional e objetivo.

keywords

passive vibration damping, viscoelastic damping treatment, modal strain energy, genetic algorithm, thin layers, thickness optimisation.

abstract

Viscoelastic treatments are one of the most efficient treatments, as far as passive damping is concerned, particularly in the case of thin and light structures. In this type of treatment, part of the strain energy generated in the viscoelastic material is dissipated to the surroundings, in the form of heat. A layer of viscoelastic material is applied to a structure in an unconstrained or constrained configuration, the latter proving to be the most efficient arrangement. This is due to the fact that the relative movement of both the host and constraining layers cause the viscoelastic material to be subjected to a relatively high strain energy.

There are studies, however, that claim that the partial application of the viscoelastic material is just as efficient, in terms of economic costs or any other form of treatment application costs. The application of patches of material in specific and selected areas of the structure, thus minimising the extension of damping material, results in an equally efficient treatment.

Since the damping mechanism of a viscoelastic material is based on the dissipation of part of the strain energy, the efficiency of the partial treatment can be correlated to the modal strain energy of the structure. Even though the results obtained with this approach in various studies are considered very satisfactory, an optimisation procedure is deemed necessary. In order to obtain optimum solutions, however, time consuming numerical simulations are required. The optimisation process to use the minimum amount of viscoelastic material is based on an evolutionary geometry re-design and calculation of the modal damping, making this procedure computationally costly. To avert this disadvantage, this study uses adaptive layerwise finite elements and applies Genetic Algorithms in the optimisation process.

Table of Contents

List of Figures

List of Tables

List of Symbols

b	Width of beam (m)
[**B**]	Deformation matrix
$[\mathbf{B}^B]$	Bending/membrane deformation matrix
$[\mathbf{B}^S]$	Transverse shear deformation matrix
[**D**]	Elasticity matrix
e_1	Modulus ratio: E_1/E_2
e_2	Modulus ratio: E_2/E_1
E	*Young*'s modulus (Pa)
E_1	*Young*'s modulus of host structure/beam (Pa)
E_2	*Young*'s modulus of viscoelastic layer (Pa)
E_3	*Young*'s modulus of constraining layer (Pa)
E'	Storage modulus (Pa)
E''	Loss modulus (Pa)
E^*	Complex extensional modulus (Pa)
f	Frequency (Hz)
G	Shear modulus (Pa)
G'	Shear storage modulus (Pa)
G''	Shear loss modulus (Pa)
G^*	Complex shear modulus (Pa)
h_1	Geometry ratio: H_1/L
h_2	Thickness ratio: H_2/L
$\bar{h}_2$	Thickness ratio: H_2/H_1
$h_2(x)$	Viscoelastic thickness function
$h_2^s(x)$	Viscoelastic thickness function (with imposed symmetry)
h_3	Thickness ratio: H_3/H_1
h_m	Homogeneous equivalent thickness
H	Thickness (m)
H_1	Thickness of host structure/beam
H_2	Thickness of viscoelastic layer
H_3	Thickness of constraining layer
H_k	Finite element thickness
I	Second moment of area of beam cross-section (m^4)
K	Stiffness (N)
[**K**]	Stiffness matrix
L	Length of beam (m)
L_e	Finite element length
[**L**]	Differential operator

M	Mass (kg)
[**M**]	Mass matrix
N	Shape function
[**N**]	Interpolation operator matrix (displacement field)
[$\mathbf{N}^{\sigma}$]	Interpolation operator matrix (stress field)
[**S**]	Flexibility matrix
t	Time (s)
T	Temperature (ºC)
u	In-plane displacement field
w	Out-plane displacement field
x_i	GA parameters of VEM thickness function
$\alpha\ (T)$	Shift factor at temperature T
δ	Phase shift (rad)
ε	Extensional strain
ϕ	Mode shape
γ	Shear strain
η	Loss factor
ν	*Poisson*'s ratio
ρ	Density (kg/m^3)
σ	Extensional stress (N/m^2)
τ	Shear stress (N/m^2)
ω	Angular frequency (rad/sec)

List of Acronyms

ADF	Anelastic Displacement Field
ATF	Augmenting Thermodynamic Fields
CLD	Constrained Layer Damping
DFA	Direct Frequency Analysis
FEM	Finite Element Method
FLD	Free Layer Damping
FOST	First-order Shear Theory
GA	Genetic Algorithm
GHM	Golla-Hughes-McTavish
HOST	High-order Shear Theory
MSE	Modal Strain Energy
RKU	Ross-Kerwin-Ungar
VEM	Viscoelastic Material

Chapter 1

Motivation, Objectives and Organisation of the Thesis

This chapter contains a brief description of the circumstances that motivated this line of research, the main objectives and the organisation of this dissertation.

1.1 Motivation

Vibration is a mechanical phenomenon that everyone is familiar with. It can be defined as the cyclic or oscillating movement of a structure, machine or machine component from its position of rest. Vibrations are occasionally desirable but usually they are unintended and unwanted. It is natural for machines and structures to vibrate and it is actually inevitable.

In general, vibrations do not cause concern; however, occasionally, when the level of vibration is sufficiently high, it can have expensive or life-threatening consequences. In order to determine whether the level of vibration deserves some attention, design engineers in the industrial world need to have a correct understanding of vibrations. Unfortunately,

vibration control has, very often, been a poorly understood technology. The design of structures and machines usually comprises some conflicting requirements and design engineers normally fail to properly address vibration control and develop adequate solutions in the designing stage.

A machine or structure needs to have the capacity to dissipate vibration energy to eliminate unwanted or excessive oscillations by means of some form of damping mechanism. It follows, therefore, that damping needs to be looked at as an essential requirement of a good mechanical design. The term *damping* refers to the removal of some part of the vibration energy from a vibrating structure. However, even the best designs are susceptible of developing problems at a later stage.

When the source of the problem cannot be controlled, the only other option is to use damping mechanisms to remove, at least, part of the vibration. Various methods are available to dampen vibrations but some polymers, namely viscoelastic materials (VEM), exhibit properties that produce favourable levels of damping in structures and machines. Basically, viscoelastic damping consists in the dissipation, as a form of heat, of the vibration energy produced during cyclic deformation. The importance of an insight into the unique characteristics of viscoelastic materials is paramount; otherwise the results of their careless application might turn out to be unsatisfactory.

Although the history of the technology based on viscoelastic damping dates from the early years of the 20th century, it was not until the 1930's that some scientific work started taking place. World War II brought about some development in the area of damping materials but it was only in the 1950's that the application and use of damping treatments to improve the characteristics of structures started to emerge.

There have been many contributions from the academic world since then but facing the impossibility of describing them all in a concise review, only some of the highlights will be mentioned.

The German team of Hermann Oberst [1] is referred to as one of the first to investigate and apply viscoelastic treatments to unconstrained structures. Ross, Ungar and Kerwin [2] were also among the first to carry out studies and in 1959 proposed the commonly known RKU equations of the 4th order, providing a simple and approximate analytical method for the analysis of unconstrained and constrained treatment configurations. These equations are still used nowadays in the analysis of beams and plates with constrained configuration.

Some pioneering work was also done by DiTaranto [3] back in 1965 by extending the work of Ross, Kerwin and Ungar. He eliminated the simply supported end condition assumption and derived a movement equation for freely vibrating beams with any end conditions. The equation is a sixth-order linear differential equation of motion for the transverse displacement of sandwich beams. The natural frequencies and modes discussed by DiTaranto constitute a special class of resonance frequencies and forced modes of vibration of the sandwich beam, which simplify the general forced vibration problem.

From the 1970's to the present day, the research of damping treatments has been overwhelming and many technical papers and textbooks have been published. Among the researchers of more relevance are Yan and Dowell [4] who derived linear differential equations governing the vibrations of unsymmetrical sandwich plates and beams. Others include Rao and Nakra [5] who analysed the flexural vibration of unsymmetrical sandwich beams and plates including transverse, longitudinal and rotary inertia.

Two important reference books on the subject were published in the eighties by Ferry [6] and Nashif *et al*. [7]. At a later stage, Roy and Ganeson developed a finite element model and examined partial damping layers for unconstrained plates [8] and unconstrained beams [9] and Johnson [10] reviewed passive damping treatments. Johnson *et al*. [11] determined the numerical solutions of modal loss factors and natural frequencies of a sandwich cantilever beam.

Other important contributions came from Mead in 1998 [12] and Jones in 2001 [13] when they published books that are still a reference today. Hufenbach *et al.* [14] performed a structural dynamic analysis of fibre-reinforced cylindrical shells based on a shear-elastic

theory following the Timoshenko theory. More recently, Zhang and Chen [15] developed a 3-D finite element model for laminated composite beams with integral viscoelastic layers and Pradeep and Ganeson [16] studied the behaviour of vibration and thermal buckling of sandwich beams.

As previously mentioned, these references constitute a small percentage of the total number of studies done on the subject of viscoelastic damping. The contribution of these scholars to the comprehension of this theme has been enormous and there have been many breakthrough conclusions. Despite that, and the number of decades dedicated to the investigation of viscoelastic damping, it continues to draw the attention of the academic community as it is felt that this topic is still not fully understood.

The research carried out in this dissertation has been directed towards finding some innovative results, hoping they can be instrumental in furthering the knowledge of viscoelastic treatments. This has been the main motivation behind this thesis. In order to achieve this main goal, innumerable parametric analyses were performed, very discouraging at times, but rewarding in the end! The specific objectives are set out in the following section.

1.2 Objective of the dissertation

An efficient damping treatment configuration is one whose viscoelastic material dissipates the most energy. These treatments are called viscoelastic damping treatments and they are effective passive control mechanisms to mitigate vibration in light structures. This ability depends on the amount of energy stored inside the VEM layer during the vibration of the structure.

The layer of viscoelastic material may cover the entire surface of the host structure or may be placed in a partial manner. In fact, partial coverage has proven to be just as efficient as total coverage [17], provided the patches are placed strategically; that constitutes the main topic of this thesis. The design of a partial viscoelastic damping treatment involves several main design parameters: layers thickness, material properties, natural mode, boundary

conditions and the location of the VEM patches. The optimisation process entails finding the correct combination of all these parameters which will result in the maximum damping for the natural vibration mode, or modes, that are of primary interest.

Taking into consideration the effectiveness of partial treatments, the development of this thesis has the following main objectives:

- Complete a thorough bibliographic review of the current state-of-the-art.
- Investigate the dynamics of Genetic Algorithms (GAs) so that this optimisation tool can be used with confidence throughout the optimisation process.
- Establish the influence that the numerous parameters that are involved in viscoelastic treatments have on their behaviour.
- Optimise the thickness of homogeneous viscoelastic layers in accordance with the dimensions of the surface that requires damping using Genetic Algorithms.
- Develop and validate various shapes of non-uniform viscoelastic layers where the thickness varies over the coverage area.
- Determine whether the variable shape thus obtained is a viable proposition by comparing a viscoelastic homogeneous shape to a variable one.
- Establish whether the distribution of the shear strain energy across the length of the beam with a VEM layer of uniform thickness may be used as an indicator for the best solutions concerning a variable configuration.
- Finally, the author hopes to provide inspiration for further improvement of this optimisation process by motivating the reader to peruse this thesis and take up some of the future work suggested in the last chapter.

1.3 Organisation of the dissertation

This dissertation is organised into nine chapters and that includes this chapter which is dedicated to describing the general motivation, the research goals and the structure of the thesis.

In the second chapter a brief introduction is presented including a concise review on the problematic subject of vibration and some vibration control solutions, particularly the viscoelastic damping treatments.

In the third chapter, viscoelastic damping treatments are analysed in more detail giving special attention to the characterisation of the properties of viscoelastic materials and the configuration and modelling of these passive damping treatments. The characterisation methods that are usually applied to determine the complex modulus of viscoelastic materials used for passive damping are also presented.

The fourth chapter deals with the analysis of the viscoelastic treatments based on the method of finite elements. Some issues regarding the finite element modelling are discussed followed by the characterisation of the VEM behaviour. The spatial model describes the high shear strain fields that are developed in the core layer. They have to be represented correctly and that can be achieved with layerwise models which are briefly described. The layerwise formulation applied in this thesis concludes this chapter.

Optimisation is at the core of this research and this is the subject of chapter 5. A brief introduction is provided followed by an equally brief description of Topology optimisation. The latter method constitutes an additional means of confirming the results obtained with the genetic algorithm, which will be the main tool used subsequently for the shape and volume optimisation of the VEM layer. The genetic algorithm is, therefore, examined in detail and a parametric study is included.

The efficiency of the damping layer depends, not only on its thickness, but also on many other parameters. After identifying these parameters, their influence on the viscoelastic layer efficiency is investigated in the parametric study of constrained layer damping of Chapter 6.

Based on some of the conclusions obtained from the previous chapter and with the assistance of the GA optimisation tool, the optimisation of a homogeneous layer for three

boundary conditions and the first three modes of vibration of a beam are dealt with in Chapter 7.

Chapter 8 covers the optimisation of the VEM layer shape (exclusively) as well as the optimisation of shape and volume. The results obtained from the latter optimisation are compared to the results obtained in the previous chapter for a uniform layer including a numeric analysis of the variable shape feasibility. The study is carried out for two boundary conditions and the first three modes of vibration.

Chapter 9 concludes this dissertation with the main conclusions and suggestions for possible future research work.

Chapter 2

Basic Concepts

This chapter introduces the reader to the subject under investigation by describing basic concepts. This includes a brief description of problems arising from excessive vibration, the necessity to find control solutions, the different methods that may be used and the method upon which this thesis is centred on - viscoelastic damping treatments.

2.1 Machines and vibration

Excluding those machines whose function and design is to create some sort of vibration, an ideal machine would produce no vibration at all because all energy would be channelled into the job of work to be done. However, machine elements react against each other, energy is dissipated through the structure in the form of vibration and even a good machine design will produce low levels of inherent vibration. As the machine wears, foundations settle, parts deform and subtle changes in the dynamic properties of the machine begin to

occur. Shafts become misaligned, parts begin to wear, rotors become unbalanced and clearances increase. All of these factors are reflected in an increase in vibration energy, which, as it is dissipated throughout the machine, excites resonances and puts considerable extra dynamic loads on bearings. Cause and effect reinforce each other and the machine progresses towards ultimate breakdown.

In the past, experienced plant engineers have been able to recognise by touch and hearing whether a machine was running smoothly or whether a fault was developing. This cannot be relied upon any longer because most modern machinery runs so fast that many vibrations occur at such high frequency that instruments are needed to detect and measure them.

Machine elements, which constrain vibration forces, for example bearing housings, are usually accessible from the outside of the machine so that the vibration resulting from the excitation forces can be measured at these points. As long as the excitation forces are constant, or vary within certain limits, the vibration level measured will also be constant and vary within similar limits.

Furthermore, for most machines, the vibration has a typical level and its frequency spectrum has a characteristic shape when the machine is in good condition. This frequency spectrum, a plot of vibration amplitude against frequency, is known as the vibration signature of the machine.

When faults begin to develop, the dynamic processes in the machine change and some of the forces acting on the machine parts are also changed, thereby influencing the vibration level and the shape of the vibration spectrum.

Vibration signals carry much information relating to the running condition of machines. This fact is the basis for using regular vibration measurement and analysis as an indicator of machine health trends and the need for maintenance or the resolution of the vibration problem by means of passive or active control methods.

2.2 Structural dynamics

It is not only machines, such as engines, rotors and turbines that are subjected to vibration related issues. Structures are also prone to vibrations that may collapse, or at least present performance faults due to vibration and noise that is generated externally or internally.

Structural dynamics analyses the behaviour of structures when subjected to loads varying in time, which might include wind, waves, traffic, people, earthquakes, etc. In the past, because structures and machines were made exceptionally stiff and massive, the lowest resonance frequency was so high that the corresponding mode of vibration would hardly be excited. Nowadays, the cost of such an approach would be particularly high and, therefore, not viable. During the last few decades, this has led structural engineers to develop and construct very efficient structures. This is mainly due to the use of lighter and more resistant materials but also more efficient and versatile production and assembly processes.

Structures tend to be as light as possible at the expense of lowering the stiffness. Modern steel frame buildings, for example, are much lighter and cheaper but they are also more flexible and if the vibration energy is not properly dissipated, it can result in a greater response during earthquakes or other extreme conditions.

Especially in large structures (bridges, buildings, airplanes, etc.) the high amplitude of vibration and low resonance frequencies will eventually lead to disaster if the structure does not have the capacity to dampen the vibrations. However, although not as evident, the same effect will occur in much smaller structures so long as their damping capacity is insufficient.

It is, therefore, of utmost importance for the designer to have an adequate knowledge of structural dynamics so that structures and machines can be designed to behave well in the expected operational environment. Nonetheless, if despite the designer's best efforts, vibration problems occur at a later stage, damping treatments or damping devices have to be developed and applied.

2.3 Vibration problems and the need for vibration control

Vibrations represent a major engineering issue in many areas of civil, mechanical, or aeronautical design, they are undesirable and, very often, engineers struggle to reduce their levels.

Vibration is normally a destructive by-product of the force that is transmitted through a structure, which if not adequately controlled provokes, amongst other things, structure fatigue. The '4-Ds' related to vibration are destruction, damage, disturbance and discomfort. One of the resulting effects of a structure or machine being excited by an external or internal dynamic force is vibration and noise [12].

Vibration is characterised by an oscillatory movement, which is the result of a cyclic energy conversion from deformation potential energy to the kinetic energy of the movement. The vibration produced by earthquakes is at the top of the vibration scale and is by far the most destructive. At the other end of the scale, lower levels of vibration may be more or less disturbing depending, not only on how long they last, but also on the part of the human body that is being affected and its capacity to tolerate vibration [12].

Motor cars and aeroplanes have always been notorious for their vibration potential due to their reciprocating engines, which, if left unchecked would lead to disastrous fatigue failure. The introduction of the jet engine in the late 40's seemed to have solved this problem until it was realised that high levels of jet noise generated damaging vibration on the external surface of the plane, causing acoustic fatigue of the structure, which represented an even bigger problem [18].

Ships are also prone to vibration problems as they carry many machines which rotate or reciprocate, known to be sources of vibration; these include the propulsion engines, water pumps, diesel engines, air compressors, air conditioning, etc. Another good example of multiple sources, paths and frequencies of vibration and their associated noise is a helicopter cabin. If uncontrolled, cabin vibration can cause discomfort to both passengers

and pilot and violent vibration of the instrument panel can impair the pilot's capability of controlling the helicopter, which may cause catastrophic consequences.

Electronic equipment is also conditioned to sustainable levels of vibration. They are usually designed to operate without malfunction or breakage within specified vibration limits that should not be exceeded. Other examples of vibrating items are bridges, skyscrapers, high-voltage power lines, tractors, cranes and trucks. It is imperative in all these cases to dampen the vibration levels so that the equipment can operate satisfactorily without vibration related failure and so that their users can be protected.

Vibration and noise problems may be solved by controlling the source of the problem, by protecting the equipment against noise and vibration or by modifying the transmission mechanism [19]. There are several methods that may be used in order to control vibration: balancing and aligning rotating systems to reduce excitation forces, avoiding changes in mass and/or stiffness that cause undesirable resonances, using vibration absorbers and the incorporation of damping mechanisms [19].

It is worthwhile noting that the control devices that can be used to dampen vibrations may have to operate under diverse environmental conditions ranging from very low temperatures to extremely high ones. The suppression of energy may involve transferring energy to other structural components or converting energy into heat or radiation.

Examples of structures in conditions of extreme temperatures are turbine blades, power transmission lines, exhaust pipes and aeroplane structures and the dampening material must be able to withstand them. Dampening materials may also have to be immersed in oil, exposed to radioactivity or corrosive environments or even rain and humidity.

2.4 The application of polymer materials in industry

Polymeric materials have played an important role in their application as structural materials due to their interesting characteristics, like low weight, corrosion resistance and associated manufacturing and transformation processes.

Polymers have been used in the construction of automobile bodies, as well as, ship and boat hulls. Glass reinforced polymers have a good strength to weight ratio and the ability to be moulded into complex shapes, making them attractive to designers. Special fibres, such as, carbon fibres and polyamide fibres have been used to stiffen the bodies of glass reinforced polymer racing cars. The inherent chemical resistant characteristics of many polymers make them ideal for transport applications, including commercial vehicle applications. Polymeric foams are used for acoustic and thermal insulation. Polymeric composites have also enjoyed wide application in aerospace technology.

Applications of polymer composites in mechanical components include bearings, gears, cams, wheels, brakes, clutches, seals, conveyors, transmission belts and many other components [20]. In practically all bearings, sliding and rubbing between materials is inevitable and polymers possess a good capability of doing it with little wear and without surface damage. There are other advantages in the usage of polymers as bearings, such as, their relatively low cost and good corrosion resistance, but they have drawbacks too, namely, low yield and low creep strengths, low temperature resistance and poor thermal conductivity. These disadvantages are taken care of by reinforcing or bonding the polymer to a rigid backing (e.g. steel) to form a composite material.

Polymer composites based on various resin matrices have been widely used as friction materials. The proportions of the different components have to be chosen correctly to suit the properties of the desired material. If there is too little resin, the strength might be insufficient; too much resin might reduce the coefficient of friction at high operating temperatures. Materials with very different friction and wear properties can be produced by juggling with the composition variables. Gears must be able to resist bending and fatigue and must also have adequate surface qualities to minimise friction and wear. Many polymers and polymer composites possess the right combination of properties to make them suitable for gears. These include, silent running, reduced vibration, reduced wear, acceptance of wide dimensional tolerances, among others.

Plastics derived from polymer composites have penetrated the furniture and housewares market for many years now and they have also found their way into the construction

industry. In the latter, polymer composites are usually ready for use; labour on site is reduced, they require little maintenance with exposure to the weather and are light in weight. They do, however, demand more sophisticated processing machinery.

Carbon fibre reinforced polymer composites are also widely used in many applications because they are potentially extremely strong, light and rigid, as well as being self-lubricating. Applications in packaging, handling and storage for polymeric composites are numerous.

2.5 Dynamic control methods

Whenever a vibration problem needs to be tackled, the understanding of its nature becomes necessary. This includes knowing the origin of the source, the path along which the vibration energy reaches the problem point and the vibration frequency. An analysis of the latter may reveal that its waveform is single-frequency, random, transient or periodic. The vibration may also be of a torsional, flexural or longitudinal nature. This means that each problem needs to be evaluated individually in accordance with its characteristics as there are various ways to deal with it. It is desirable to primarily solve vibration problems by controlling the source of the problem, for example, by controlling the stiffness and/or mass characteristics; another way is to isolate the system from the excitation forces. If the previous options are not possible, the remaining one is to add some sort of damping. There are, basically, three control methods to address vibration problems: passive, active, and semi-active control.

2.5.1 Passive vibration control

Passive control is obtained with an alteration of the dynamic behaviour of the structure, which is associated with the stiffness, mass and damping characteristics of passive elements that may be added to the structure [21]. These elements include mass, springs, rubbers or fluid dampers which react passively in opposition to the velocities, acceleration

and deflections that are imposed on them by the vibration and they do not require external assistance. These mechanisms are often based on an energy dissipation mechanism.

There are basically four different approaches to passive vibration control: by structural design, by localised addition, by resilient isolation and by added damping [12]. Most problems concerning noise and vibration are generated by components that exhibit low levels of material damping; the latter is now being used as a structural design parameter rather than being applied only when faulty conditions occur. These '*structural design'* concepts include methods such as, the reduction of the number of responding modes, nodalising, de-coupling, structural stiffening, selection of the best material, etc.

In some situations, the most effective and economic way to reduce vibration is to resort to localised additions. The insertion of extra devices or materials as '*auxiliary systems'* in the form of a mass, spring, damper or their combination provide a means of absorbing vibration that neutralise the exciting force over a narrow frequency range. This constitutes a localised addition as the added system is located at a particular point rather than being distributed over a portion of the structure. A simple neutraliser may have only one extra device, but if it is carefully located, it can have a large influence on the system.

In most of the non-resonant cases, vibration problems can be solved with any of the above mentioned methods or by '*resilient isolation'*. Resilient isolation consists in the interconnection of structural systems by means of resilient elements, thereby, isolating the source where vibration is generated, from the receiver where the vibration is unwanted. These anti-vibration mounts are applied, for example, on the supports of car, ship or aeroplane engines acting mainly on the vibration energy path as vibration inhibitors.

Nonetheless, the most commonly used method of increasing damping is to insert highly damped polymers (viscoelastic materials) at strategic locations in the structure. These passive damping treatments are nowadays regarded as the most effective process of controlling and suppressing noise and vibration. In this type of treatment, the dissipation mechanism absorbs the deformation energy during vibration motion and then dissipates it to the ambient air in the form of heat. When this happens, the system is said to be damped.

In real situations, a combination of the above methods may be used acting simultaneously on the vibration source, path and location. Furthermore, straightforward vibration problems can often be solved by using ready-made anti-vibration hardware or material selected from manufacturer's catalogues. That is the case with vibration neutralisers, damping materials and vibration analysers. However, their selection and matching requires a detailed knowledge of the structure, otherwise these treatments may be rendered ineffective.

2.5.2 Active vibration control

In contrast to passive treatments, active control systems rely on external assistance. They consist of sensors, whose function is to detect vibration and emit a signal that is then processed by an electronic system or computer. Power amplifiers receive the processed signal and drive the actuators that will reduce the vibration.

Active control involves the production of a reaction signal to electronically cancel the disturbance. Generally, active systems are more costly than passive ones but in some cases of severe vibration they are the only viable solution, especially in low frequency situations. They should, in any case, be considered only after other passive treatments have been exhausted. However, with the on-going development of technology and the availability of low cost electronic components, for the same level of performance, active solutions may become cheaper than passive ones for an increasing number of applications [12].

It should also be noted that a control system cannot compensate for a bad design and that external disturbances can only be controlled over a limited band frequency. This is called the *bandwidth* and it is important to remember that outside the bandwidth the disturbance can actually be amplified by the active control system.

Smart materials used in active control systems are materials where strain energy is generated (by mechanisms involving temperature, electric or magnetic field) as a result of some coupling in their constitutive equations. Smart fluids, shape memory alloys and

piezoelectrics fall under the rubric of smart materials[1] [22]. Shape Memory Alloys (SMA) have a recoverable strain up to 5%, piezoelectric materials a recoverable strain of 0.1% under electric field and magnetostrictive materials a recoverable strain of 0.15% under magnetic field [23].

Piezoelectric materials can be used as actuators or sensors and there are two broad categories: ceramics and polymers. Piezopolymers are mostly used as sensors whereas piezoceramics are widely used as both actuators and sensors and for a wide range of frequencies. Magnetostrictive materials have a long life-time and their maximum response is obtained when the material is subjected to compressive loading.

2.5.3 Semi-active vibration control

Semi-active methods involve the enhancement of the damping properties of passive elements by active control. Examples of this type of control include the two main classes of smart fluids, the electro-rheological fluids (ERFs) and magneto-rheological (MRFs) fluids [23, 24]. It also includes active constrained-layer damping (ACLD) [25] in which an active layer replaces the traditional constraining layer. The ERFs and MRFs are fluids that can change state instantly through the application of an electric or magnetic charge, respectively.

Smart fluids are resurging with the emergence of commercial demand due to their unique properties. Besides being used as dampers in vehicle and seismic vibration control, they are used in a wide range of applications, such as, special-purpose devices for medical rehabilitation, virtual surgery, etc. [22, 26].

[1] The term “active materials” is more appropriate since they do not exhibit any “decision” ability and should not, therefore, be considered “smart”. Nevertheless the term “smart materials” is often applied to denote those materials with sensing and/or actuation capabilities.

2.6 Viscoelastic damping treatments

As the name implies, viscoelastic materials possess both elastic and viscous properties, that is, some of the strain energy stored in a viscoelastic structure is recovered upon removal of the load and the remainder is dissipated by the material in the form of heat. This dissipation mechanism is a decisive factor in the damping capability of these materials.

Since viscoelastic materials possess a high material damping capability, as a result from the internal dissipative effect provided by its molecular structure, they can be used in conjunction with high performance structural materials, for example, aluminium and steel alloys, carbon composites, etc. Viscoelastic materials cannot be used as structural materials on their own due to lack of strength and rigidity but they may be used to provide some form of remedy to unacceptable levels of vibration in problematic structures.

The application of add-on viscoelastic material layers, either superficially (without any coverage), in a constrained manner or embedded in the structure in the design phase, provides an efficient form of combining the properties of the two types of materials. Nowadays, there is an increasing interest in the market in providing solutions for structural materials with adequate damping properties and these products are available commercially in the form of sandwich metal sheet with various VEM cores.

Passive damping treatments based on VEMs have been used since the early fifties due to the emerging interest in aerospace development and the need to study passive treatments that, with an additional reduced mass, would offer the required efficiency. The relatively reduced cost of this type of treatment and the easiness of its application led to the expansion of damping treatments to other fields of structural engineering, as previously described.

Avoiding resonances in machinery and structures may be difficult as excitations cover a wide range of frequencies and many resonances get excited. In these cases, the use of damping treatments is particularly effective in the reduction of the vibration response and

dynamic stresses. The latest efforts place an emphasis on optimised solutions in order to reduce the weight and cost of the materials.

Optimisation by means of partial coverage

A layer of viscoelastic material can be applied directly on the surface of the structure to be treated or embedded in it in the form of a sandwich construction. Usually, this layer covers the extent of the whole surface, and that can hardly be considered economically efficient. It has been shown numerically and experimentally [17] that partial and localised coverage can be applied successfully to plate and beam structures without compromising its efficiency. This partial coverage solution minimises structural modifications, particularly mass increase, while reducing the treatment cost.

The effectiveness of partial treatments depends on their strategic location on the structure surface; it is, therefore, important to define the relative position of the damping material patches. In addition, the procedure to obtain an optimised partial location involves trade-offs between the extension of the treatment, its location and the resultant efficiency. This type of optimisation requires not only several numeric calculations, but also some knowledge on the part of the designer.

Partial treatment coverage of a vibrating plate or beam can be further enhanced by varying the thickness of the viscoelastic damping layer over the covered area. An optimisation routine can be used to find the ideal distribution but this should only be used on one vibration mode at a time. Different modes require different optimum distributions. It follows that, if one resonant mode dominates the vibration response, only then becomes realistic to optimise the partial distribution in order to increase the damping effect. If different resonant modes are present in the bandwidth of interest, uniform coverage may be advisable [12].

2.7 Summary

This introductory chapter first presents an overview on the effects of vibration on structures and machines. Machines and structures need to have the capability to dampen out vibrations to which they will inevitably be subjected to. In order to avoid structural failure, this relevant aspect should be taken care of in the designing stage of the structure or machine. However, even the best design can subsequently develop vibration problems. When the source of the problem cannot be solved, damping mechanisms may be used to remove, at least, part of the vibration.

Various options to dampen vibrations are presented; however, passive damping treatments have become the most popular and are regarded as very efficient in dampening vibrations. It involves the use of polymers, particularly viscoelastic materials, which are in essence polymer composites. They have been widely used in industry for many years and the subject of many academic studies.

A short overview is then presented on viscoelastic treatments and the partial coverage of viscoelastic treatments. A more thorough description of these topics is presented in the following chapter.

Chapter 3

Viscoelastic Damping Treatments

This chapter examines viscoelastic materials and some of their more relevant properties. It also presents in more detail the viscoelastic damping treatments, namely the possible configurations and modelling methods.

Many real vibration problems associated with resonance can always be mitigated by adding damping layers to the structure. Damping layers based on viscoelastic materials are very much in demand because they are effective, relatively inexpensive and able to develop a self-sufficient dissipative mechanism.

The objective of adding viscoelastic materials to a structure is to ensure that the cyclic deformation of the material will occur as the structure vibrates in the modes of interest in order to dissipate as much energy as possible during each cycle. This requires, not only, an understanding of the dynamic behaviour of the structure, but also, the behaviour and properties of viscoelastic materials.

3.1 Viscoelastic materials

Viscoelastic materials are polymers made up of long molecular chains that, when subjected to stresses, deform by either one or both of the following mechanisms:

- The lengths and angles of the chemical bonds that connect the atoms may become distorted and the atoms may be moved to positions of bigger internal energy.
- Large scale rearrangement of the atoms can occur if the molecular mobility of the polymer is high enough. Various physical and chemical factors can affect the molecular mobility, such as, temperature, the presence of fluid phases or the molecular architecture.

Polymeric materials are complex agglomerates of long, entwined, thread-like molecules. According to Mead [12], Ferry [6] describes the molecules as having 'kinks, curls and convulsions' and they 'wriggle and writhe with their thermal energy'. When this wriggling and writhing is suitably restrained, polymers become extremely efficient energy absorbers.

Viscoelastic models, also known as rheological models, possess a combination of elastic and viscous properties. According to the elastic model, *Hooke*'s law applies where stress (σ) is proportional to strain (ε) and *Young's* modulus (E) is defined as the ratio between stress and strain (σ = E * ε). Deformation is instantaneous, which means that total deformation occurs the instant the stress is applied or released, i.e. strain is independent of time. Upon release of the external load, the specimen assumes its original dimensions as the deformation is totally recovered.

On the contrary, viscous behaviour is characterised by a deformation that is not instantaneous; it is delayed or dependent on time. In addition, the deformation is not reversible or completely recovered immediately after the stress is removed. A material that exhibits a combination of the mechanical characteristics of these two extremes is called a viscoelastic material. The application of a stress on a VEM results in an instantaneous elastic strain, followed by a viscous time-dependent strain. Figure 3.1 shows a plot of strain versus time where t_a denotes the instant where the load is applied and t_r the instant

load is released. A VEM returns to its original shape after being stressed, but does it slowly enough to oppose the next cycle of vibration.

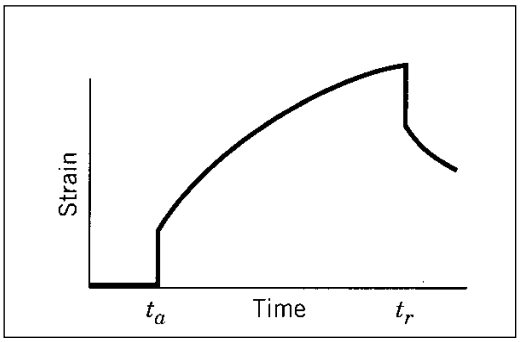

Figure 3.1: Strain vs. time response for a viscoelastic material [27]

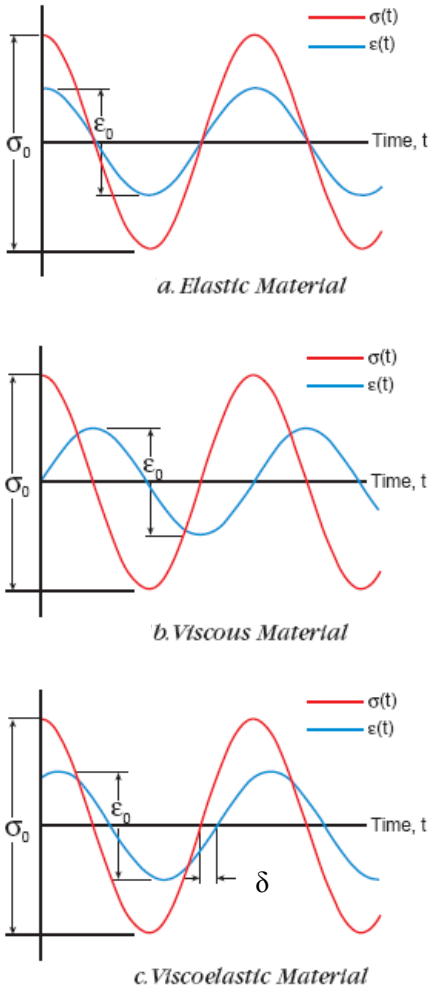

Furthermore, as a result of the elastic behaviour of a viscoelastic material, all the energy stored in the sample during loading is returned when the load is removed and the stress and strain curves move completely in phase.

Conversely, when the load is removed in a viscous material, no energy is returned and the stress is out-of-phase with the strain. In the case of a viscoelastic material the stress is out-of-phase with the strain by an angle δ ($0 < \delta < \pi/2$), as shown in Figure 3.2 [28].

Figure 3.2: Cyclic stress and strain curves vs. time for various materials (adapted from [28])

When a harmonic loading is applied, the viscoelastic material modulus can be represented by a complex quantity. The real part of the complex modulus defines the stiffness and it is related to the elastic behaviour. The imaginary component defines the capability of the material to dissipate energy and it is related to the viscous behaviour.

The damping performance of a material is measured by the phase shift between the maximum stress and maximum strain and it does not exceed 90º. The larger the phase shift δ, the more effective the material is at damping unwanted vibration.

3.1.1 Viscoelastic relaxation modulus

Stress relaxation measurements represent an experimental technique that may be used to measure and quantify the viscoelastic behaviour of polymeric materials. These tests consist in rapidly straining a specimen in tension to a relatively low strain level. With the temperature being held constant, the stress necessary to keep this strain level is measured as a function of time. It is found that stress decreases with time and this is due to molecular relaxation processes that take place within the polymer. Relaxation Modulus $E_r(t)$ is a time-dependent elastic modulus for viscoelastic polymers that may be defined as:

$$E_r(t) = \frac{\sigma(t)}{\varepsilon_0} \tag{3.1}$$

where $\sigma(t)$ is the measured time-dependent stress and ε_0 is the strain level, which is maintained constant. Moreover, the magnitude of the relaxation modulus is a function of temperature *T*, so isothermal stress relaxation measurements must be carried out over a range of temperatures, as represented in Figure 3.3.

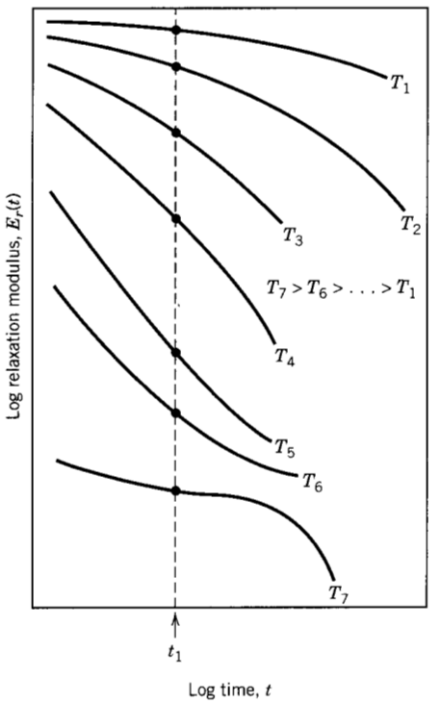

Figure 3.3: Temperature dependence of the relaxation modulus generated from T_1 to T_7 [27]

3.1.2 Viscoelastic creep

Many polymeric materials are susceptible to time-dependent deformation when the stress level is kept constant [27]. This is called viscoelastic creep. Modest stresses below the yield strength of the material, even at room temperature, may cause significant deformation. A good example of this is the flat spot that develops on the tyre contact surface when a motor car is parked for prolonged periods of time. Creep tests on polymers are conducted in the same manner as the tensile tests that are performed on metals. Under isothermal conditions, a tensile stress is applied instantaneously and is kept at a constant level while the strain is measured as a function of time. The results are represented as time-dependent creep compliance $E_c(t)$, which is defined by:

$$E_c(t) = \frac{\sigma_0}{\varepsilon(t)} \tag{3.2}$$

where σ_0 is the constant applied stress and $\varepsilon(t)$ is the time-dependent strain. Creep compliance is sensitive to temperature and it decreases with increasing temperature.

3.1.3 Modelling of viscoelastic materials

The development of representative models of the VEM behaviour and the characterisation of its properties are imperative in the design and optimisation of these passive treatments. Due to VEM high sensitivity to temperature and frequency, the experimental characterisation of the mechanical properties is a complex and critical task. A model that properly represents the material properties is also one of the main difficulties encountered in the analysis and modelling of viscoelastic treatments.

Since the early fifties, there has been a growing interest and development in the evaluation and description of the dynamic behaviour of polymers and their dissipative mechanism. Ferry [29, 30, 6], Maxwell [31], Oberst [1] and others developed and worked on numerous publications on models that have remained practically unaltered and are still used nowadays. The advances that have been made in this field are mostly concerned with the

treatment methods and the confirmation of the results, which have been obtained by means of available computer tools that are increasingly powerful.

At the time, the mechanical response of real viscoelastic systems was represented by a combination of simple mechanical elements, such as, springs and dashpots, in order to gain a greater insight into the relaxation behaviour of the material and its relationship to the structure. The Maxwell rheological model associates in series a spring and a dashpot. The viscosity of the liquid in the dashpot defines the viscous behaviour while the response of the spring characterises the elastic behaviour.

Although this is a simple model, it is not a realistic one. Also unrealistic is the Voigt-Kelvin model made up of a spring and a dashpot in parallel instead of being in series. The most widely used model is a three-element model which combines in series a spring and a Voigt-Kelvin model. It was also in the fifties that the complex modulus concept was first introduced to represent the behaviour of the viscoelastic materials.

In the eighties, the concept of partial derivatives proposed by Bagley and Torvik [32, 33] was used in the representation of VEM behaviour and this model is still used today in the analysis of passive damping treatments. More recently, in the early nineties, Lesieutre *et al.* [34] proposed an alternative model - *Anelastic Displacement Field* – in which a series of additional variables were included to represent the varying properties of the viscoelastic material with the increase of frequency. The *Golla-Hughes-McTavish* model [35] uses a set of additional oscillators to represent the same effect.

Molecular theories constitute another modelling alternative where a reasonable representation of a polymer molecule is assumed and the motion of such a molecule in a viscous medium is deduced [36]. The molecular theories predict the distribution of relaxation times and partial moduli associated with each relaxation time. Although molecular theories are not based on mechanical models, they are equivalent in many aspects.

3.1.4 Characterisation of VEM taking into account the frequency

As previously mentioned, contrary to the elastic behaviour of a material, a VEM under harmonic excitation displays a phase shift between the stress and strain maximums; it is a measure of the material damping performance and does not to exceed 90 degrees (Figure 3.4).

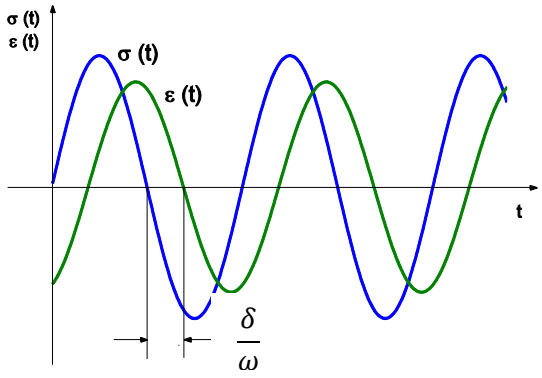

Figure 3.4: Harmonic excitation and response of a viscoelastic material [57]

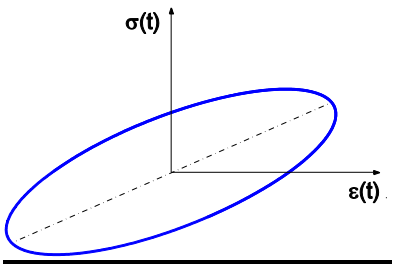

Figure 3.5: Hysteretic loop of a viscoelastic material [57]

For a viscoelastic material subjected to the cyclic loading as shown in Figure 3.4, the hysteresis of the material can be defined by plotting the input stress $\sigma(t)$ versus responding strain $\varepsilon(t)$ for one cycle of motion. The elliptical shape shown in Figure 3.5 is defined as the hysteresis loop. The area within the hysteresis loop is equal to the dissipated energy per cycle of harmonic motion by the material. By calculating the energy loss per cycle of oscillation due to steady state harmonic loading, an estimate of damping can be obtained.

The stress $\sigma(t)$ and strain $\varepsilon(t)$ induced by a sinusoidal harmonic force in a viscoelastic specimen are:

$$\sigma(t) = \sigma_0 \sin(\omega t) \tag{3.3}$$

and

$$\varepsilon(t) = \varepsilon_0 \sin(\omega t - \delta) \tag{3.4}$$

where δ represents the phase shift between stress and strain.

Equation (3.3) can be written in the following form:

$$\begin{aligned}\sigma(t) &= \sigma_0 \sin(\omega t - \delta + \delta) \\ &= \sigma_0 \sin(\omega t - \delta)\cos(\delta) + \sigma_0 \cos(\omega t - \delta)\sin(\delta)\end{aligned} \tag{3.5}$$

Assuming that the frequency ω is a positive variable and substituting sin(ωt - δ) and cos(ωt - δ) by (3.3) and its derivative, we obtain:

$$\sigma(t) = \frac{\sigma_0}{\varepsilon_0}\varepsilon(t)\cos(\delta) + \frac{\sigma_0}{\varepsilon_0 \omega}\frac{d\varepsilon(t)}{dt}\sin(\delta) \tag{3.6}$$

Substituting $\frac{\sigma_0}{\varepsilon_0}$ cos (δ) by the storage modulus E', the constitutive relationship of the material can be written in the form:

$$\sigma(t) = E'\varepsilon(t) + \frac{E'}{\omega}\frac{d\varepsilon(t)}{dt}\mathrm{tg}(\delta) \tag{3.7}$$

Similarly, the shear strain $\gamma(t)$ is:

$$\tau(t) = G'\gamma(t) + \frac{G'}{\omega}\frac{d\gamma(t)}{dt}\mathrm{tg}(\delta) \tag{3.8}$$

where $\tau(t)$ represents shear stress and G' shear storage modulus. The term tg(δ) is equivalent to the material loss factor η (term used in structural engineering).

3.1.5 Complex modulus of a viscoelastic material

Viscoelastic material properties are usually modelled in the complex domain when subjected to harmonic excitation. The resulting harmonic strain function can be represented by the following complex exponential function:

$$\varepsilon(t) = \varepsilon_0 e^{(j\omega t)} \tag{3.9}$$

and (3.7) can be written in the frequency domain as:

$$\sigma(\omega) = E'(\omega)\varepsilon(\omega) + jE'(\omega)\,\eta(\omega)\varepsilon(\omega) = E^*(\omega)\varepsilon(\omega) \tag{3.10}$$

where $E^*(\omega)$ is the complex extensional modulus [37].

The term *E'* represents the real part and *E''* the imaginary part. The real part of the complex modulus, *E',* is known as the storage modulus and it is associated with the elastic behaviour of the VEM representing the deformation energy that is stored and recovered on removal of the load. The imaginary part, *E'',* is called the loss modulus, represents the VEM viscous behaviour and defines its dissipation capacity. The loss factor η of the viscoelastic material is defined as the ratio between the imaginary component and the real component of the complex modulus

$$\eta = \frac{E''}{E'} \tag{3.11}$$

Equation (3.10) can be expressed in the form

$$\frac{\sigma(\omega)}{\varepsilon(\omega)} = E'(\omega)(1 + j\frac{E''(\omega)}{E'(\omega)}) \tag{3.12}$$

and written as

$$E^* = E'(1 + j\eta) \tag{3.13}$$

The shear stress-strain relation can be derived in an identical manner resulting in a complex shear modulus entity, which is defined as

$$G^* = G'(1 + j\eta_G) \tag{3.14}$$

where G' denotes the shear storage modulus, G" the shear loss modulus and η_G the shear loss factor.

Although *Poisson´*s ratio, denoted by ν, is frequency-temperature dependent, it is usually assumed to be constant [38] as a good approximation; the real parts of both moduli can then be related as:

$$E' = 2(1 + \nu)G' \tag{3.15}$$

and η_G can be assumed to be equal to η.

Moreover, both the imaginary and real parts depend upon temperature, frequency, dynamic strain rate, static pre-load, time effects (such as creep and relaxation), aging and other environmental conditions [28, 12]. The most important are the temperature and frequency effects.

3.1.6 The effect of temperature on the dynamic properties of VEM

When viscoelastic materials are subjected to different temperatures, their properties, namely the complex moduli represented by *E'*, *G'* and η, can change significantly. Viscoelastic materials are much more sensitive to temperature than metals or some composites due to their particular molecular structure. In fact, temperature is considered the factor with the highest impact on the variation of VEM properties. This effect is illustrated in Figure 3.6 in which the main temperature regions can be seen, namely the glassy region, the transition region, and the rubbery region.

In the glassy region, VEMs exhibit much higher storage moduli than in the transition or rubbery regions.

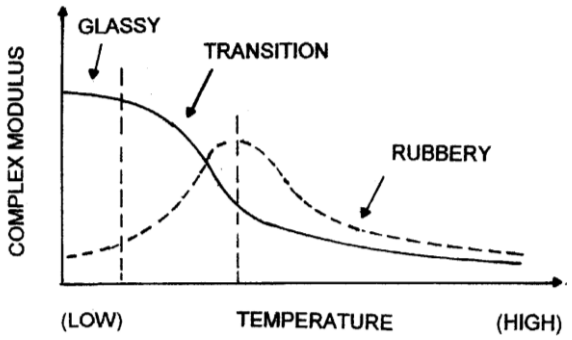

Figure 3.6: Variation of the storage modulus - *G'*(continuous line) and loss factor - η (dashed line) of a VEM with temperature (adapted from [13])

However, it needs to be said that different materials can have different temperatures defining their glassy regions, because the range of temperatures which characterises the glassy region of a polymer depends a great deal on the type and composition of the viscoelastic material. High values of storage moduli (stiffness) intrinsically correspond to low loss factors.

The rate of conformational change measures the degree of molecular mobility, which in the glassy region is so slow that it can be considered negligible. The polymer chains are rigidly ordered and possess a glass-like behaviour which is very close to an elastic behaviour. Thus, when the polymer is submitted to an applied stress, it responds by bond stretching making it unable to sustain large deformation increases without brittle fracture.

In a region of higher temperatures, the rate of conformational change is so high that the changes occur almost instantaneously and the material behaves in a rubbery manner. In this region the material is easily deformed and takes longer to reach equilibrium after the load is removed. Within this temperature range, the storage modulus and the loss factor hardly vary with the temperature and typically both have low values. At even higher temperatures, the material starts exhibiting fluid properties; it will then begin to disintegrate and have a storage modulus and loss factor of zero effectiveness.

Between the glassy and rubbery regions there is a transition region which is a combination of elastic solidity and viscous fluidity. In this phase, the variation of the storage modulus is high and due to the higher mobility of the molecular chains, storage modulus decreases significantly with the rise in temperature. It is in this region where the change in stiffness is the fastest.

For a polymer to work efficiently as a damping material, it must have a high loss modulus. It is in this region where the loss factor rises to a maximum value and where the material is, therefore, most effective. This is due to the fact that the molecular chains are in a semi-rigid or semi-flow state and are able to rub against adjacent chains. It is these frictional effects that produce the damping characteristics of a viscoelastic material. It is, therefore, extremely important to know the operating temperature so that a material, whose transition region falls within this range, can be used in the design. Moreover, it is the manner in which the modulus (G' or E') and the loss factor (η) vary with temperature and frequency that distinguishes the different viscoelastic polymers [13].

3.1.7 The effect of frequency on the dynamic properties of VEM

Frequency also has an intense effect on the dynamic properties of a viscoelastic polymer but with an inverse relationship compared to the effect of the temperature. The increase of excitation frequency causes the same effect as low temperatures, that is, high values of storage moduli; this is called temperature-frequency equivalence and this property is used in experimental measurement techniques for the characterisation of the dynamic properties of materials. At low frequencies, both the storage moduli and loss factors values are low; at high frequencies, the storage modulus is high but the loss factor is low (Figure 3.7). Similarly to the temperature effect, there is a transition region and that is where the loss factor reaches its maximum value and the storage modulus varies from low to high values. The selection of the viscoelastic material should, therefore, be based on the transition region of the material to coincide with the operating range (or selected range) of frequencies of the host structure to be treated.

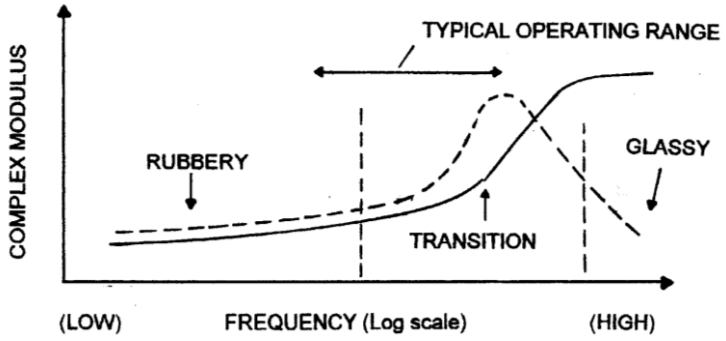

Figure 3.7: Variation of the storage modulus - *G'*(continuous line) and loss factor - η (dashed line) of a VEM with frequency (adapted from [13])

3.1.8 The effect of cyclic strain amplitude

The effect of the cyclic strain amplitude on the viscoelastic polymer is dependent on its molecular structure, which is difficult to evaluate due to the high dissipative effect that occurs within its structure. However, the effect of the cyclic strain is comparatively lower than the temperature effect [7]. Furthermore, most of the damping viscoelastic materials behave linearly at low strain amplitudes and non-linearly at high strain amplitudes.

3.1.9 Other environmental effects

The exposure of polymers to some environmental factors may be detrimental and lead to irreversible changes of the complex modulus properties. These include ultraviolet and nuclear radiation, humidity, fuels and lubricants. Some elements may be more important than others, depending on the operating conditions but by doing realistic simulations it can be established whether a damped structure will behave well.

3.1.10 Combined effects of temperature and frequency

In practice both the frequency and temperature may vary simultaneously. What is known as *reduced frequency* (f_r) refers to the combined effect of frequency and temperature into a single variable. The interpolation, extrapolation and correlation of experimental values rely on the application of the concept of frequency-temperature equivalence. This concept is

based on the assumption that the values of the complex modulus at any given frequency f_1 and temperature T_1 are identical to the values at another frequency f_2 and another temperature T_2, so that

$$G^*(f_1, T_1) = G^*\big(f_2 \alpha(T_2)\big) \tag{3.16}$$

The values of $\alpha(T)$ are determined by sliding the modulus and loss factor points to the left or to the right [13] in order to limit a single storage modulus, loss modulus or loss factor curve. This shifting represents a factor applied to the frequency at any temperature T so that

$$f_r = \alpha(T) f \tag{3.17}$$

The outcome of this process is illustrated in Figure 3.8 where several datasets of storage modulus E' and loss factor η measured at different temperatures (T_{-2}, T_{-1}, T_0, T_1 and T_2) are shifted horizontally forming a master curve for both storage modulus and loss factor.

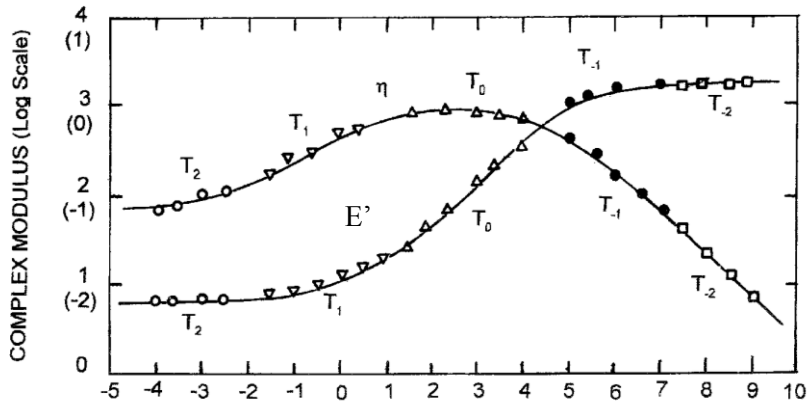

Figure 3.8: Reduced frequency plot of complex modulus data (adapted from [13])

3.1.11 Temperature-frequency nomograms

Once the reduced frequency analysis of the complex modulus values has been carried out, it is possible to obtain the modulus and loss factor at any temperature and frequency. However, this is time-consuming as it involves first reading the value of $\alpha(T)$ corresponding to the chosen temperature, then multiplying it by the frequency to obtain the reduced frequency so that finally the modulus and loss factor can be read. There are other

methods to calculate them but the graphical plots in the form of nomograms are the best option. Nomograms, provided by the manufacturer of the material, have become widely used and recognised as a very useful tool. They present the properties of the material as a function of both the frequency and temperature. Figure 3.9 represents a nomogram of a material which is specifically used in vibration control (3M SJ 2015 – ISD 112).

A nomogram is a graphical calculating tool designed to allow the approximate computation of a function. It consists of a set of scales, one for each variable of an equation. The precision with which physical markings are drawn, viewed and aligned limits the accuracy of the nomogram. Most nomograms are used in applications where an approximate answer is appropriate. The result is obtained by laying a straightedge across the known values on the scales and reading the unknown value from where it crosses the scale for that variable. The results from a nomogram are obtained very quickly and reliably and they can be read as follows: for a given temperature and frequency, the intersection between the horizontal frequency and the oblique temperature is determined. A vertical line is then drawn to intersect the storage modulus or the loss factor curves so that their values may be read on the left ordinate scale.

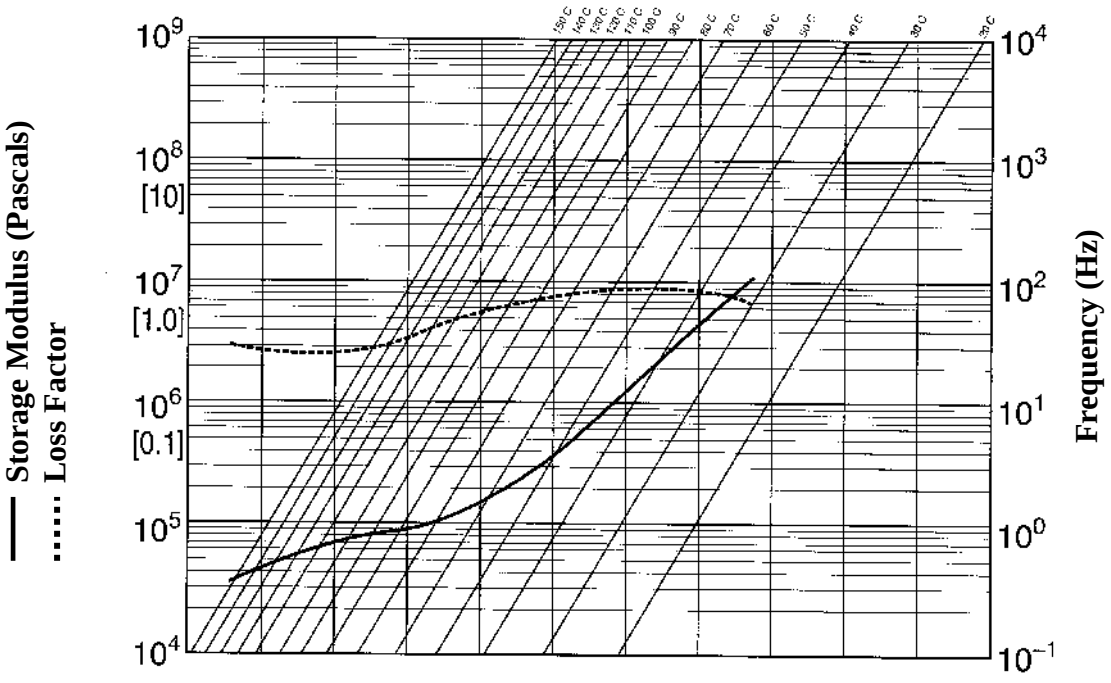

Figure 3.9: Nomogram of VEM 3M - ISD 112 [57]

3.2 Configuration of viscoelastic treatments

There are basically two configurations in which the viscoelastic material may be applied to the structure and passive damping treatments based on VEM are classified into two categories: constrained (Constrained Layer Damping - CLD) and unconstrained (Free Layer Damping - FLD). Their characteristics are distinct and so is their application. When a damping layer is added to a vibrating beam or plate, it undergoes fluctuating extensional strains and in the case of CLD, shear strains are also present. These strains vary over the surface and through the depth of the plate or beam, the direct strain being proportional to the local bending moment and the shear strain to the local shear force. The manner in which the damping layers are incorporated into the structures for greatest efficiency is related to the type of strain (shear or extensional).

3.2.1 Unconstrained damping treatments

The unconstrained treatment (also called free layer damping) refers to a structure where a viscoelastic layer (2) is attached or bonded to the host structure (1) and the generation and dissipation of energy occurs due to the alternate tension and compression of the VEM layer (Figure 3.10).

In such a structure, the extensional strain varies through its depth and in proportion to the distance from the neutral plane of bending. It follows that the locations furthest from the neutral plane present the highest extensional strains. If the structure is required to dissipate energy by extensional strain, the best location for the damping layer would be those outer surfaces. On the other hand, the outer surface of the damping layer is free of any shear strain.

In free layer damping, the application of viscoelastic material of considerable thickness is needed. However, VEM layer thicknesses higher than twice the thickness of the base layer do not contribute to an increase in efficiency, which remains practically constant; they are impractical and from the point of view of weight and cost, ineffective [13]. Nevertheless,

this type of treatment has some advantages, namely the low cost and simple applicability. Additionally, this configuration may constitute an efficient thermal and noise insulation.

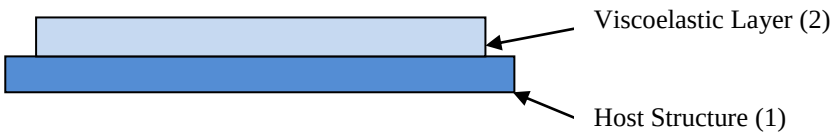

Figure 3.10: Unconstrained treatment

In the FLD configuration, the thickness of the viscoelastic layer has a direct impact on the amount of dissipation energy that is stored in the VEM layer, i.e. a thicker layer represents higher extensional deformation and simultaneously more material volume acting upon the total deformation energy. This direct effect simplifies the design and optimisation of viscoelastic treatments based on the free layer configuration, where the amount of VEM is defined by a balance between the damping efficiency and the added mass and subsequent treatment cost.

3.2.2 Constrained damping treatments

A CLD treatment consists of a viscoelastic core (2) sandwiched together between two stiff layers, the host structure (1) and a constraining layer (3) as shown in Figure 3.11. In a constrained configuration the transverse shear stress and strain in a vibrating structure are both zero at the outer surfaces and greatest at the neutral surface. If the damping layer is supposed to dissipate energy by shear strain, then the best option would be to place it close to the neutral surface, sandwiched between two plates. A symmetrical beam is, for this reason, the most efficient, as will be demonstrated in Chapter 6.

As the laminate is subjected to cyclic flexural vibrations, the base beam and constraining layer move relatively to each other, resulting in the core material being highly deformed in shear. These so-called sandwich structures are very effective in controlling and reducing the vibration response of flexible and light structures. The vibration energy in the viscoelastic material caused by its shear deformation is transferred to the surrounding layers or ambient medium as heat.

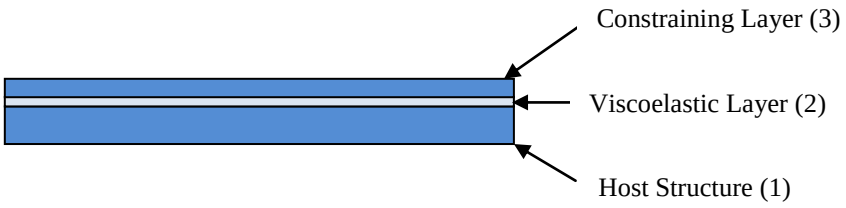

Figure 3.11: Constrained treatment

High strength-to-weight ratio and a good thermal insulation are some of the advantages of composite sandwich structures. Another great advantage is that one can obtain optimal designs for the various applications by selecting different geometric configurations and different materials of the face sheets and the cores. Contrary to the unconstrained configuration, thin viscoelastic layers are used, usually less than 0.5 mm [39].

Apart from restricting the upper surface of the viscoelastic material, the constraining layer also acts as a core protection. Its thickness may vary and any material with a high *Young*'s modulus may be used for this purpose. The applicability of these treatments is also relatively simple and mainly used for correction purposes when faulty conditions occur.

3.2.3 Embedded treatments

Embedded treatments are symmetrical forms of the CLD configuration. This type of damping treatment is normally used as a design parameter, that is, it is incorporated in the structure in the manufacturing phase. The efficiency of the embedded treatments is, in this way, maximised. In fact, the shear strain imposed on the VEM layer is particularly high due to the position of the core relatively to the neutral plane (illustrated in Figure 3.12).

There are ready-to-use commercial solutions on the market in the form of sandwich aluminium or stainless steel sheets with a polymer core [40]. The Minnesota Mining and Manufacturing Company (3M) manufactures and supplies many acrylic polymer adhesives (e.g. 3M-467) and other polymer products [13, 39]. The Soundcoat company also supplies self-adhesive film products, the most typical being the N5 [13, 41]. There may be various

grades for different temperature ranges and may come in sheets, rolls and custom cut sizes. Where metals cannot be used, a wide range of specialised non-metallic constraining layer dampers are also available, for example for electrical, military and medical applications [42].

Figure 3.12: Embedded treatment

3.2.4 The application of VEM treatments

In the case of unconstrained viscoelastic treatments, the VEM may be applied to any surface ranging from different metals to polymer-based composites. The adhesion of the VEM to the structure surface needs to be effective and the material limitations need to be observed, namely, the operational temperature range, the humidity and vapour conditions and the absence of solvents and other chemical products.

As far as the constrained configuration is concerned, some considerations need to be addressed. In the case of the embedded structure, seeing that the viscoelastic material has to be incorporated in the structure during the manufacturing process and does not support extreme temperatures, the production process needs to be selective. The thermal processes of adhesion should be substituted by joints with adhesive tape or mechanical connections.

3.3 Optimisation of viscoelastic treatments

Passive damping treatments based on the use of viscoelastic material constitute a self-sufficient dissipative mechanism, are very efficient and not costly. Nevertheless, it is possible to introduce some optimisation techniques to increase its efficiency range and reduce the material and application costs even further.

3.3.1 Partial treatments

The total coverage of the surface to be treated may present a high cost/benefit relation. Experiments have been done by Moreira and Rodrigues [17] to distribute the damping material in a partial and localised manner in selected areas. According to these authors, not only there are experimental studies that show that the partial application of the viscoelastic material is as effective as the total treatment, but that the coverage of the whole area does not produce significant improvement in damping. This methodology is specially recommended for unconstrained configurations. Normally, partial treatment consists in placing the viscoelastic material in strategic places on the area to be treated.

According to Moreira and Rodrigues [17], there are different opinions as to the optimum location of the partial patches. Some authors defend that they should be placed over areas close to the nodes of the natural mode, whereas others advocate that the viscoelastic patches should be placed close to the anti-nodes of each mode. The authors concluded that these opinions are both correct but that it depends on the position of the viscoelastic material in relation to the structure.

In the case of sandwich structures, where the base beam and constraining layer have the same thickness and the viscoelastic core is placed between them in the neutral plane where the shear stresses and strains reach their maximum, the viscoelastic material must be placed on the nodal areas.

On the other hand, in unconstrained treatments, the viscoelastic layer is located away from the neutral axis. The direct bending strains vary over the surface of a vibrating plane or along the length of a beam. At the nodal areas of a resonating mode, the direct bending strains are almost non-existing and there is little or no energy dissipated. On the contrary, the direct strains and energy dissipation are greatest close to the anti-nodes. In this case, the viscoelastic layer should be placed on the anti-nodal areas because these are the areas where the base plate deforms the most [12].

Lumsdaine and Scott [43] also presented an interesting work on the shape optimisation of free layer damping treatments where the viscoelastic layer thickness distribution is defined

following a numerical optimisation procedure. Stevens and Shostein [44] analysed the effects of partial free layer damping treatments on the modal parameters of circular plates. Akanda *et al.* [45] proposed a partial optimised distribution of an unconstrained damping treatment based on perforated VEM layers to 50 – 60 % of the total area thereby reducing the added mass significantly.

3.3.2 Spacers and amplifying mechanisms

These treatments consist of spacers that are applied between the host layer and the viscoelastic layer [46, 47]. The effect of the spacer is to increase the distance between the centroid of the VEM layer and the centroid of the whole composite structure. The aim is to increase the deformation of the bottom surface of the viscoelastic layer, since the higher the strain energy stored in the viscoelastic layer is, the higher the structure damping ratio. The spacer acts, thus, as a "strain magnifier". Moreover, for best effectiveness the spacer should be thick in comparison with the other two layers and its shear stiffness should be much greater than that of the damping layers [12].

3.3.3 Multiple layer and multiple material treatments

Another efficient way of optimising viscoelastic treatments is to place various layers of VEM in a multiple layer configuration. The multi-layer configuration consists in the application of various overlapping VEM layers and constraining layers allowing the shear strain energy in each of the VEM layers to be maximised. The damping capacity of VEM is, not only confined to a narrow temperature range, but it is also conditioned by its transition temperature thereby limiting the efficiency of a one-layer configuration. By applying layers of VEM with different transition temperatures, the combination of the relative efficiency of each material results in a higher overall efficiency [48, 49].

3.3.4 Hybrid treatments

Compared with other forms of structural dynamic control, viscoelastic treatments, especially the constrained configuration, are capable of handling high damping levels, are

safe and fairly reliable. Viscoelastic treatments are, however, temperature and frequency dependent and not very efficient at low excitation frequencies. On the other hand, active control mechanisms are particularly efficient in this frequency range while exhibiting poor performance at high frequencies.

There has been an increasing interest recently in combining two different forms of dynamic control that have different efficiency ranges and dissipative action. One of the main forms of hybrid mechanisms is obtained by substituting the constraining layer by piezoelectric crystals in the control and maximisation of the shear strain energy imposed on the VEM [50]. In addition, the high VEM damping properties at medium and high frequencies dampens the control instability present in the piezoelectric actuators in an effect known as *spillover* [51].

3.3.5 Fibre enhanced treatments

The objective of introducing fibre into the viscoelastic material is to increase the stiffness and the loss factor of the structure based on the direction of application [52]. These treatments are mainly applied to unconstrained configurations. The fibre enhancement makes these treatments as efficient as the constrained configurations while maintaining the advantages of the unconstrained structures, namely their application simplicity. The fibres act as entangled linear constraining agents promoting the shear strain effect within the VEM layer.

3.4 Modelling of viscoelastic treatments

Since the late 50's, many analytical mathematical models have been developed to properly analyse the response of damped structures. Constrained treatments are viewed as more efficient than free layer treatments but, especially for complex structures, the difficulty of analytical solutions is greater. In this case, the use of finite element methods is recommended and further development of finite element software has increased the accuracy of predictions of the dynamic behaviour of damping treatments. However, finite

element packages are computationally expensive and can be avoided when dealing with simple systems. The best known set of equations to derive a simple damping model is referred to as the RKU equations and they were developed by Ross-Kerwin-Ungar [2]. They can be used as a valuable and expedite tool for an initial analysis of damped structures.

The Modal Strain Energy (MSE) is an alternative method with a much lower computational cost proposed by Johnson *et al.* [11]. It is based on the energy ratios proposed by Ungar and Kerwin [53] and states that the ratio between the system damping ratio (or system loss factor) and the viscoelastic material damping ratio can be evaluated from the ratio of the strain energy in the viscoelastic elements and the total strain energy in the structure for a given mode. Shin and Maurer [54] compared the results obtained with MSE and the results obtained with other methods, whose values were validated experimentally, and came to the conclusion that the MSE method provided a fairly good approximation.

3.4.1 RKU method

The RKU method considers a three-layer structure and it can handle both extensional and shear types of treatment applied on beams. This analytical method, however, relies on some assumptions that may compromise the validity of the analysis. The most important one is that the RKU equations were developed using sinusoidal expansions for the mode shapes of bare beams, therefore, implying simply-supported boundary conditions. When working with other boundary conditions, such as, built-in, cantilever and free-free, approximations must be made depending on the mode shape [7]. Other major assumptions include:

1. The neutral axis of the entire structure cross-section varies with frequency.
2. Damping is mainly due to the shearing of the viscoelastic material, whose modulus is represented by complex quantities (in the case of constrained treatments).
3. There is no slipping between the elastic and viscoelastic layers at their interfaces.
4. The beam is simply supported and vibrating at a natural frequency or the beam is infinitely long and the end effects may be neglected.

This is a simplified method which is very effective for the initial screening of different materials by confining the options to a few choices and can be a valuable tool for initial design stages of damping treatments. Other approaches can then be used to obtain more accurate results. Within the constraints of the Euler- Bernoulli beam theory, Rao [55] developed more exact solutions at the expense of more numerical processing and added complexity.

RKU equations

The composite beam is made up of three layers, the middle one being the only one subjected to shear strain [2]. The external layers are assumed to behave according to *Kirchoff-Love* hypothesis.

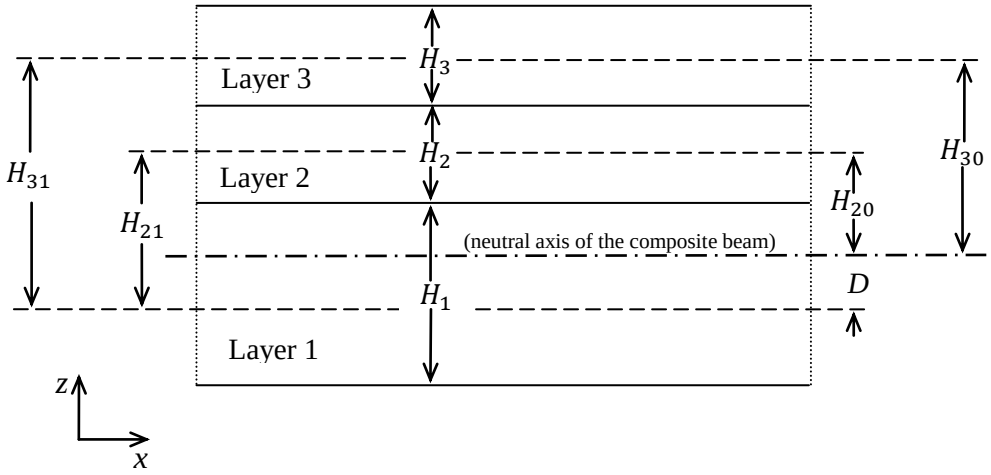

Figure 3.13: Geometry of a composite structure

Using this analytical model, the complex flexural rigidity EI^* for the composite beam representing the treated structure is calculated and the ratio between the imaginary and the real parts of this rigidity represents the loss factor of the structure. Layer 1, 2 and 3 represent the host structure, damping layer and constraining layer, respectively.

For a sandwich beam, the flexural rigidity is given by:

$$EI = \frac{E_1 H_1^3}{12} + \frac{E_2 H_2^3}{12} + \frac{E_3 H_3^3}{12} - \frac{E_2 H_2^2}{12}\left(\frac{H_{3_1} - D}{1+g}\right) + E_1 H_1 D^2 + E_2 H_2 \left(H_{2_1} - D\right)^2 + E_3 H_3 \left(H_{3_1} - D\right)^2 - \left(\frac{E_2 H_2 \left(H_{2_1} - D\right)}{2} + E_3 H_3 \left(H_{3_1} - D\right)\right)\left(\frac{H_{3_1} - D}{1+g}\right) \quad (3.18)$$

where D is the distance from the neutral axis of the composite 3-layer beam to the neutral axis of the host beam; E_1, E_2, E_3 and H_1, H_2, H_3 are the elastic moduli and thicknesses of the host structure, core layer and constraining layer, respectively; H_{21} and H_{31} are geometric parameters. The dimensional parameters are defined as follows:

$$D = \frac{E_2 H_2 \left(H_{21} - \frac{H_{31}}{2}\right) + (E_2 H_2 H_{21} + E_3 H_3 H_{31}) g}{E_1 H_1 + \frac{E_2 H_2}{2} + g\,(E_1 H_1 + E_2 H_2 + E_3 H_3)} \quad (3.19)$$

$$H_{21} = \frac{H_1 + H_2}{2} \quad (3.20)$$

$$H_{31} = H_2 + \frac{H_1 + H_2}{2} \quad (3.21)$$

The Shear parameter g is defined as:

$$g = \frac{G_2(\lambda/2)}{E_3 H_2 H_3 \pi^2} \quad (3.22)$$

where G_2 is the shear modulus of the core material and λ is the wave length of the natural mode, namely the n^{th} eigenvalue divided by the beam length. The shear parameter can also be expressed in terms of modal frequencies by:

$$g = \frac{G_2 L^2}{E_3 H_2 H_3 \xi_n^2 \sqrt{C_n}} \quad (3.23)$$

where:

$$\xi_n^4 = \frac{\rho_1 b H_1 \omega_n^2 L^4}{E_1 I_1} \tag{3.24}$$

The parameters L, b and ρ_1 are the length, width and density of the beam respectively, I_1 the second moment of inertia, ξ the beam eigenvalue, ω_n is the n^{th} modal frequency and C_n is the correction factor proposed by Rao [55] for the specific mode and boundary condition involved, which is presented in Table 3.1.

Table 3.1: Correction factors for shear parameter in RKU equations (adapted from [13])

Boundary Conditions	Correction Factor	
	Mode 1	Mode 2+
Pinned-Pinned	1	1
Clamped-Clamped	1.4	1
Clamped-Pinned	1	1
Clamped-Free	0.9	1
Free-Free	1	1

Oberst's Equations

In the *Oberst*'s beam theory, due to the fact that the constraining layer is absent (layer 3), layer 2 is extensionally deformed; this configuration represents an FLD treatment for beams. The RKU equations are the equations that Oberst used to characterise a viscoelastic material by estimating its complex modulus; they may be applied considering the following conditions:

$$H_3 = 0; E_3 = 0 \tag{3.25}$$

As the thickness of the constraining layer H_3 tends to zero, the shear parameter tends to infinity. Parameter D can be determined by calculating the limit defined by:

$$D = \lim_{\substack{H_3 \to 0 \\ g \to \infty}} \left[\frac{K_2 \left(H_{21} - \frac{H_{31}}{2} \right) + g(K_2 H_{21} + K_3 H_{31})}{K_1 + \frac{K_2}{2} + g(K_1 + K_2 + K_3)} \right] = \frac{K_2}{K_1 + K_2} \left[\frac{H_1 + H_2}{2} \right] \tag{3.26}$$

where $K_i = E_i H_i$.

Substituting (3.26) in (3.18) and considering the conditions in (3.25), the expression that defines the flexural rigidity of the *Oberst*'s beam may be written as follows:

$$EI = K_1 \frac{H_1^2}{12} + K_2 \frac{H_2^2}{12} + \frac{K_1 K_2}{K_1 + K_2} \left[\frac{H_1 + H_2}{2} \right]^2 \tag{3.27}$$

Introducing the non-dimensional $e_2 = \frac{E_2}{E_1}$ and $\bar{h}_2 = \frac{H_2}{H_1}$, (3.27) can be re-written in an equivalent form

$$\frac{EI}{E_1 I_1} = 1 + e_2 \bar{h}_2^3 + 3\left(1 + \bar{h}_2\right)^2 \left[\frac{e_2 \bar{h}_2}{1 + e_2 \bar{h}_2} \right] \tag{3.28}$$

Symmetrical Sandwich Beam Equation

A symmetrical sandwich beam represents a configuration formed by skins of identical thickness. The following conditions apply to a symmetrical sandwich beam:

$$H_3 = H_1; E_3 = E_1; K_3 = K_1 \tag{3.29}$$

and H_{21} then becomes:

$$H_{21} = \frac{H_{31}}{2} \tag{3.30}$$

If the previous conditions are applied, we can define the position of the neutral axis as:

$$D = H_{21}\frac{g}{g+\frac{1}{2}} = (H_1 + H_2)\frac{g}{1+2g} \tag{3.31}$$

and the flexural rigidity of the symmetric beam is defined as:

$$\begin{aligned} EI = {} & K_1\frac{H_1^2}{6} + K_2\frac{H_2^2}{12} + K_1(H_1+H_2)^2\left(\frac{g}{1+2g}\right)^2 + \\ & + K_2(H_1+H_2)^2\left(\frac{1}{2}-\frac{g}{1+2g}\right)^2 + K_1(H_1+H_2)^2\left(\frac{1+g}{1+2g}\right)^2 \\ & - K_2\frac{H_2}{12}\frac{H_1+H_2}{1+2g} - \frac{K_2}{4}\frac{(H_1+H_2)^2}{(1+2g)^2} - K_3\frac{(H_1+H_2)^2(1+g)}{(1+2g)^2} \\ = {} & K_1\frac{H_1^2}{6} + K_1(H_1+H_2)^2\left(\frac{g}{1+2g}\right) + K_2\left[\frac{H_2^2}{12} - \frac{H_2}{12(1+2g)}\right] \end{aligned} \tag{3.32}$$

If the extensional stiffness of layer 2 is ignored ($E_2 = 0$), then the previous expression may be simplified and written in the form:

$$EI = K_1\frac{H_1^2}{6} + K_1(H_1+H_2)^2\left(\frac{g}{1+2g}\right) \tag{3.33}$$

or in the following equivalent form:

$$\frac{EI}{E_1 I_1} = 2 + 12\left(1+\bar{h}_2\right)^2\frac{g}{1+2g} \tag{3.34}$$

3.4.2 Modal strain energy (MSE)

The Modal Strain Energy (MSE) method was proposed by Johnson and Kienholz [11] with the intention of providing an accurate and flexible tool in the day-to-day design analysis. The method uses simple approximate formula to calculate the loss factor for each mode. The approximation was shown to be reasonable compared with the true complex eigenvalue solutions, especially for lightly damped structures. This method can be used directly in a numerical analysis based on the finite element method, where the main assumption relies on the fact that undamped mode shapes are considered to be

representative of the mode shapes for the damped solution. This assumption does not have a major effect in the case of unconstrained and asymmetric constrained configurations with very thin damping treatments.

In the case of symmetric, or close to symmetric constrained configurations, where the VEM core may produce important modifications on the order of natural modes, especially on the corresponding natural frequencies, it should not be overlooked. In this analysis, this drawback is minimised by considering the dissipation core to be represented by an elastic material with a *Young*'s modulus identical to the storage modulus of the viscoelastic material. It is important to recall here that, in this study, the storage modulus is considered constant and frequency independent; when frequency dependent properties must be considered, iterative procedures [15, 56] should be used.

The MSE principle states that the ratio between the obtained damping ratio for the entire damped structure ($\eta^n_{structure}$) and the viscoelastic material damping ratio (η^n_{VEM}) can be evaluated from the ratio between the strain energy stored in the viscoelastic layer ($\mathbf{U}^n_{VEM}$) and the strain energy of the entire structure ($\mathbf{U}^n_{TOTAL}$) for a given mode n, as:

$$\frac{\eta^n_{structure}}{\eta^n_{VEM}} = \frac{\mathbf{U}^n_{VEM}}{\mathbf{U}^n_{TOTAL}} \tag{3.35}$$

The structure loss factor for a particular natural mode n can, therefore, be computed from the following equation:

$$\eta^n_{structure} = \eta^n_{VEM} \frac{\{\phi\}^{\mathrm{T}}_n [\mathbf{K}_{VEM}] \{\phi\}_n}{\{\phi\}^{\mathrm{T}}_n [\mathbf{K}] \{\phi\}_n} \tag{3.36}$$

where $\{\phi\}_n$ is the mode shape for the n-*th* mode, $[\mathbf{K}_{VEM}]$ represents the stiffness matrix of the damping layer and $[\mathbf{K}]$ represents the finite element stiffness matrix of the entire sandwich structure. The superscript $^{\mathrm{T}}$ means matrix or vector transpose.

3.4.3 Iterative modal strain energy (IMSE)

As previously stated, the calculation of the loss factor with the MSE method is restricted to lightly damped structures as only in these cases is the undamped model effectively represented. In the case of highly damped structures, where the thicker VEM induces a considerable alteration to the mass and stiffness, the modal strain energy method proves to be conducive to inaccuracy.

In view of this, an iterative procedure was formulated [57] so that stiffness changes can be introduced and the effects of the variation of the storage and loss moduli with frequency can more efficiently be taken into account. This approach involves the calculation of the real part of the stiffness matrix to be updated iteratively. The updating is based on the properties of the VEM at the frequency value (in the vicinity of the natural mode being considered) of the current iteration. Once convergence has been reached, the methodology of the original MSE is used to determine the correspondent modal loss factor, the exception being the use of the correspondent imaginary part of the stiffness matrix defined at the converged value of frequency.

3.4.4 Iterative complex eigensolution (ICE)

The Modal Strain Energy method provides an approximate modal loss factor and computationally speaking it is a rather cost-effective method. The Iterative Complex Eigensolution, on the contrary, calculates an exact solution as it uses the determined complex eigenvalue to find the exact modal loss factor [56]. Similarly to the IMSE, this method starts off by determining the real eigensolution of the finite element model at a specific initial frequency. After the initial estimate of the value of the damped natural frequencies, the ICE updates the complex stiffness matrix and the corresponding complex eigenvalues. The updating continues until convergence is achieved and the required accuracy is obtained. This approach represents an improvement on the IMSE approach but it requires a higher computational effort.

3.5 Summary

This chapter starts off by analysing the concept of viscoelasticity and the relationship between the maximum stress and maximum strain phase shift and the damping performance of a viscoelastic material. Due to the elastic and viscous behaviour of a VEM and since harmonic excitation can be assumed, their properties are normally modelled in the complex domain. A complex modulus is thus derived in order to compute the material damping capacity, also known as the material loss factor. It is defined as the ratio between the VEM capacity to dissipate the energy related to the viscous behaviour and the strain energy associated with the elastic behaviour. The higher the energy dissipation, in the form of heat, the higher the VEM loss factor and, hence, the more effective the material is. The effect of temperature and frequency on the dynamic properties of VEM is also analysed.

Being very effective in the control and suppression of vibration, these polymers (viscoelastic materials) are nowadays widely used in different configurations in order to obtain highly damped structures. The optimised way in which these materials can be applied in damping treatments is also subject of an analysis, be it in the form of amplifying mechanisms, multiple layers, fibre enhancement or, in particular, partial coverage.

In order to evaluate the efficiency of a structure treated with a damping material, its response has to be analysed. Many models have been developed, among them, the RKU and the MSE methods. The latter was used in this study to predict the structure damping ratio for a particular natural mode. To be able to compute the damping ratio through the MSE method, the shear strain energy developed inside the VEM layer needs to be calculated; in order to do that, it has to be accurately represented by spatial discretisation into what is commonly known as finite elements. Finite element analysis of viscoelastic treatments is the subject of the next chapter.

Chapter 4

Finite Element Analysis of Structures with Viscoelastic Treatments

This chapter introduces the numerical analysis of viscoelastic damping treatments. The main issues regarding the use of the finite element method to simulate these damping treatments are briefly highlighted. The layerwise spatial model is presented, as well as the layerwise finite element formulation used in this work.

The method of finite elements is considered the most widespread method in the resolution of problems concerning static and dynamic behaviour of structures. The analysis developed in this work is based on this numerical method, and this chapter introduces the applied methodology and the numerical issues resulting from the present application, as well as the corresponding solutions used.

Despite the general and widespread use of the finite element method (FEM) for simulation purposes, the application of this method in the modelling of the viscoelastic damping

treatments requires some specific considerations. Due to the fact that viscoelastic damping treatments consist of a total or partial layerwise distribution in the structure, and that the damping mechanism relies on the shear strain field developed inside the VEM layer, it is important to take into consideration their spatial discretisation. The variation of the viscoelastic properties with temperature and frequency, either in the time or frequency domain, requires special attention too. The most adequate method of analysis also needs to be selected based on the modelling method used, the simulation objective and the type of solution required.

4.1 The finite element method

The analysis methodology applied in this work is based on the finite element method which is a numerical tool widely used in the analysis of structures. Nevertheless, several issues must be considered when dealing with plates and beams with either constrained or embedded (symmetrical) thin viscoelastic layers [58]. These issues are described and the methods and main assumed simplifications are identified and presented.

The finite element method relies on the spatial discretisation of a structure into uniform sub-domains, commonly known as finite elements. Within the finite element domain a predefined description of the unknown field, such as, displacement, strain or stress field is deduced and represented by a limited set of variables. The continuity conditions between adjacent finite elements, the boundary conditions and vector of loads are applied to construct the whole set of equations of motion, whose solution leads to the complete definition of the unknowns that characterise the field within each finite element domain.

The results from a finite element scheme depend closely on the assumed distribution of the unknown field and the ability of the model to represent the physical phenomena and material properties. These are usually described as spatial model and constitutive model, respectively. The accuracy and adequacy of the method of analysis used to solve the resulting numerical problem is also decisive.

4.2 Simulation of VEM structures - main issues concerning finite element modelling

Contrary to the simplicity of the damping treatment working principle, its design and optimisation is complex, especially for the constrained layer configuration, requiring the use of numerical modelling techniques. The optimisation of CLD treatments is a function of several parameters, namely, size, thickness and shape of the host structure, the thickness and configuration of the treatment layers and the intrinsic properties of the applied materials. In addition, the frequency and temperature dependent properties of the VEMs also play an important role upon the complexity associated with the correct design and optimisation of viscoelastic damping treatments.

For the correct simulation of the dynamic response of damped structures using VEM damping treatments, special care should be taken when selecting the proper spatial model, the viscoelastic constitutive model and the solution method. The correct discretisation or spatial modelling of beams and plates with viscoelastic treatments plays a fundamental role in the accuracy and validity of the results obtained in numeric simulation. The discretisation approach to the problem depends obviously on the treatment configuration.

Another important aspect to be taken into account in the analysis of viscoelastic treatments by means of finite elements is the difficulty dealing with the introduction of the properties of viscoelastic materials in the calculation and characterisation of viscoelastic damping. Apart from sustaining a high loss factor, some of their properties are highly dependent on the temperature and excitation frequency that they are subjected to. These factors need to be taken into consideration so that the correct characterisation and simulation process of viscoelastic damping can be obtained.

Even though temperature is an important parameter, isothermal conditions may be assumed and the treatment behaviour can be analysed for various levels of temperature within the expected temperature range. Isothermal conditions were considered in this study, thereby, disregarding temperature dependency. However, this procedure is far from ideal and realistic and Lesieutre [59] developed the method - *Augmenting Thermodynamic Fields*

(*ATF*) based on a thermodynamic process. The introduction of a variable temperature is sometimes essential as in the case of viscoelastic materials being applied in structures with low thermal conductivity.

Finally, the solution method is not only selected by the type of expected results, but is also conditioned by the applied constitutive model used to characterise the VEM behaviour.

4.3 Characterisation of the behaviour of the VEM

The science of deformation and flow of matter, known as rheology, provides the basis for the mathematical approach to the modelling of the damping phenomenon. Rheology may be classified into microscopic and macroscopic theories. The latter is the most useful in engineering and works in terms of state equations based on the laws of thermodynamics of irreversible processes. The state equations are models that describe the material behaviour and can be written in the following general form:

$$f[D_1(\sigma), D_2(\varepsilon), t, T, \cdot, \cdot] = 0 \tag{4.1}$$

where f is the vector function of variables, σ and ε are the stress and strain tensors, respectively, t is the time, T the temperature, the other variables represent the physiochemical properties of environment conditions and D_1 and D_2 represent differential, integral or combined operators. One of the best known representations of the state equations is the standard linear model. Other models include the generalised standard model that introduces additional derivatives and generalised derivatives model that replaces integral derivatives by fractional derivatives. The complex modulus model is an approach that describes the viscoelastic behaviour more conveniently than the previously mentioned methods. It introduces the rheologic model of the complex modulus (discussed in Chapter 3) in the finite elements approach and it is the constitutive model used in this study.

Other constitutive models are presented in recent open literature, which demonstrate the interest in this specific research field and the continuous search for improved constitutive

models for VEMs. *Golla-Hughes-McTavish* (*GHM*) [35] model and *Anelastic Displacement Fields* (*ADF*) proposed by Lesieutre and co-workers [34, 59] are two interesting and broadly used time domain constitutive models that can be directly introduced in a time domain solution method. Nevertheless, these methods require, at least, the duplication of the dimension of the system of equations [57]. The fractional derivative model [32, 33] is also an interesting constitutive model, providing a good representation of the material behaviour with a minimum set of parameters. However, it requires special solution methodologies [60, 61, 62].

4.4 Method of analysis

The selected constitutive model used to represent the VEM behaviour may dictate the method of analysis. In fact, if time domain constitutive models are applied, then time domain solution methods must be used. On the contrary, frequency domain models, such as, the complex modulus approach, require that the solution be obtained in the frequency domain using a *Direct Frequency Analysis* (*DFA*).

The direct evaluation of energy dissipation in structures is very complex and so, the evaluation of the dissipation of energy in terms of damping ratio is generally accepted. One of the ways of predicting the damping level is known as the Modal Strain Energy (MSE) method, which is an accurate predictor in structures of elastic and viscoelastic elements, as previously discussed. In this study the MSE method was used in conjunction with the complex modulus approach to represent the VEM properties.

4.5 Spatial model

One of the key issues for the design of these treatments is related to the correct description of the strain field developed inside the damping layer resulting from the deformation imposed by the host structure during vibration, in conjunction with the proper representation of the material behaviour, i.e. the viscoelastic constitutive model.

The spatial modelling of unconstrained treatments is relatively simple. The generation and subsequent dissipation of energy that occurs in the VEM, results from the alternate tension/compression strain of the viscoelastic material. In the case of this configuration, a correct description of the strain field can be obtained by the application of beam and plate elements.

The spatial modelling of constrained treatments requires that the high shear strain energy generated in the VEM be correctly represented and the classical theory of laminated structures seems inadequate to do it. It is, therefore, necessary to use a different spatial discretisation method. There are alternative modelling methods that are able to represent correctly the shear strain fields generated in the viscoelastic core. These alternative modelling methods include combined models and layerwise models.

4.5.1 Combined models

Combined models consist of beam finite elements and quadrilateral finite elements based on plane strain conditions that are combined in a stratified form and modelled individually. The model, depicted in Figure 4.1, is based on the concept proposed by Killian and Lu [63] and describes the shear strain generated in the viscoelastic layer rather accurately; therefore, the simulation results obtained with this model are satisfactory. In its simplest form, the two outer layers are represented by two beam elements and the dissipative layer is represented by another two beam elements. The beam degrees of freedom are coincident. The generation of the required finite element mesh is difficult and time consuming and, therefore, this model is not widely used.

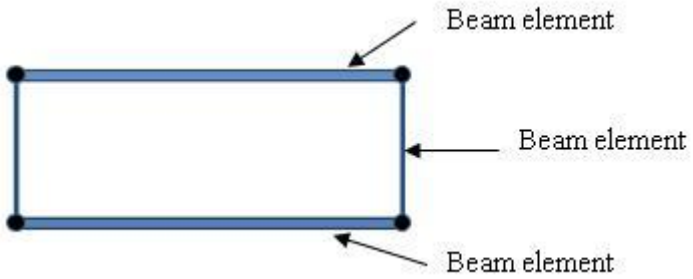

Figure 4.1: Combined model of beam elements

There is another method that uses two beam finite elements to represent the outer layers and a quadrangular finite element to represent the dissipative core [57]. This model requires the three element layers, as well, as the four node layers to be modelled separately; it also requires rigid linking elements between the nodes of the quadrangular element and the nodes of the adjacent beam; this model is shown in Figure 4.2. It is a suitable modelling method for multi-layer and curved structures but it is also a time consuming model.

Figure 4.2: Rigidly connected combined model of beam and quadrangular elements

In another model proposed by Johnson and Kienholz [11], the beam elements that represent the face layers and the quadrangular finite element representing the VEM core share the nodal positions. This way, the need for rigid connecting elements of the previous model is avoided (Figure 4.3). This model contemplates the introduction of an offset node corresponding to half the thickness of the layer of the outer beams.

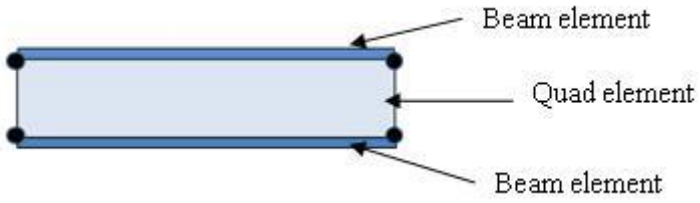

Figure 4.3: Combined model of beam and quadrangular elements

The last of the combined models presented here, uses three quadrangular finite elements to represent the three layers that make up the sandwich structure [57]. The main advantage of this model is the simplicity and speed that is associated with the spatial modelling. A

comparison study of the performance of these models has been done by Moreira and Rodrigues [58] and they concluded that this model allowed a rapid convergence.

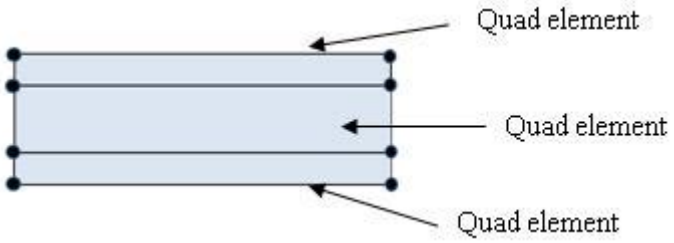

Figure 4.4: Combined model of quadrangular elements

4.5.2 Layerwise models

Layerwise theories based on a piecewise description of the displacement field have been developed and provide a very accurate simulation of the damping layer effect. Combined models have drawbacks concerning their application in structures of complex geometry and in multiple layer treatments, because their modeling is both difficult and lengthy.

By comparison, the layerwise model has several advantages that justify its choice (also for this study), especially when applied in the dynamic control of light structures with very thin viscoelastic damping layers. Since the material properties, the treatment configuration and the layer dimensional parameters are introduced directly in the analysis process by means of a numeric table, it is possible to change data without having to alter the finite element mesh. The computational cost is reduced, which is an evident advantage when optimising treatments or developing designs at an initial stage.

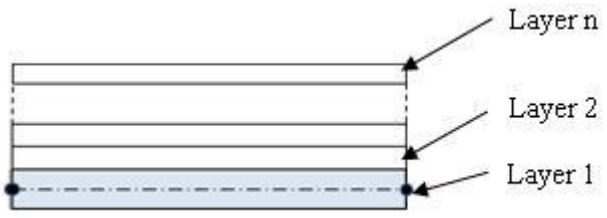

Figure 4.5: Layerwise element model with multiple layers

Each layer may be described individually based on *First-order shear theory* (*FOST*) or *Higher-order Shear Theory* (*HOST*) beam models or quadrilateral models based on plane strain conditions. These modelling theories assume continuity of the displacement fields over the laminate thickness; the continuity of the transverse shear stresses can also be directly imposed in the finite element formulation when using stress continuity conditions.

The majority of layerwise theory publications either deal with passive or active damping treatment of beams or sandwich plate structures with a single viscoelastic core. Although the FOST and HOST models are able to represent the treatment configuration in an appropriate manner, their application is not adequate in multiple layer configurations. The analysis of multiple layer treatments can be done using a generalised model presented by Saravanos [64] and Saravanos and Pereira [65] based on a generalised layerwise theory proposed by Robbins and Reddy [66].

Displacement-based layerwise theories may be divided into two categories: the partial layerwise theory which uses layerwise expansions for the in-plane displacement components but not the transverse displacement component and the full layerwise theory which uses expansions for the three displacement components.

4.6 Layerwise finite element formulation

This section presents the layerwise finite element that will be applied along the subsequent chapters devoted to the analysis of constant (Chapters 6 and 7) and variable (Chapter 8) thickness VEM layers. The spatial model replicating the sandwich construction of the treated structure must be able to accurately represent the shear deformation pattern developed inside the VEM layer, while avoiding the usual numerical locking issues related to the high aspect ratio of the finite element [58]. Furthermore, it must provide an easy and flexible modelling approach to simplify the spatial model construction and redesign during an optimisation procedure [67, 68]. In this work, a layerwise beam finite element based on a stress-displacement mixed formulation is used. A brief description on this finite element is presented hereby but more details can be found in reference [69].

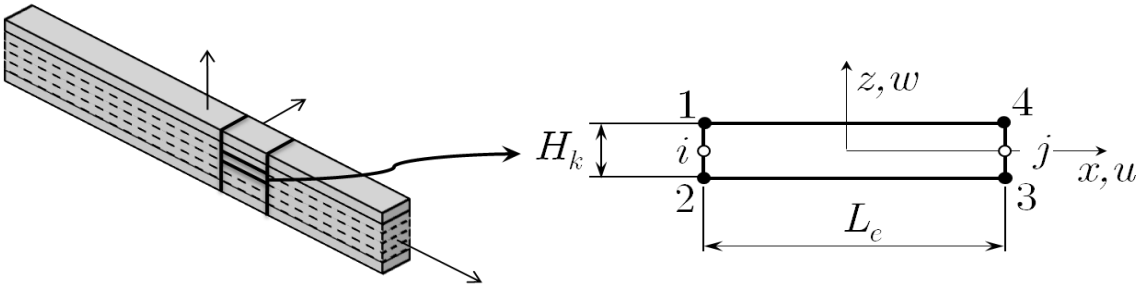

a) beam laminate b) generic layer finite element

Figure 4.6: Generic layer configuration of the laminate beam finite element

Figure 4.6 presents a generic layer k of the beam finite element configuration, represented by four corner nodes (1-4) used to interpolate the in-plane displacement field $u(x, y, t)$ and two mid-side nodes (i and j) that represent the displacement field $w(x, t)$ considered uniform along the direction z of the laminate. The stiffness and mass matrices for a generic layer k of the beam finite element are determined. The laminate finite element stiffness and mass matrices are assembled from the generic layer matrices using a standard numerical assembling technique.

Displacement field

The displacement field within the layer finite element domain is interpolated from the nodal values as:

$$\begin{aligned} u(x,z) &= N_{1x}N_{1z}u_1 + N_{2x}N_{2z}u_2 + N_{3x}N_{3z}u_3 + N_{4x}N_{4z}u_4 \\ w(x) &= N_i w_i + N_j w_j \end{aligned} \tag{4.2}$$

where the interpolation functions are defined as:

$$\begin{aligned} N_{1z} = N_{4z} &= \frac{1}{H_k}\left(z + \frac{H_k}{2}\right) \qquad N_{1x} = N_{2x} = N_i = -\frac{1}{L_e}\left(x - \frac{L_e}{2}\right) \\ N_{2z} = N_{3z} &= -\frac{1}{H_k}\left(z - \frac{H_k}{2}\right) \qquad N_{3x} = N_{4x} = N_j = \frac{1}{L_e}\left(x + \frac{L_e}{2}\right) \end{aligned} \tag{4.3}$$

where $x \in [-L_e/2, L_e/2]$ and $z \in [-H_k/2, H_k/2]$, L_e and H_k being the length of the finite element and the thickness of the layer respectively. The displacement field (4.2) can be written in matrix form as:

$$\{\mathbf{u}(x,z)\} = [\mathbf{N}(x,z)]\{d\} \tag{4.4}$$

where $\{d\}$ represents the generalised displacement vector:

$$\{d\} = \{w_i \quad u_1 \quad u_2 \quad w_j \quad u_3 \quad u_4\}^T \tag{4.5}$$

and matrix $[\mathbf{N}(x,z)]$ represents the interpolation operator described by (4.3).

Strain field

Plane stress conditions and linear elastic deformation are assumed and therefore the strain field of the beam finite element is defined as:

$$\{\varepsilon(x,z)\} = \begin{Bmatrix} \varepsilon_{xx} \\ \gamma_{xz} \end{Bmatrix} \tag{4.6}$$

where ε_{xx} and γ_{xz} are the normal and the shear strains, respectively. The strain field is obtained applying the differential operator $[\mathbf{L}]$ to the displacement field (4.4) as:

$$\{\varepsilon(x,z)\} = [\mathbf{L}][\mathbf{N}(x,z)]\{d\} = [\mathbf{B}(x,z)]\{d\} \tag{4.7}$$

where $[\mathbf{B}(x,y)]$ is the deformation matrix defined by the membrane and bending strain $[\mathbf{B}^B]$ and shear strain $[\mathbf{B}^S]$ terms.

Stress field

The stress field is defined independently from the strain field following an interpolation procedure similar to the displacement field description, as:

$$\{\sigma(x,z)\} = [\mathbf{N}^\sigma(x,z)]\{\sigma\} \tag{4.8}$$

where the nodal stress vector $\{\sigma\}$ is described by the stress nodal parameters:

$$\{\sigma\} = \{\sigma_{x1} \quad \sigma_{x2} \quad \sigma_{x3} \quad \sigma_{x4} \quad \tau_{xz1} \quad \tau_{xz2} \quad \tau_{xz3} \quad \tau_{xz4}\}^T \tag{4.9}$$

and the stress related interpolation matrix is defined by the set of terms:

$$[\mathbf{N}^{\sigma}(x,z)] = [N_{1x}N_{1z} \quad N_{2x}N_{2z} \quad N_{3x}N_{3z} \quad N_{4x}N_{4z}] \tag{4.10}$$

using the same interpolation operator applied to the displacement field.

Variational formulation

The constitutive operator can be used to describe the stress-strain relation as:

$$\{\sigma(x,z)\} = [\mathbf{D}]\{\varepsilon(x,z)\} \tag{4.11}$$

where [**D**] is the elasticity matrix containing the elastic properties of the material (the *Young*'s modulus E and the *Poisson*'s ratio ν). The constitutive operator can alternatively be represented by the flexibility matrix as:

$$[\mathbf{D}]^{-1}\{\sigma(x,z)\} = \{\varepsilon(x,z)\} \tag{4.12}$$

The *Hellinger-Reissner* variational principle is applied to determine the total energy, resulting from the superposition of the elastic strain energy (first term of (4.13), the complementary energy (second term of (4.13)) and the work performed by external forces:

$$\Pi_P = \frac{1}{2}\int_{-L_e/2}^{L_e/2}\int_{-H_k/2}^{H_k/2}\{\sigma\}^T[\mathbf{D}]^{-1}\{\sigma\}\,dxdz - \int_{-L_e/2}^{L_e/2}\int_{-H_k/2}^{H_k/2}\{\sigma\}^T[B]\{d\}\,dxdz + W_e \tag{4.13}$$

The variational form of the equilibrium equation arises from the minimisation of the total energy Π_P in relation to the nodal stress $\{\sigma_e\}$ and displacement $\{d_e\}$, (parameters of the finite element), resulting in the following system of equations of motion:

$$\begin{bmatrix}[\mathbf{S}_{ss}] & [\mathbf{S}_{sd}] \\ [\mathbf{S}_{sd}]^T & [0]\end{bmatrix}\begin{Bmatrix}\{\overline{\sigma}_e\} \\ \{d_e\}\end{Bmatrix} = \begin{Bmatrix}\{0\} \\ \{F_e\}\end{Bmatrix} \tag{4.14}$$

The sub-matrices $[\mathbf{S}_{ss}]$ and $[\mathbf{S}_{sd}]$ can be decomposed as:

$$[\mathbf{S}_{ss}] = \begin{bmatrix}[\mathbf{S}_{\sigma\sigma}] & [0] \\ [0] & [\mathbf{S}_{\tau\tau}]\end{bmatrix} \tag{4.15.a}$$

$$[\mathbf{S}_{sd}] = \begin{bmatrix}[\mathbf{S}_{\sigma d}] \\ [\mathbf{S}_{\tau d}]\end{bmatrix} \tag{4.15.b}$$

whose sub-matrices $[\mathbf{S}_{\sigma\sigma}]$, $[\mathbf{S}_{\tau\tau}]$, $[\mathbf{S}_{\sigma d}]$ and $[\mathbf{S}_{\tau d}]$ are defined as:

$$[\mathbf{S}_{\sigma\sigma}] = D_\sigma^{-1} \int_{-L_e/2}^{L_e/2} \int_{-H_k/2}^{H_k/2} [\mathbf{N}_{\sigma\sigma}(x,z)]^T [\mathbf{N}_{\sigma\sigma}(x,z)]\, dzdx \tag{4.16.a}$$

$$[\mathbf{S}_{\tau\tau}] = D_\tau^{-1} \int_{-L_e/2}^{L_e/2} \int_{-H_k/2}^{H_k/2} [\mathbf{N}_{\tau\tau}(x,z)]^T [\mathbf{N}_{\tau\tau}(x,z)]\, dzdx \tag{4.16.b}$$

$$[\mathbf{S}_{\sigma d}] = \int_{-L_e/2}^{L_e/2} \int_{-H_k/2}^{H_k/2} [\mathbf{N}_{\sigma\sigma}(x,z)]^T [\mathbf{B}^B(x,z)]\, dzdx \tag{4.16.c}$$

$$[\mathbf{S}_{\tau d}] = \int_{-L_e/2}^{L_e/2} \int_{-H_k/2}^{H_k/2} [\mathbf{N}_{\tau\tau}(x,z)]^T [\mathbf{B}^S(x,z)]\, dzdx \tag{4.16.d}$$

The first two matrices (4.16.a) and (4.16.b) are obtained with exact integration and represent the normal and shear stresses flexibility matrices, respectively. The third matrix (4.16.c), which is also obtained by full quadrature, represents the effect of normal stresses on the respective strains participates. The complementary work performed by the shear

stresses against the shear strains is described by the matrix defined in (4.16.d), calculated by a reduced integration procedure at point $x = z = 0$. The global mixed matrix equation described by the equations of motion (4.14) can be condensed at the element level as:

$$-([\mathbf{S}_{sd}]^T[\mathbf{S}_{ss}]^{-1}[\mathbf{S}_{sd}])\,\{d_e\} = \{F_e\} \tag{4.17}$$

where the inverse of $[\mathbf{S}_{ss}]$ is defined by:

$$[\mathbf{S}_{ss}]^{-1} = \begin{bmatrix} [\mathbf{S}_{\sigma\sigma}]^{-1} & [0] \\ [0] & [\mathbf{S}_{\tau\tau}]^{-1} \end{bmatrix} \tag{4.18}$$

The displacement vector $\{d_e\}$ can be calculated from the assembled reduced form (4.17) whose solution can then be applied to the original assembled mixed form (4.14), prescribing the natural shear stresses boundary conditions at the top and bottom faces of the beam in order to determine the full stress field.

The consistent form of the mass matrix is defined as:

$$[\mathbf{M}] = \rho b \int_{-L_e/2}^{L_e/2} \int_{-H_k/2}^{H_k/2} [\mathbf{N}(x,z)]^T [\mathbf{N}(x,z)]\, dz dx \tag{4.19}$$

4.6.1 Numerical implementation

The numerical implementation of the proposed finite element formulation is straightforward and it can easily be introduced in an open source finite element program.

The stiffness matrix for a generic layer *k* of the beam finite element is defined as:

$$[\mathrm{K}]_k = b.\begin{bmatrix} \frac{GH_k}{L_e} & -\frac{1}{2}G & \frac{1}{2}G & -\frac{GH_k}{L_e} & -\frac{1}{2}G & \frac{1}{2}G \\ -\frac{1}{2}G & \frac{EH_k}{3L_e}+\frac{GL_e}{4H_k} & \frac{EH_k}{6L_e}-\frac{GL_e}{4H_k} & \frac{1}{2}G & -\frac{EH_k}{3L_e}+\frac{GL_e}{4H_k} & -\frac{EH_k}{6L_e}-\frac{GL_e}{4H_k} \\ \frac{1}{2}G & \frac{EH_k}{6L_e}-\frac{GL_e}{4H_k} & \frac{EH_k}{3L_e}+\frac{GL_e}{4H_k} & -\frac{1}{2}G & -\frac{EH_k}{6L_e}+\frac{GL_e}{4H_k} & -\frac{EH_k}{3L_e}+\frac{GL_e}{4H_k} \\ -\frac{GH_k}{L_e} & \frac{1}{2}G & -\frac{1}{2}G & \frac{GH_k}{L_e} & \frac{1}{2}G & -\frac{1}{2}G \\ -\frac{1}{2}G & -\frac{EH_k}{3L_e}+\frac{GL_e}{4H_k} & -\frac{EH_k}{6L_e}+\frac{GL_e}{4H_k} & \frac{1}{2}G & \frac{EH_k}{3L_e}+\frac{GL_e}{4H_k} & \frac{EH_k}{6L_e}-\frac{GL_e}{4H_k} \\ \frac{1}{2}G & -\frac{EH_k}{6L_e}-\frac{GL_e}{4H_k} & -\frac{EH_k}{3L_e}+\frac{GL_e}{4H_k} & -\frac{1}{2}G & \frac{EH_k}{6L_e}-\frac{GL_e}{4H_k} & \frac{EH_k}{3L_e}+\frac{GL_e}{4H_k} \end{bmatrix} \tag{4.20}$$

where G and E represent the shear modulus and *Young*'s modulus for the material of the generic layer k respectively.

From (4.19), representing the consistent mass matrix of a generic k layer, the diagonal form of the mass matrix can be derived. The lumped mass matrix or diagonal mass matrix is, therefore, defined as:

$$[\mathbf{M}]_k = \frac{\rho \cdot b}{4} L_e H_k \begin{bmatrix} 2 & & & \cdots & & 0 \\ & 1 & & & & \\ & & 1 & & & \vdots \\ \vdots & & & 2 & & \\ & & & & 1 & \\ 0 & & \cdots & & & 1 \end{bmatrix} \tag{4.21}$$

where ρ represents the layer material density and b, L_e and H_k stand for the width, the length of the finite element and the layer thickness, respectively. The lumped mass matrix is herein used due to the inherent reduced computational cost.

4.6.2 MATLAB implementation

MATLAB® programming environment was used in this study for the numerical analyses (in Chapter 8 the commercial software was additionally used for assessment purposes). The finite element implementation, optimisation tasks and results analysis and presentation were performed in this powerful numerical tool.

The detailed flowcharts of the routines used are presented in Appendix "A" and the algorithms created for the numerical implementation of the proposed finite element model, in Appendix "B". The MATLAB code "ebeam.m" is the routine that computes the finite element stiffness and mass matrices. To be able to obtain the stiffness and mass global matrices, it is necessary to use a code that assembles the individual finite element matrices. The MATLAB code used for that purpose is called "assembly.m". The routine "boundaryC.m" defines the boundary conditions to be applied to the beam.

4.7 Summary

This chapter addresses the application of the finite element method (FEM) in the modelling of VEM treatments. It is, by far, the most widely used method due to its enormous applicability in structural engineering. This method is capable of simulating the behaviour of structures treated with VEM fairly efficiently. However, the manner in which these layered structures are spatially discretised, demands particular attention. Especially in the case of constrained treatments, where the shear strain that is generated in the viscoelastic core is relatively high and localised, special discretisation methods are required. They include combined models and layerwise models, the latter being the model used in this work.

Layerwise finite element models are usually based on the description of the displacement field. This study, however, applies a different spatial discretisation method in which the layerwise beam finite element is based on a combined formulation of stress and displacement fields. This spatial model is applied in the analysis of the damping layer effect performed in Chapters 6, 7 and 8.

After applying the FEM to calculate the mass and stiffness matrices that represent the structure spatial model, it is necessary to develop an analysis process to determine the treatment effects on the structure dynamic behaviour. Analysis processes have been developed that are, nonetheless, computationally costly as they involve calculations in the complex domain. Less computationally expensive is the MSE method used in the study. The finite element formulation is then presented and completes this chapter.

Chapter 5

Optimisation with Genetic Algorithms

This chapter briefly describes the concept of optimisation. An optimisation tool, the Genetic Algorithm is analysed in detail and a parametric study is included.

One of the main research goals of this dissertation is to find an optimised viscoelastic layer configuration whose shape and dimensions vary across the length of a beam while achieving a better damping efficiency than a layer of uniform thickness.

There are various types of optimisation procedures available, each having advantages and disadvantages. However, random search optimisation methods, such as, Genetic Algorithms seem to be the most suitable to achieve the proposed goal.

In order to confirm the results obtained with Genetic Algorithms, another method was also selected for that effect, the method of Topology optimisation.

5.1 Optimisation as a tool for structural efficiency

In order to understand how a system works and to study the performance of a design and how it can be influenced, models need to be developed. To model a design, one has to define it and assign values to each quantity whose values need to satisfy mathematical relations. The model description contains variables, parameters and constants defined as follows:

Variables – They specify different states of the design and assume different values.
Parameters – These are quantities that are given one specific value.
Constants – These are typically natural fixed quantities that the design cannot influence.

To be able to determine how these quantities relate to each other so that the design function performs well, an analysis needs to be conducted. Stress, thermal and vibration analysis are examples of the various analyses that may be done. The modification of the design can generate various alternatives that, according to a criterion, are then evaluated and ranked so that the designer can choose one of the alternatives. The "best" alternative can take many forms and it depends on the designer's point of view. A criterion may also change with time, that is, what used to be an important issue in the past, may no longer be considered as such.

Optimisation is defined as a procedure that will render a design or a structure as functional or as efficient as possible. When the design model is subjected to an evaluation, the best design is called the optimal design and the criterion used is the objective of the model. The reason for the objective function to sometimes be called "cost function" is that the minimum cost often characterises the best design. Optimisation studies require several iterations until an improvement has been obtained and may, therefore, be computationally expensive.

The optimisation of a model involves various steps [70]:

1. The selection of a set of variables to describe the various alternatives.
2. The selection of a criterion (objective) that is expressed in terms of the variables

and which is to be minimised or maximised.

3. The constraints that are expressed in terms of the variables that must be satisfied.
4. The determination of the variable values that minimise or maximise the cost function.

When problems are multi-criteria, the objective may be competing in nature, in which case some trade-offs are required. In multi-criteria problems, if no point exists that reduces one criterion without increasing the other/others, a point in such design space is called a Pareto optimal point [70].

The design objectives may be met by different configurations and in the search for the optimum configuration, they need to be compared. This can be obtained by the discretisation of the design space into finite elements and there are several methods that can then be used. These include the homogenisation method, artificial intelligence methods or Genetic Algorithms, the latter presenting a very important approach in recent times.

The feasible domain of the model refers to the variable values that satisfy the constraints; the establishment of boundaries (upper and lower) is of utmost importance. Functions may have more than one optimum value in which case these values need to be viewed relatively to the points in the vicinity. There may be various local minimums, such as points 2, 5 and 7 in Figure 5.1; the smallest value of these local minima is the global minimum. Similarly, the global maximum will be the maximum value of the local maxima (points 1, 3 and 6). Point 4 is a point of horizontal inflection (all points refer to Figure 5.1).

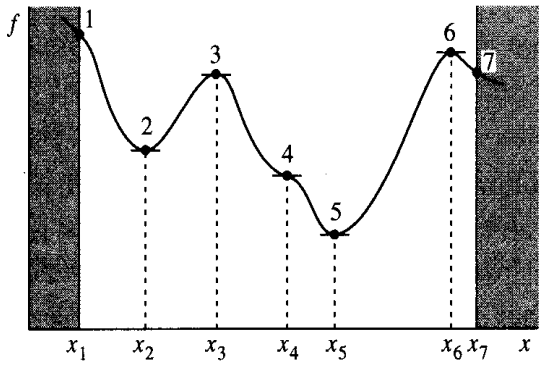

Figure 5.1: Local and global optima [70]

The identification of all the local optima and the determination of the global optimum for different ranges of parameters are desirable if a thorough design optimisation is to be carried out. Different parameter values may alter the design space drastically and shift the location of the global and local solutions. An optimum may be shifted from the interior to the boundary and vice-versa, or a global solution may be shifted from a local minimum to another if parameter values are changed. A *parametric study* involves the solution of the problem, often with different sets of parameter values, so that optimal solutions may be found for a range of parameters. However, from the mathematical point of view, such optimisation may turn out to be a difficult task or expensive from a computational point of view.

5.2 Optimisation procedures

According to Goldberg [71], conventional optimisation search methods are divided into three groups: the calculus-based algorithms that make use of gradients, the enumerative schemes and random methods. The algorithms based on gradients use the derivatives of the objective function and of the constraints with respect to the problem variables. They assume the continuity of the search space and in real world problems that is seldom the case. Furthermore, in multidimensional problems, the relations between variables are complex and it is, thus, not viable and practical to use analytical derivatives as the computational effort becomes excessive. These calculus-based methods, generally lack robustness over the large spectrum of optimisation functions.

Concerning the enumerative schemes, the algorithm looks at the objective function values at every point in space, one at a time within a finite search space or a discritised infinite search space. They are simple but lack efficiency and are also computationally costly. The disadvantages of the calculus-based and enumerative methods prompted the development and the popularity expansion of the random search algorithms, also known as evolutionary algorithms. Furthermore, enumerative schemes do not use any knowledge from previous results, which randomised techniques do. The latter use the knowledge obtained from previous results to direct the search through the parameter space and this way, become

comparatively more efficient. The Genetic Algorithms fall under this category of optimisation methods and are one of the most popular.

5.3 Topology optimisation

Before the 1990's structural Topology optimisation consisted in using size and shape optimisation to improve designs with a predetermined topology. The initial layout of the design relied upon the intuition and experience of the designer and the subsequent design worked on a subset of possible shapes with fixed topologic properties.

In 1988, Bendsϕe and Kikuchi [72] introduced the homogenisation method and did some pioneering work on the theory on which the methodology of the modern Topology optimisation is based. Various commercial software that use this type of optimisation with application to day-to-day practical problems have since been released on the market. Methods, such as, Optimality Criteria (OC), Sequential Linear Programming (SLP), and the Method of Moving Asymptotes (MMA) are some solution methods. According to Papalambros [70], the Optimality Criteria was used to determine the optimal topology of the damping material on plates. The versatile MMA is an algorithm suited for large scale Topology optimisation problems that was developed by Svanberg in 1987 [73] and improved in 1999 by developing a more convergent version [74].

Nowadays, Topology optimisation is used at the concept level of the design process as it allows designers to generate the best option that meets the design requirements at an initial stage. Knowing the design targets right from the start makes it easy to apply the computational method. Although design changes are part of all the phases of the design, after a certain stage they become rather costly and should, therefore, be avoided.

The layout of the material within a determined design space for a set of loads and boundary conditions is optimised through a mathematical approach. The design space is the allowable volume within which the design can exist. This space contemplates factors, such as, human and tool accessibility, packaging and assembly requirements. Topology optimisation allows a substantial design improvement by altering the arrangement of cavity

distribution inside the structure. The concept design generated by Topology optimisation is then fine-tuned for performance of a chosen topology with shape optimisation.

However, one of the disadvantages of Topology optimisation is the manufacturing of the optimal proposal as it may either be too expensive or not feasible to manufacture. Some solutions have been developed by imposing performance constraints or extrusion constraints.

5.4 Genetic Algorithms as an optimisation tool

Living organisms consist of cells and within cells the DNA is organised into structures called chromosomes. A chromosome is made up of genes which are responsible for a trait of an individual. The gene's locus will determine which trait it will influence and the gene's allele how it will be influenced. During sexual reproduction, genes are exchanged between each pair of chromosomes by recombination (or crossover) and the offspring may be subjected to mutation. The ability of an organism to survive and to reproduce depends on the organism fitness. It was based on natural evolution and survival of the fittest that the Genetic Algorithm was developed.

Genetic Algorithms have become increasingly important in solving real-world optimisation problems and since its development by Holland [75], researchers and practitioners have made remarkable additions to the field of genetic algorithm optimisation. According to the principle of survival of the fittest, the genetic algorithm allows populations of candidate solutions to evolve towards improved solutions.

Genetic Algorithms have been applied to numerous problems and in many practical applications they are able to find good solutions in a reasonable amount of time. Economics, Immune Systems, Ecology, Population Genetics and Social Systems are some examples of GA applications [76]. They have, consequently, been the subject of numerous technical papers and research by many scholars investigating the role of the parameters in the success of the GA performance.

5.4.1 The development of GAs

In the sixties and seventies, various evolution strategies and evolutionary programming techniques were developed with the view that evolution could be used as an optimisation tool for engineering problems. During the same period, the natural process of evolution of species inspired John Holland [75], his colleagues and students to invent the Genetic Algorithm. Holland's initial motivation was to study the mechanisms of adaptation that can be found in nature and to include those mechanisms in computer-simulated systems.

The second major landmark came in 1989 when Goldberg [71] published a book called Genetic Algorithms in Search, Optimization and Machine Learning devoted to search and optimisation. He presented the genetic algorithm as a problem solving tool by applying GAs in machine learning systems. Since then, the interest in this type of algorithm has continued to rise and this is revealed not only by the number of publications but also by the number of engineers who use GAs to solve industrial-scale problems.

Whitley and Starkweather [77] studied the reproduction process and developed an approach where the offspring replace the low ranking individuals of the population and not their parents, as in the standard GAs. Their algorithm (GENITOR) also ranks the "genotype" in the current population and assigns a fitness value to it, abandoning the conventional method of fitness values being directly based on the evaluation function. Hesser and Manner [78] investigated the dependence of the mutation probability upon two parameters, the population size and the dimension of the configuration space.

Later in 1996, Smith and Fogarty [79] investigated the use of genetically encoded mutation rates within a steady state genetic algorithm in order to provide a self-adapting mutation mechanism for incremental evolution. Ochoa *et al.* [80] claim that the determination of the optimum mutation rates is dependent on whether recombination is used or not. They suggest that if recombination is not used, the best strategy would be to start with a relatively high mutation rate and decrease it over the course of a single run. If, on the other hand, recombination is used, the optimal strategy is to use both a fixed and low mutation rate, as a high rate actually affects the performance of the GA. Harik and Lobo [81]

explored the development of a robust and simple genetic algorithm with no parameters whatsoever, where the algorithm relieves the user from having to set the parameters.

Eiben *et al.* [82] revised the terminology and surveyed the different forms of control that had been studied by the evolutionary computation community. The success of solving a problem with a genetic algorithm is highly dependent on the proper selection of the crossover and mutation operators. Different operators are suitable for different problems and also for the various stages of the process. So Tzung-Pei *et al.* [83] proposed a dynamic GA where the crossover and mutation rates are automatically and dynamically adjusted according to the fitness values of the respective offspring that it produces. The ratios of suitable operators are thus increased, whereas the ratios of unsuitable operators are decreased.

In 2002, Dirk Thierens [84] acknowledges the merit of adaptive mutation rates that vary along the runs but which end up not being used by novice users due to their complexity; with this in mind he proposed two simple adaptive mutation rate schemes. Rechenberg [85] developed the 1/5 success rule and Affenzeller [86] developed an advanced selection method for the GAs that allow a self-adaptive control of the selection pressure. This selection model is able to detect premature convergence, which is one of the most frequent difficulties when GAs are applied to complex problems. Sadjadi [87] developed scaling methods in 2004 to overcome the difficulty encountered when there are multiple peaks in close proximity. Herrera *et al.* [88] undertook an extensive study examining the synergetic effects among real-parameter crossover operators (GAs based on real number representation) that belong to different categories. They designed a hybrid real-parameter crossover operator that generates two offspring for every pair of parents, each one with a crossover operator that belongs to a different category.

5.4.2 Genetic Algorithm encoding

The chromosomes in biological terms are often encoded as bit strings in Genetic Algorithms and they typically represent a candidate solution to a problem. The genes that make up the chromosomes are features in artificial genetic systems. In binary encoding the

features are equivalent to bits. Bits may be located at different positions in the string in analogy to the locus (its position) of a gene on the chromosome. An allele in a bit string is either a "0" or "1".

0	1	0	0	0	1	1	1	0	1
1	1	0	1	0	0	1	0	0	0
1	1	1	0	1	0	0	0	1	0
0	0	1	0	1	0	1	1	0	0
1	1	1	1	0	1	0	1	0	0
0	0	1	1	0	0	0	1	1	1

Figure 5.2: Binary encoding

For historical reasons, binary encodings are the most common (Figure 5.2) but the alphabet, integers or real numbers can also be used to form the chromosomes. Figure 5.2 represents the binary encoding of six individuals having a bit string length of ten. Although extensively used, the binary coding can become problematic in real life situations. When the problem has several variables, the population size and the individual bit length tend to become unmanageably large, affecting the computational speed and proper convergence.

A phenomenon known as the *Hamming cliff* also presents a problem. As an example, the representation of 127 in binary code is 01111111 whereas the consecutive integer, 128, is represented by 10000000; in other words, the corresponding bits of these two consecutive integers are all different. The *Hamming distance* refers to the number of corresponding bits that differ between two binary strings. When this happens, the GA operators have difficulty in changing so many bits for a small integer change and the genetic algorithm does not perform well. The *Gray coding* attempts to overcome the problem of the Hamming cliff as any two integers always differ by one bit only.

5.4.3 Control parameters

The main control parameters that affect the search behaviour are: the population, the selection method, the type of crossover and mutation and the crossover and mutation rates. The selection of these parameters influences the convergence speed of the optimisation process and if incorrectly chosen will also compromise the success in obtaining global solutions.

Population

In generational GAs, as described by Holland [75] there are always two sets of populations: the current population and the future one. In each generation, the current population is subjected to the different operators thereby constructing a new population, which then becomes the current population for the next generation. Some of the individuals in the new population result from crossover, others from mutation and the rest may be simply copied unchanged from the previous population. In some cases, mutation may be applied to some individuals that are selected randomly from the new population, after crossover.

Concerning the population size, there are advantages and disadvantages in both large and small populations [89]. Large populations are computationally intensive due to the increase in time that is needed to evaluate the function and to apply the operators. However, by diversifying the search directions, the genetic algorithm avoids premature convergence to local optima. On the other hand, if the population size is too small, a strong individual may become dominant and, thereby, restrict the search space making the algorithm converge to a local solution instead of a global optimum. A homogeneous population will not yield new solutions. According to Faulknauer [90], a population of 50 individuals seems to be an adequate size, used by many researchers.

The concept of a chromosome "age" may also be used. This process, defended by Michalewicz [91], is equivalent to the number of generations that the chromosome stays "alive" and it replaces the concept of selection. Since the age of the chromosome depends on the fitness of the individual, the size of the population varies at every stage of this process.

Some researchers have also done experiments with subdivided populations and found that in certain cases, GAs performed better when the population was split into several small subpopulations with each subpopulation sending out migrants at some fixed time intervals [92].

A random construction of the initial population is important since, at that stage, there is no knowledge of the regions in the search domain where the global optima could be searched for. In the case of a random initial construction, it is wise to use a population size that gives a high enough probability for each solution building block to be included [93].

Nevertheless, there is always the danger of the points represented by the initial population being too far from the global optimum, i.e. it can happen that the search space associated with the population does not represent the promising regions of the function to be optimised. This phenomenon is known as sampling error and it cannot be totally avoided [90]. The sampling error can, however, be corrected by allowing a small percentage of the worse individuals to reproduce and survive. If only the best individuals are allowed to survive, all the individuals that do not represent points in the apparent, but false optimum region, are eliminated. The average distance between individuals in a population is referred to as "Diversity".

As previously mentioned, in generational GAs, the whole population is updated in each generation. In a "Steady-state GA", in one generation only a small portion of the population is changed. An extreme Steady-state GA would refer to an algorithm where in one generation only one individual is changed.

Selection methods

The selection operator selects individuals from the population for reproduction by first evaluating the fitness of each individual and then, based on their fitness values, parents are selected to form a mating pool. It is a process where the stronger individuals must have preference for the generation of offspring. This gives rise to a phenomenon called selective pressure, which is influenced by various types of selection methods.

There are different methods of selection of the individuals for the mating pool and they may be classified roughly in two groups: fitness-proportionate and rank-based selection. A common rank-based selection is the "Tournament" selection; in this type of selection, a certain number of individuals are drawn at random from the whole population and the best

individual from this group is selected as a parent for the next generation. The process ends when the number of individuals in the mating pool is equal to the number of individuals in the initial population.

The tournament type of selection ensures that the worst individual is never chosen as parent for the following generation. The outcome is that the average fitness value of the new population is higher than the average fitness value of the previous population. The number of individuals in tournament (tournament size) must also be taken into consideration. A high percentage of individuals (in relation to the total number of individuals), will represent a higher selective pressure.

Another popular method of selection is the "Roulette Wheel" (Figure 5.3). This type of fitness-proportionate selection, used in Holland's original GA [75], is based on the theory that if an individual is twice as fit as another one, it should reproduce twice as many times as the other. This is usually implemented by using the roulette wheel strategy that runs as follows: Each individual is assigned a slice of a roulette wheel, the size of the slice being proportional to the individual's fitness, i.e. the higher the fitness value, the larger the slice. The roulette wheel is spun and when it stops, the corresponding individual is selected as a parent for the next generation.

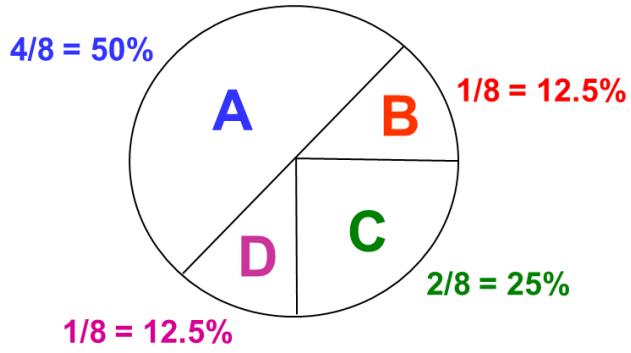

Figure 5.3: Roulette wheel selection method

The roulette wheel selection pressure is weaker than tournament selection pressure [94] as, unlike the latter, there is always the possibility of the worst individuals being selected for the mating pool. Their probability of being chosen as parents for the next generation is lower, but it exists.

The mating pool can also be made up of individuals that are selected randomly. In comparison with tournament and roulette wheel strategies, the Random selection method is the least selective. An individual from a previous generation has the same probability of being chosen for the formation of the next generation as the rest of the individuals.

Elitism is another selection operator which ensures that the individual/ individuals with the highest fitness value is /are carried over from the precedent generation to the next one [95]. This process guarantees that the best individuals are not lost if they are not selected for reproduction or destroyed by crossover or mutation.

Some of the less fit offspring in the population may also be eliminated (according to predefined fitness values) in a process this author calls "Selective Breeding". They are eliminated before the selection of parents for the mating pool takes place. This process ensures that only the better offspring are eligible for selection.

The fitness of an individual often depends on complex patterns of features which the operator must be able to transmit to the offspring. The extent to which, the contribution to fitness of one gene depends on the values of the other genes, is known as epistasis [96]. This concept refers to parameter interaction among genes. High epistasis means that building blocks (a group of genes that give a chromosome a high fitness) cannot form.

Types of crossover

The crossover operator is the most used operator in the algorithm as most of the individuals in the new population are generated by this operator. The idea is to recombine parts of different individuals in the hope that the best traits may be transmitted over the generations and produce better offspring. The crossover operator exchanges some genes from two chosen individuals to generate offspring that consequently inherit some traits from each parent.

The simplest form of crossover is that of single-point crossover where a position in the string is chosen at random and two individuals are thus divided by this cutting point. Two

offspring are generated by combining the first part of one parent and the second part of the other parent. This type of crossover is illustrated in Figure 5.4.

Figure 5.4: Single-point crossover

Many other types of crossover may be used, such as, multipoint, uniform, arithmetic, intermediate, scattered, heuristic, shuffle and others. In the shuffle crossover [97], a single point is selected, but before the bits are exchanged, they are randomly shuffled in both parents. In this way the positional bias is removed as the bits are randomly reassigned each time crossover is performed.

Types of mutation

The mutation operator can also present different configurations. The most widely used is the "Bit-flip" mutation (Figure 5.5); other types include the "One-zero exchange" mutation, "Inversion" mutation and "Swapping" mutation [83]. Bit-flip mutation (also known as One-point mutation) involves the flipping of a bit in a string from 1 to 0 and vice-versa. The point of mutation is chosen at random (e.g. individual 011111 becomes 011011).

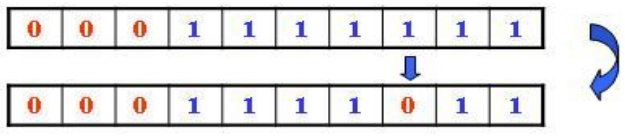

Figure 5.5: Additional example of bit-flip mutation

Figure 5.6 shows one-zero exchange mutation where in a string all the bit values "0" change to "1" and "1" change to "0" (e.g. individual 001100 becomes 110011).

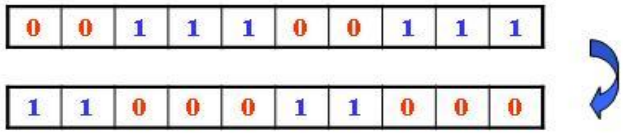

Figure 5.6: Additional example of one-zero exchange mutation

Inversion mutation (Figure 5.7) inverts the bit order in an interval of the string (e.g. individual 12|345|6 becomes 12|543|6).

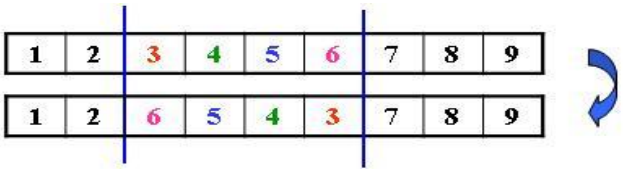

Figure 5.7: Additional example of inversion mutation

Finally, shown in Figure 5.8, the swapping mutation arbitrarily exchanges any two bits in a single string (e.g. individual 123456 becomes 623451 by exchanging the first and last bits).

Figure 5.8: Additional example of swapping mutation

Crossover and mutation rates

The crossover rate determines the percentage of individuals that are recombined i.e. it determines the probability that an individual has of being recombined with another individual. Identically, the mutation rate determines the probability that a bit or individual has (depending on the type of mutation) of being mutated. Generally, the elite solutions propagate unchanged; they are not recombined or mutated.

Some settings on the crossover rate and mutation rate (also known as crossover probability and mutation probability) have been advanced in the past but there are no conclusive results on what is best. It depends on the problem being solved, on the encoding used and other parameters.

The most encouraging strategy is to have rates that evolve over the course of a single run, i.e. the design of dynamic algorithms that automatically chooses the appropriate probability of crossover and mutation and adjusts their rates according to the average progress values [76, 83].

5.4.4 Genetic Algorithm implementation

The optimisation algorithm can be easily implemented in any programming language; MATLAB® was the language used in this work.

The first step consists in choosing the way the candidate solutions are to be encoded. This is a very important aspect for the success of a genetic algorithm. An initial random population is then generated, bearing in mind that the diversity should be neither too high nor too low in order to enhance the performance of the GA.

The fitness value of each individual in the population must also be calculated so that it reflects the way an individual is closer to the optimum, in comparison with the others. Based on the individuals' fitness, parents are selected from the current population to form a mating pool using any of the selection methods previously mentioned. Some individuals with the best fitness values may be chosen as elite individuals. The individuals in the mating pool are then crossed-over and mutated to create offspring and the existing population is replaced by its children.

The generational process is repeated until a stopping criterion has been reached; the most common are:

- The number of generations has reached the specified maximum number of generations.
- A solution has been found that satisfies the minimum criteria.
- Successive generations do not produce better results in terms of the fitness of the best solutions.
- Computation time has been reached.
- Any combinations of the above mentioned criteria [98].

The genetic algorithm flow chart is illustrated in Figure 5.9.

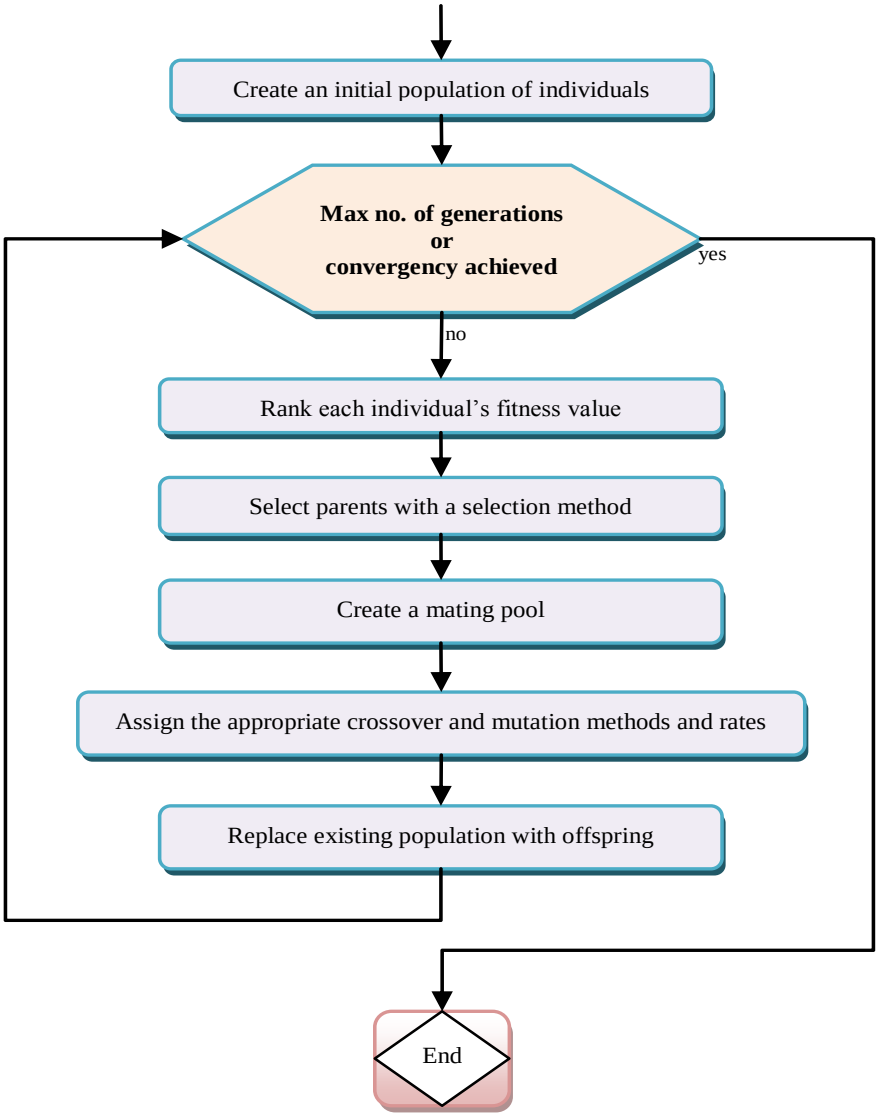

Figure 5.9: Genetic Algorithm flow chart

5.5 Parametric study of GAs

Initially and according to Holland's Adaptation in Natural and Artificial Systems [75], crossover was viewed as the main parameter for the variation and innovation in GAs. Later, according to Mitchell [76], the power of crossover versus the power of mutation was

compared in various studies; also according to Spears [99], crossover was a more robust constructor of new schemas, whereas Muhlenbein [100] argued that the power of mutation had been underestimated. Although crossover is a very powerful way of exploiting the search space, it has a disadvantage of not being able to produce new alleles. It can also happen that during the genetic search some important traits are lost in the process and this operator is unable to recover them. That is where the mutation operator comes in; it has the ability of, not only reintroducing the lost alleles into the mating pool, but also of introducing entirely new randomly generated elements into the gene pool. The mutation operator chooses at random one or more bits from the individual and alters its attributes. The purpose of this process is to reduce the probability of the search ending in a local optimum.

However, what has since been advanced by researchers is that, what is important is not the choice between crossover and mutation but rather a balance among crossover, mutation and selection (the exploitation/exploration balance). When selective pressure is increased, the search focuses on the individuals with the highest fitness value and due to the higher 'exploitation' some diversity is lost. On the other hand, by decreasing the selective pressure the 'exploration' is increased because there are more schemata (bit chromosome patterns) involved in the search and the diversity increases. In order to help the algorithm stay out of local minima, new regions of a search space have to be randomly explored, whereas information from visited points determines which points might be beneficial to be exploited next [101].

5.5.1 The balance between selective pressure and population diversity

The purpose of selection is to give preference to the fitter individuals to be chosen as parents in the hope that their offspring will have an even better fitness. However, if the selection is too strong, the highly fit individuals will take over the population and the population diversity that is needed for further progress, decreases. On the contrary, if the selection is too weak, the slow evolution can compromise the convergence success. On the other hand, the population diversity is associated with the distribution of the population in the search space. The population size and the crossover and mutation rates are the main

parameters that have an effective impact on the population diversity; the higher these rates, the higher the diversity.

The balance needed between the two opposing factors, selective pressure and population diversity, is crucial for a successful search. In order to achieve this balance, one has to take into account the relative weight of the different control parameters. If the diversity of the population is high, a highly selective process must be chosen in order to achieve the correct balance that will lead to a successful global optimisation search. On the other hand, lower diversity requires a less selective method.

In general, as the exploitation increases due to a selective pressure increase, the diversity decreases, whereas an exploration increase caused by a selective pressure decrease will increase the diversity. In order to maximise the success of the optimisation procedure, an exploitation/exploration balance must be reached. The understanding of the balance between the various operators (selection, crossover and mutation) and their effect on the algorithm efficiency is very important and some examples on how the balance may be achieved are presented; this involved a parametric study involving two functions and different types of selection and mutation.

Parameters used

In order to validate the relationship between selective pressure and the population diversity, tests were undertaken based on two selected functions and with the following common parameters: the size of the population used throughout the tests is 50 and the string length is 71 bits. One-point crossover and crossover ratio of 0.8 were also used. Elitism is present in all tests and unless specified, the method of selection is tournament and the tournament size is 2. Unless otherwise stated, the mutation type used was the one-zero exchange. Graph lines represent, on average, 7 runs. The scale of all graph ordinates is logarithmic so that minimum function values can be more adequately visualised.

5.5.2 Selected functions

The selected functions are shown in Figure 5.10 and Figure 5.11 and they are defined by the following equations:

$$f = x^2 + y^2 \tag{5.1}$$

$$f = \frac{1 - \sin(r)}{r}; r = \sqrt{x^2 + y^2} \tag{5.2}$$

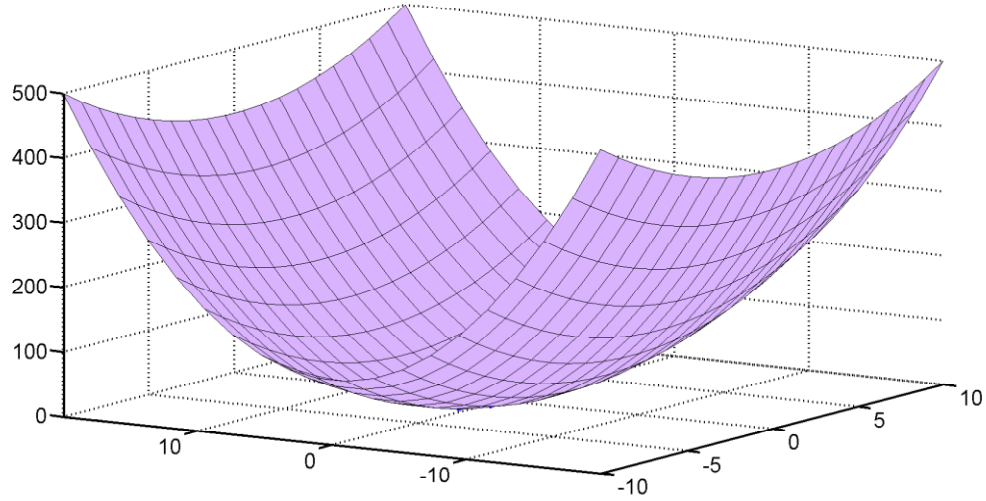

Figure 5.10: Graphical representation of Function (5.1)

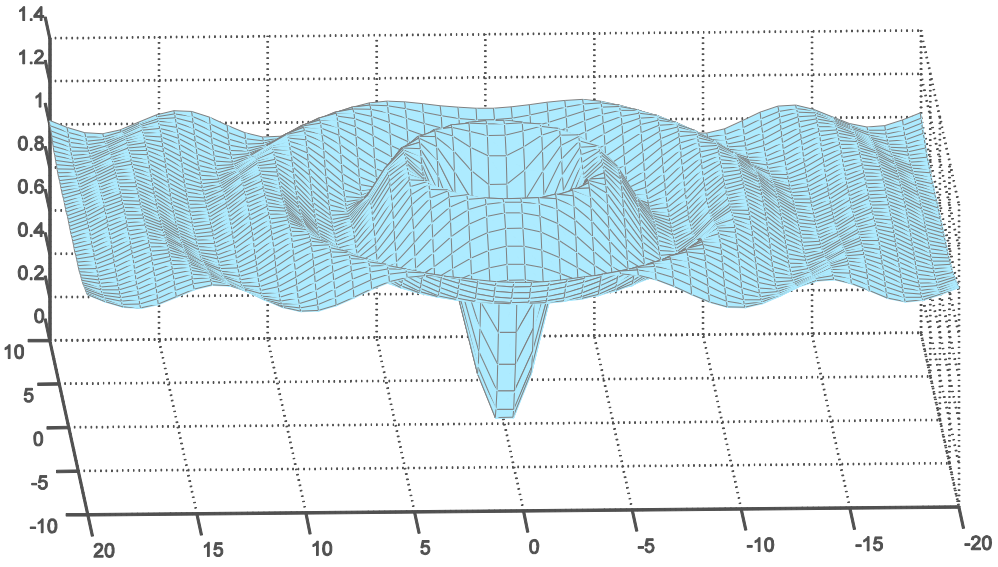

Figure 5.11: Graphical representation of Function (5.2)

5.5.3 Balance indicator

An indicator of the balance between the population diversity and the selective pressure can be shown by plotting the minimum and the mean function values (considering the objective to be the minimisation of a function).

One of the best ways to monitor the progress of an algorithm is convergence, i.e. when the mean and minimum fitness scores are close [87], as shown in Figure 5.12. If the mean values approach the minimum function values, an adequate diversity has been produced thereby preventing convergence to a local minimum. Conversely, Figure 5.13 shows a diversity imbalance causing premature stagnation and failure to find the minimum global values.

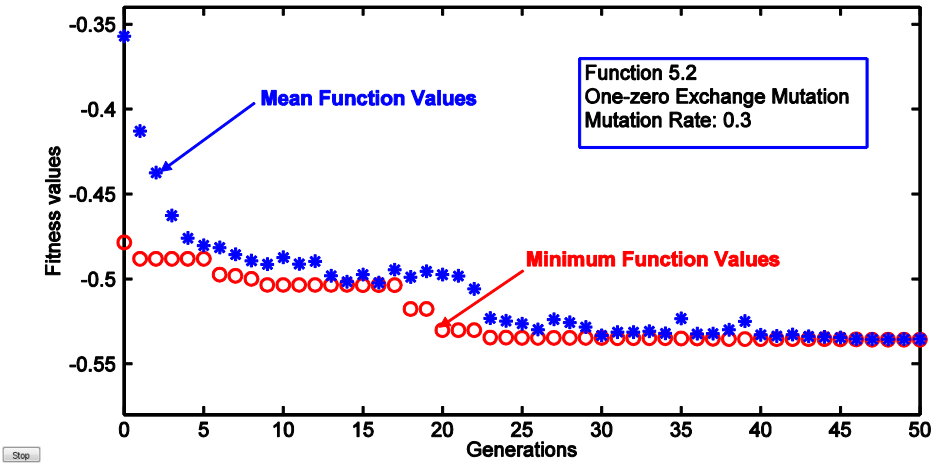

Figure 5.12: Correct balance between diversity and selection

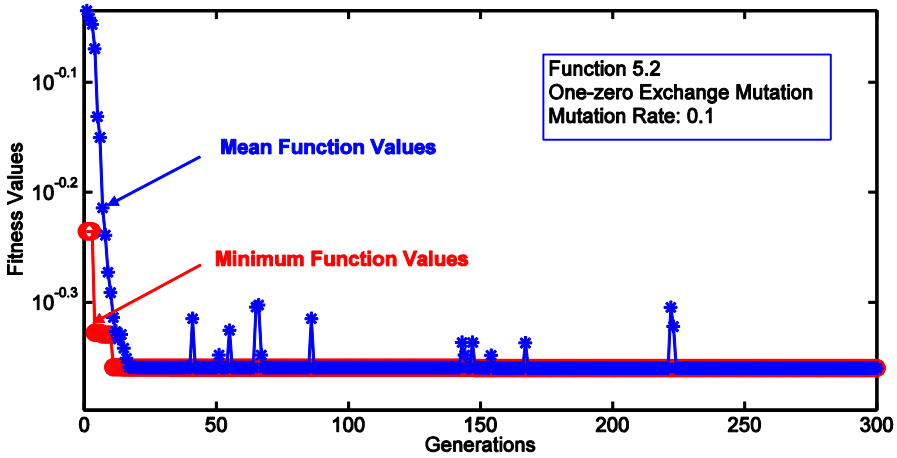

Figure 5.13: Incorrect balance between diversity and selection

5.5.4 The most suitable mutation rate for the selected functions

At first, in order to find the best mutation rate for the set of parameters previously mentioned, the selective pressure was kept constant (by applying elitism and tournament to all tests) and the population diversity was varied by using different mutation rates. Figure 5.14, Figure 5.15 and Figure 5.16 show the algorithm performance for different mutation rates as they search for a global minimum.

Figure 5.14 shows that, in the case of (5.1), the mutation rate that is capable of obtaining the lowest minimum function value is a mutation rate of 0.4 and that higher rates (0.5, 0.6 & 0.7) or lower rates (0.1, 0.2 & 0.3) perform worse than the former rate. In other words, for this set of parameters, the balance between the selective pressure and the population diversity is best accomplished when a mutation rate of 0.4 is used.

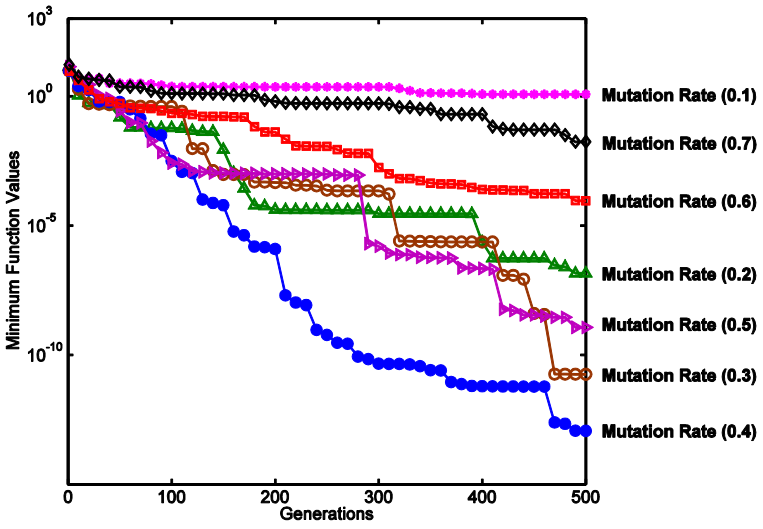

Figure 5.14: Convergence graph of mutation rates for Function (5.1)

In the case of (5.2) the best mutation rate is 0.3, as shown in Figure 5.15. Figure 5.16 provides another perspective of the algorithm behaviour, showing a plot of the minimum function values obtained for the various mutation rates.

We can, therefore, conclude that lower mutation rates (in relation to the best rate) provide a population diversity that is insufficient to cope with a very selective process while higher mutation rates diversify excessively. Similar experiments were done with other types of

mutation and the results obtained were consistent with these observations, providing decisive conclusions on this issue.

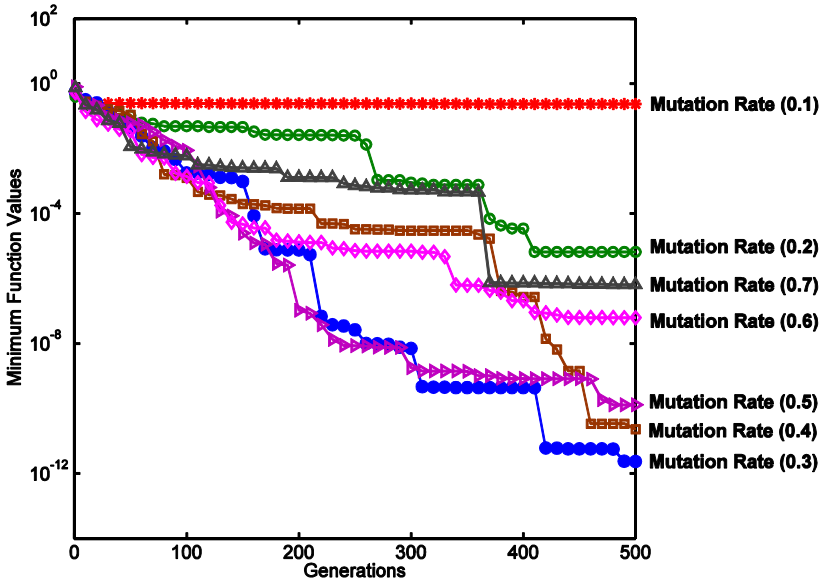

Figure 5.15: Convergence graph of mutation rates for Function (5.2)

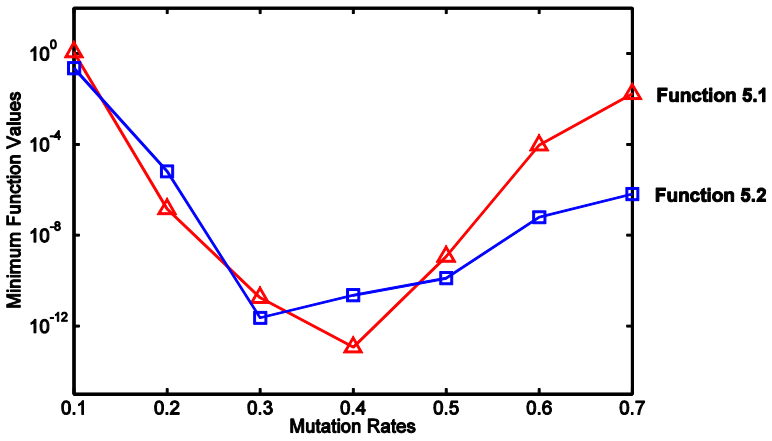

Figure 5.16: Minimum values obtained with different mutation rates

5.5.5 Selective pressure increase

The behaviour of the algorithm when subjected to a higher selective pressure was then analysed. One way of incrementing the selection pressure may be by means of selective breeding, i.e. by the elimination of the less fit offspring from the population before the selection processes (tournament and elitism) choose the parents. Another way may be the increase of the tournament size, i.e. the number of individuals in tournament. The influence

of selective breeding in the selective pressure is shown in Figure 5.17 and Figure 5.18, whereas Figure 5.19 and Figure 5.20 show how the tournament size affects the algorithm.

Function (5.1)

Figures 5.14 and 5.16 show that the best mutation rate for (5.1) is 0.4. Figure 5.17 compares the function values obtained previously with the values that resulted from the application of selective breeding. The figure shows that the minimum function values obtained for the mutation rates 0.1, 0.2, 0.3, 0.4, 0.7 and 0.8 did not improve with the introduction of selective breeding. The lower mutation rates (0.1, 0.2, 0.3 and 0.4) were unable to keep up with a more selective process, whereas 0.7 and 0.8 seemed disproportionate. The mutation rate 0.4 was no longer the best mutation rate, but 0.5, the latter showing a slight improvement as far as the minimum value is concerned.

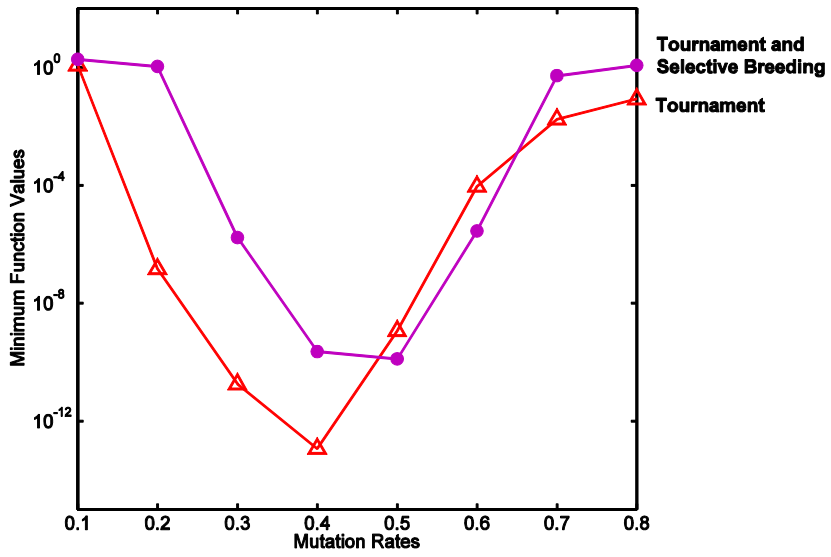

Figure 5.17: Effect of introduction of selective breeding

A lower global minimum was also obtained in the case of 0.6 mutation rate. In both of these two cases, it was due to the fact that the higher selective pressure (brought about by the selective breeding) was compensated by the higher population diversity (due to higher mutation rates) and the balance was recuperated. This is evidenced in the graph (Figure 5.17) by the shifting of the curve to the right.

The convergence graphs of two mutation rates, 0.4 and 0.6, before and after the increase of the selective pressure (due to selective breeding), are shown in Figure 5.18. In the case of the best rate (0.4), the selection pressure increase did not yield better results. The same did not occur in the case of the higher mutation (0.6) because the higher diversity that it produced was balanced by the higher selection.

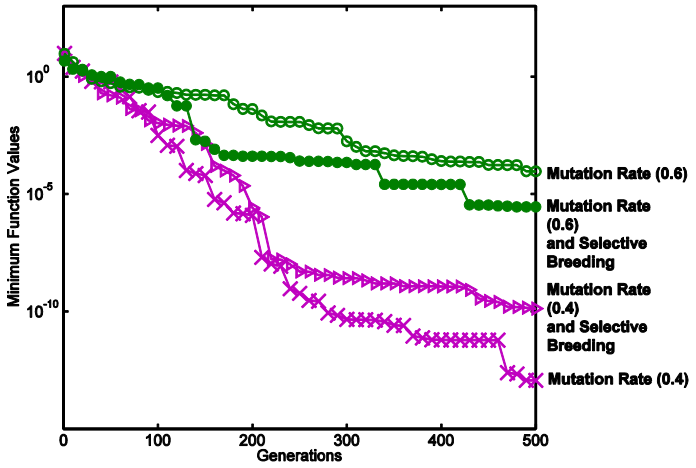

Figure 5.18: Effect of selective breeding on two mutation rates

The algorithm was also tested with other types of mutation. The value of the best mutation rate differed according to the type of mutation. Less mutating types, for example the bit-flip type requires lower mutation rates (0.05 – see Figure 5.29). However, when selective breeding was applied to higher mutation rates, similar conclusive results were obtained as in the case of one-zero exchange mutation.

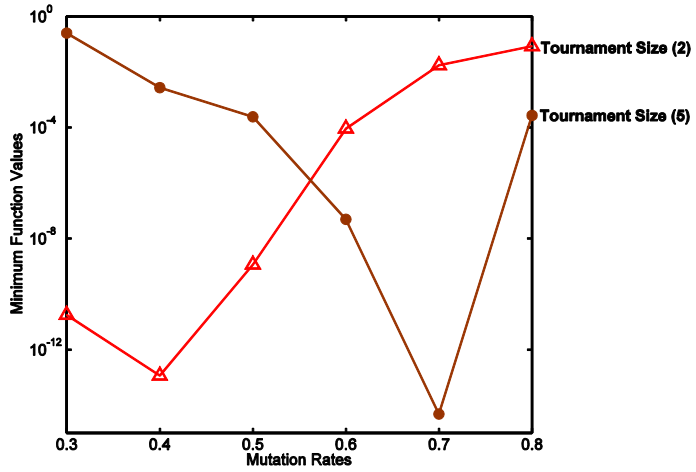

Figure 5.19: Effect of tournament size

The increase in the tournament size from two to five individuals was observed and the search for a global minimum shown in Figure 5.19. This rise in the number of individuals in tournament represents an increase of the selection pressure [102] producing an improvement in relation to the minimum values only in the case of higher mutation rates (0.6, 0.7 and 0.8). Again, higher mutation rates were necessary to keep up with more selection.

Figure 5.20 shows the convergence trend relatively to the effect that the increase in tournament size had on two different rates. It may be seen that in the case of the best mutation rate (0.4), that it produced a premature stagnation; however, the inverse happened to a higher mutation rate (0.7), where an adequate balance between selection pressure and diversity seems to have been obtained, as the algorithm was able to find a global minimum.

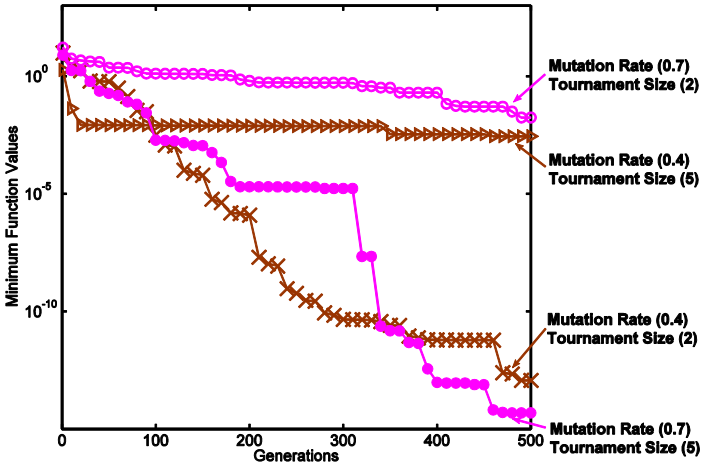

Figure 5.20: Effect of tournament size on two mutation rates

Function (5.2)

It may be observed from Figures 5.15 and 5.16 that the best mutation rate for (5.2) is 0.3. a similar study to the one carried out for (5.1) was also performed on (5.2). Figure 5.21 shows a plot of the minimum function values obtained comparing the values shown in Figure 5.16, and the effect that the increase in the selection pressure produced by the introduction of selective breeding.

According to these results, the selective breeding produced worse results for the mutation rates 0.1, 0.2, 0.3, 0.6, and 0.7, whereas the opposite happened with mutation rates 0.4 and 0.5. The improvement of the latter rates is due to a more adequate balance between diversity and selection, and the graphical representation clearly shows a shift of balance towards slightly higher mutation rates (0.4 and 0.5).

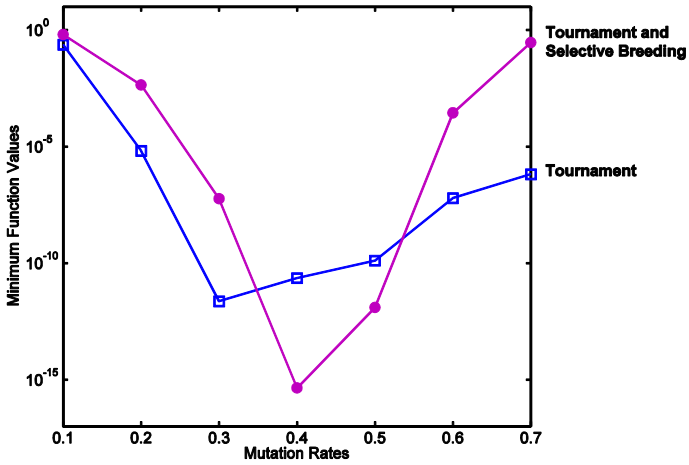

Figure 5.21: Effect of introduction of selective breeding

The convergence graphs of two mutation rates before and after the introduction of selective breeding are shown in Figure 5.22, where it can be seen that improved results only occurred in the case of the higher rate (0.4). In analogy to (5.1) (see Figure 5.19), Figure 5.23 also shows a shift of balance towards higher mutation rates due to an increase in the tournament size.

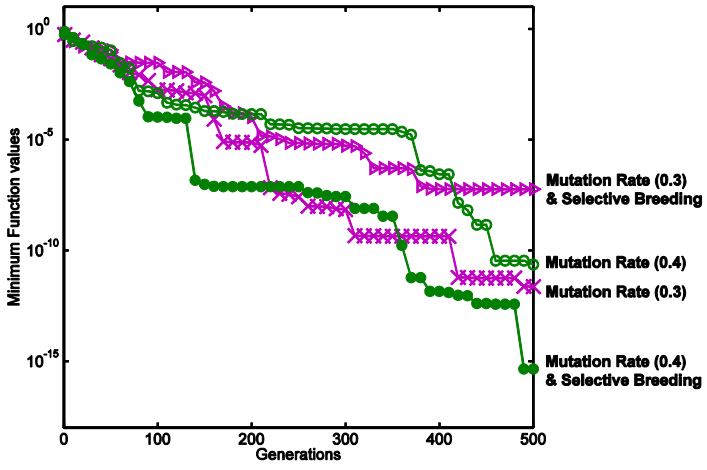

Figure 5.22: Effect of selective breeding on two mutation rates

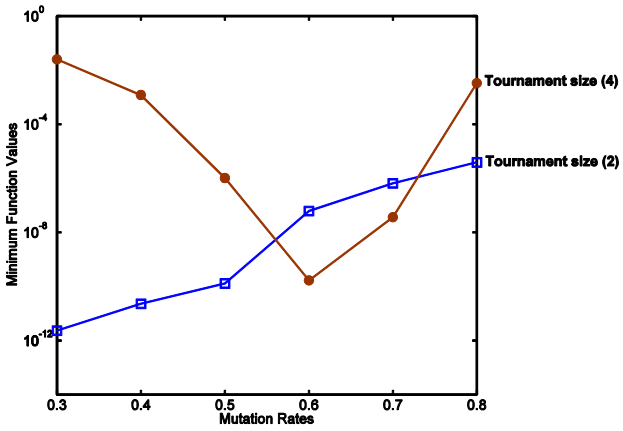

Figure 5.23: Effect of tournament size

5.5.6 Selective pressure decrease

In order to find out how the GA behaves when the pressure on the selection is decreased and its effect on the best mutation rates (0.4 in (5.1) and 0.3 in (5.2)), another study was done. This reduction in the selective pressure may be achieved by selecting the parents for mating by means of the roulette wheel process. As previously mentioned, this is a less selective process [94] compared to the tournament selection used in the previous tests (elitism is still being used).

Function (5.1)

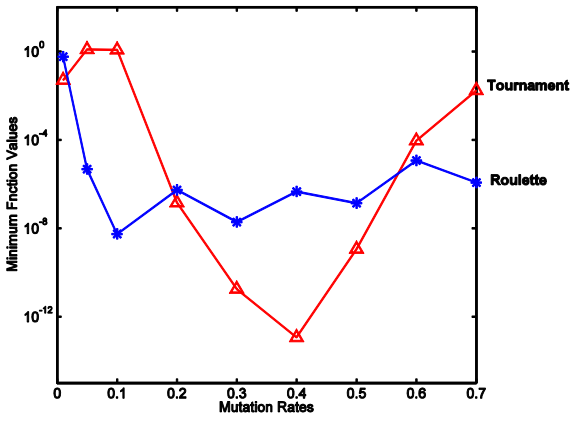

Figure 5.24: Effect produced by the roulette wheel

Figure 5.24 compares the minimum function values obtained with tournament selection (see Figure 5.16) and roulette selection. It shows that the performance of the best mutation

rate (0.4) does not improve with less selection and the same can be said for the rates close to it. However, if the roulette wheel is applied to low mutation rates (0.1), the opposite happens, because the balance between selective pressure and population diversity is again obtained. That observation can also be seen in Figure 5.25.

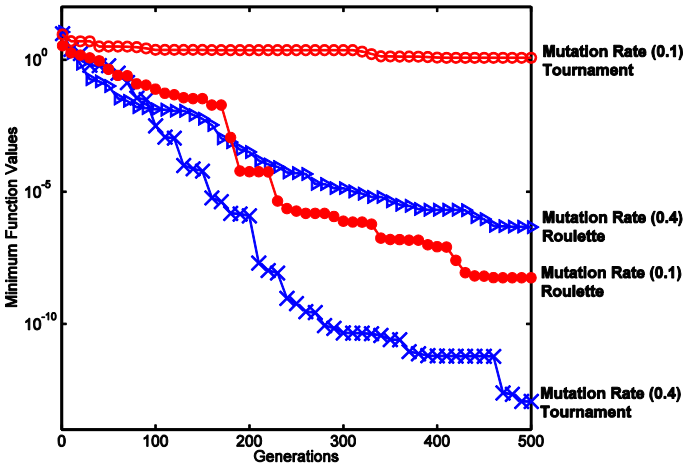

Figure 5.25: Effect of the roulette wheel on two mutation rates

Function (5.2)

When the roulette wheel was applied to the best mutation rate (0.3), the results worsened (Figure 5.26). On the contrary, the roulette wheel produced considerable improvement in the search for a global minimum when applied to a lower mutation rate (0.1) as shown in and Figure 5.27.

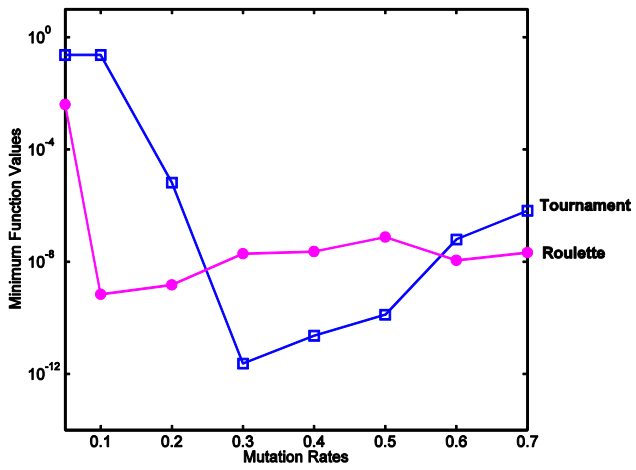

Figure 5.26: Effect produced by the roulette wheel

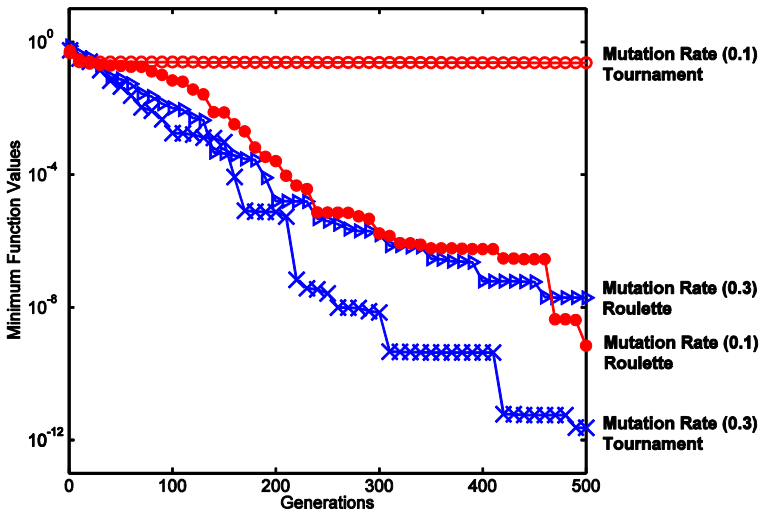

Figure 5.27: Effect of the roulette wheel on two mutation rates

The same type of analysis was done with other types of mutation, namely the bit-flip and inversion. A similar procedure was applied in that the mutation rate that performed the best in tournament was first found; the behaviour of this rate and other rates were then analysed when subjected to higher or lower selective pressures. In both types of mutation, results showed a similar trend as the ones obtained for one-zero mutation, i.e. higher selective pressures demanded higher mutation rates, whereas lower selective pressures required lower mutation rates in order to achieve an adequate balance.

5.5.7 Analysis of tournament versus roulette

In the vast majority of the literature available on the subject of selection methods, the tournament selection is pointed out as being more efficient than roulette wheel. This was analysed by applying the technique of balancing the selective pressure and the population diversity in a comparative study between the two types of selection. Taking into consideration the three different types of mutation examined, the tournament selection proves to be the selection method that is capable of obtaining the lowest global minimum values, thereby corroborating the preference given to tournament selection (Figures 5.28, 5.29 and 5.30).

This was done by running numerous tests using various mutation rates to determine the best mutation rate for tournament and for roulette (using Function (5.2)). Figure 5.28 shows the best mutation rates for each case (the best mutation rate for tournament has already been shown in Figure 5.15). In other words, the two plots shown in Figure 5.28 represent the mutation rates that are capable of obtaining the lowest minimum function values for each of the two selection methods mentioned. Both Figures 5.29 and 5.30 show identical results for the other two types of mutation.

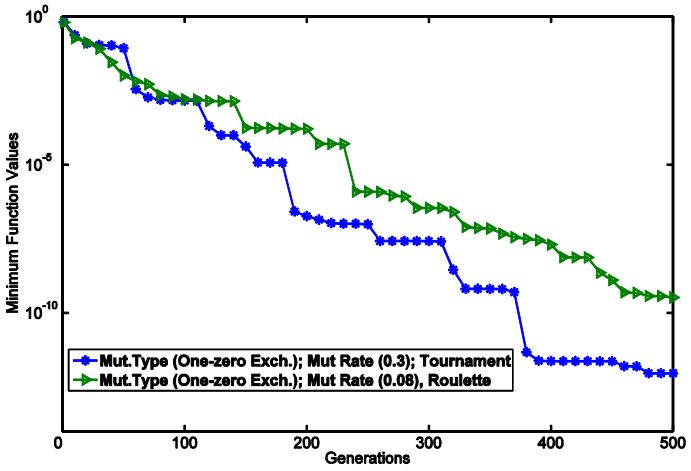

Figure 5.28: Tournament vs. roulette for one-zero exchange mutation

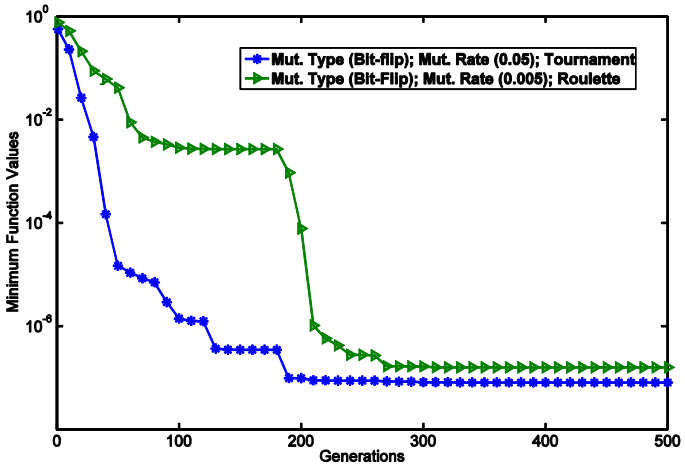

Figure 5.29: Tournament vs. roulette for bit-flip mutation

It is also interesting to note that, as tournament is a higher selective process than the roulette wheel, one would expect the best mutation rate for tournament to be of a higher

value than the best mutation rate for roulette. In fact, that was confirmed in all three types of mutation analysed and shown in Figures 5.28, 5.29 and 5.30.

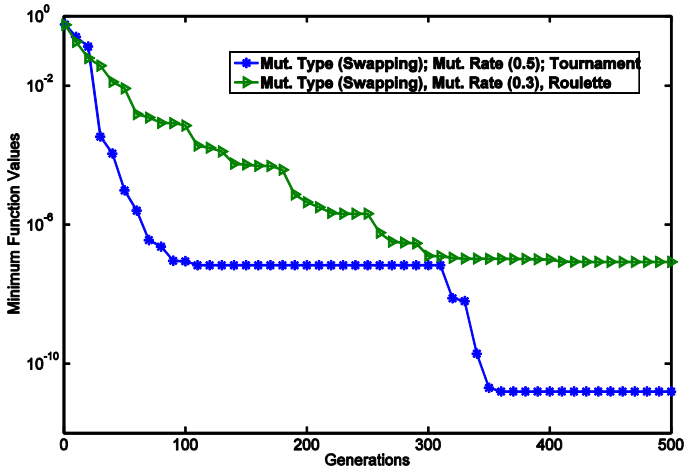

Figure 5.30: Tournament vs. roulette for swapping mutation

5.6 Summary

This chapter deals with the subject of optimisation. The general concept of optimisation and Topology optimisation, in particular, are briefly reviewed and then the use of Genetic Algorithms as an optimisation tool is examined at length. Firstly, the supporting theory leading to the algorithm implementation is presented followed by a parametric study.

The parametric study focuses on the analysis of the balance that is required between diversity and the selective pressure. For a successful search of solutions to be obtained with a Genetic Algorithm, that is of paramount importance.

The main aim of the study carried out in this chapter is to understand the dynamics of the genetic algorithm so that it can be used with confidence in the optimisation procedure dealing with the optimal design of viscoelastic layers, of both homogeneous thickness and variable thickness. The former is dealt with in Chapter 7, whereas the latter is presented in Chapter 8.

Chapter 6

Parametric Analysis of CLD Treatments

In this chapter an analysis is first made on the main contributors to damping efficiency. Then an analysis on the influence that the various parameters have on the behaviour of constrained layer damping treatments is presented.

In order to understand the behaviour of a viscoelastic core layer when subjected to constrained circumstances, there is a need to first have the correct perception of the parameters that affect the performance of the VEM layer. Secondly, the effects that the multiple design parameters have on the efficiency vs. VEM thickness curve need to be explored.

In addition, it is an objective of the study carried out in this chapter to provide some useful and straightforward guidelines towards the efficient design of thin CLD damping treatments.

6.1 Design parameters of constrained layer damping treatments

The design complexity of CLD treatments is justified by the fact that the thickness of the viscoelastic layer acts distinctly on the two principal contributors for the total strain energy: the amount or volume of VEM that is being deformed by the vibration of the host structure and the imposed shear deformation. In fact, while a low thickness VEM represents a reduced volume to store deformation energy, it is responsible for higher shear strain levels when the outer skins perform a flexural motion during vibration. This dual effect, in addition to the effect of the constraining layer thickness, has motivated the interest of the research community as it can be observed from the numerous studies on this particular issue [21, 103, 104], especially those looking for an optimised placing or layering strategy [47, 105 - 107].

However, this complexity offers some design flexibility, especially when partial coverage is also considered [108, 109]. The type and thickness of the VEM and the stiff skin layers can thus be modified in order to optimise the effectiveness of the composite product. One common observation drawn from most of the published studies and from the basilar textbooks on this subject [7, 13] establishes a direct relation between the symmetry of the sandwich construction of the CLD treated structure (complete symmetry implies a constraining layer with the same thickness as the base structure) and the damping efficiency of the treatment. This obvious observation is related to the shear deformation distribution inside the layered structure.

Another perceived general observation is the direct relation between the thickness of the damping layer and the damping efficiency. In general, the thickness of the VEM layer seems to have a strong impact on the damping efficiency of the treated structure for low values of the VEM layer thickness. However, this effect reduces significantly as the VEM thickness increases [21]. This observation results from the dual effect mentioned before, and it is not entirely true for all thickness ratio scenarios.

A numerical analysis is applied to totally covered beams with CLD treatments, where the most important design parameters are explored in order to identify the individual effects on

the efficiency curve shape and peak location. Non-dimensional parameters are applied to provide general design guidelines that may be followed by the designer, regardless of the dimensions and material of the host structure. Even though the study is conducted on simple beams, the most important observations can easily be extrapolated to plates and shells.

A simple sandwich beam with elastic skins and a single viscoelastic core is used in this study. This geometry represents both the constrained and the integrated configurations of the viscoelastic damping treatments.

The parameters H_1, H_2 and H_3 are the thickness of each of the three layers, representing the host base beam (layer 1), the viscoelastic sheet (layer 2) and the constraining or upper skin (layer 3), respectively. By using the following dimensional ratios, the results are made non-dimensional:

$$\begin{aligned} h_1 &= H_1/L \\ h_2 &= H_2/L \\ h_3 &= H_3/H_1 \end{aligned} \tag{6.1}$$

6.2 The viscoelastic constitutive model and material properties

The representation of the viscoelastic material using a proper constitutive model is also an important issue when dealing with viscoelastic damping treatments. Besides the effect of other application conditions, like load amplitude and, in some cases humidity, viscoelastic materials are frequency and temperature dependent and can be represented by the complex modulus approach when the analysis is performed in the frequency domain and when it is assumed that both the applied excitation and the resulting response are harmonic.

For the purpose of this study, the complex modulus approach is used considering a constant complex modulus representing the viscoelastic material. This simplification removes the effect of the storage modulus and loss factor variation with the frequency and temperature but do not imply any limitation to the observed results. In fact, all the

observations are valid and can easily be extrapolated for the cases when the frequency dependence must be considered. This frequency dependency can then be easily introduced taking into consideration that treatment efficiency is proportional to the VEM loss factor and observing and considering the main effects of the VEM modulus on the efficiency curve and peak position. These observations rely on the assumption that the material damping of the host structure and constraining layer is negligible or significantly reduced when compared to the damping effect produced by the VEM layer.

Since the loss factor is related to a strain energy ratio, it depends upon the material properties acting directly on the deformation energy. On a close analysis of the membrane/bending and transverse shear deformation energies for the three layers, it is possible to identify that while the shear strain energy contribution in the skins is almost negligible it becomes dominant in the core damping layer. On the other hand, the membrane/bending energy is of significance in the skins but negligible in the core. Hence, the system damping ratio mostly depends on *Young*'s modulus of the outer layers and the storage shear modulus and loss factor of the viscoelastic material in the core.

According to Arnold Lumsdaine [110], there is very little data on the *Poisson*'s ratio of viscoelastic materials. For low frequencies and high temperatures, it is usually assumed that viscoelastic materials are incompressible ($\upsilon = 0.5$), whereas for low temperatures and high frequencies, $\upsilon = 0.33$ is more adequate. Although the variation of *Poisson*'s ratio is well documented, due to the fact that the measurement of this variation is not easy to obtain experimentally, this information is not available for most viscoelastic materials. In this study, since the viscoelastic material is commonly used near its transition temperature range covering its vitreous transition region, a *Poisson*'s ratio of 0.49 (a commonly used numerical value that is close to the value that represents the incompressible condition) was assumed, thus solving the potential numerical issue known as volumetric locking.

The material density plays a direct role on the mass characteristics of the individual layers, which merely affects the natural frequencies of the sandwich beam, having no direct effect on the damping efficiency of the treatment. The effect of material density can be easily considered through the analysis of the effect of the natural mode frequency alteration on

the associated storage modulus and loss factor, which can finally be taken into account through the analysis of the modulus ratio effect.

$$e_1 = \frac{E_1}{E_2} \tag{6.2}$$

where E_1 and E_2 represent the *Young*'s modulus of the bare beam and the storage modulus of the VEM layer, respectively. In this study, the constraining layer is assumed to be made of the same material as the host structure.

6.3 Analysis on the damping efficiency contributors

As described by (3.35), the dissipative effect of energy provided by the damping layer is directly responsible for the damping achieved when using passive damping treatments based on viscoelastic materials. Since the viscoelastic layer will dissipate part of the stored energy when subjected to deformation during vibration, the main goal of an optimisation design procedure of these treatments is to maximise the strain energy stored in this layer. The storage size that is represented by the volume of the VEM layer and the deformation level imposed to this particular layer are directly responsible for the global strain energy that is stored in the structure.

To perform an initial and detailed analysis on the effect that the thickness of the VEM layer produces on the damping efficiency of a constrained damping treatment configuration, a simple numerical analysis is herein presented. The main goal of this initial step is to understand the role that the two contributors play on the stored strain energy, namely the volume of the VEM layer that is able to deform and store energy, and the shear deformation pattern that is induced inside this damping layer during the vibration of a beam.

A beam with length L and width b is discretised by a 40-finite element mesh where each material layer is represented by a single numerical layer. Free-free boundary conditions were considered, and a symmetric configuration ($H_1 = H_3$) was selected. Other boundary

conditions and asymmetric configurations were also considered in the analysis, whose results are not presented in this section but the same general observations were obtained (a detailed analysis on these design parameters is provided in the remaining study presented in section 4).

The host structure and the constraining layer are identical and are made of aluminium. The viscoelastic layer is represented by a thin layer of acrylic-based polymer commercially available for damping purposes at normal ambient temperature ranges; it represents approximately the properties of ISD112 from 3M (within the temperature range 20-30ºC and the frequency band 10-50 Hz [111]). Table 6.1 lists the properties used in this study, corresponding to a modulus ratio of e_1 = 7 E4.

Table 6.1: Material properties

	Aluminium (1,3)	*Viscoelastic Material* (2)
Density	2710 kg/m^3	1140 kg/m^3
Modulus of Elasticity	70 GPa	1 MPa
Poisson's Ratio	0.32	0.49

When looking at a standard constrained layer damping curve relating the viscoelastic layer thickness and the loss factor of the treated structure for a particular mode shape, the unique and most obvious observation that one can take is the fact that, although the efficiency continuously increases for thicker layers of VEM, the relative increase becomes smaller. In other words, the benefit that one gets when introducing additional damping material by using thicker layers becomes smaller for the same incremental addition. This behaviour can be observed in Figure 6.1 where the solid line represents the normalised loss factor distribution (ratio between the treated structure loss factor and the VEM loss factor) for different values of normalised thickness of the VEM layer (h_2). Following this general observation, the thickness of the viscoelastic layer is often ruled by a balance between the cost and weight of the added damping material and the global efficiency obtained.

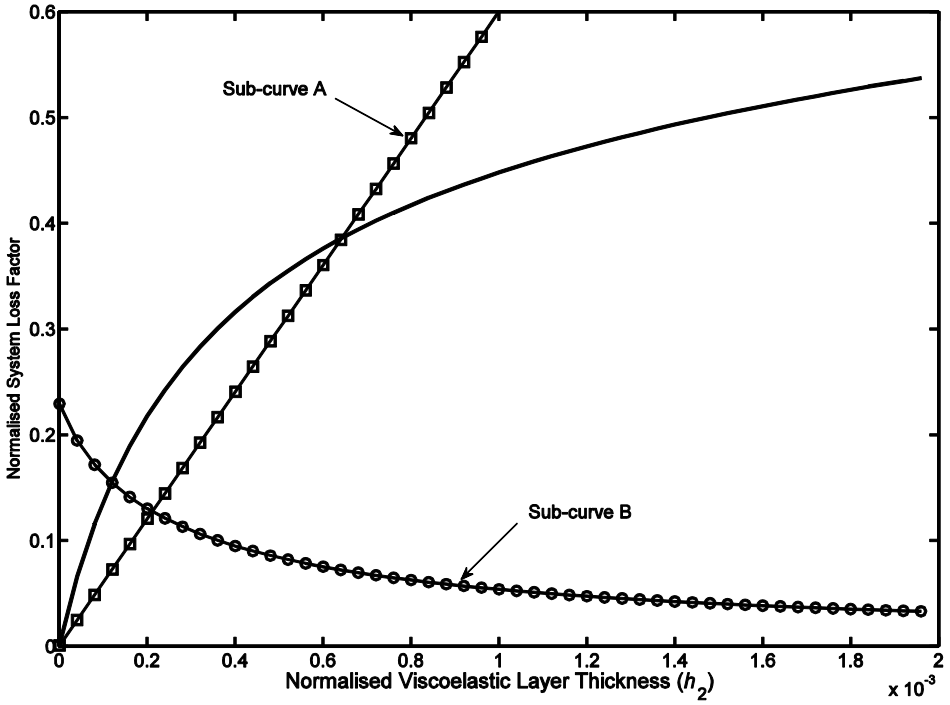

Figure 6.1: Normalised efficiency curve, sub-curve A and sub-curve B (h_1 = 0.001)

The solid line curve of Figure 6.1 can be decomposed into sub-curve A representing the volume of the damping layer ($H_2 * L * b$) and sub-curve B representing the specific strain energy ratio per unit volume (strain energy of VEM layer divided by the layer volume). A close observation of these curves (represented in different scales to fit the figure) identifies the direct action of the thickness of the damping layer on the two main contributors for the stored deformation energy.

One is a direct linear relation with the thickness variable representing the volume energy (sub-curve A); the other is an indirect relation representing a shear deformation produced inside the damping layer (sub-curve B). This last observation is accepted by common sense, i.e. for the same flexural pattern produced by the external skins (mostly dictated by the skin properties and geometry), a thinner layer will present more transverse shear than a thicker one.

Dealing directly with the thickness of the damping layer and analysing the behaviour of the two sub-curves A and B, an interesting feature can be observed when using very thin VEM

layers in high h_1 ratios – the shear deformation curve (sub-curve B) shifts to the left hand side and increases its maximum value (Figure 6.2).

This effect produces a steep rise of the efficiency curve that reaches a maximum peak before it starts decreasing in value. This interesting feature contradicts the commonly accepted monotonic damping efficiency vs. VEM layer thickness curve and it was initially observed by Yu and Huang [103] in three-layer VEM sandwich circular plates.

However, since this feature was never thoroughly explored or properly explained, a careful analysis of the effects of the design parameters, namely the length of the structure, base and constraining layer thickness and the intrinsic properties of the materials is presented in the next section.

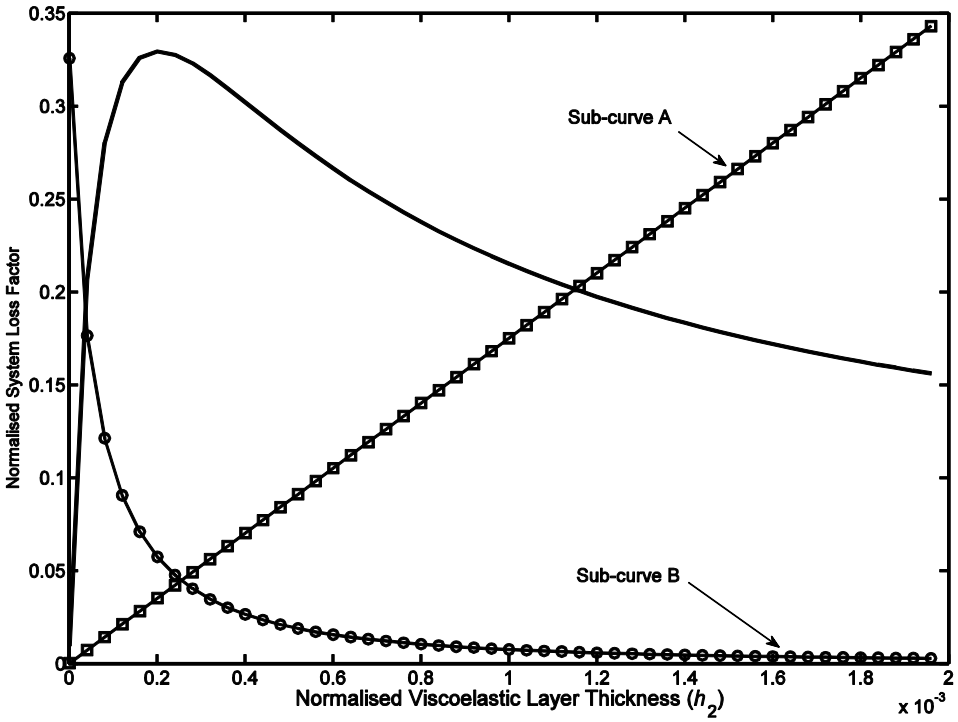

Figure 6.2: Normalised efficiency curve, sub-curve A and sub-curve B ($h_1 = 0.01$)

6.4 Parametric study and analysis of the results

Since the interaction among the various parameters is of paramount importance in the analysis of the system damping ratio, a study was done on their effect on the system loss factor. The normalised thickness of the VEM layer (h_2) versus the base thickness-length ratio (h_1), the base structure-constraining layer ratio (h_3) and the modulus ratio (e_1) were analysed. Furthermore, the consequence of the application of different boundary conditions and the effect of higher natural modes are briefly examined. Graphs in this section are plotted with the code "verif_strain_energy.m" and the associated codes "strain_energy.m", "assembly.m", "ebeam.m" and "boundaryC.m". The flowcharts of these and other codes used in this dissertation are displayed in Appendix "A" and the respective algorithms in Appendix "B".

6.4.1 Thickness/length ratio effect

Figure 6.3 describes the behaviour of a free-free constrained beam (in the 1st mode of vibration) as the thickness ratio h_2 of the viscoelastic layer varies up to 0.002. Each line in Figure 6.3 represents a different ratio h_1, defined as the ratio between the thickness of the base beam (H_1) and the length of the beam (L). It refers to a symmetric constrained configuration where the thickness of the base beam (H_1) is the same as the thickness of the constraining layer (H_3), i.e. ratio $h_3 = 1$. On the abscissa the thickness of the viscoelastic layer is divided by the length of the beam, thus defining the ratio h_2, while on the ordinate, the system loss factor is divided by the VEM loss factor.

As evidenced from Figure 6.3, the relative thickness of the base layer has an impact on the shape of the efficiency curve. For thin beams, for example those with ratio $h_1 = 0.001$, there is no sharp increase in the loss factor for very thin damping layers, but it is evident that the damping of the structure will benefit from an increasingly thicker core layer. Thicker damping materials will, however, add extra cost and weight to the composite.

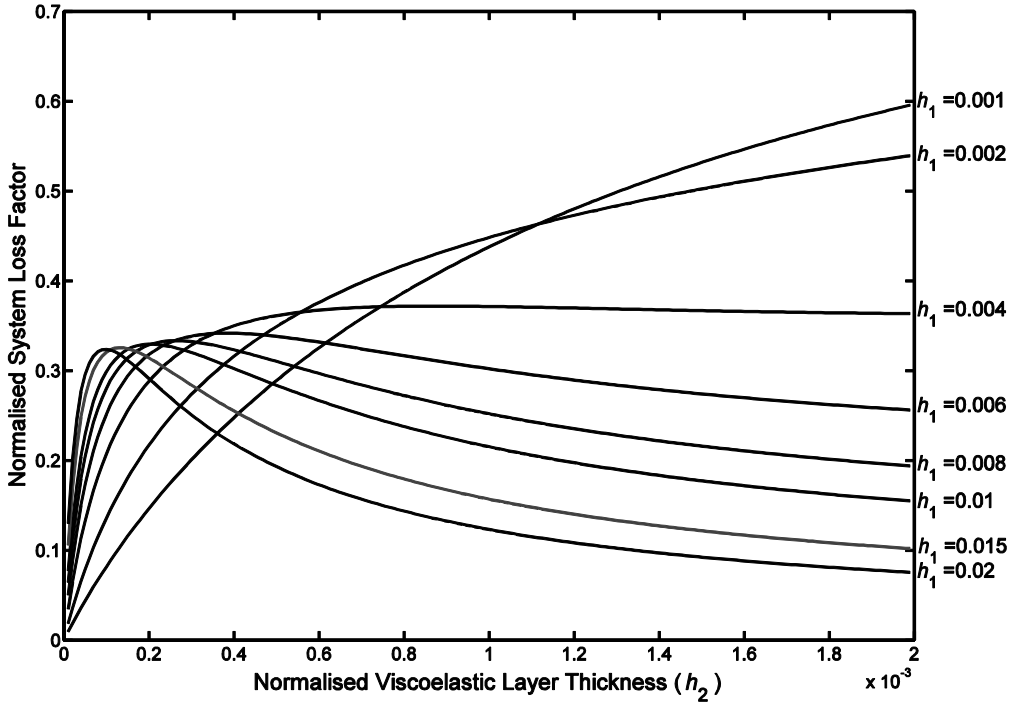

Figure 6.3: Efficiency curves for symmetric sandwich beam, $h_3 = 1$

For moderately thick beams, (e.g. $h_1 = 0.004$), the modal strain energy method predicts a substantial increase in the loss factor for low thicknesses of core layer. If the thickness of the viscoelastic material is progressively increased to higher values, the loss factor actually decreases slightly before starting to gradually increase again. This effect can be better observed in Figure 6.4, where the thickness ratio h_2 of the VEM layer varies up to 0.01.

On the opposite spectrum, considering relatively thick beams (e.g. $h_1 = 0.02$) the most significant increase in damping will occur for low additions in weight, that is, for small increases in thin damping layer thicknesses. However, if the viscoelastic thickness is augmented beyond the optimum value (the thickness that generates the highest loss factor) the damping effect will in fact decrease significantly. The use of thicker and therefore more costly damping materials would be quite wasteful, meaning that a further increase of the optimum thickness of the viscoelastic layer would have two negative consequences.

Bearing in mind that, for the same length of the beam, H_1 of a 0.02 ratio is thicker than H_1 of a 0.001 ratio, Figure 6.3 (and Figure 6.4 where the analysis has been broadened to

include thicker VEM layers) show that the optimum thickness of the viscoelastic material is lower for thicker host structures (peak shifts to the left as the thickness of the beam increases). In other words, there is an inverse relationship between the thickness of the host beam and the optimum thickness of the VEM.

Assuming the length of the beam is known, the designer can choose from the various curves the condition that is most appropriate, whereby the thickness of the host beam can then be determined from the ratios shown in Figure 6.3. It is clear from observation of the figure that the curves that form a peak present a better solution than the smooth ones. The curves with a peak provide an indication of the optimum thickness of core material that will produce the highest loss factor. With low increase in weight, the damping layer can then be kept as thin as possible while achieving maximum damping.

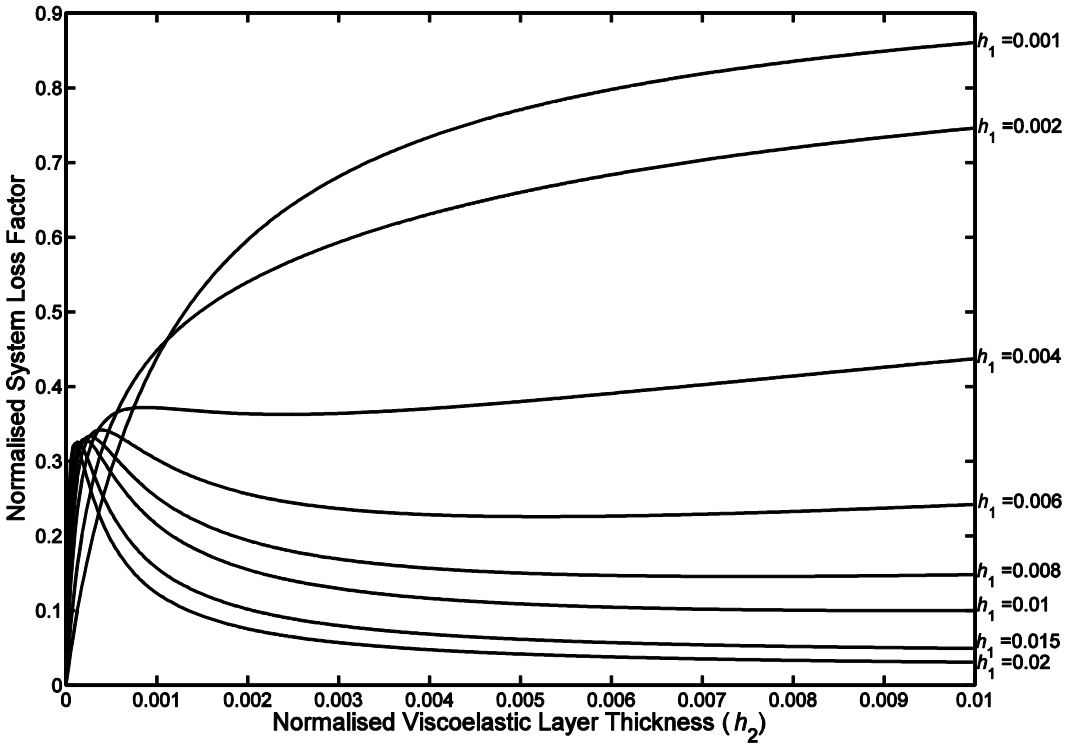

Figure 6.4: Efficiency curves for symmetric sandwich beam, $h_3 = 1$, h_2 max = 0.01

6.4.2 Constraining layer thickness effect

The effect that the variation of the thickness of the constraining layer (H_3) has on the loss factor is shown in Figure 6.5 and Figure 6.6. They also refer to a CLD configuration where the thickness of the restraining layer is, in the case of Figure 6.5, half of the thickness of the base layer. All the other parameters have been kept constant. It can be seen that there is a generalised slight decrease of the system damping. This may be explained by the fact that thinner constraining layers produce less shear strain energy in the viscoelastic material; this will affect the damping effect on the structure because the system loss factor is directly proportional to the strain energy in the VEM; an increase of the latter will produce a higher loss factor, as shown in (3.35).

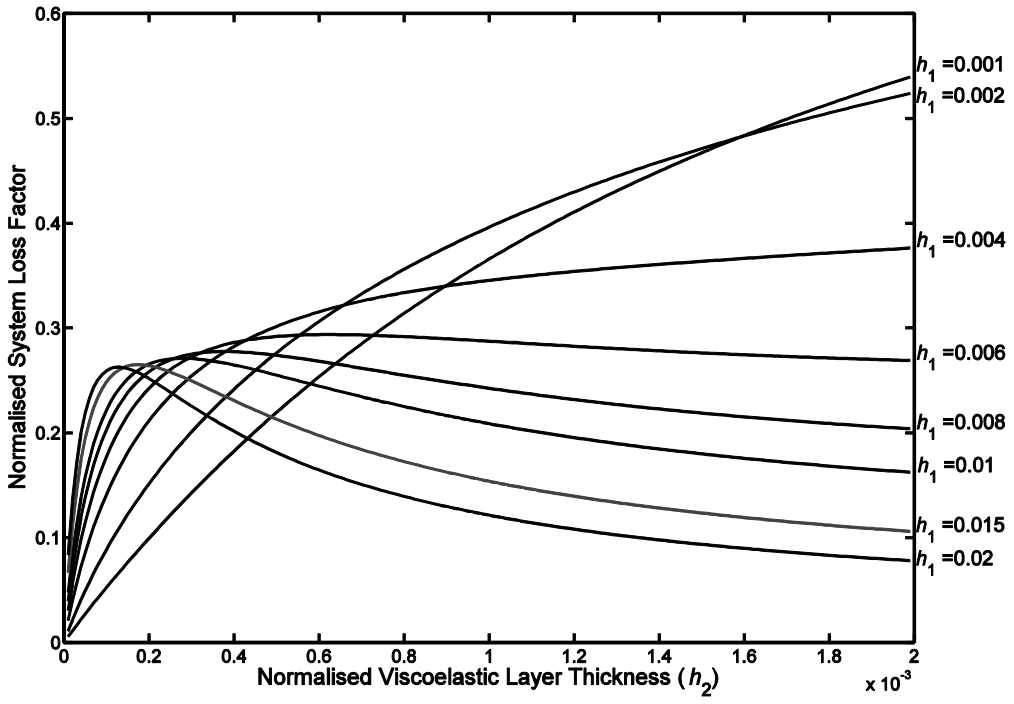

Figure 6.5: Efficiency curves for constrained damped beam, h_3 = 1/2

In Figure 6.6, all parameters have been kept constant except the constraining layer thickness which is one third the base layer. When compared to the two previous cases (Figure 6.3 and Figure 6.5), a further decrease of the loss factor can be observed. In general, the loss factor for h_3 = 1 is above 0.3, whereas for h_3 = 1/3 is below 0.2. It follows, therefore, that the damping effect increases with the increase of the constraining layer

thickness. Another observation is the relationship between the optimum thickness of the core material (VEM thickness that renders the highest loss factor) and the thickness of the constraining layer. By comparing Figure 6.3 and Figure 6.6, there is a shift of the optimum viscoelastic thickness to the left hand side with the increase of the constraining layer thickness i.e. symmetrical structures, not only bring about a higher damping effect, but require less viscoelastic material than constrained structures with thinner constraining layers.

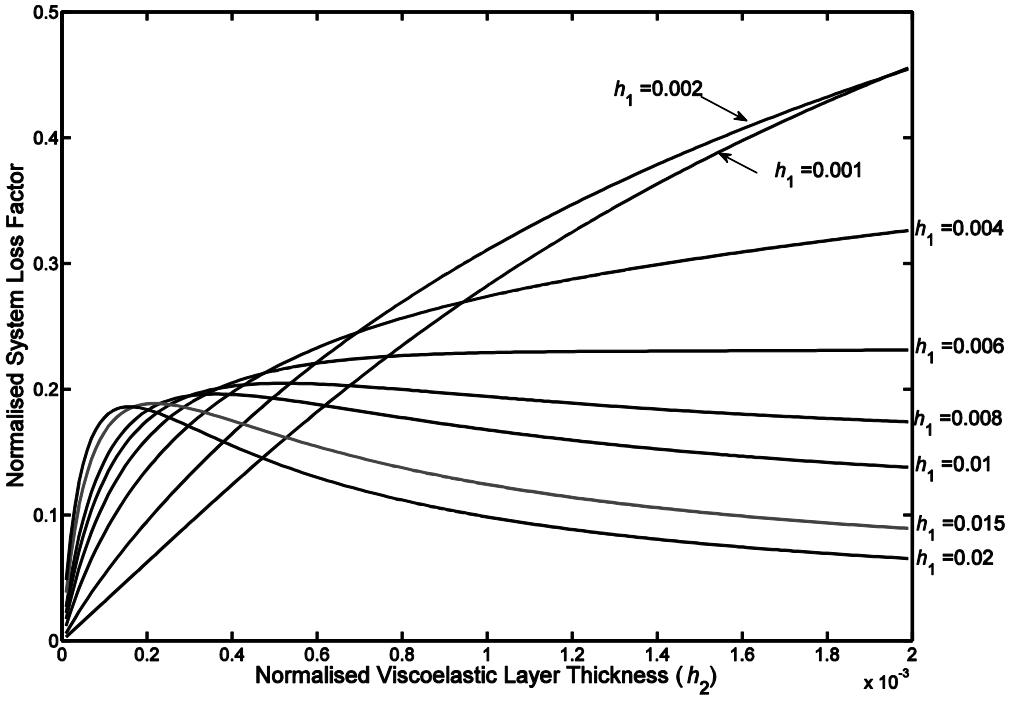

Figure 6.6: Efficiency curves for constrained damped beam, h_3 = 1/3

This effect is further analysed for h_1 = 0.01 and for various constraining layer thicknesses and it is shown in Figure 6.7. Again, two observations are possible: one is that the thicker the constraining layer, the higher the damping effect, as explained previously. The other is the displacement of the optimum VEM thickness to the left hand side with the increase of the constraining layer thickness reaffirming the advantage of symmetric constrained configurations. The dotted line in Figure 6.7 highlights the main effect of the constraining layer thickness on the efficiency curve peak.

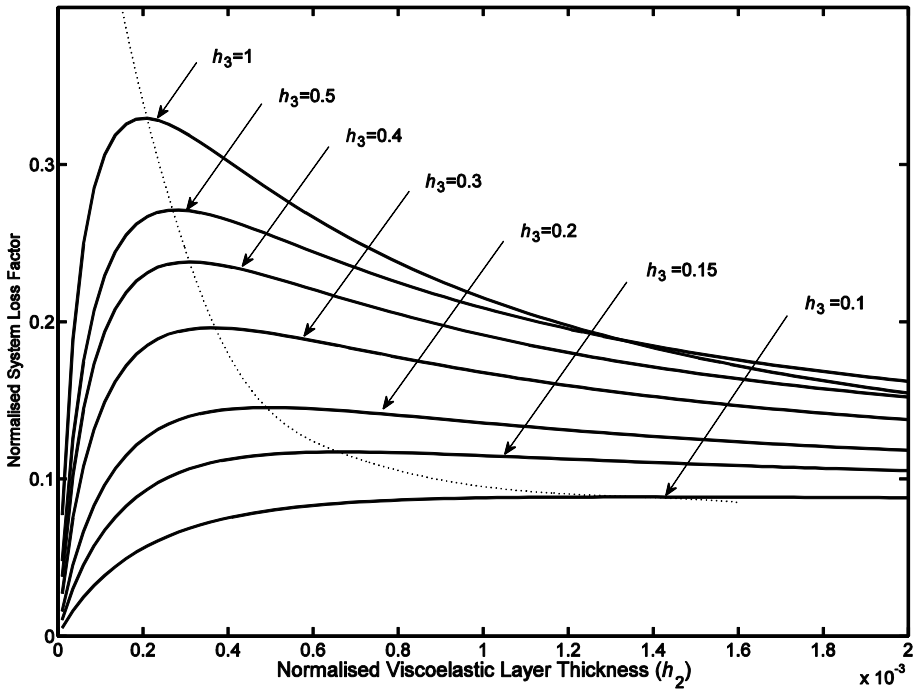

Figure 6.7: Effect of constraining layer thickness

6.4.3 Material properties effect

The material properties play a direct role on the strain energy of each of the three beam layers. In the outer layers, the membrane/bending deformation energy is the dominant contributor, whereas the main contribution in the VEM layer comes from the shear strain energy. Since the strain energy ratio is related to the structure damping ratio, the latter is mostly dependant on *Young*'s modulus of the outer layers and the storage shear modulus and loss factor of the viscoelastic core.

To illustrate the effects of the material pair used in sandwich constructions, Figure 6.8 depicts the modal loss factor ratio versus the thickness ratio h_2 for different modulus ratios (e_1), which is valid for any pair of materials with identical modulus ratio. Although the analysis shown in Figure 6.8 concerns a symmetrical sandwich configuration (h_3 = 1) and h_1 = 0.01, the effects of other design variables can easily be superposed and considered. As an example of the superposition, the depicted curves will shift to the right hand side if

lower h_1 ratios are considered (see Figure 6.3) and will move downwards and present a slight shift towards the right hand side for lower h_3 ratios (see Figure 6.7).

The efficiency curves for several modulus ratios are plotted according to standard configurations using metallic skins and commercially available viscoelastic materials for damping applications. For example, the modulus ratio of e_1 = 7E4 resembles a beam made of aluminium skins and an acrylic-based damping material for low-medium temperature applications (3M ISD112 at 20-30ºC and a frequency range 10-50 Hz) while the modulus ratio e_1 = 1E5 represents a steel sandwich beam with a higher temperature viscoelastic material (3M ISD110 for a temperature 50-60ºC and frequency range 10-50Hz).

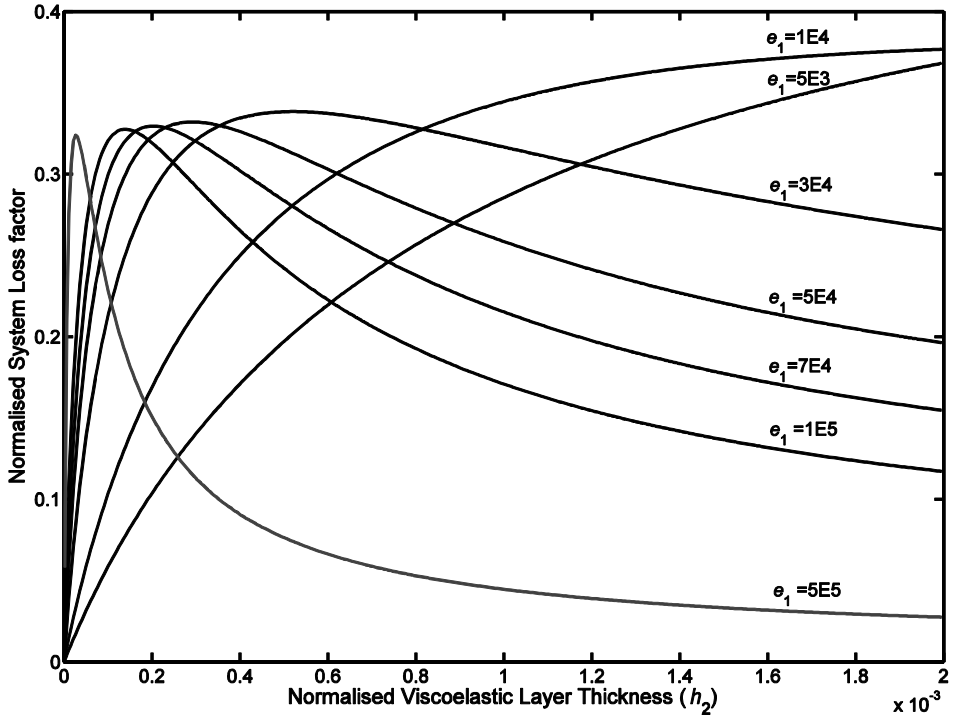

Figure 6.8: Effect of the elastic modulus variability on the loss factor for h_1 = 0.01

The results presented in Figure 6.8 are also important in introducing the frequency and temperature effect on the viscoelastic material properties. These results complement the observations obtained considering a constant and frequency-temperature independent elastic modulus. The curves depicted in Figure 6.8 show mainly that when the modulus of the viscoelastic material increases, i.e. the modulus ratio becomes smaller, the efficiency

curve peak moves to higher values of the viscoelastic layer thickness ratio. The opposite also applies.

Thus, when designing a CLD treatment, the effect of the frequency and temperature on the peak location can be taken into consideration by using the modulus ratio effect. On one hand, unlike the storage modulus of the VEM, the modulus of the host structure and the constraining layer are normally considered temperature and frequency independent.

On the other hand, the effects of frequency and temperature on the loss factor of the viscoelastic material can easily be taken into account as the efficiency of the damping treatment is directly proportional to the loss factor of the damping material. The designer is thus able to identify how and to what extent the change of the material storage modulus reshapes the efficiency curve.

6.4.4 Natural mode effect

Comparing the efficiency curve of the first three modes of a free-free symmetrical beam, one can easily verify that the peak of the higher order mode curve corresponds to progressively lower h_2 ratios. This effect seems to be simply justified by the continuous reduction of the wavelength for higher mode shapes.

Lower wavelengths lead to a more intense shear deformation pattern produced inside the dissipative core, which produce a direct effect on the sub-curve B of Figure 6.2. This feature is easily verified when analysing an experimental or numerical frequency response of a beam with constrained damping layer – for very thin VEM layers, the damping level becomes more pronounced for higher frequency modes.

The main conclusion that can be drawn from this brief study indicates that the higher the order of the natural mode, the lower will be the viscoelastic thickness ratio corresponding to the efficiency peak.

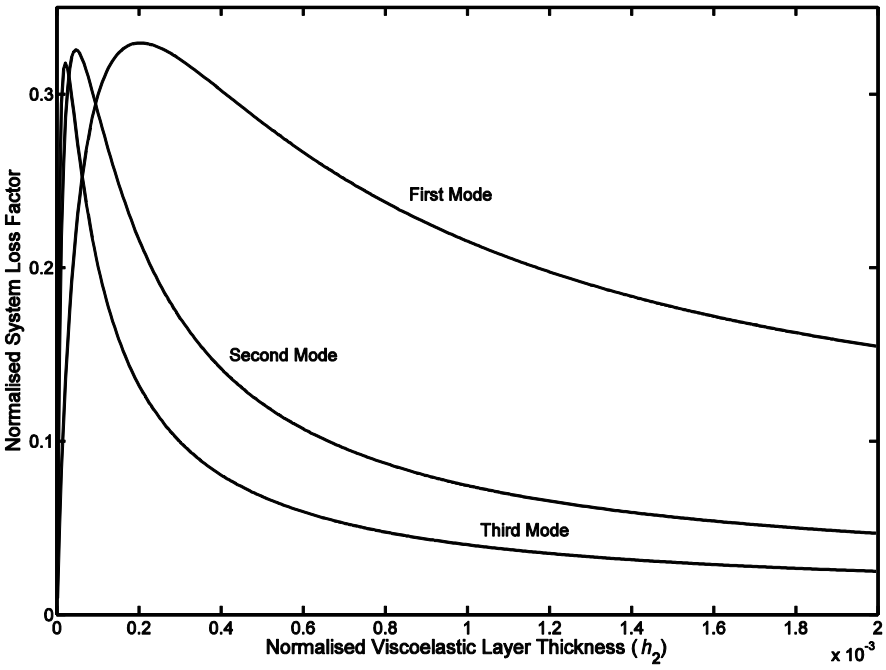

Figure 6.9: Effect of the mode variability on the loss factor for $h_1 = 0.01$

6.4.5 Boundary conditions effect

As a result of the applied constraints, the effect of the application of different boundary conditions is expected to be directly related to the intensity of the transverse shear pattern produced inside the viscoelastic layer. According to the graph of Figure 6.10, the applied boundary conditions affect the shape of the efficiency curve rather significantly, moving the curve peak to lower viscoelastic thickness ratios for those boundary conditions where the shear deformation pattern is more evident. This effect is easily observed for the simply supported beam (SS), the free-free beam (FF), the built-in beam (FX) and the combined fixed-simply supported (FX-SS) cases. The cantilever case demonstrates the effect of the boundary conditions on the wavelength of the fundamental natural mode – in this case, the shear deformation pattern is less intense.

As a conclusion, the effects of the boundary conditions can be directly evaluated from the modifications produced on the shear deformation pattern, reshaping the efficiency curve according to the intensity of the shear strain field of the dissipative layer.

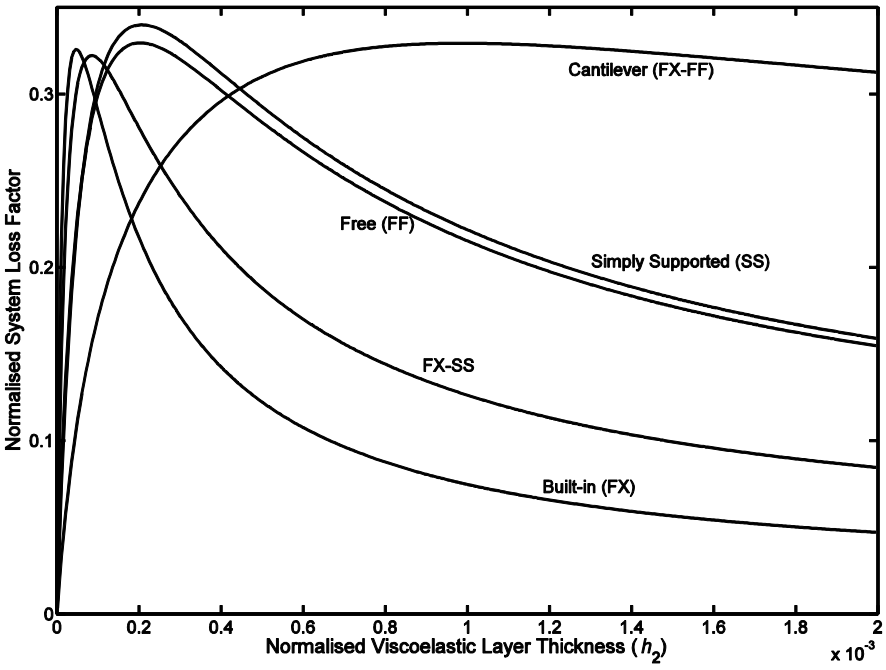

Figure 6.10: Effect of the boundary conditions variability on the loss factor for $h_1 = 0.01$

6.5 Summary

In this chapter a dimensionless analysis was performed on CLD structures. The shear strain energy produced by the viscoelastic layer energy versus volume energy is initially analysed followed by a study of the contribution that each one has on the total stored strain energy.

Then, the effect that the thickness of the host and constraining layers have on the stored strain energy of the VEM layer in a CLD configuration is also investigated. Special attention is given to the thickness ratios that produce non-monotonic efficiency curves. The effect of the boundary conditions, mode of vibration and the elastic modulus complete the study of this chapter.

Chapter 7

Optimisation of Homogeneous Thickness CLD Treatments

The search for the optimum homogeneous thickness of a VEM layer in a constrained configuration is the topic of this chapter. The genetic algorithm is the tool used in the optimisation process and results are confronted with the results from the previous chapter.

The design and optimisation of constrained layer damping treatments is a rather complex procedure due to the fact that it is dependent on several parameters, such as, size, thickness and shape of the host structure, thickness and configuration of the treatment layers and the intrinsic properties of the applied materials.

The previous chapter was dedicated to the parametric analysis of the variables that are involved in CLD treatments. On one hand, the results thus obtained, not only provide a reference to the GA optimisation analysis, but can also be confronted to the results obtained in this chapter; on the other hand, the validation of the results from Chapter 6

with the Genetic Algorithms is of paramount importance as this optimisation tool will assume a substantial relevance in the next chapter.

Hence, the study proposes an extensive analysis on the optimum viscoelastic thickness of a symmetric constrained configuration (where the thickness of the base beam (H_1) is the same as the thickness of the constraining layer (H_3) i.e. ratio $h_3 = 1$. This optimisation analysis is performed on a homogeneous cross-section of the viscoelastic layer in order to obtain the minimum thickness (h_2) conducive to the highest loss factor, where h_2 is the ratio between the thickness of the VEM layer (H_2) and the length of the beam (L), following the configuration applied in the parametric study of chapter 6. The first three vibration modes were studied for three boundary conditions, namely, free-free, built-in and cantilever conditions. The study is performed on different h_1 ratios, defined as the ratio between the thickness of the base beam (H_1) and the length of the beam (L). At the end of the chapter a brief analysis of a different h_3 ratio ($h_3 = 1/3$) is added.

The material properties are identical to those used in the preceding chapter. The base beam and constraining layer are made of aluminium, which have a *Young*'s modulus (E) =70GPa, *Poisson*'s ratio (ν) = 0.32 and density (ρ) = 2710Kg/m^3. The viscoelastic material has a storage modulus (E) = 1MPa, *Poisson*'s ratio (ν) = 0.49 and density (ρ) = 1140Kg/m^3.

7.1 Using GAs to obtain the optimum homogeneous VEM thickness

A genetic algorithm fitness function was used to optimise the minimum viscoelastic layer thickness that produces the highest loss factor. The optimisation uses an objective function whose aim is to maximise the modal strain energy for the natural modes of interest. However, the objective function only takes into consideration a benefit factor that corresponds to the efficiency of the treatment based on the structure damping ratio. The cost function represented or related to the economic cost of the viscoelastic material, added mass or any other factor associated with the cost of application of the treatment, was not introduced in the objective function used in this study. The cost function is dependent on many factors, namely the type of structure, the way the cost is to be evaluated, etc. making

it difficult and exempted of objectivity to be considered in the study. The analysis that has been done does not reflect the cost/benefit of the VEM optimum thickness but rather the thickness that will render the highest loss factor, making it impossible to optimise those curves that do not present a peak.

The Genetic Algorithm MATLAB Tool is the problem solver used in the numerical analysis where several functions are implemented in MATLAB code in order to exploit the optimisation procedure and to evaluate the cost function. The routine concerning the finite element "ebeam.m" determines the stiffness and mass matrices of the CLD structure. The routine "assembly.m" assembles the element matrices so that the stiffness and mass global matrices can be obtained. The code "boundaryC.m" establishes the boundary conditions by conditioning the stiffness and mass matrices so that the matrix elements related to the restricted degrees of freedom are removed.

The fitness function code "totalcld.m" uses the global matrices to solve the eigenproblem in order to determine the natural frequency values and their respective modal vectors. This function is written as follows: having defined the material properties, such as, *Young*'s modulus, density, *Poisson*'s ratio, the number of finite elements and number of layers, the computer code calculates the stiffness and mass matrices and degrees of freedom vector using the functions "assembly.m" and "ebeam.m". It then applies the boundary conditions with the ''boundaryC.m" function. The fitness function then calculates natural frequencies, system damping ratio and mode shape using the Modal Strain Energy (MSE) approach. As previously mentioned, the flowcharts of these and other codes used in this dissertation are displayed in Appendix "A" and the algorithms in Appendix "B".

It is important to stress that the resolution of the eigenproblem only takes into consideration the real part of the stiffness matrix. Similarly to the previous chapter, the study only takes into account the storage modulus of the viscoelastic layer. This simplification does not compromise the results, as the aim of the study is to analyse the storage mechanism of the VEM and the maximisation of the latter implies a maximisation of the energy loss by the core layer. By using the MSE method, the "totalcld.m" routine determines the treatment efficiency by evaluating the CLD damping ratio which is

introduced in the cost function, once the objective is to precisely optimise the efficiency of the treatment. The homogeneous thickness function of the viscoelastic layer is described in (7.1) as:

$$h_2\,(x) = x_1 \tag{7.1}$$

where x_1 defines the uniform thickness of the viscoelastic material.

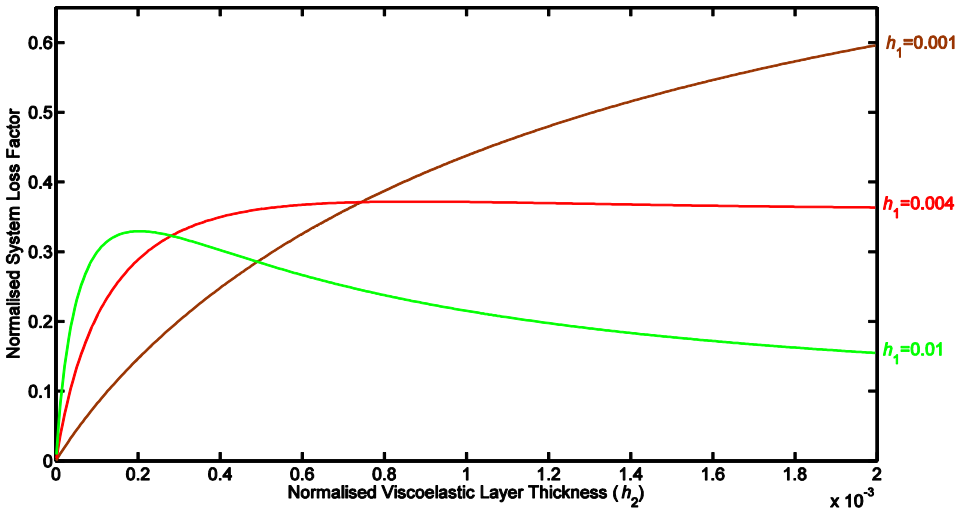

Figure 7.1: Efficiency curves for free-free boundary condition (1st mode)

Three h_1 ratios were selected, ranging from thinner to thicker structures to plot the value of the loss factors for multiple core thicknesses (Figure 7.1). It can be seen that, since the h_1 = 0.001 ratio does not exhibit a peak, it results in increasingly thicker VEM having higher loss factors. The disadvantage is, naturally, that the thicker the VEM is, the higher the cost and weight will be. In the case of this ratio, it is, therefore, not possible to find an optimum solution for the core thickness, that is, a minimum thickness value that corresponds to the highest damping factor.

As it can be observed by the curve without a peak value, the increase of the loss factor versus the cost associated with the amount of VEM used can be optimised if such cost can be expressed as a function; the latter can be introduced in the objective function of the optimisation process. The associated VEM cost may be expressed in terms of an effective economic cost or in terms of structural modification, namely the additional mass. In other

words, it is clear from the figure that, in these cases, the addition of thicker layers does not justify the cost.

Using merely the efficiency of the treatment as the cost function, the impossibility of finding the optimised VEM thickness will, obviously, occur in all cases in which the plot of VEM thickness versus loss factor does not exhibit a peak. This is confirmed by the genetic algorithm which, for ratios that do not have a peak, converges to a false solution (upper *x* limit) instead of a global optimum as illustrated in Figure 7.2.

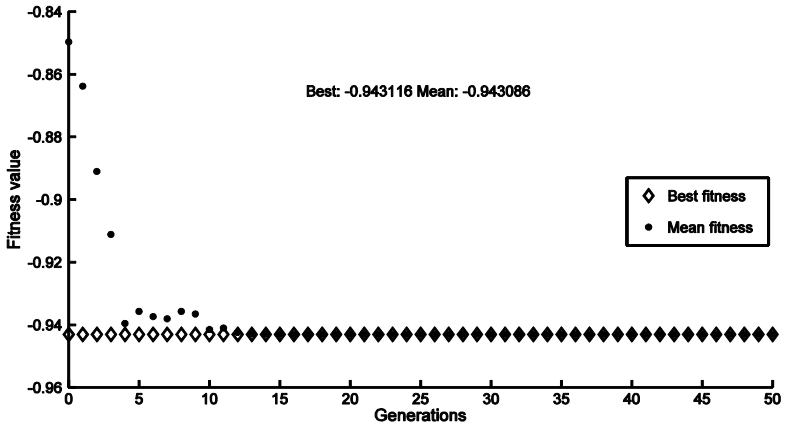

Figure 7.2: Convergence graph for $h_1 = 0.001$

Figure 7.2 shows the premature stagnation and failure of the algorithm to find a minimum global value. The optimum viscoelastic thickness found in these cases corresponds to the upper bound specified as a constraint in the algorithm, and is in agreement with the curve of the $h_1 = 0.001$ ratio where the thicker the VEM is, the higher the damping ratio.

Contrary to the previously mentioned ratio, the GA is able to search for a global minimum and find the lowest VEM thickness that generates the highest loss factor for all the ratios that exhibit peak values for the loss factor. As one example, the convergence graph of $h_1 = 0.01$ ratio showing the ability of the GA to find an optimum solution is presented in Figure 7.3.

Figure 7.4 displays the problem setup including the constraints that were set between zero, the lower bound and 10E-3, the upper bound. Due to the constraints that were introduced

to limit the search space, the algorithm uses a constraint dependent function to create the initial population, whose size is defined as twenty individuals. Although it is thought that, in general, a population of fifty individuals is an adequate size [90], a smaller population seemed appropriate in this case, as the algorithm converged rather well.

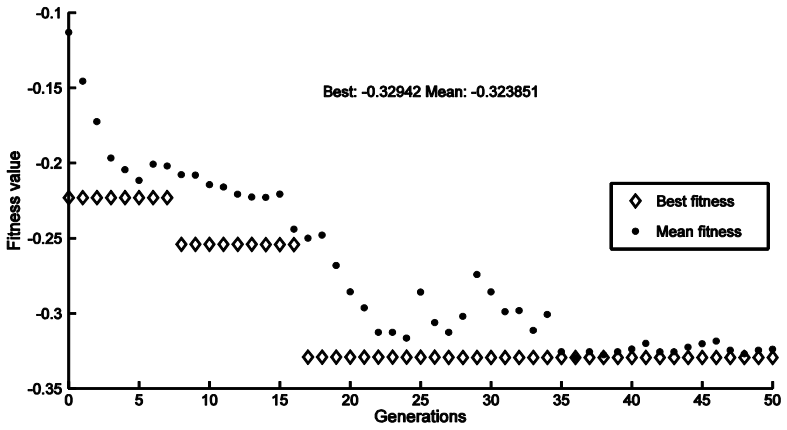

Figure 7.3: Convergence graph for $h_1 = 0.01$

Being the default fitness scaling option of the MATLAB toolbox, "Rank fitness scaling" function was chosen for the selection of the individuals for the mating pool. It scales the individuals so that the rank of the fittest individual is one, the next fittest is two, and so on. Then the "Tournament" selection function chooses the parents for the next generation by selecting four individuals (by default) at random; of these four, the best individual is chosen to be a parent. Other selection functions included in the optimisation tool are: Roulette, Uniform, Stochastic and Remainder.

In the reproduction, two of the best individuals are carried over from the precedent to the next generation to guarantee that they are not destroyed by crossover or mutation, in the process known as "Elitism". The "Crossover" fraction of individuals that are recombined in the following generation is 0.8 and the "Mutation" operator produces the remaining individuals. The "Scattered Crossover" function is the function used to form the new individuals for the following generation by creating a random binary vector. Then, it selects the genes where the vector element is a 1 from the first parent and the genes where the vector element is a 0 from the second parent. For example, if:

Parent 1 = [a b c d e f g];

Parent 2 = [1 2 3 4 5 6 7];

and random crossover vector = [1 0 1 1 0 0 0];

then, the new individual (child) = [a 2 c d 5 6 7]

The Mutation function is also a constraint dependent function. The GA tool offers other crossover and mutation functions described in Chapter 5. A specified maximum number of generations as the stopping criterion is applied, which in this case is 50 generations.

The optimum solution for ratio 0.01 found by the algorithm is given by the variable x = 2.0416E-4, as shown in Figure 7.5. This VEM thickness ratio coincides with the value of h_2 in Figure 6.1 at the curve peak.

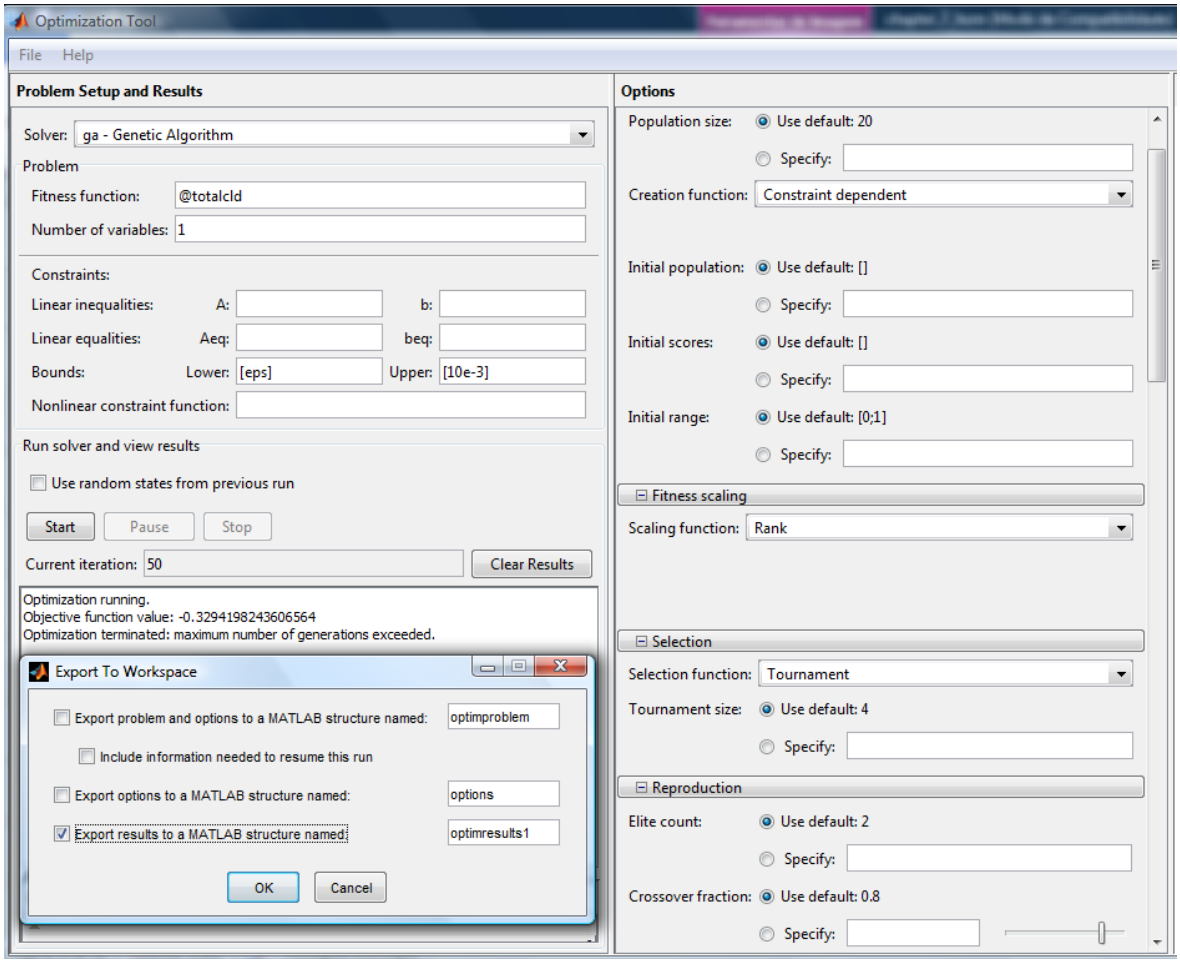

Figure 7.4: GA problem setup for h_1 = 0.01

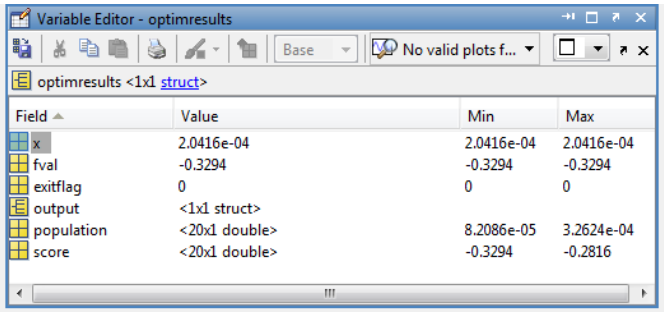

Figure 7.5: GA results for h_1 = 0.01

As far as the ratio h_1 = 0.004 is concerned, the loss factor increases for VEM thickness ratios up to about 0.7E-3. For higher ratios, it remains practically constant causing the algorithm to sometimes behave erratically in this range of values as it struggles to find a minimum solution.

7.2 Results

Results are presented for three boundary conditions, free-free, built-in and cantilever, for both symmetrical and unsymmetrical treatments.

7.2.1 Free-free beam

The first study hereby presented has free-free boundary conditions, i.e. both ends of the beam are free; they have no force or torque constraints.

As previously mentioned the purpose of the study concerning this chapter is to confirm the findings of Chapter 6 and simultaneously validate them by means of GA optimisation. The results obtained are presented hereafter and grouped in Table 7.1. It shows the optimum VEM thickness ratios for different boundary conditions and the first three vibration modes using the genetic algorithm in the manner previously described.

To compare the results from the parametric analysis of chapter 6 with the optimisation results herein obtained, the latter are superposed to the efficiency curves of Chapter 6. It

can easily be perceived from the graphs presented here that the values in Table 7.1 (Optimum viscoelastic thickness obtained with GA optimisation) coincide very closely to the corresponding values at the curve peaks. The values on this table are also identified on all figures by vertical lines corresponding to each case.

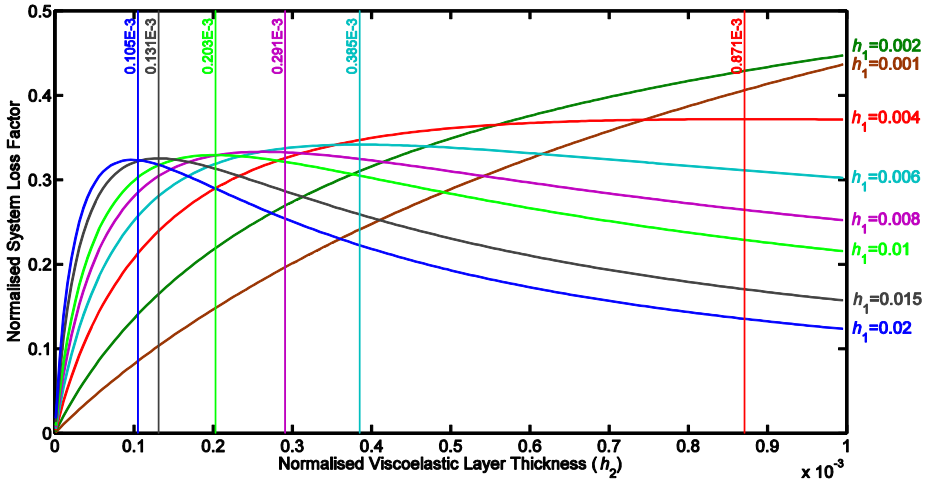

Figure 7.6: Efficiency curves for free-free boundary condition (1st mode)

In line with the conclusions that may be drawn from Figure 7.6, the perusal of Table 7.1 also shows that the optimum thickness of the viscoelastic material is lower for thicker host structures. By analysing each individual column, and bearing in mind that $h_1 = 0.02$ corresponds to a thicker host structure, an inverse relationship can be observed between the thickness of the host beam and the optimum thickness of the VEM.

Figure 7.7 represents the efficiency curves for the 2nd mode and the abscissa scale is different from that of Figure 7.6. Figure 6.10 (chapter 6) shows that the higher the order of the natural mode, the lower will be the optimum viscoelastic thickness. For this reason, the abscissa amplitude has been shortened for each of the higher modes so that the curves and their peaks can be more easily distinguished.

In addition, the VEM values in Table 7.1 corroborate the findings of Chapter 6. By comparing the different modes for each boundary condition, the evidence of the relationship between the order of frequency and the optimum VEM thickness is clear. In accordance with what has been observed in the previous two modes, it is clear that the 3rd

mode requires thinner cores (Figure 7.8). It is also noteworthy to point out that some figures might look similar, as in the case of Figures 7.7 and 7.8; this is due to the fact that the scale of the abscissa in the case of the former is 4.5E-4 and the latter is 1.4E-4. The reason for the expansion of the abscissa accordingly is to avoid cramming curve peaks in one spot thereby rendering the understanding of the figure less effective. The ordinate scale has also been adjusted.

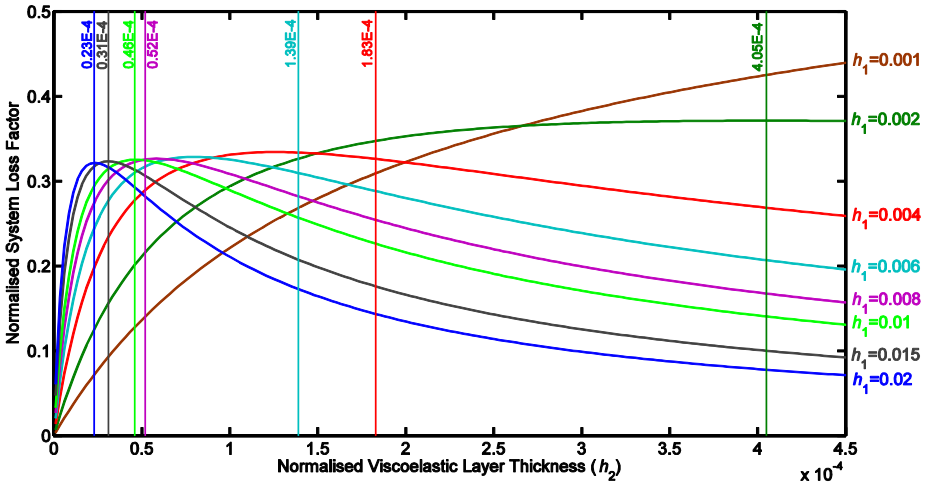

Figure 7.7: Efficiency curves for free-free boundary condition (2nd mode)

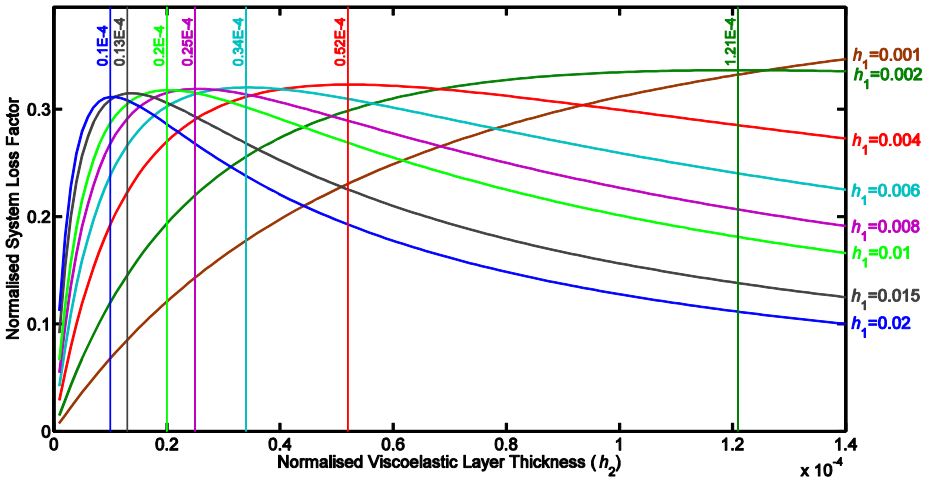

Figure 7.8: Efficiency curves for free-free boundary condition (3rd mode)

However, by actually comparing the values shown on the vertical lines, it can be concluded that higher modes move the curve peak to lower viscoelastic thickness ratios. That is, an increase in the order of the natural mode is accompanied a shift of the efficiency peak to the left hand side and this observation is in accordance with the findings in Chapter 6.

7.2.2 Built-in beam

A built-in beam, otherwise known as clamped-clamped beam or encastre, implies that both extremities are clamped and displacements and rotations are restrained. The comparison between some boundary conditions can be verified both in Figure 6.10 (chapter 6) and Table 7.1, where the curve peak moves to lower viscoelastic thickness for those boundary conditions where the shear deformation pattern is more evident. If one compares the values in Table 7.1 obtained for the built-in condition (where shear deformation is considerable), each mode exhibits lower values comparatively to the other boundary conditions (taking into consideration the same h_1 ratio).

Using the h_1 = 0.01 ratio again in the 1st mode of vibration as an example, the optimal VEM thickness ratio in a free-free boundary condition is approximately 0.2, whereas a built-in structure would only require an h_2 ratio of approximately 0.05. The normalised VEM thickness versus the normalised system loss factor in the 1st mode of a built-in structure is shown in Figure 7.9.

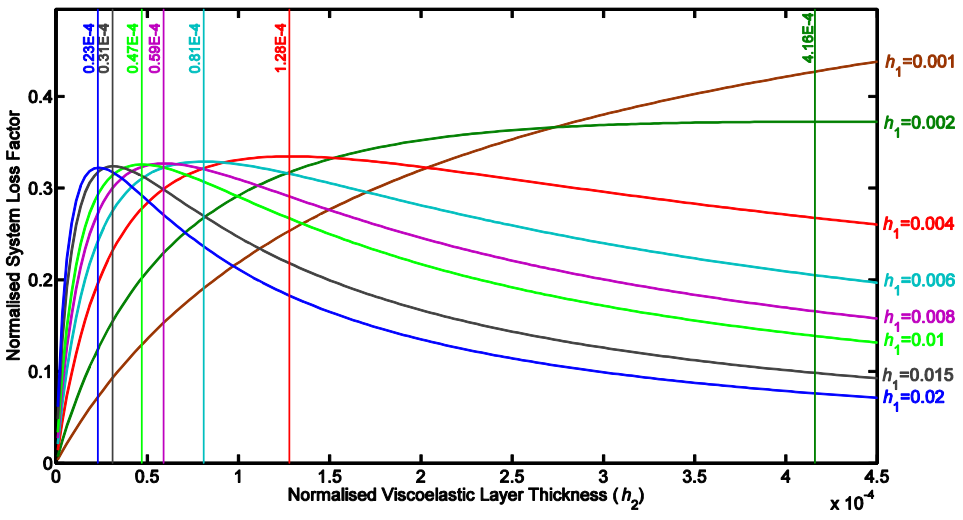

Figure 7.9: Efficiency curves for built-in boundary condition (1st mode)

Figure 7.10 illustrates the efficiency curves in the 2nd natural mode of vibration and Figure 7.11 the 3rd mode for the same boundary condition. Once more, the coordinate scales have been modified in order to accommodate the lower viscoelastic layer thickness ratios that

are required to obtain the corresponding highest damping ratios as the order of the mode increases. This only becomes apparent when the values of the curve peaks are examined, either on the vertical lines or in Table 7.1. As explained in the free-free boundary condition, the adjustment of the abscissa was deemed necessary to prevent compactness of the curve peaks in the case of the 2nd and 3rd modes.

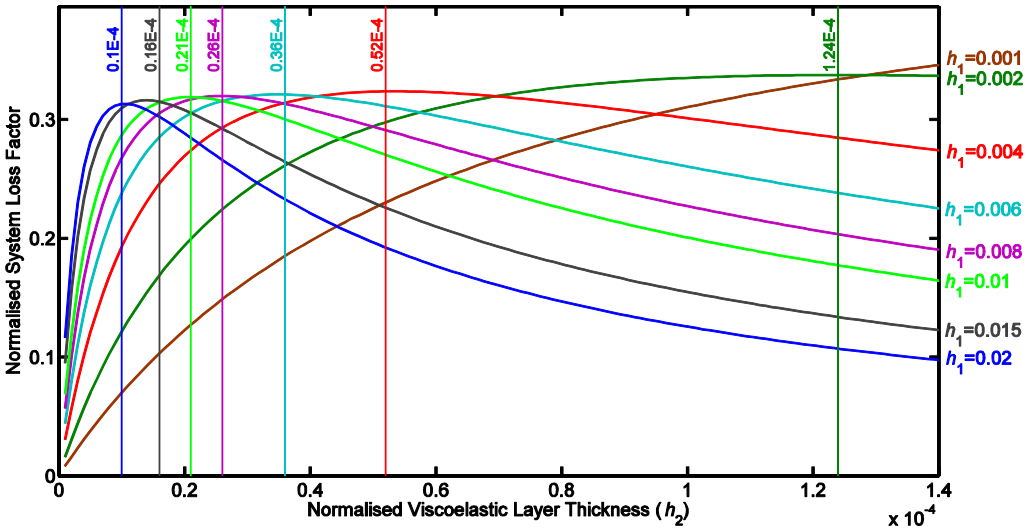

Figure 7.10: Efficiency curves for built-in boundary condition (2nd mode)

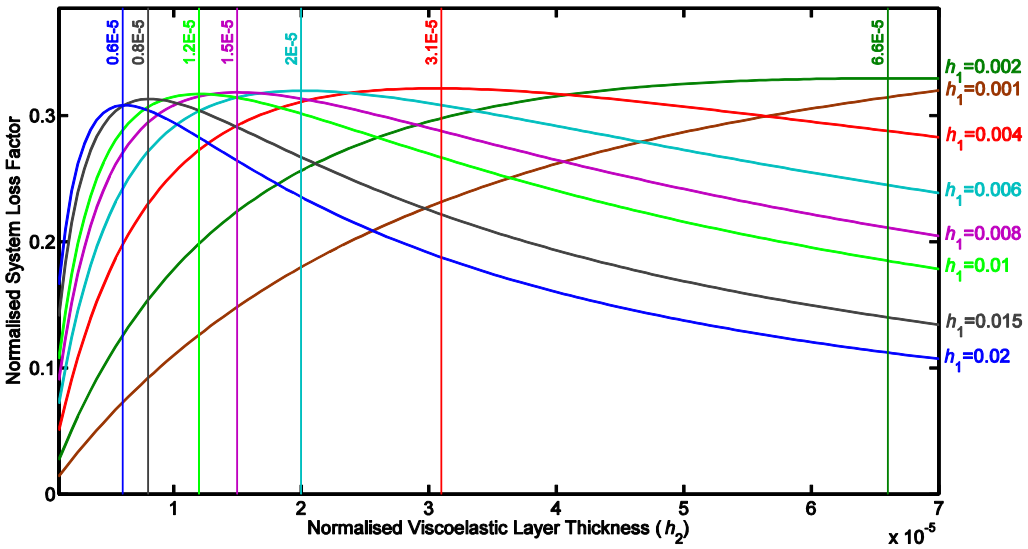

Figure 7.11: Efficiency curves for built-in boundary condition (3rd mode)

7.2.3 Cantilever

Referring once more to Figure 6.10, it is evident that a fixed-free boundary condition, otherwise known as a cantilever, requires thicker damping layers because the shear strain is not as intensive as in the case of the other boundary conditions. Contrary to the case of a built-in structure with very high shear strain levels, requiring an h_2 ratio of approximately 0.05, the cantilever demands a VEM thickness ratio of almost one (1st mode, $h_1 = 0.01$).

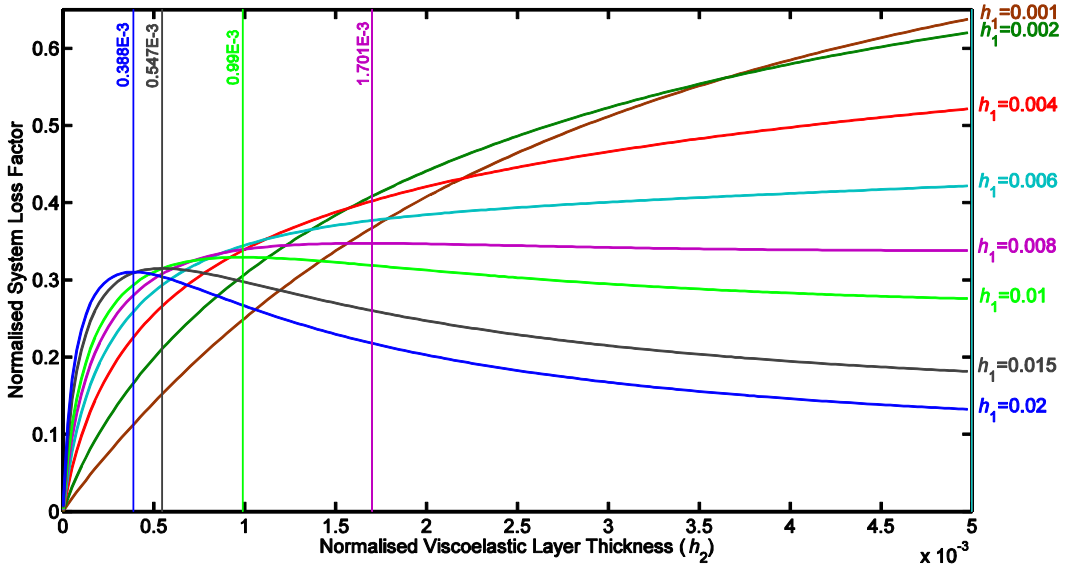

Figure 7.12: Efficiency curves for the cantilever (1st mode)

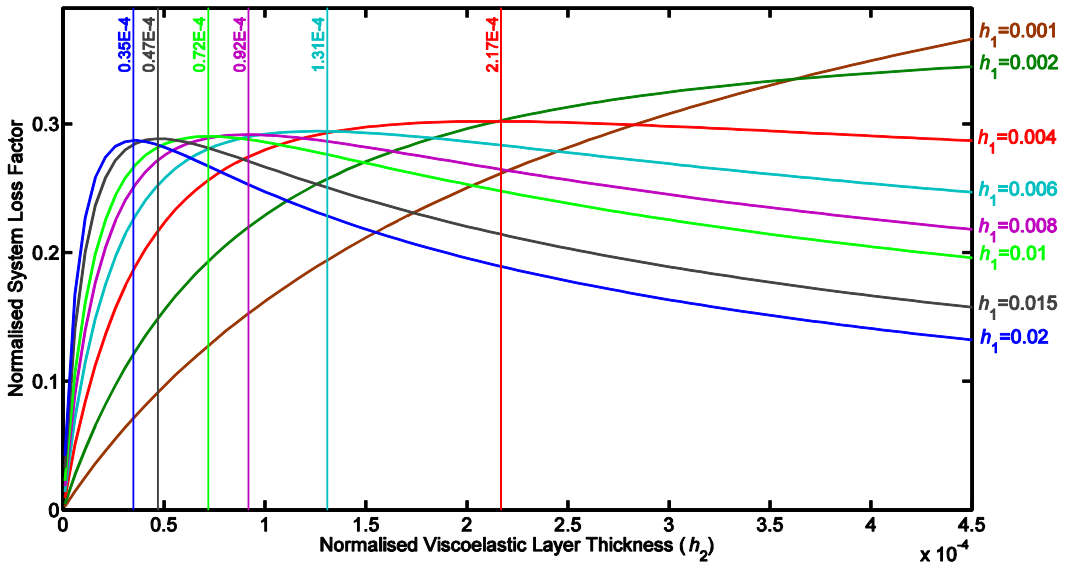

Figure 7.13: Efficiency curves for the cantilever (2nd mode)

The efficiency curves in the 2nd and 3rd natural mode of vibration for the cantilever are shown in Figures 7.13 and 7.14, respectively. The coordinate scales have been modified in order to accommodate, in this case, thinner viscoelastic layer ratios.

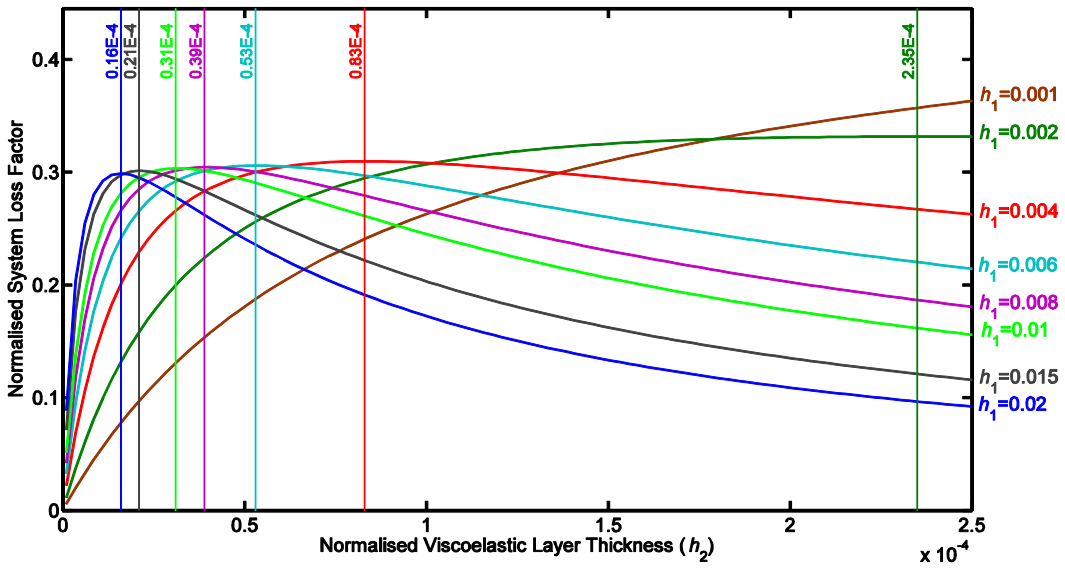

Figure 7.14: Efficiency curves for the cantilever (3rd mode)

Table 7.1 presents the optimum VEM thickness ratios for different boundary conditions and the first three vibration modes (obtained with GAs). The order in which the results for the three boundary conditions analysed are presented (first the cantilever, free-free and then built-in), correspond to the order of the boundary conditions that impose higher deformation gradients (see also Figure 6.10). This way, it is possible to identify the fact that lower VEM thickness is needed in those boundary conditions that impose higher deformation gradients (e.g. built-in).

The inverse relationship concerning the mode order and the optimum thickness of the VEM can also be observed (see Figure 6.9). In fact, higher mode orders produce higher deformation gradients in the viscoelastic layer requiring, therefore, thinner VEM thicknesses. All values of h_2 in Table 7.1 have the same exponent (E-3).

Table 7.1: Optimum viscoelastic thickness ratios obtained with GA optimisation

	CANTILEVER			FREE-FREE			BUILT-IN		
	VEM Thickness Ratio (h_2)			VEM Thickness Ratio (h_2)			VEM Thickness Ratio (h_2)		
Ratio (h_1)	1st Mode	2nd Mode	3rd Mode	1st Mode	2nd Mode	3rd Mode	1st Mode	2nd Mode	3rd Mode
0.001	----	----	----	-----	-----	-----	-----	-----	0.249
0.002	----	----	0.235	-----	0.405	0.121	0.416	0.124	0.066
0.004	----	0.217	0.083	0.871	0.183	0.052	0.128	0.052	0.031
0.006	----	0.131	0.053	0.385	0.139	0.034	0.081	0.036	0.020
0.008	1.701	0.092	0.039	0.291	0.052	0.025	0.059	0.026	0.015
0.01	0.990	0.072	0.031	0.203	0.046	0.020	0.047	0.021	0.012
0.015	0.547	0.047	0.021	0.131	0.031	0.013	0.031	0.016	0.008
0.02	0.388	0.035	0.016	0.105	0.023	0.010	0.023	0.010	0.006

7.2.4 Thin constraining layers

As previously discussed in Section 6.4.2, thinner constraining layers require thicker VEM, as they produce less shear strain (and naturally lower loss factors) in the viscoelastic material. This is particularly evident in Figure 6.7 of the same chapter. In this section, only one boundary condition is analysed to avoid unnecessary repetition.

By observation of Figure 7.15, the curves for the ratios 0.001, 0.002, 0.004, 0.006, 0.008 and 0.01 do not have peak values and as such, the genetic algorithm was unable to converge and find an optimum solution. The viscoelastic thickness ratios that generate the highest loss factor for the other two ratios coincide with the values on Table 7.2.

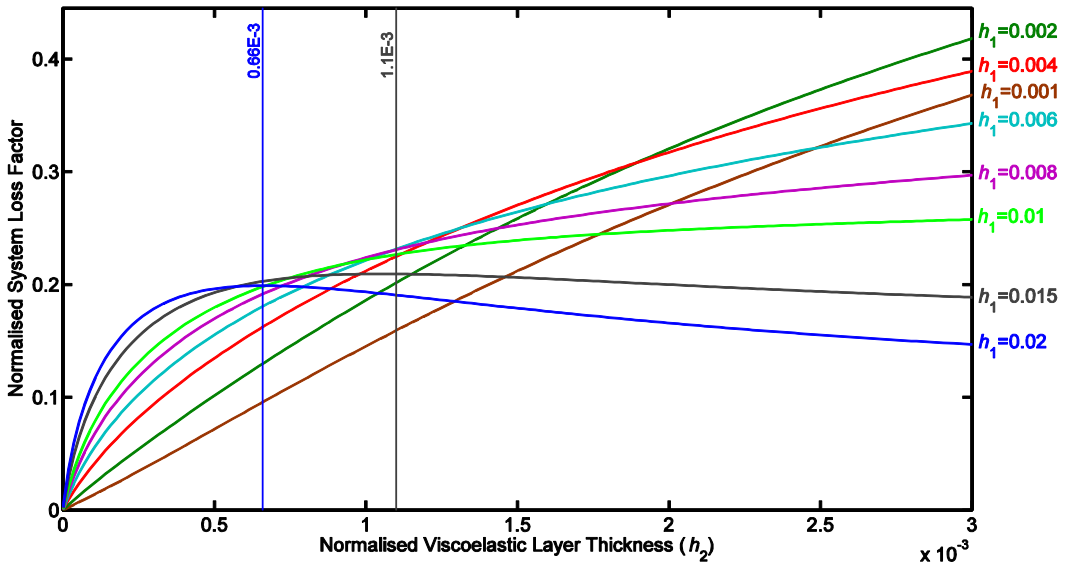

Figure 7.15: Efficiency curves for the cantilever (1st mode and h_3 = 1/3)

Figure 7.16 and Figure 7.17 show the efficiency curves for the cantilever in the 2nd and 3rd modes respectively.

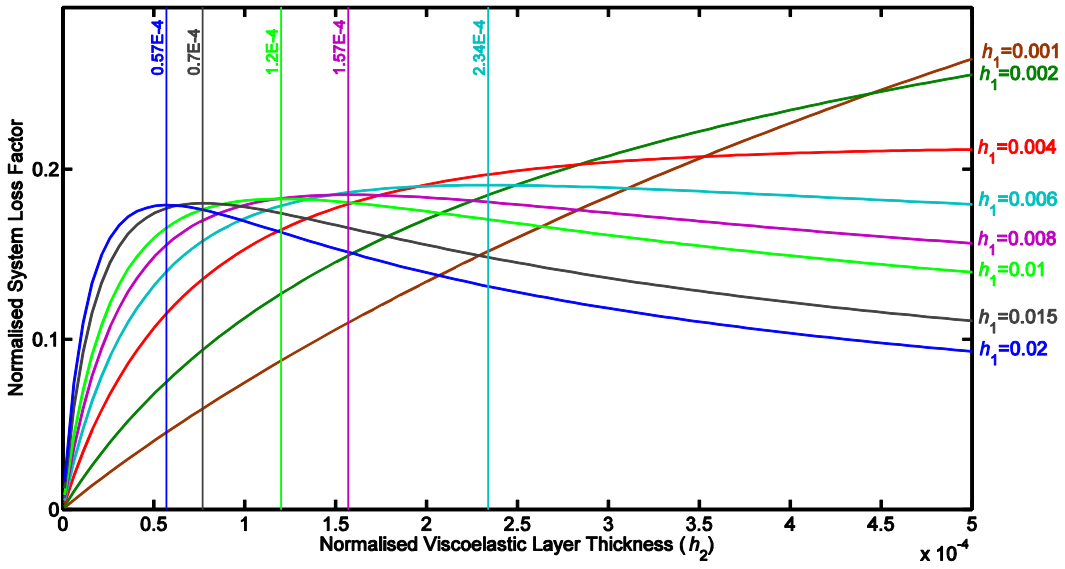

Figure 7.16: Efficiency curves for the cantilever (2nd mode and h_3 = 1/3)

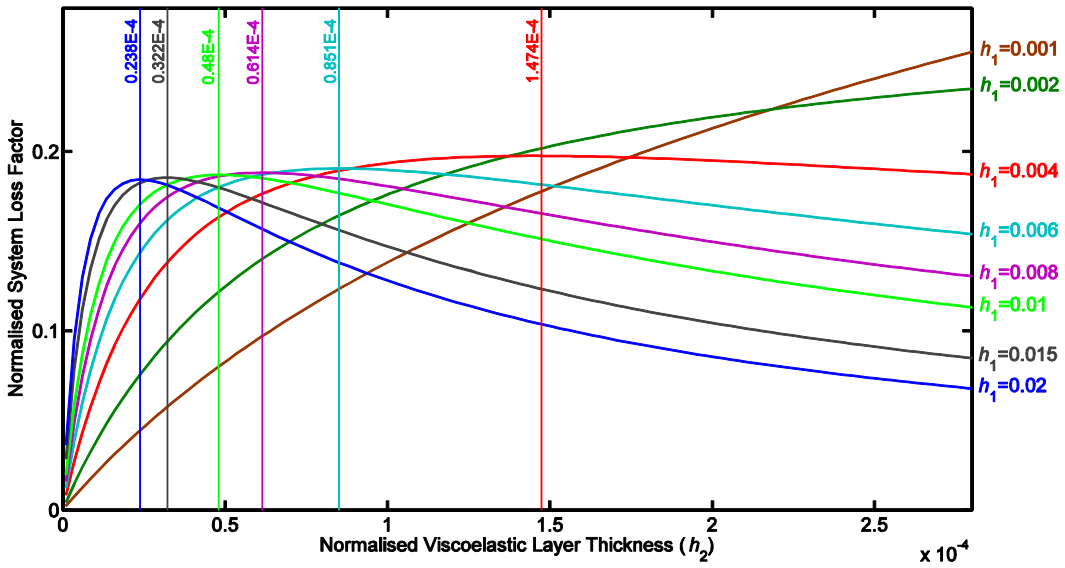

Figure 7.17: Efficiency curves for the cantilever (3rd mode and h_3 = 1/3)

Table 7.2 shows the optimised viscoelastic thickness values that were obtained with GAs for a cantilever in the first three natural modes of frequency but with a constraining layer whose thickness is one third of the host layer thickness ($h_3 = 1/3$). All values of h_2 in Table 7.2 have the same exponent (E-3).

Table 7.2: Optimum viscoelastic thickness ratios (cantilever and non-symmetric CLD)

	Ratio (h_1)							
	0.001	**0.002**	**0.004**	**0.006**	**0.008**	**0.010**	**0.015**	**0.020**
1st Mode	-----	-----	-----	-----	-----	-----	1.100	0.660
2nd Mode	-----	-----	-----	0.234	0.157	0.120	0.077	0.057
3rd Mode	-----	-----	0.147	0.085	0.061	0.048	0.032	0.023

This table confirms what had been observed in the previous chapter, in that the thinner the constraining layer is, the lower the damping effect. As the deformation gradient is lower in the non-symmetrical structure, it requires thicker VEM layers (see Figure 6.7). This is also clear from the comparison between the values on this table to the ones in Table 7.1 (for the cantilever). As an example, in the case of the cantilever and unsymmetrical treatments,

only h_1 ratios equal or higher than 0.015 show a curve peak, whereas in the symmetrical structure that happens for $h_1 \geq 0.08$. Another example (also the cantilever) is that for h_1 = 0.015, in a symmetrical situation the optimum VEM thickness ratio is 0.547E-3 whereas the ratio in the non-symmetric case is 1.1E-3. The inverse relationship between the order of the mode and the VEM thickness is obvious.

7.3 Summary

The search for the optimum homogeneous thickness of a viscoelastic layer in a constrained configuration is the topic of this chapter. The Genetic Algorithm is the optimisation tool used in this search. Firstly, the parameters are defined and the genetic algorithm problem is set up. The optimal solutions are then explored for eight different h_1 ratios in a symmetric configuration. Three boundary conditions, namely, free-free, built-in and cantilever conditions in the first three natural modes of vibration are considered. The values obtained in the optimisation process are tabulated for better perception of the results and are also compared graphically to the values obtained in Chapter 6.

An analysis is also carried out for an unsymmetrical constrained configuration, that is, a structure with a much thinner constraining layer relatively to the host layer. In this case only the cantilever condition in the first three modes of vibration was considered.

The results obtained are consistent with those observed in the previous chapter concerning the parametric study of CLD treatments, thereby, assessing the optimisation methodology that will be used in the subsequent analysis presented in Chapter 8.

Chapter 8

Optimisation of Variable Thickness CLD Treatments

In this chapter, the search for the optimum variable thickness of a VEM layer in a constrained configuration is carried out. The genetic algorithm is, once more, the tool used in the optimisation process and results are confronted with the optimum uniform thickness from the previous chapter.

As mentioned in the introduction to this dissertation, covering the surface of the structure to be treated with viscoelastic material in a partial manner provides a means of reducing the cost of the treatment without jeopardising its efficiency. However, the solution is feasible if only one resonant mode is present in the bandwidth of interest, as the optimum distribution of the VEM varies from one mode to another. In the case of the presence of different modes, coverage of the whole surface with a homogeneous VEM thickness is usually recommended [12]. Nevertheless, optimisation strategies can be applied to reach a partial treatment that is able to efficiently dampen a set of selected modes.

8.1 Optimisation strategy

This section of the study has two main objectives: one is to determine whether the optimisation codes that were used place the largest amount of material in the sections of the beam where the shear strain energy is the highest. In view of the contradictory effects of the volume and strain energies discussed in chapter 6, this analysis aims to determine if it can be assumed in a straight forward manner that the areas of the beam that exhibit the highest strain energy in a layer of homogeneous thickness are the areas where most damping material should be placed; this assumption would simplify the design of partial optimised damping treatments to a great extent.

The other objective is to obtain an approximate shape of a viscoelastic variable cross-section, the dimensions that generate the highest damping effect and confront those results to the loss factors of a VEM layer of homogeneous thickness. This will determine whether a VEM treatment with variable cross-section is a favourable solution comparatively to the homogeneous one.

In order to meet these objectives, two different optimisation tools were used, namely, topology optimisation and optimisation using Genetic Algorithms. The results obtained with the two methods will determine whether the material variable configuration complies with the dissertation objectives.

8.1.1 Genetic Algorithm approach

The genetic algorithm procedure relies on a set of variables to describe the way the VEM layer is distributed on the beam. Several strategies can be used, including the direct attribution of a genetic code for the entire set of finite elements used to represent the host structure. In this study, a different approach is used. Relying on the assumption that the VEM distribution is related to the shear deformation energy distribution along the beam, and due to the relationship between shear strain energy and the deformation that the beam undergoes for a specific mode shape, a trigonometric function was used in the genetic algorithm optimisation.

The genetic algorithm tool from MATLAB uses a code (totalcld.m) to find the variable thickness function of the viscoelastic layer, being described as:

$$h_2(x) = x_1 \left[0.5 \cos\left(\frac{2\pi x}{L}\, x_2 + x_3\right) + 0.5\right] + x_4 \tag{8.1}$$

where four parameters are used: x_1 defines the amplitude of the trigonometric function, x_2 sets the wave length, x_3 introduces a phase shift to the function and x_4 defines a constant, or homogeneous thickness, into the function. This function complies with the distribution of the shear strain energy for both boundary conditions studied in this work (free-free and built-in). Alternative functions should be considered for other boundary conditions.

Establishing a volume equivalence between the variable configuration and a homogeneous distribution of VEM with thickness h_m

$$h_m * L = \int_0^L h_2(x)\, dx \tag{8.2}$$

and integrating (8.1), x_1 can be determined

$$x_1 = \frac{4\pi x_2 (h_m - x_4)}{2\pi x_2 + \sin(2\pi x_2 + x_3) - \sin(x_3)} \tag{8.3}$$

When considering symmetric boundary conditions, the symmetry of the distribution of the VEM over the beam seems to be a plausible assumption. If the symmetry pre-condition is applied to (8.1), a relation between the two parameters x_2 and x_3 can be established as:

$$x_2 = -\frac{x_3}{\pi} \tag{8.4}$$

Replacing this symmetry condition into (8.1) it becomes:

$$h_2^s(x) = x_1\left[\frac{1}{2}\cos\left(\frac{2\pi x}{L} * \left(-\frac{x_3}{\pi}\right) + x_3\right) + \frac{1}{2}\right] + x_4 \tag{8.5}$$

Again, if the volume equivalence is introduced, which can be described by:

$$h_m * L = \int_0^L h_2^s\,(x)dx \tag{8.6}$$

the parameter x_1 can be related to the remaining parameters, x_3 and x_4, as:

$$x_1^s = \frac{2x_3(h_m - x_4)}{x_3 + \sin(x_3)} \tag{8.7}$$

Based on the trigonometric function previously described, the GA code attempts to find a variable shape for the viscoelastic layer that will render a more effective sandwich structure, that is, a structure with a higher loss factor. The genetic algorithm control parameters used in the previous chapter optimisation of a homogeneous cross-section of the VEM have been kept constant.

8.1.2 Topology optimisation

In this work an additional optimisation approach was used so that, on one hand, other optimisation strategies could be tested and, on the other hand, so that an assessment on the reliability of the GA results could be obtained. The topology optimisation method was selected for this purpose due to its suitability for this type of problems. The codes used for this type of optimisation are: "topology.m" and the codes associated with it namely, "strain_energy_topology.m", "assembly.m", "ebeam.m" and "boundaryC.m".

As discussed before (Chapter 5), topology optimisation is based on an operator that defines optimisation in accordance with a selected objective variable. In this case, the optimisation code calculates the distribution of the strain energy for the elements that make up the cross-section of the beam. Depending on the distribution of energy, the allocation of the

viscoelastic material thickness by the code is proportional to the contribution that each finite element has on the total strain energy of the VEM layer. The topologic code is, therefore, designed to place more material in the section of the beam that contributes the most to the damping of the structure. The robustness of this procedure is weak, as evidenced by the results in this chapter; however, the implementation of the topology optimisation proved to be a simple and expeditious method that can produce satisfactory results for some problems, such as the ones in this study.

8.1.3 Commercial applications used

To aid the analysis of the results obtained in this part of the study, a finite element commercial software is also used. The NASTRAN (MSC NASTRAN) software is used in conjunction with FEMAP pre- and post-processor.

NASTRAN is mainly a solver for finite element analysis (FEA); it is a program that was originally developed for NASA in the late 1960s for the Aerospace industry. It consists of several modules. Each module is a collection of FORTRAN subroutines that are designed to perform a specific task, for example, assembling matrices, solving matrix problems, applying constraints, processing model geometry, etc. All input and output to the program is in the form of text files; however, the program is not designed to build or mesh a model graphically.

There are various software programs available in the market to import the results from NASTRAN and show them graphically. One is FEMAP which is an advanced engineering simulation software program that works as a pre- and post-processor to several finite element packages, including NASTRAN. The pre-processing creates finite element analysis models of complex engineering products and systems, and the post-processing displays the solution results. It is also able to model beams, generate high-quality meshing and provide visualisation of the elements as solid components. Visualisation capability is a key feature so that results and the model behaviour can be interpreted and understood quickly.

The simulation applications include basic strength analysis, frequency and transient dynamic simulation, system-level performance evaluation, advanced response, etc. In the case of the analysis being done in this chapter, FEMAP was used to visualise the results from NASTRAN simulations, which include the distribution of the shear strain energy across the beam and the mode shapes for each boundary condition.

8.1.4 Methodology

One of the main goals of this study is to get observations on the main assumption of this thesis concerning the ability to design partial CLD treatments, either based on a variable thickness VEM layer or a stepwise VEM layer configuration, simply by following the shear strain energy distribution of a homogeneous CLD. As such, the study first analyses the extensional energy and the shear strain energy that is developed across the length of the beam in the outer and core layers, respectively.

Then it compares the loss factor values obtained in a core layer of uniform thickness and the loss factors of two variable viscoelastic layer shapes generated by different optimisation processes (genetic and topologic algorithms). In this part of the study, the variable thickness solutions are required to have the same viscoelastic quantity of material used in the homogeneous solution. Several VEM thickness values are considered. The GA procedure used in this study is based on the thickness function described by Equation (8.5).

The variable shape configurations between the topologic and GA are explored for various h_2 ratios.

The complete set of parameters is then used in (8.1) towards the definition of a unique solution with an optimised variable distribution and an optimised volume of VEM. The objective of this last part of the study is to identify, not only the shape of the VEM layer configuration following a variable distribution, but also the volume of VEM that renders the best damping efficiency.

These results will then be compared to the observations obtained in chapter 7 establishing a relation between the optimum volume of VEM for the homogeneous treatment and the volume of VEM obtained for the variable configuration using (8.1). In other words, the comparison aims to identify the relation between the best VEM layer thickness for the homogeneous case, the one located at the efficiency curve peak, and the mean value for the VEM layer thickness of the variable configuration. The comparison between the variable and homogeneous configurations, in so far as material savings and loss factor increase are concerned, is also performed.

Safeguarding the aspect that partial coverage only makes sense when one vibration mode is present, the first three vibration modes were studied separately. Two boundary conditions, namely, free-free and built-in conditions were analysed. The materials used in the CLD structure concerning the study in this chapter are the same as in Chapter 6 and 7.

8.2 Free-free beam

Both ends of the free-free beam have no force or torque constraints.

All structures vibrate at certain frequencies called natural or modal frequencies and when the structure vibrates at these frequencies, the deformation pattern will assume, for all practical purposes, a certain shape that is very similar to the mode shape. The mode shape describes the shape of the structure and it depends on the structure configuration as well as the boundary conditions.

8.2.1 Mode shapes

The shapes of the 1st, 2nd and 3rd natural vibration modes of the laminated beam in free-free boundary conditions are shown in Figure 8.1. They were generated by FEMAP, which was used to post-process the simulation performed by NASTRAN.

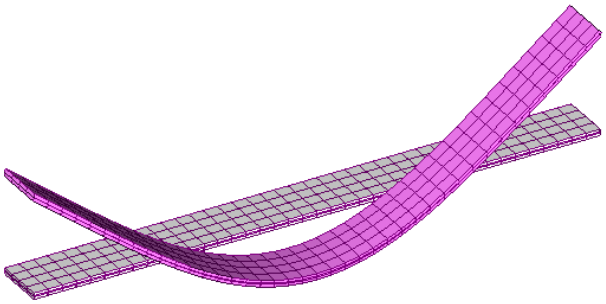

1st natural vibration mode

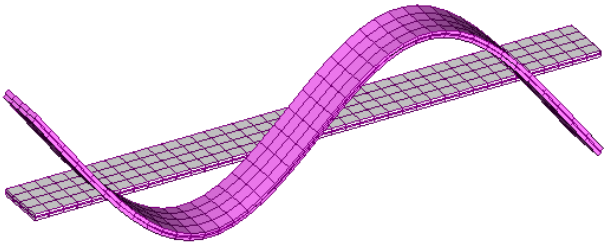

2nd natural vibration mode

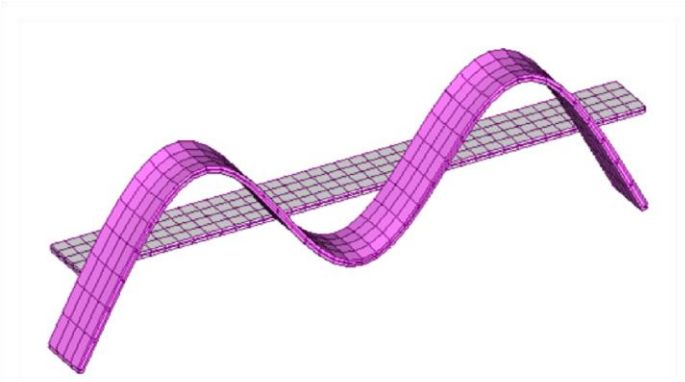

3rd natural vibration mode

Figure 8.1: Natural mode shapes of a free-free beam

8.2.2 First mode

Lengthwise distribution of the extensional strain energy in the base layer

Figure 8.2 and Figure 8.3 are obtained with the MATLAB code "verif_strain_energy.m" and associated codes. The figures show the lengthwise distribution of the extensional strain energy in the base layer of a sandwich structure (being a symmetric configuration, the

observations are the same for the constraining layer). The strain energy in the base layer and in the constraining layer results mainly from the bending and direct (membrane) stresses that act on the beam when it vibrates. In the 1st mode of vibration, this results in the extensional strain having its highest value in the centre of the beam, which is the anti-nodal location for the 1st mode.

The analysis was done on the lowest and highest h_1 ratios considered in the study, namely h_1 = 0.001 (Figure 8.2) and h_1 = 0.02 (Figure 8.3) so that the response of the layers, in so far as the extensional strain energy is concerned, may be compared. It can be observed that in the case of the lowest h_1 ratio (0.001), as the thickness of the VEM increases, the extensional strain energy decreases. This may be explained by the fact that, in the case of very thin aluminium adjoining layers, a much thicker core layer places a higher restriction on the bending of the whole structure. In other words, the thickness increase of the VEM causes a very significant decoupling, which reduces the level of stress and strain in the external layers.

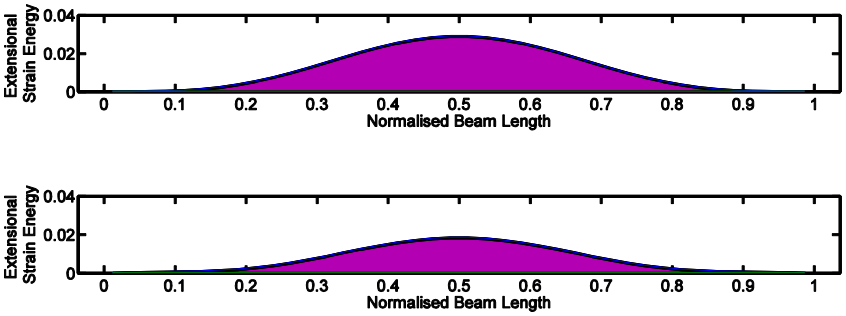

Figure 8.2: Extensional strain energy for h_1 = 0.001

On the contrary, when considering much thicker base and constraining layers (h_1 = 0.02), the opposite happens, that is, as the thickness of the viscoelastic layer increases, the extensional strain energy also increases, as shown in Figure 8.3. A possible explanation could be that the stiffness of the outer layers is sufficiently high to cause the decoupling effect resulting from thicker VEM layers to be less evident.

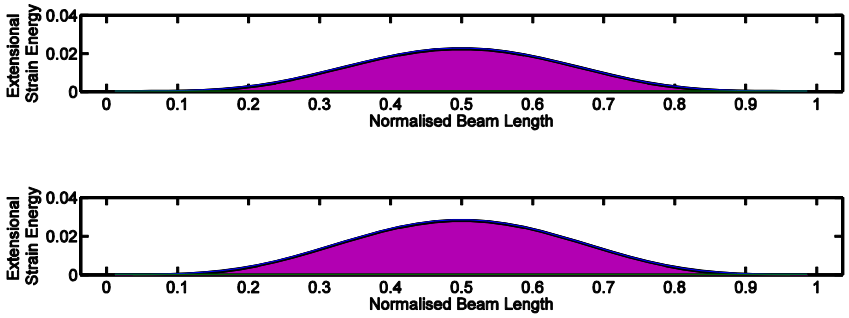

Figure 8.3: Extensional strain energy for $h_1 = 0.02$

Lengthwise distribution of the shear strain energy in a VEM uniform layer

The following figures (Figure 8.4 to 8.7) represent the shear strain energy produced in a viscoelastic layer of homogeneous thickness and they were also generated by the MATLAB code "verif_strain_energy.m".

The shear strain energy accumulated in the VEM is mainly due to shearing stresses imposed by its adjoining layers and, generally speaking, the figures show that the highest strain energy values occur at the nodal points. The above mentioned figures represent various h_1 and h_2 ratios.

For very small h_1 ratios (h_1 = 0.001 and h_1 = 0.002), as the thickness of the viscoelastic material increases, there is an overall increase of the strain energy, not only at the nodes, but also at the extremities. As these ratios do not exhibit the loss factor peak values discussed in the previous two chapters, an increase of the h_2 ratio is accompanied by an increase in the shear strain energy. This is illustrated in Figure 8.4 and Figure 8.5.

As the thickness of the base and constraining layers increase (h_1 = 0.006 and higher ratios), the shear strain energy at the extremities becomes increasingly more relevant reaching, in some cases, almost the same value as the strain energy at the nodes.

However, the shear strain energy in the case of these higher h_1 ratios increases only up to a certain h_2 ratio and starts to decrease after that, that is, up to the peak value an increase in

the h_2 ratio corresponds to higher shear strain energy; after the peak, thicker viscoelastic layers exhibit lower values of shear strain energy. The inversion of the relationship happens at the peak of the loss factor curves. This occurrence is particularly evident in Figure 8.7.

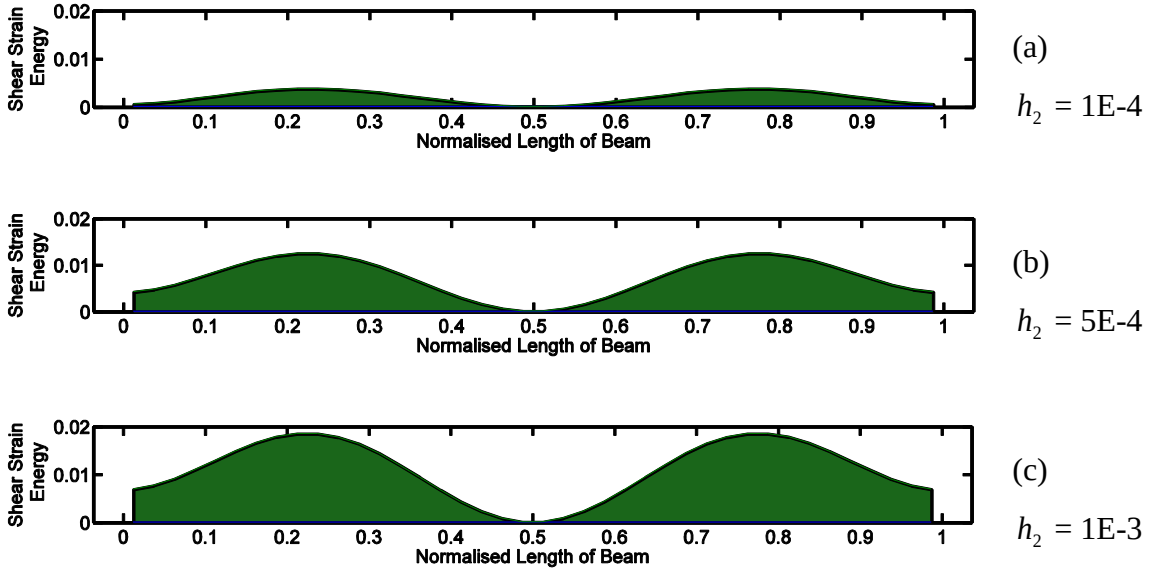

Figure 8.4: VEM layer shear strain energy for h_1 = 0.001

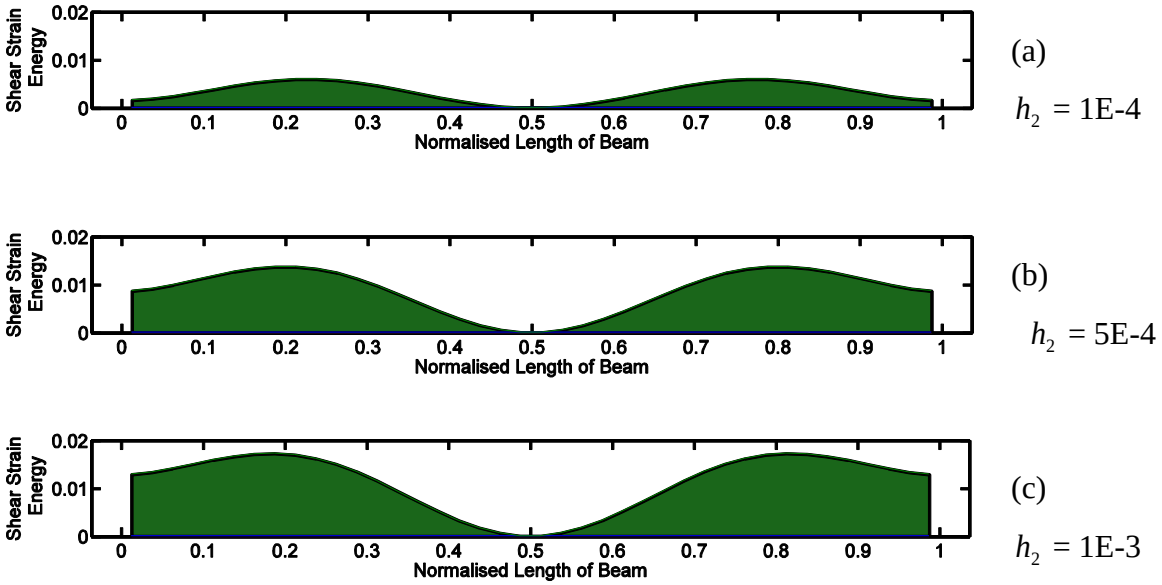

Figure 8.5: VEM layer shear strain energy for h_1 = 0.002

If a comparison is done between core layers of the same thickness (e.g. h_2 = 1E-4) but with different h_1 ratios, it can be observed that thicker adjoining layers produce higher shear strain energy (comparison between the (a) subplot of each figure). This finding is coherent with the analysis that was done in Chapters 6 and 7 on the effect of the constraining layer thickness, where thicker constraining layers produce higher loss factors (Figure 6.7).

The analysis carried out in this section of the study involves not only the constraining layer, but the host layer as well. However, this difference does not invalidate the analogy between the two cases and the conclusion that thicker adjoining layers generate higher loss factors.

Since the damping ratio is related to the strain energy stored in the viscoelastic layer, one would expect its increase when dealing with thicker host and core layers, which is the case in the comparison mentioned in the previous paragraph.

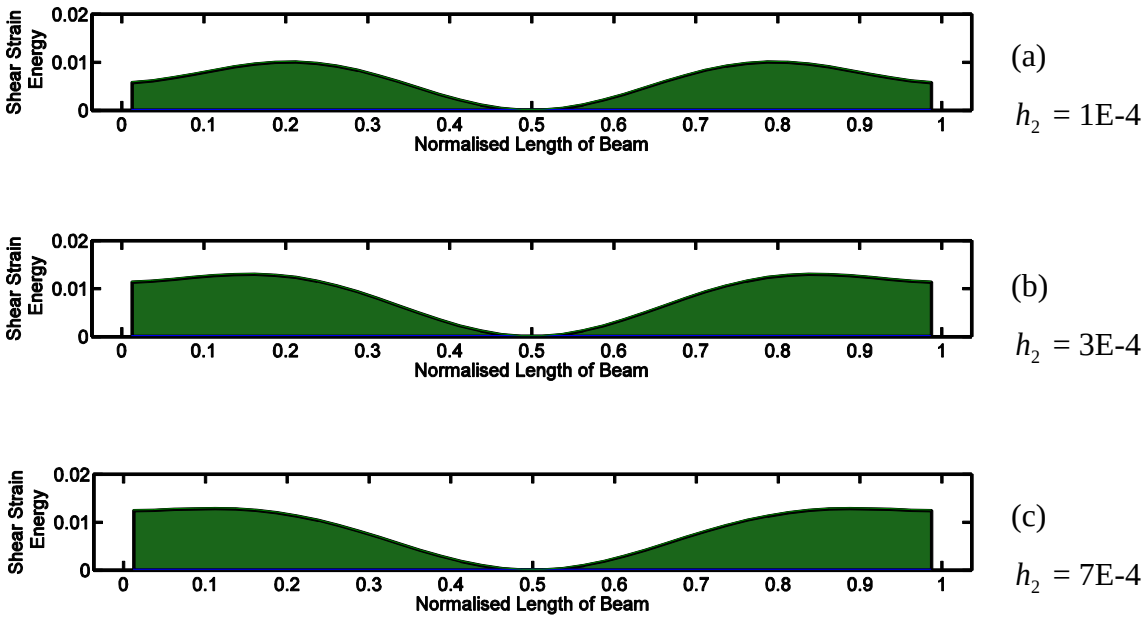

Figure 8.6: VEM layer shear strain energy for h_1 = 0.006

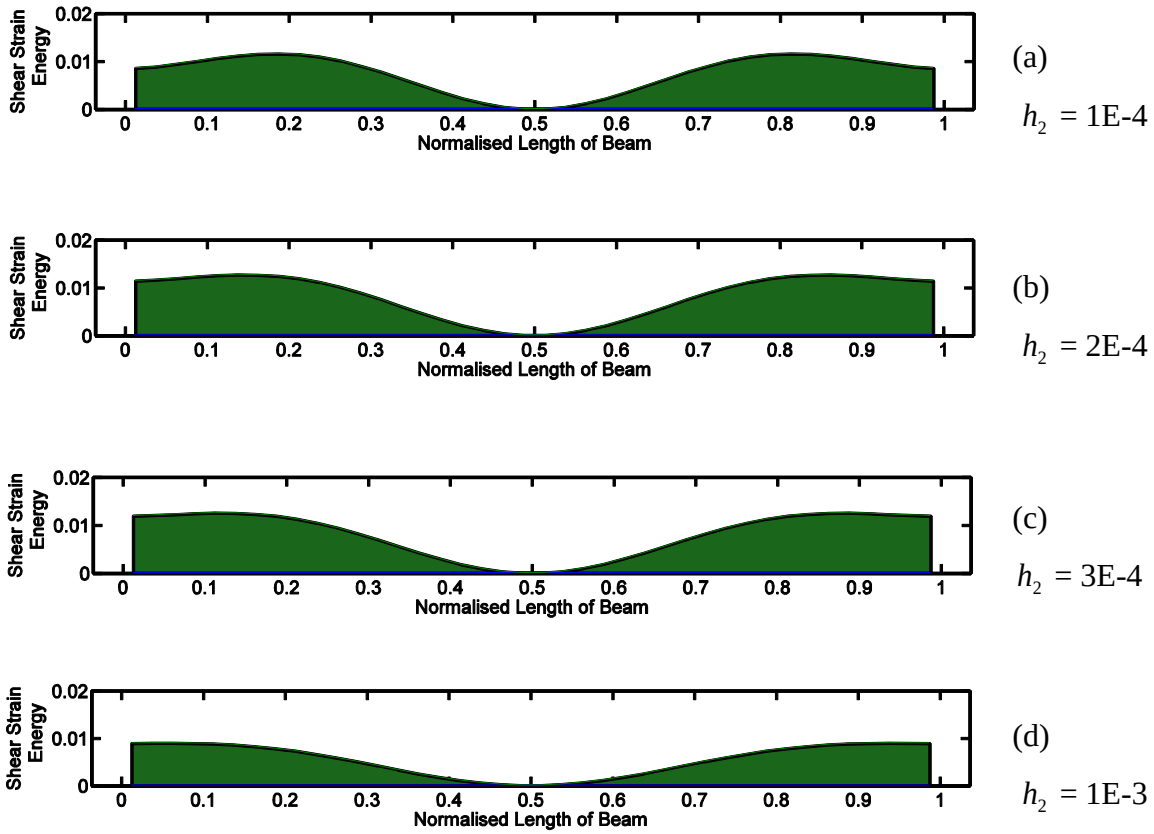

Figure 8.7: VEM layer shear strain energy for $h_1 = 0.01$

To confirm the results obtained in the above figures, an independent analysis was performed using NASTRAN. The beam was modelled as a 3D body using three layers of low order (8-node) hexaedral finite elements to represent the three material layers of the composite beam: host beam, VEM layer and constraining layer. The FEMAP software program was then used to visualise the results concerning the distribution of the shear strain energy in the viscoelastic layer of the composite structure. A top view of the VEM layer (length/width) with the distribution of the shear strain energy is represented in Figure 8.8 (ratio $h_1 = 0.01$ and h_2 = 3E-4). The highest levels of strain energy are shown in darker shades of grey, that is, at the extremities and nodal areas.

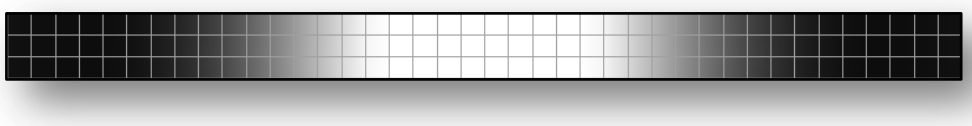

Figure 8.8: Shear strain distribution: VEM layer top view (FEMAP)

Shape optimisation of a variable VEM layer

This section of the study analyses two aspects regarding the optimisation of the core layer. Firstly, the values of the loss factors obtained for a homogeneous VEM layer are compared to the loss factors of the topologic and GA optimisation. Secondly, the GA and topologic algorithms generate the variable shape for the VEM layer that will produce higher loss factors than that of a uniformly distributed layer.

Analysis of the loss factor for various thicknesses of VEM layers

Regarding the analysis of the loss factor versus the thickness of uniform and variable layers, there are four representations under comparison. The reference curve (solid black line) represents the efficiency for a homogeneous CLD configuration. The curve (solid red line) represents a variable configuration rendering the best efficiency following a topology optimisation procedure. The two previously mentioned curves were generated simultaneously by the code "topology.m".

The loss factor values obtained with the Genetic Algorithm MATLAB tool and code "totalcld.m" (blue star markers) are represented at specific core thicknesses. The ratio between the loss factors produced by the GA and the ones obtained for a uniform thickness is also represented (green curve with triangular markers). The sandwich structure is symmetrical and multiple h_1 ratios are examined (Figures 8.9, 8.11, 8.13, 8.15, 8.17 and 8.19).

The GA optimisation is based on the trigonometric functions (Equations (8.5) and (8.7)) where two restrictions are imposed: the predefined volume of the VEM layer and the symmetry of the distribution function. Symmetry is imposed by making the period (x_2) dependent on the phase shift (x_3), as described by Equation (8.4). The volume constraint is introduced by Equation (8.6) establishing that the variable configuration will have the same amount of viscoelastic material as a predefined homogeneous one. The genetic algorithm is, therefore, left with two variables to be optimised, x_3 and x_4 (the vertical shift) using Equation (8.5) in conjunction with Equation (8.7).

The GA constraint bounds are set within a wide range of values so as to avoid conditioning the results. Broadly speaking, as an example, the phase shift represented by the variable x_3 in Equation 8.5 is allowed to vary between $0.1*\pi$ and $10*\pi$. The loss factors thus obtained by the genetic algorithm configuration are higher than the homogeneous configuration loss factors for all h_1 ratios that have been studied. It also produces better results than the topologic configuration for all but one h_1 ratio (0.001).

Seeing that the function used by the GA is based on the optimisation of a VEM layer whose thickness is equivalent to a uniform thickness, the satisfying results obtained with GAs means that with the same amount of material, a variable shape proves to be more efficient. This fact is evident, both in the case of the monotonic and non-monotonic efficiency curves. As far as the former are concerned, the GA consistently obtains higher damping values. The non-monotonic curves reveal that the peak of the variable cross-section happens for smaller h_2 ratios, that is, to the left (and above) the homogeneous curve peak. This means that a reduction of material on the part of the variable shape is translated into higher loss factors.

The curve of the ratio between the loss factor of the variable shape generated by the genetic algorithm and the loss factor obtained for a layer of homogeneous thickness (green curve) also demonstrates the performance superiority of the variable shape, especially for thinner core layers.

A careful examination of the ratio curves for the various h_1 ratios show different trends. In the monotonic efficiency curves, the ratio tends towards an asymptotic loss factor value, meaning that after a certain point, the use of a variable shape is not considered beneficial. In the efficiency curves with a peak, although the ratio curves pick up slightly at the end of their trajectory, it is expected that they will also decrease towards an asymptotic unity level. Common sense presumes that when the amount of VEM is too high, the effect of the optimised placement of the damping material may be rendered null.

Figure 8.13 (also Figure 8.46) displays a slightly different tendency in comparison with other h_1 ratios. With respect to the efficiency curves, the peak is initially followed by a

slight decrease and then a clear tendency to increase after that. These curves correspond to a set of parameters evidencing a mixed behaviour between a configuration with an efficiency curve with a distinct peak (e.g. Figure 8.15) and a configuration with the conventional monotonic and asymptotic efficiency curve (e.g. Figure 8.13). Concerning the ratio between the optimised configuration efficiency (from GA) and the efficiency obtained with the homogeneous configuration, it decreases drastically near the peak of the efficiency curve; after the peak, the ratio starts increasing. In other words, in stark contrast to the other ratio curves, the one in Figure 8.13 exhibits a dip in its shape.

With respect to the topologic variable shape and the ratios with an evident peak, there are two distinct situations: before and after the damping factor peak value. Up to the peak, both the topologic and GA configurations obtain higher loss factors than the uniform thickness.

After the peak, the GA configuration continues to perform well, obtaining higher loss factors than the topologic or the uniform configurations. On the contrary, the topologic performs even worse than the uniform thickness. The reason for this is that the topologic algorithm is based on a direct relationship between the efficiency of the treatment and the thickness of the VEM at a specific point in the beam. This relationship is only feasible in the region of the efficiency curve where this direct relation exists, that is, before the peak value. After the peak occurrence, there is an inversion of this relationship and the topology algorithm operates against the real optimisation aim. This explains the fact that for ratios without a peak (h_1 = 0.001 and h_1 = 0.002), the performances of the topologic and GA configurations are both better than the homogeneous thickness configuration (Figure 8.9 and 8.11).

Distribution of VEM across the beam

As far as the thickness distribution of the viscoelastic material across the beam is concerned and considering each h_1 ratio, the viscoelastic variable shape is analysed for various VEM thicknesses (usually at the beginning, middle or peak value and end of the

respective analysis spectrum). Figures 8.10, 8.12, 8.14, 8.16, 8.18 and 8.20 represent the variable configurations for selected h_2 ratios.

Both the topologic and the Genetic Algorithms produce similar results, that is, both show the same trend in the placement of the material. They reveal the tendency to concentrate most of the damping material away from the centre of the beam.

At the beam extremities, the distribution is slightly different for the various h_1 ratios. This is a result of the limited representation of the thickness function used in the GA optimisation. The topologic optimisation minimises the amount of material at mid-span of the beam while concentrating most of the the available material near the anti-nodal locations of the natural mode (in accordance with the strain energy of the VEM layer, as depicted in Figures 8.4 to 8.7). The GA tries to get a similar result using the available thickness function. This tendency is present in all h_1 ratios but is particularly noticeable in Figure 8.10 which illustrates the variable shapes generated by the topologic and GA codes for the lowest h_1 ratio (0.001). It can be seen that the two optimisation codes placed very little material at the extremities of the beam, coinciding with the low shear strain energy at those points (see Figure 8.4).

With the increase of both the h_1 and h_2 ratios, there is also an increase of material thickness at the very tip of the beam (in compliance with the increase of the shear strain energy previously shown).

It is important to recall here that no symmetry constraints are imposed to the topologic optimisation; even so, its results show that symmetry has been preserved. The volume of the VEM layer is maintained by the topologic procedure since it operates by moving material from one element to another, depending on its contribution to damping.

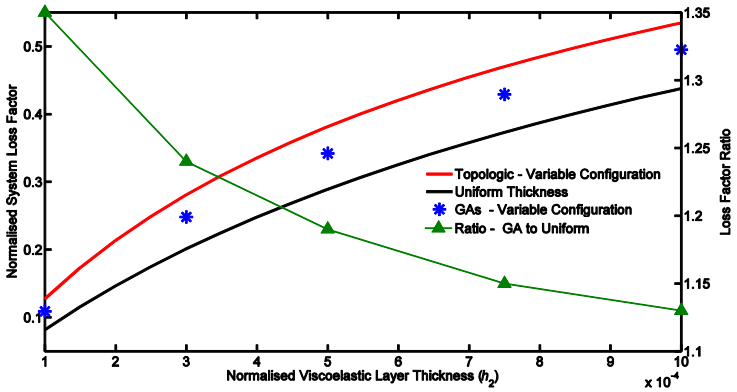

Figure 8.9: Loss factor vs. thickness of uniform and variable layers for h_1 = 0.001

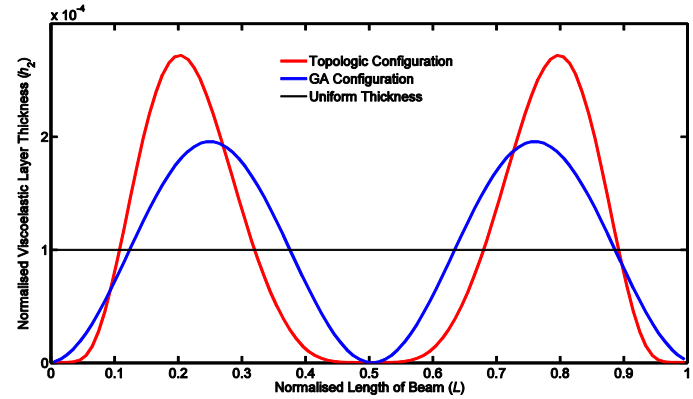

(a) h_2 = 1E-4

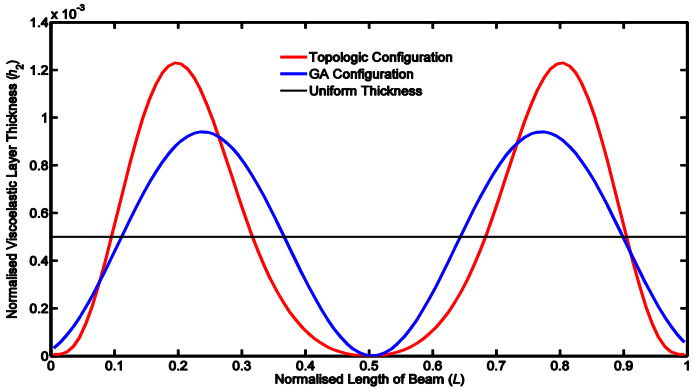

(b) h_2 = 5E-4

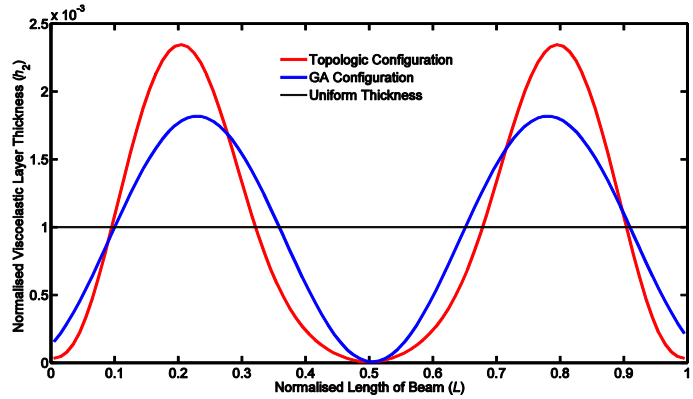

(c) h_2 = 1E-3

Figure 8.10: Uniform thickness and variable configurations for h_1 = 0.001

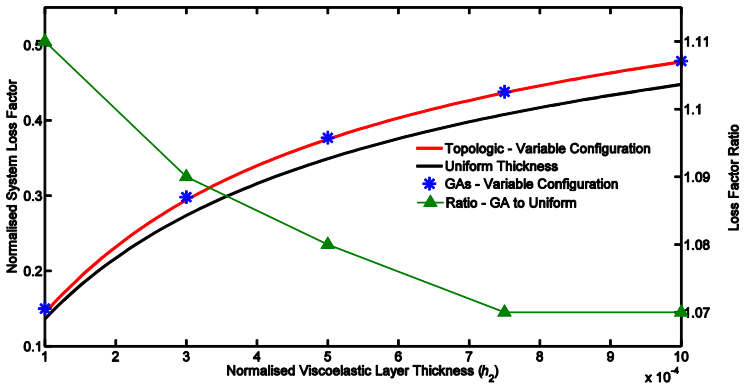

Figure 8.11: Loss factor vs. thickness of uniform and variable layers for h_1 = 0.002

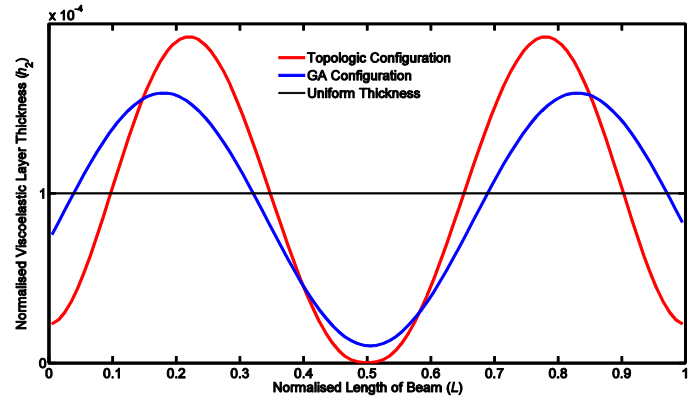

(a) h_2 = 1E-4

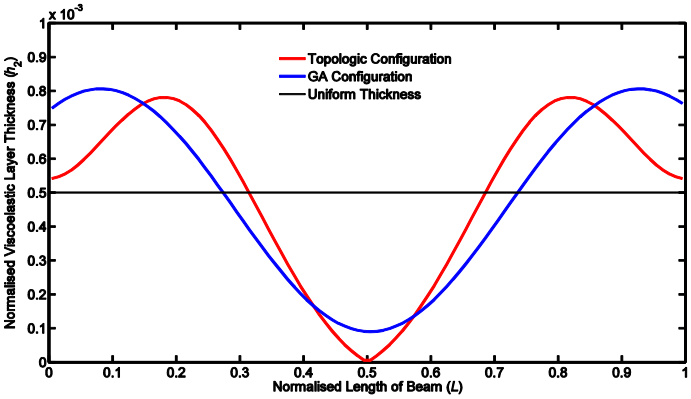

(b) h_2 = 5E-4

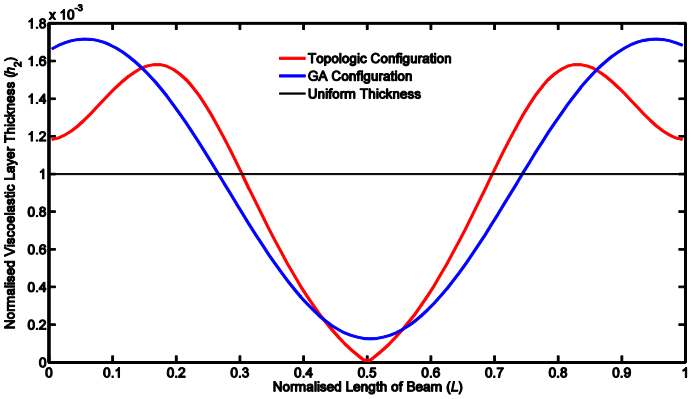

(c) h_2 = 1E-3

Figure 8.12: Uniform thickness and variable configurations for h_1 = 0.002

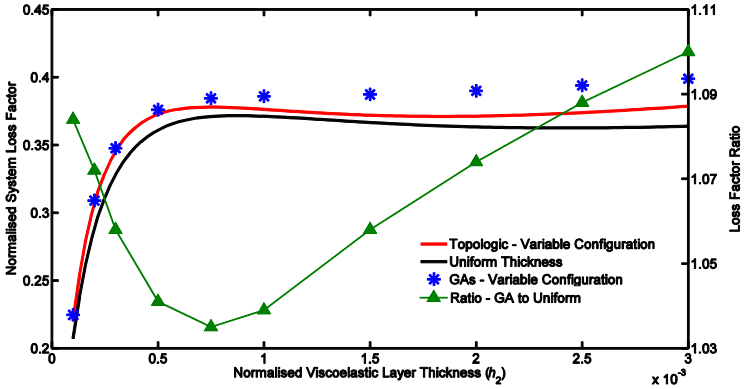

Figure 8.13: Loss factor vs. thickness of uniform and variable layers for h_1 = 0.004

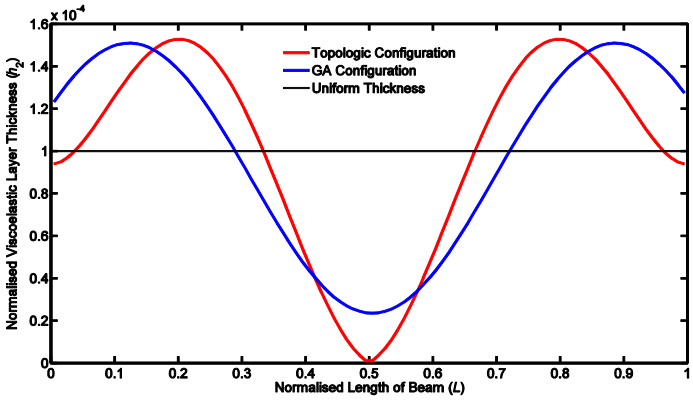

(a) h_2 = 1E-4

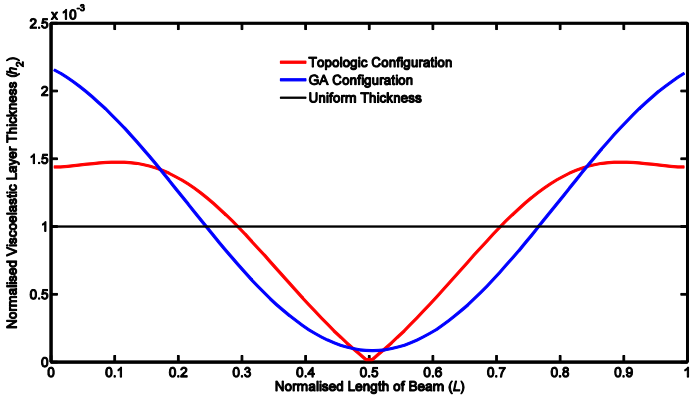

(b) h_2 = 1E-3

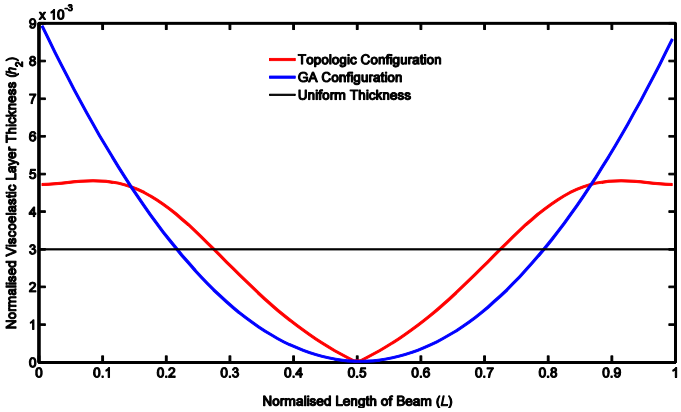

(c) h_2 = 3E-3

Figure 8.14: Uniform thickness and variable configurations for h_1 = 0.004

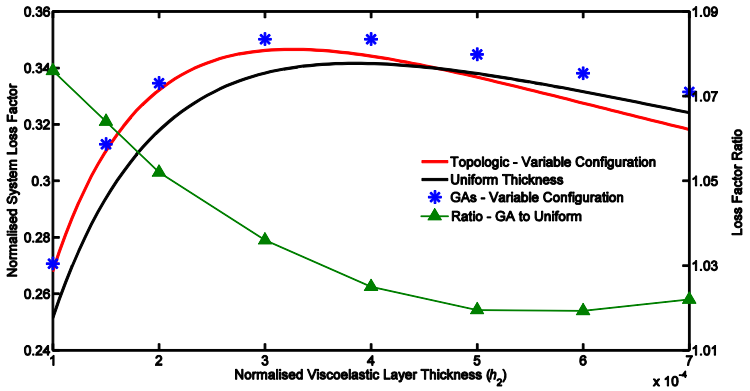

Figure 8.15: Loss factor vs. thickness of uniform and variable layers for h_1 = 0.006

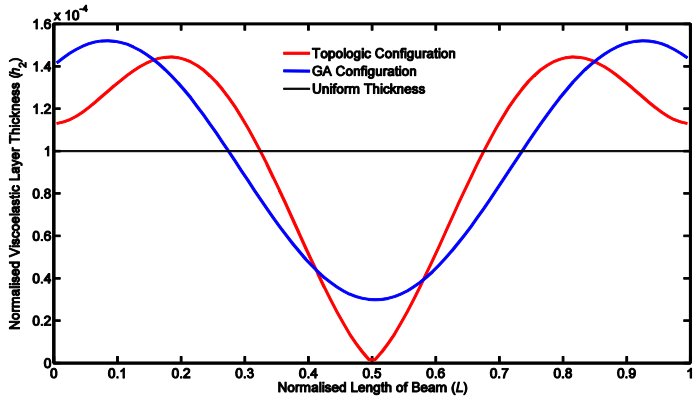

(a) h_2 = 1E-4

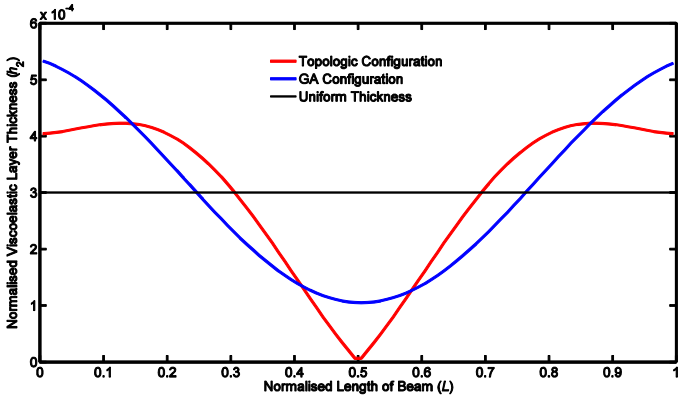

(b) h_2 = 3E-4

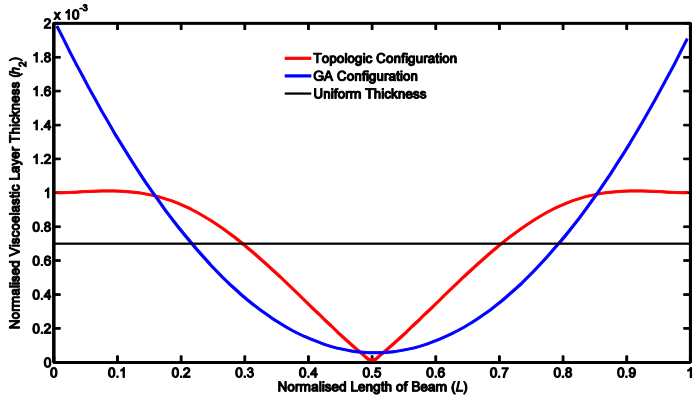

(c) h_2 = 7E-4

Figure 8.16: Uniform thickness and variable configurations for h_1 = 0.006

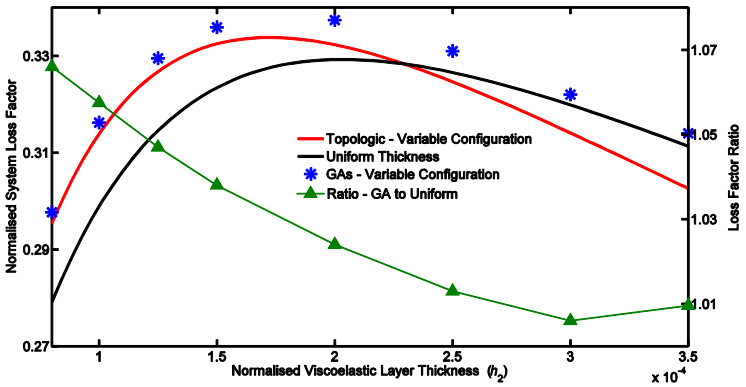

Figure 8.17: Loss factor vs. thickness of uniform and variable layers for h_1 = 0.01

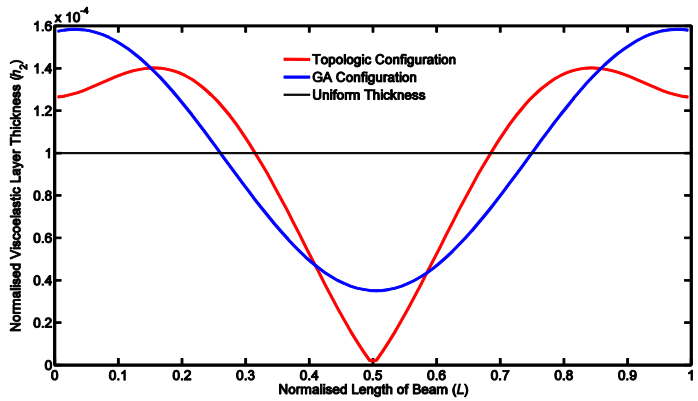

(a) h_2 = 1E-4

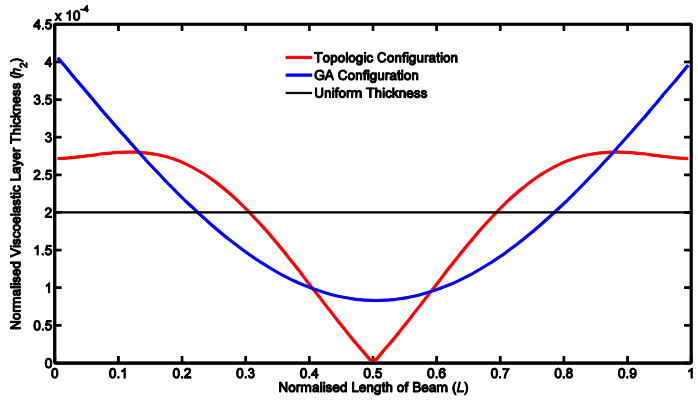

(b) h_2 = 2E-4

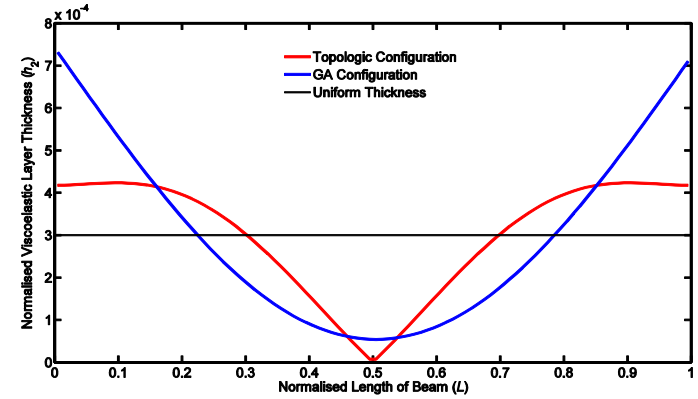

(c) h_2 = 3E-4

Figure 8.18: Uniform thickness and variable configurations for h_1 = 0.01

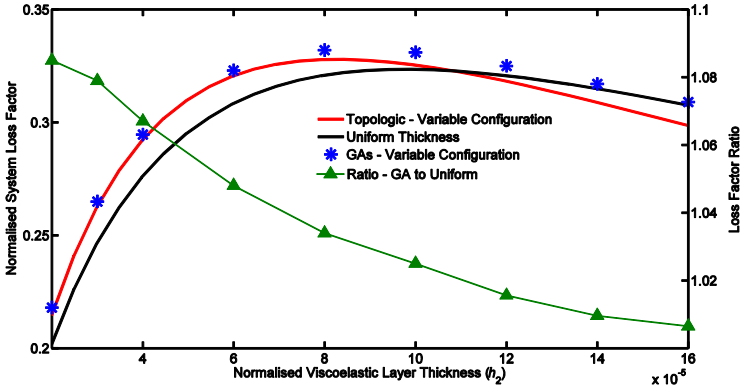

Figure 8.19: Loss factor vs. thickness of uniform and variable layers for h_1 = 0.02

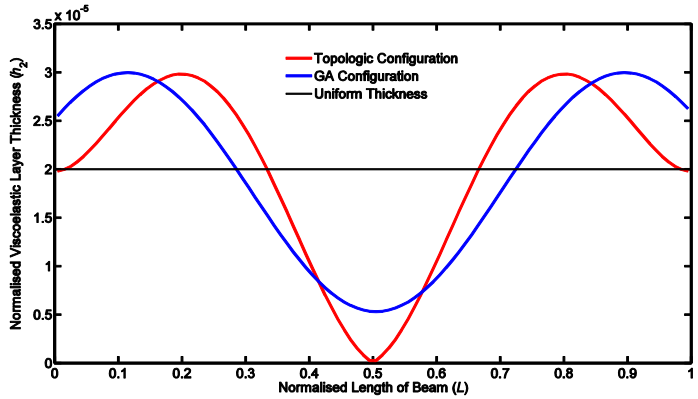

(a) h_2 = 2E-5

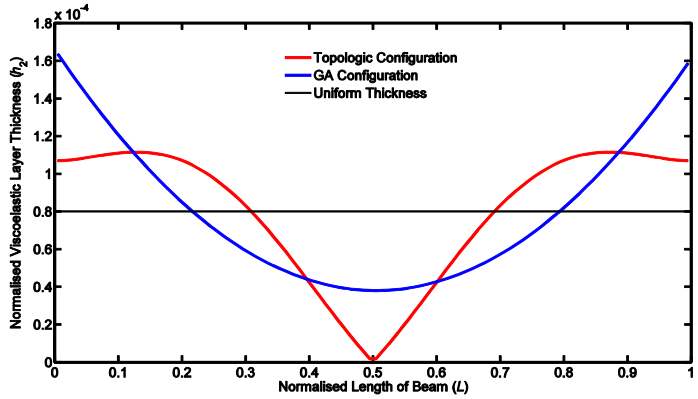

(b) h_2 = 8E-5

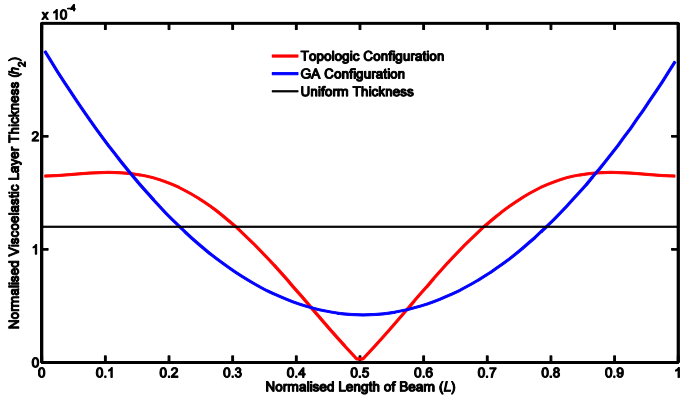

(c) h_2 = 1.2E-4

Figure 8.20: Uniform thickness and variable configurations for h_1 = 0.02

Volume and shape optimisation with GAs of a variable VEM layer

This optimisation is based on the general trigonometric function represented in (8.1) where the GA tool optimises its four variables, that is, the restrictions imposed on the volume and symmetry of the previous section are no longer present (code – "totalcld"). Since no constraint on the amount of VEM is imposed, the optimisation procedure will simultaneously produce an optimised shape of the variable distribution of VEM and an optimum value of VEM volume (quantified here as an equivalent homogeneous thickness). Table 8.1 shows the variables lower and upper constraint bounds that were set for the genetic algorithm optimisation of four variables and the results obtained. The variable x_1 represents the amplitude of the configuration and in the case of h_1 = 0.006, (as an example) it is set between zero and 2E-3, which is believed to provide an adequate search space as the thickness of most viscoelastic materials is approximately one-tenth [39, 41] of the mentioned upper bound. The variable x_2 represents the period and x_3, the phase shift. As it can be seen in Table 8.1, the former is broadly set between 0.1 and 10 to avoid conditioning the results and the latter between zero and π. The genetic algorithm is able to find compensatory values for these two variables, thus, providing a symmetric configuration (see Figure 8.21). Finally x_4 represents the vertical shift, which is allowed to vary between zero and 0.5E-3.

Table 8.1: Constraint bounds and results for three h_1 ratios

Ratios	**h_1 = 0.006**				**h_1 = 0.01**				**h_1 = 0.02**			
Variables	x_1	x_2	x_3	x_4	x_1	x_2	x_3	x_4	x_1	x_2	x_3	x_4
GA Lower Bounds	0	0.1	0	0	0	0.1	0	0	0	0.1	0	0
GA Upper Bounds	2 E-3	10	π	0.5 E-3	1 E-3	10	π	0.1 E-3	1 E-3	10	π	0.05 E-3
GA Results	0.59 E-3	0.76	0.72	0.13 E-3	0.35 E-3	0.67	1.02	0.07 E-3	0.15 E-3	0.89	0.27	0.027 E-3

The GA results shown in Table 8.1 were used to plot the dotted line configuration in Figure 8.21, which represents the three h_1 ratios with a peak loss factor. The figure

compares the configuration resulting from volume and shape optimisation to the configuration obtained exclusively with shape optimisation for a VEM thickness that generates the highest loss factor. The configurations are somewhat identical, thereby confirming the reliability of the results obtained for the four variables.

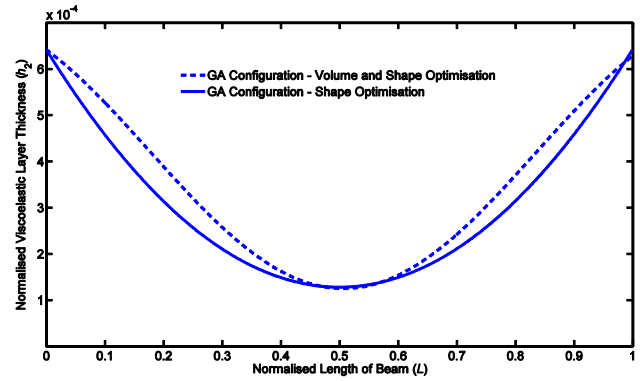

(a) $h_1 = 0.006$

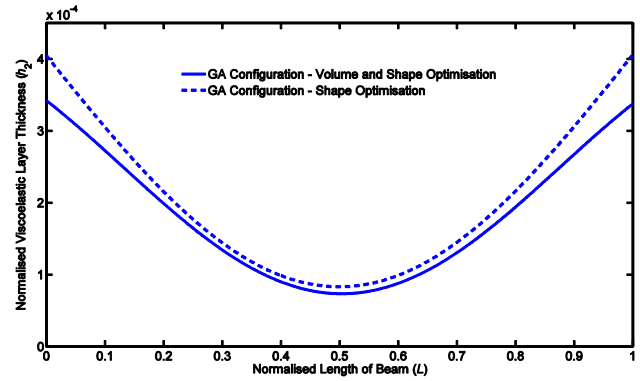

(b) $h_1 = 0.01$

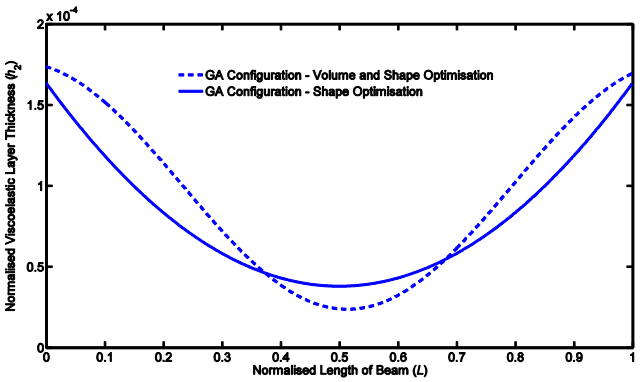

(c) $h_1 = 0.02$

Figure 8.21: GA variable configurations for 3 h_1 ratios

Analysis of uniform versus variable configurations (three h_1 ratios)

Table 8.2 presents a comparison between the average thickness of the variable VEM layer (average amount of material) obtained with the results from Table 8.1 using the generic

function with four paramenters and the thickness of the homogeneous layer rendering the highest efficiency (Table 7.1). These are h_2 ratios that correspond to the highest loss factor.

Table 8.2: Optimum VEM layer thickness for three h_1 ratios

	h_1 = 0.006	h_1 = 0.01	h_1 = 0.02
Average h_2 (4 var.)	3.35 E-4	1.77 E-4	9 E-5
Uniform configuration	3.85 E-4	2.03 E-4	10.5 E-5

Based on the results from Table 8.2, Figure 8.22 represents the percentage saving, in terms of viscoelastic material, that the configuration obtained with the volume and shape optimisation has over the homogeneous configuration.

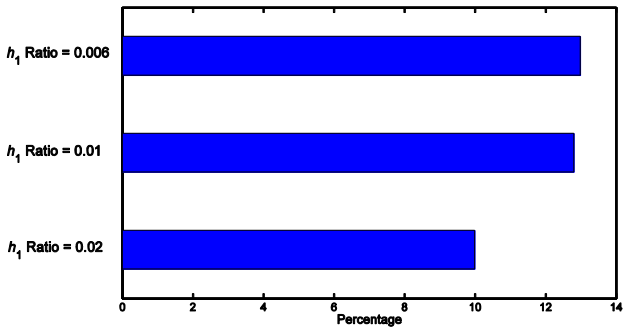

Figure 8.22: Percentage reduction of VEM

Table 8.3 presents the loss factor values corresponding to the optimum viscoelastic layer thicknesses shown in Table 8.2 and Figure 8.23 shows the respective percentage increase of the variable configuration (obtained with shape and volume optimisation) over the uniform configuration loss factors.

Table 8.3: Optimum loss factors for three h_1 ratios

Ratios	h_1 = 0.006	h_1 = 0.01	h_1 = 0.02
Average h_2 (4 var.)	0.3506	0.3379	0.3304
Uniform configuration	0.3417	0.3294	0.323

These results coincide with the ones generated by the shape optimisation, that is, with less viscoelastic material the variable configuration is able to obtain higher loss factors.

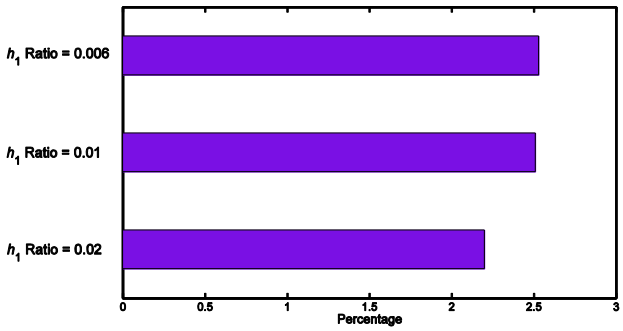

Figure 8.23: Percentage increase of loss factors

8.2.3 Second mode

Lengthwise distribution of the extensional strain energy in the base layer

The extensional strain energy generated in a structure undergoing vibrations in the second natural mode and whose dimensions are equivalent to a ratio $h_1 = 0.001$ is represented in Figure 8.24. Figure 8.25 represents the extensional strain energy in the case of $h_1 = 0.01$.

The findings observed in the 1st mode of vibration also apply to the 2nd mode, that is, with an increase in the VEM thickness, there is a slight decrease of strain energy in low h_1 ratios and the inverse happens in higher h_1 ratios. The same conclusions are applicable to the constraining layer of a CLD symmetrical configuration.

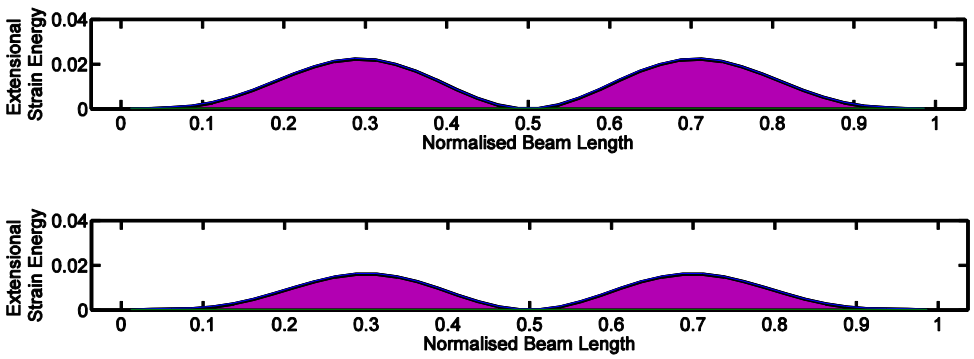

Figure 8.24: Extensional strain energy for $h_1 = 0.001$

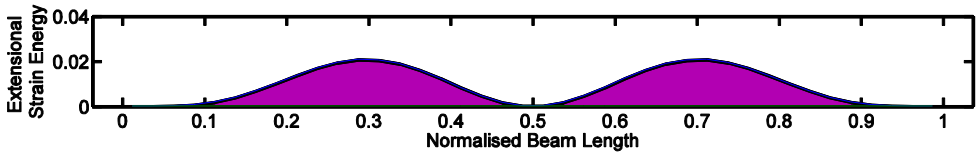

(a)

h_2 = 1E-4

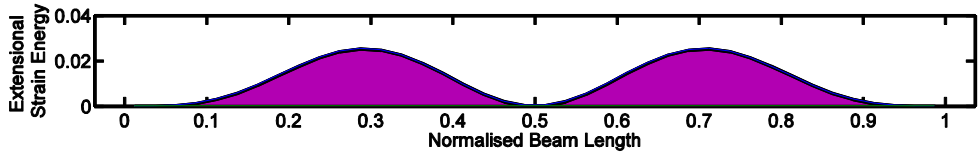

(b)

h_2 = 5E-4

Figure 8.25: Extensional strain energy for h_1 = 0.01

Lengthwise distribution of the shear strain energy in a VEM uniform layer

The shear strain energy for h_1 = 0.001 is shown in Figure 8.26 where an increase in the h_2 ratio corresponds to an increase in shear strain energy, as in the case of the 1st mode. In the 2nd natural mode of vibration, the concentration of the shear strain energy occurs at the three nodes and extremities; however, it exhibits its highest value in the centre of the beam.

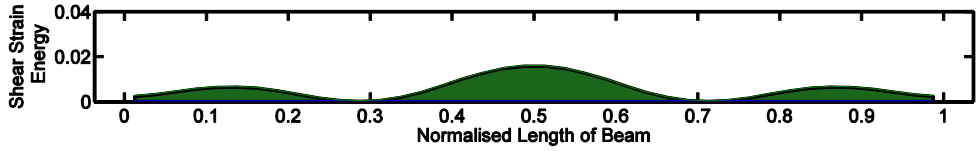

(a)

h_2 = 1E-4

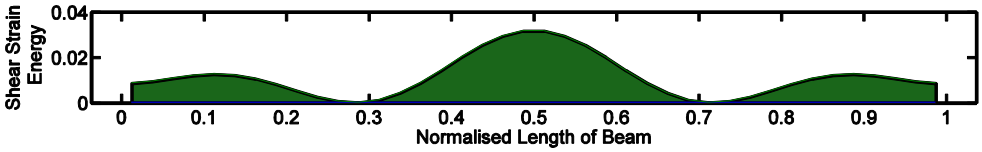

(b)

h_2 = 5E-4

Figure 8.26: VEM layer shear strain energy for h_1 = 0.001

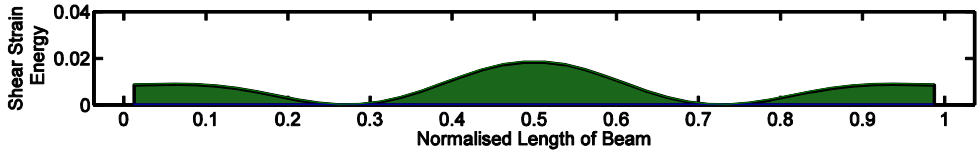

(a)

h_2 = 1E-4

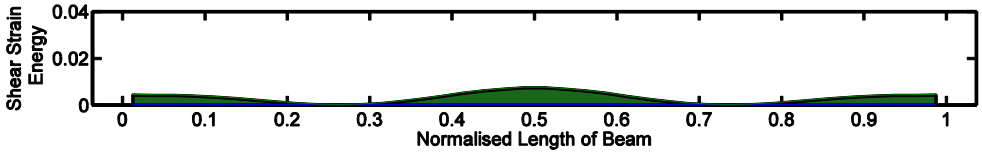

(b)

h_2 = 5E-4

Figure 8.27: VEM layer shear strain energy for h_1 = 0.01

However, for higher ratios and similarly to what happens in the 1st mode, once the loss factor reaches its peak value an increase in the amount of viscoelastic material corresponds to a reduction of the strain energy (Figure 8.27).

Once more, an analysis was performed with NASTRAN to confirm the results from the MATLAB routines. The darker grey shade in Figure 8.28 clearly shows a higher incidence of shearing strain energy in the centre of the beam relatively to the extremities (h_1 = 0.001 and h_2 = 5E-4). This distribution can be favourably compared to Figure 8.26 (b).

Figure 8.28: Shear strain distribution: VEM layer top view (FEMAP)

Shape optimisation of a variable VEM layer

The comparison between the loss factors obtained with the GA and topologic variable cross-sections and a uniform one, is shown in Figure 8.29 and it represents three different h_1 ratios. In the case of the lowest h_1 ratio (0.001), both the GA and topologic configurations obtain better results than the uniform configuration.

In the cases where the damping factor forms a peak (h_1 = 0.006 and h_1 = 0.01), after the peak, the GA configuration practically coincides with the homogeneous configuration (or is even slightly inferior). This may be due to the limitation of the GA function representation. In other words, after the peak, the GA variable shape does not represent a major advantage over the uniform configuration as the corresponding results rapidly tend towards the efficiency curve of the homogeneous configuration. This observation is consistent with the general view that for higher VE thicknesses, the gain obtained with the optimal placement is reduced or even negligible, thereby, not justifying the optimised configuration relatively to the homogeneous layer. The topologic variable core layer obtains considerably lower damping factors. The shapes of the topologic and GA configurations are shown in Figure 8.30 and it refers to h_1 = 0.001 and h_2 = 5 E-4. This configuration remains somewhat constant for the different h_1 and h_2 ratios.

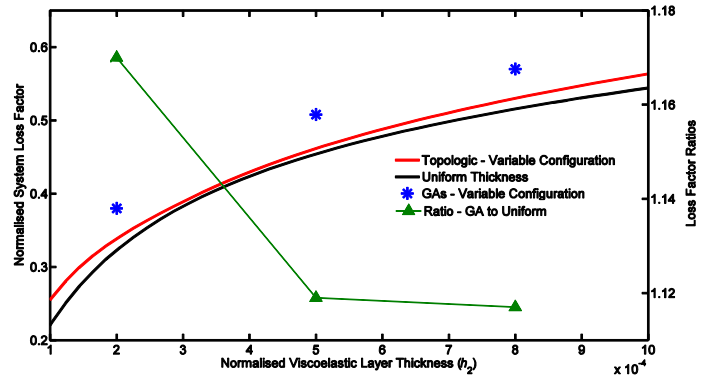

(a) $h_1 = 0.001$

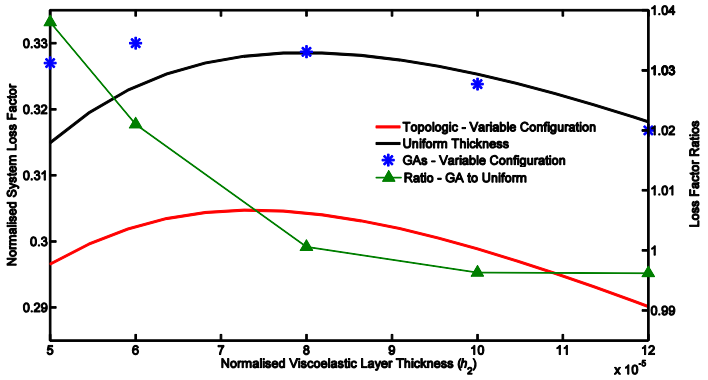

(b) $h_1 = 0.006$

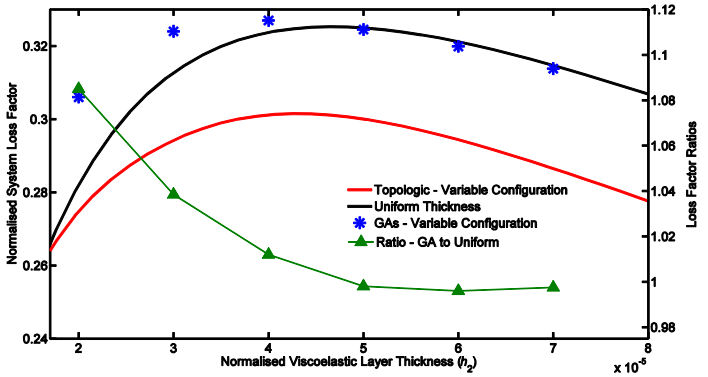

(c) $h_1 = 0.01$

Figure 8.29: Loss factor vs. thickness of uniform and variable layers for 3 h_1 ratios

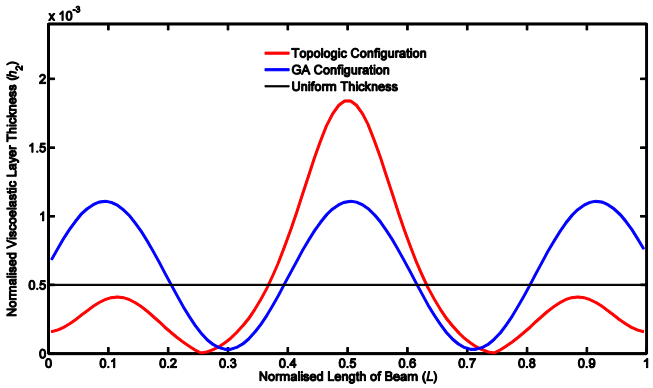

Figure 8.30: Uniform thickness and variable configurations

Volume and shape optimisation with GAs of a variable VEM layer

The genetic algorithm optimisation of the shape and volume taking into consideration the four variables in (8.1) was also carried out for the second mode of vibration and h_1 = 0.01 in order to obtain an optimal variable core layer.

The results are presented in Table 8.4 and Figure 8.31 compares the configuration thus obtained to the configuration produced by the optimisation based on volume and symmetry constraints (Equations 8.5 and 8.7) i.e. based on shape optimisation only.

Table 8.4: Constraint bounds and results for h_1 = 0.01

Variables	GA Lower Bounds	GA Upper Bounds	GA Results
x_1	0	1 E-4	6.02 E-5
x_2	1	10	1.92
x_3	0	π	0.235
x_4	0	0.1 E-4	9.7 E-6

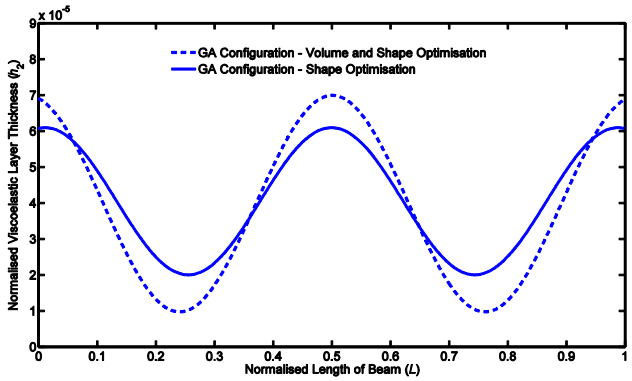

Figure 8.31: GA variable configurations for h_1 = 0.01

8.2.4 Third mode

Lengthwise distribution of the extensional strain energy in the base layer

In the 3rd natural mode of vibration, taking into consideration various h_1 and h_2 ratios, it was observed that the variance in the extensional strain energy is insignificant and does not warrant the graphical representation of different figures. One example is shown in Figure 8.32 to illustrate the general contour, which also applies to the constraining layer of a CLD symmetrical configuration.

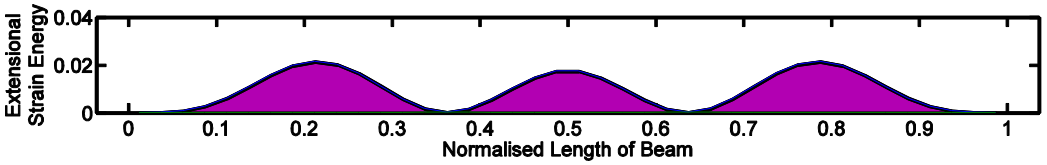

Figure 8.32: Extensional strain energy for h_1 = 0.01

Lengthwise distribution of the shear strain energy in a VEM uniform layer

In line with the previous two modes, the strain energy higher levels also occur at the nodes and both tips of the beam. The observations with respect to the 3rd mode concerning the variation of the shear strain energy with different h_1 and h_2 ratios are consistent with the results obtained in the 2nd mode. Figures 8.33 and 8.34 are representative of h_1 ratio = 0.01 and they show that at both tips of the beam, thicker viscoelastic layers undergo higher shear strain energy.

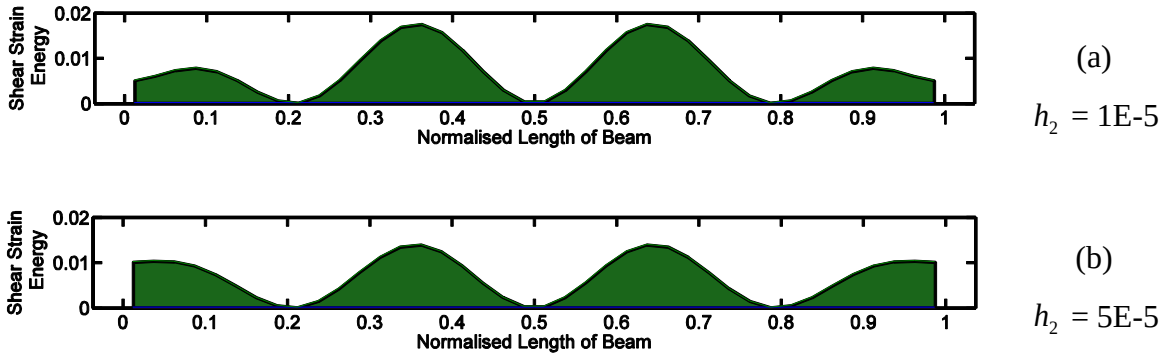

Figure 8.33: VEM layer shear strain energy for h_1 = 0.01

In accordance with the procedure used in the two previous modes, Figure 8.34 shows the results obtained by the NASTRAN simulation software.

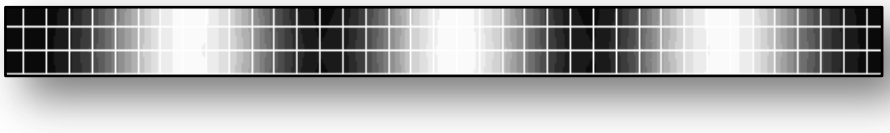

Figure 8.34: Shear strain distribution: VEM layer top view (FEMAP)

Shape optimisation of variable VEM layer

With respect to the lowest h_1 ratio, Figure 8.35 (a) shows (similarly to the modes previously analysed) the prevalence of the configuration generated by the genetic algorithm over the uniform pattern. The higher ratios with a loss factor peak perform identically in relation to the 2nd mode.

The damping factors produced by the topologic shape are generally inferior to the other options.

As far as the GA configuration is concerned, it performs well only up to the damping factor peak values. This is made clear in Figure 8.35 (b) and Figure 8.35 (c). As indicated before, the optimisation for higher variable VEM thicknesses produces distributions with efficiencies close to the values obtained for the homogeneous configurations (the volume of the two configurations being the same). This clearly shows that optimisation may be worthless for high VEM thicknesses.

Figure 8.36 depicts a typical variable distribution of the viscoelastic material for h_1 = 0.01, h_2 = 3 E-5 in the 3rd mode of vibration.

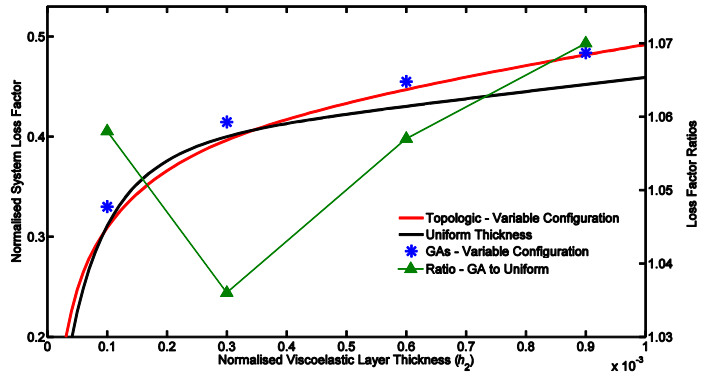

(a) $h_1 = 0.001$

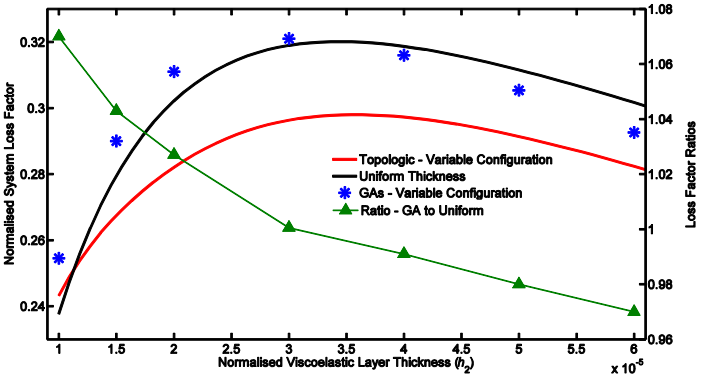

(b) $h_1 = 0.006$

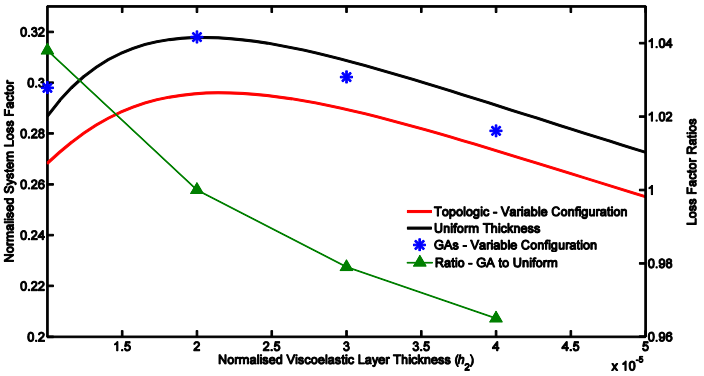

(c) $h_1 = 0.01$

Figure 8.35: Loss factor vs. thickness of uniform and variable layers for 3 h_1 ratios

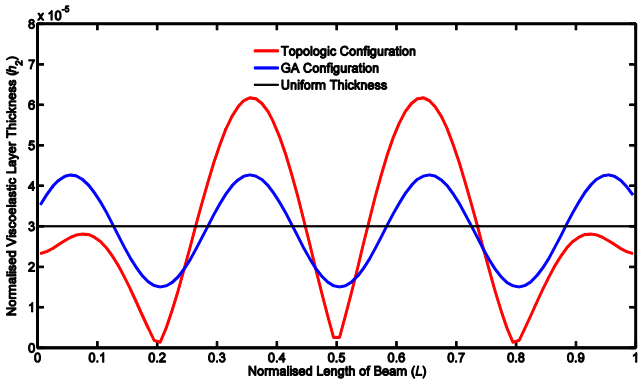

Figure 8.36: Uniform thickness and variable configurations

Volume and shape optimisation with GAs of a variable VEM layer

The GA volume and shape optimisation results are shown in Table 8.5. Figure 8.37 illustrates the comparison between two variable configurations. The dotted line reflects the volume and shape optimisation, whereas the configuration resulting from the volume restricted optimisation is shown in a continuous line.

Table 8.5: Constraint bounds and results for $h_1 = 0.01$

Variables	GA Lower Bounds	GA Upper Bounds	GA Results
x_1	0	5 E-5	4.4 E-5
x_2	1	4	3.07
x_3	0	π	2.2 E-16
x_4	0	0.5 E-5	4.77 E-6

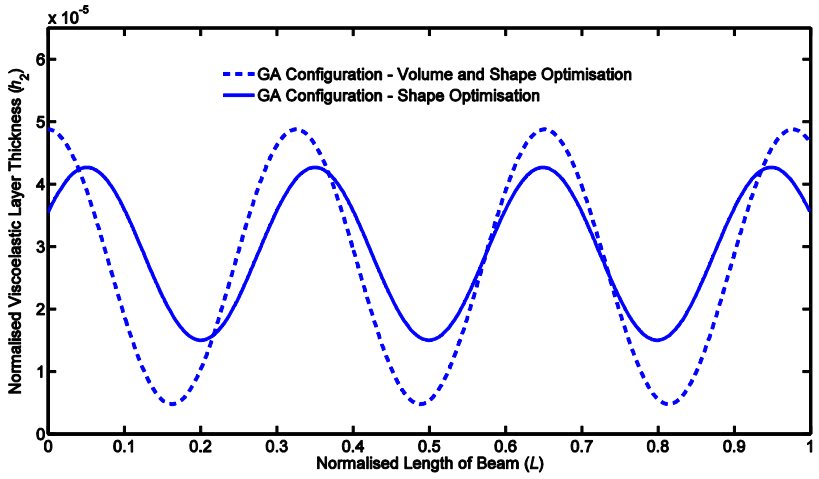

Figure 8.37: GA variable configurations for $h_1 = 0.01$

Analysis of uniform versus variable configurations (3 modes)

Table 8.6 makes a comparison between two sets of values concerning the ratio $h_1 = 0.01$ in the first three modes. It compares the average thickness of the variable VEM layer obtained with the results from Tables 8.1 ($h_1 = 0.01$ only), 8.4 and 8.5 (1st, 2nd and 3rd

modes, respectively) to the thickness of the homogeneous layer rendering the highest efficiency (Table 7.1). These are h_2 ratios that correspond to the highest loss factor.

Based on the results from Table 8.6, Figure 8.38 represents the percentage saving, in terms of viscoelastic material, that the configuration obtained with the volume and shape optimisation has over the homogeneous configuration.

Table 8.6: Optimum VEM layer thickness for $h_1 = 0.01$

	Average h_2 (4 var.)	Uniform configuration
1st Mode	1.77 E-4	2.03 E-4
2nd Mode	3.85 E-5	4.6 E-5
3rd Mode	1.69 E-5	2 E-5

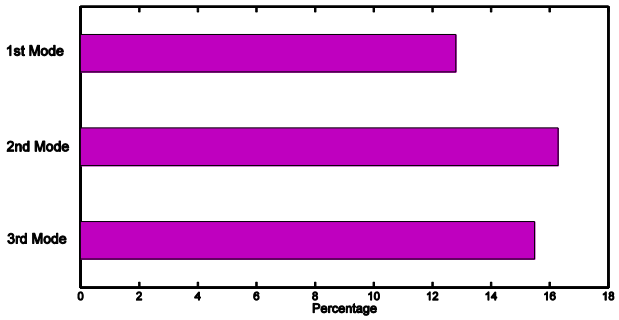

Figure 8.38: Percentage reduction of VEM

Table 8.7 presents the loss factor values corresponding to the optimum viscoelastic layer thicknesses shown in Table 8.6 and Figure 8.39 shows the respective percentage increase of the variable configuration (obtained with both shape and volume optimisation) over the uniform configuration loss factors.

In the cases analysed, (considering different h_1 ratios and the first three modes) the percentage savings of VEM vary between roughly 10% and 20%, which can be considered significant, especially in sizable structures. Not only does the variable shape use less

viscoelastic material, but there is also an increase of the loss factor (with the exception of the 2nd and 3rd modes).

Table 8.7: Optimum loss factors for $h_1 = 0.01$

	Average h_2 (4 var.)	Uniform configuration
1st Mode	0.3379	0.3294
2nd Mode	0.3227	0.325
3rd Mode	0.311	0.3179

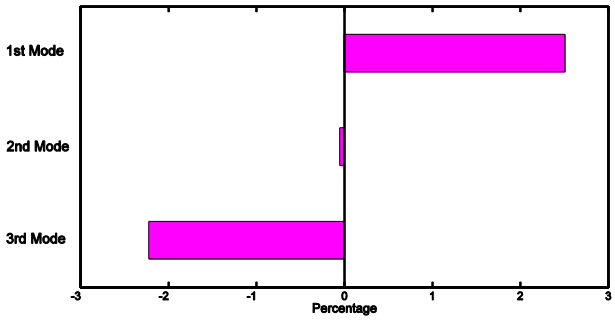

Figure 8.39: Percentage increase of loss factors

8.3 Built-in beam

The built-in beam is also symmetric and the strain energy distribution can be approximately represented by the selected trigonometric thickness functions. In the boundary condition related to this type of beam, extremities are clamped and displacements and rotations are restrained.

8.3.1 Mode shapes

The shapes of the 1st, 2nd and 3rd natural vibration modes of the laminated built-in beam are shown in Figure 8.40 and have been generated by FEMAP.

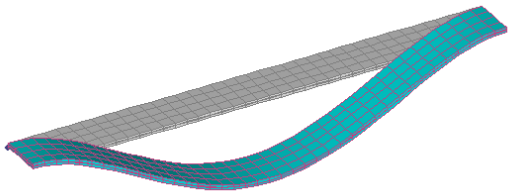

1st natural vibration mode

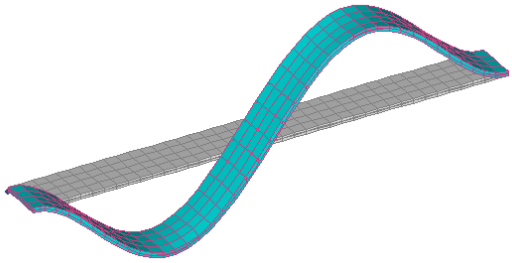

2nd natural vibration mode

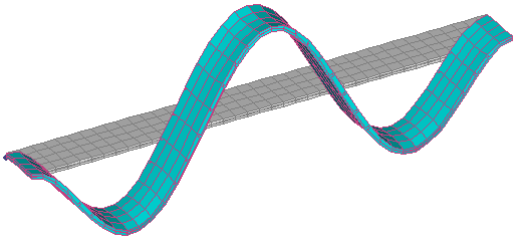

3rd natural mode of vibration

Figure 8.40: Natural mode shapes for the built-in beam

8.3.2 First mode

Lengthwise distribution of the extensional strain energy in the base layer

In the case of a built-in structure, the extensional strain energy (obtained with the MATLAB code "verif_strain_energy.m") is mostly noticeable at the tips and the centre of the beam. In this case, and contrary to the results observed for the free-free beam, the extremities evidence peak levels of strain energy for the outer layers; this is the direct result of the clamped effect. As in the case of the free-free boundary condition, in beams where the base and constraining layers are very thin, an increase of the viscoelastic layer produces an overall reduction of the extensional strain energy (Figure 8.41). In thicker base and constraining layers, the inverse occurs, that is, if the thickness of the VEM layer is increased, the extensional strain energy in the adjoining layers also increases slightly

(Figure 8.42). These conclusions also apply to the constraining layer of a CLD symmetrical configuration.

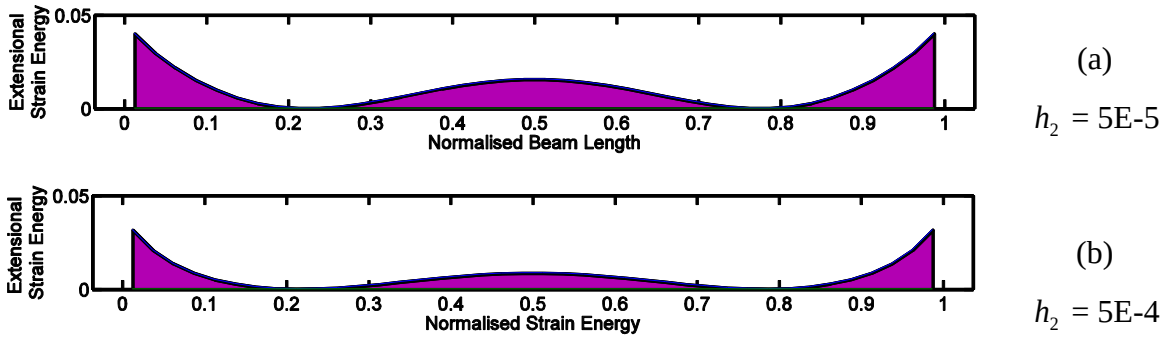

Figure 8.41: Extensional strain energy for h_1 = 0.001

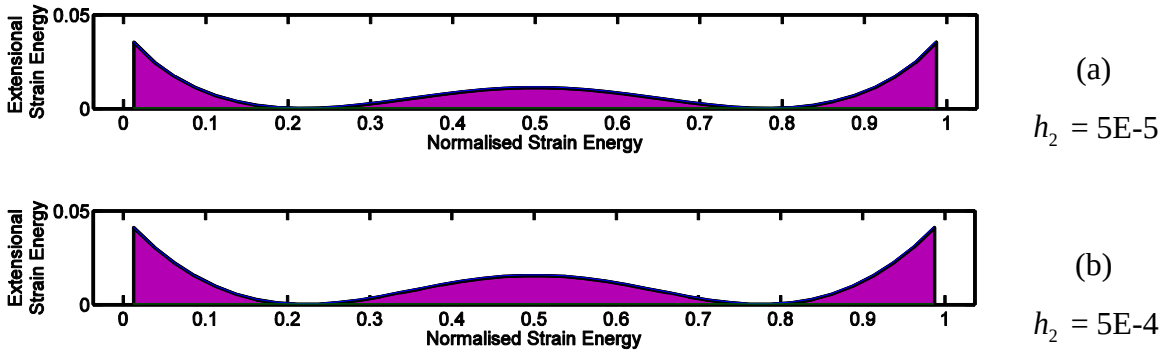

Figure 8.42: Extensional strain energy for h_1 = 0.01

Lengthwise distribution of the shear strain energy in a VEM uniform layer

The observation of Figures 8.43 and 8.44 reveals that two beams having the same base and constraining layer thicknesses, but different core thicknesses, will have different shear strain energies. An increase in the core thickness corresponds to an increase in shear energy in the case of thin adjoining layers with no peak loss factor values (Figure 8.43). If the base and constraining layers are thicker, (h_1 = 0.01) considering an increase in the VEM thickness up to the loss factor peak value, the shear strain energy increase is confirmed. For core layers that correspond to loss factor values after the peak, there is a reduction of the shear strain energy and that is illustrated in Figure 8.44 (b).

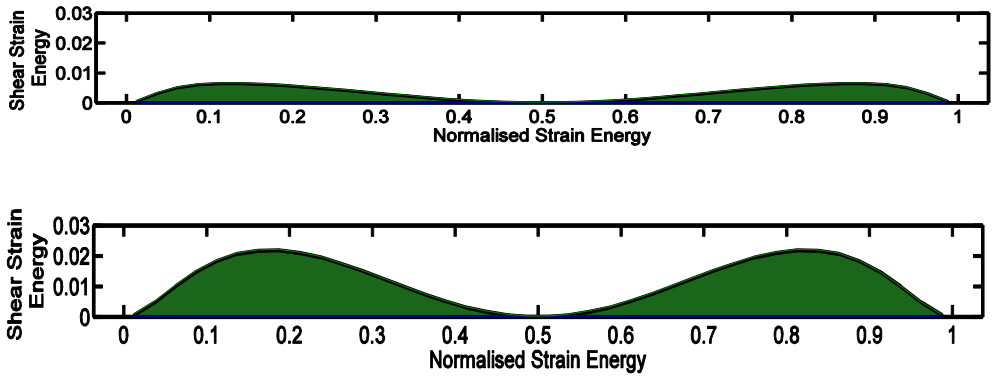

Figure 8.43: VEM layer shear strain energy for h_1 = 0.001

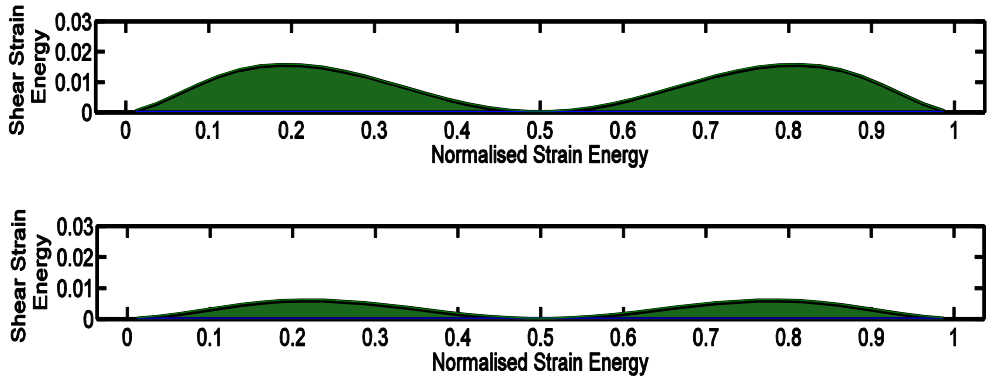

Figure 8.44: VEM layer shear strain energy for h_1 = 0.01

The visualisation provided by FEMAP of the results obtained by NASTRAN confirms the distribution of the shear strain energy and that is shown in Figure 8.45.

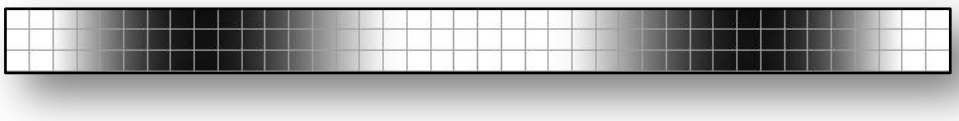

Figure 8.45: Shear strain distribution: VEM layer top view (FEMAP)

Shape optimisation of a variable VEM layer

A similar study to the one carried out on the free-free boundary condition, was done for the built-in beam. The progress of the loss factors for the three configurations (GA, topologic and uniform) was evaluated and a variable shape was optimised. In general, the

configuration generated by the genetic algorithm produces slightly higher loss factors for all the h_1 ratios under analysis. For the ratio without a peak ($h_1 = 0.001$) in Figure 8.46, the performances of the topologic and GA configurations are both better than the homogeneous thickness and present similar results.

In the case of the ratio with a less pronounced peak ($h_1 = 0.002$) in Figure 8.48, the GA shape produces significantly higher damping factors. This result evidences the topologic issue discussed in the free beam section when dealing with homogeneous thickness after the efficiency peak.

Concerning the ratios with a distinct peak, the topologic configuration only fares well for very small thicknesses of viscoelastic material, i.e. low h_2 ratios; the reason for this has been explained previously in the free-free section. Generally speaking, the topologic configuration performs worse than both configurations (uniform thickness and GA) near and after the efficiency peak.

With respect to shape optimisation, the contours generated by the topologic code do not contain any material at the tips where the beam is clamped. For thin viscoelastic layers, the GA optimisation performed similarly; as the loss factor starts approaching the peak value, the GA code places some damping material at the tips, which is incongruent with the distribution of the shear strain energy.

A possible justification might be related to some limitations of the thickness function used in the GA procedure. Once more, for high VEM thicknesses, the GA optimised shape configuration presents loss factor values that tend towards the uniform configuration ones.

This is in agreement with previous observations (free beam section) in that, for high volumes of VEM, the VEM configuration does not provide a significant improvement over the homogeneous configuration. The different trend of the ratio curve (GA to uniform) shown in Figure 8.48 has also been commented previously (refer to Figure 8.13).

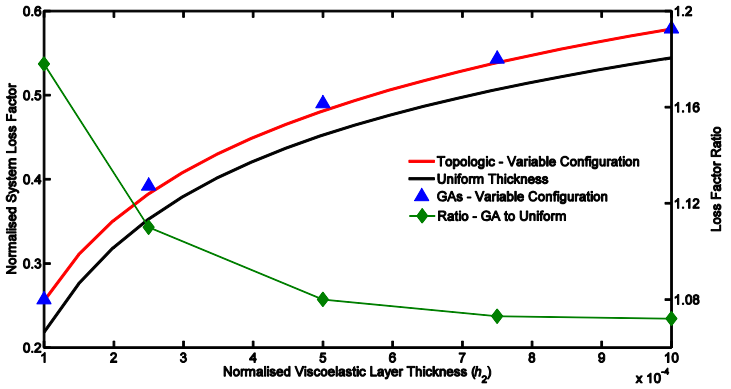

Figure 8.46: Loss factor vs. thickness of uniform and variable layers for h_1 = 0.001

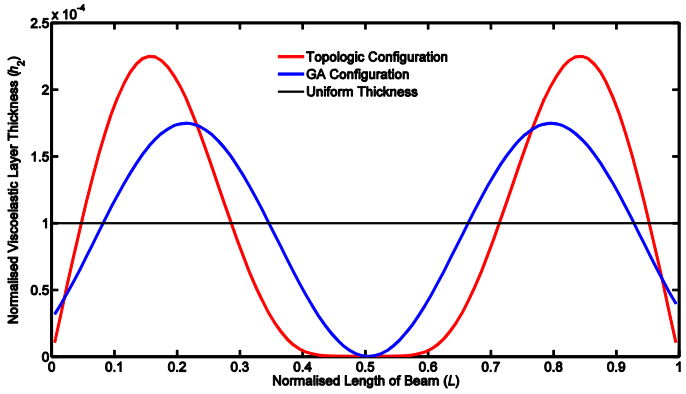

(a) h_2 = 1E-4

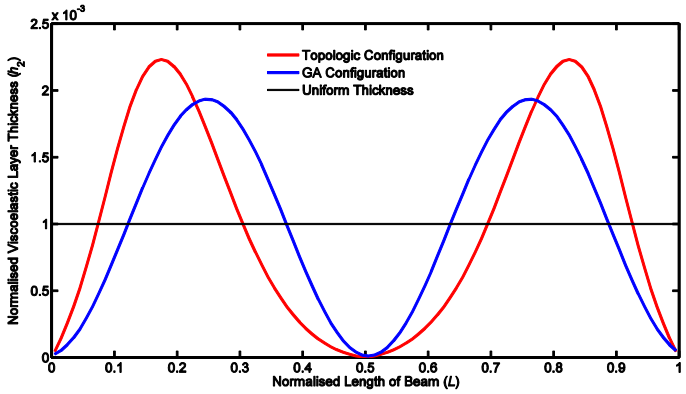

(b) h_2 = 1E-3

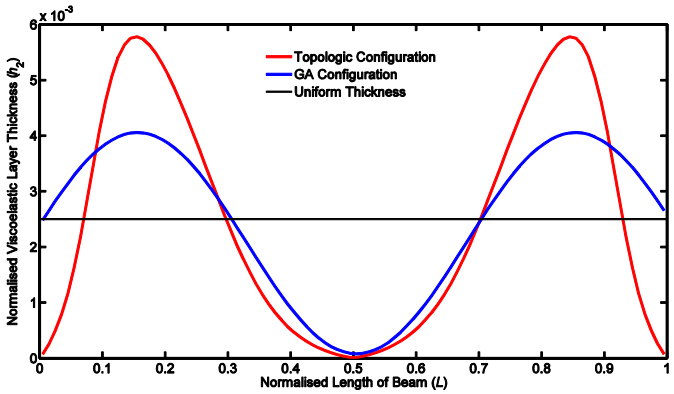

(c) h_2 = 2.5E-3

Figure 8.47: Uniform thickness and variable configurations for h_1 = 0.001

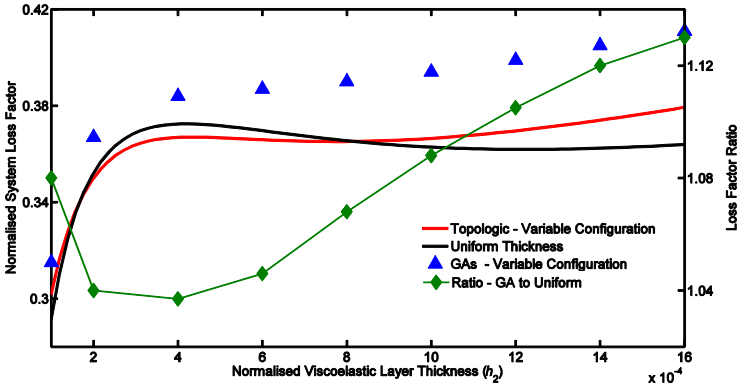

Figure 8.48: Loss factor vs. thickness of uniform and variable layers for h_1 = 0.002

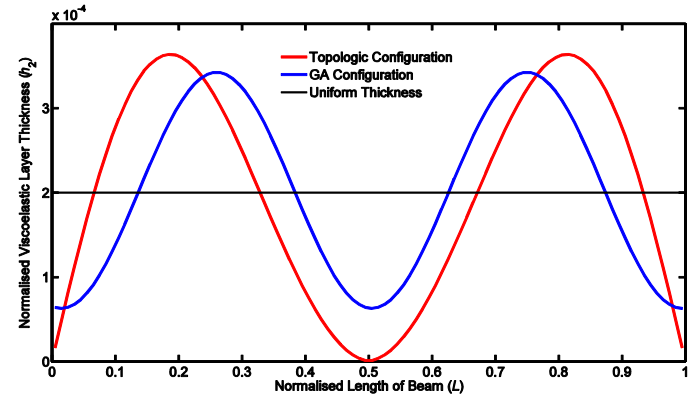

(a) h_2 = 2E-4

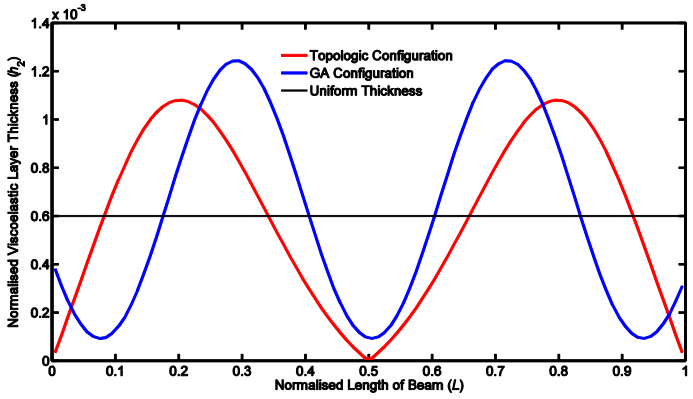

(b) h_2 = 6E-4

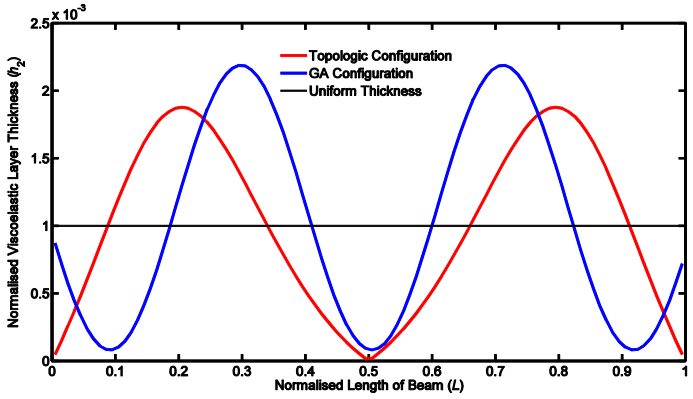

(c) h_2 = 1E-3

Figure 8.49: Uniform thickness and variable configurations for h_1 = 0.002

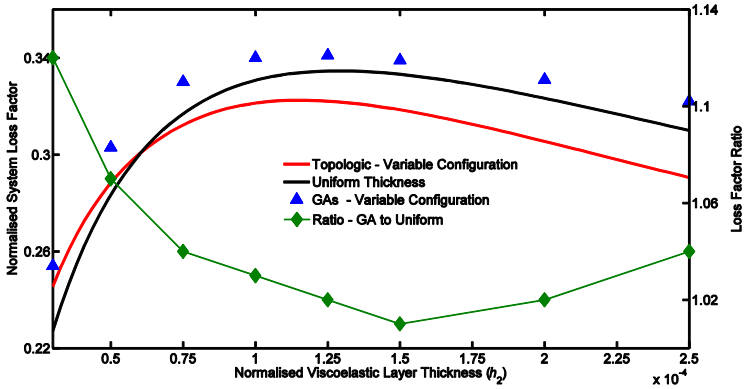

Figure 8.50: Loss factor vs. thickness of uniform and variable layers for h_1 = 0.004

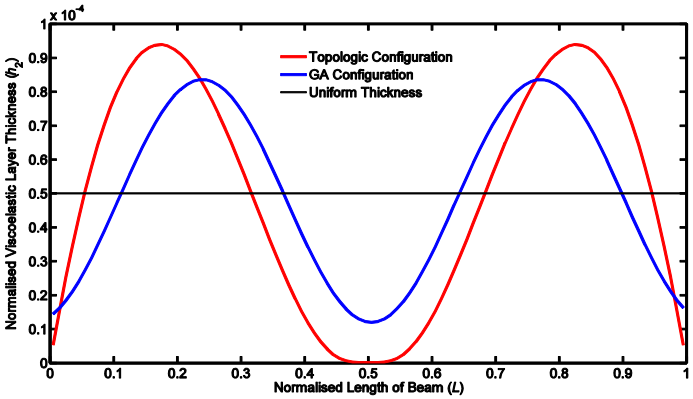

(a) h_2 = 5E-5

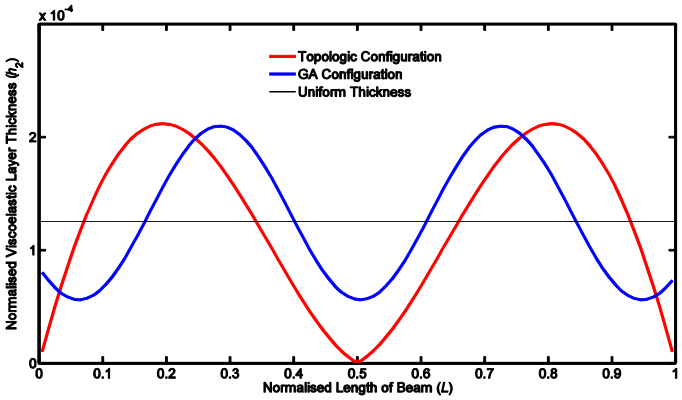

(b) h_2 = 1.2E-4

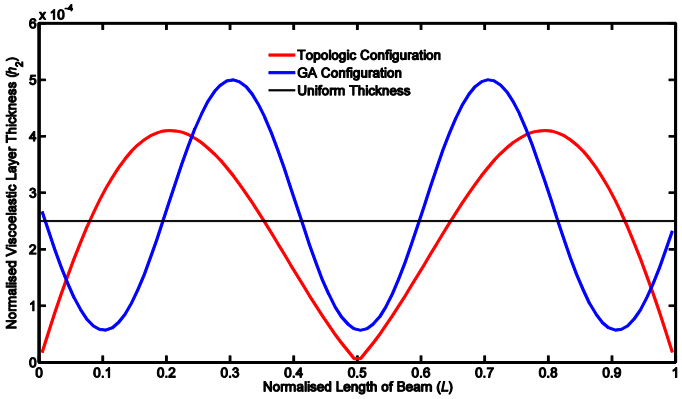

(c) h_2 = 2.5E-4

Figure 8.51: Uniform thickness and variable configurations for h_1 = 0.004

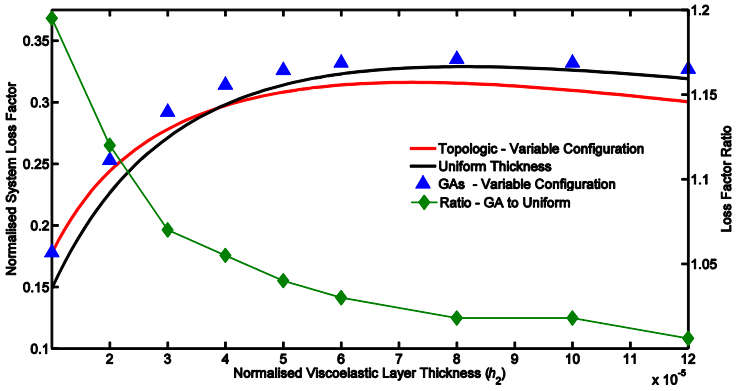

Figure 8.52: Loss factor vs. thickness of uniform and variable layers for h_1 = 0.006

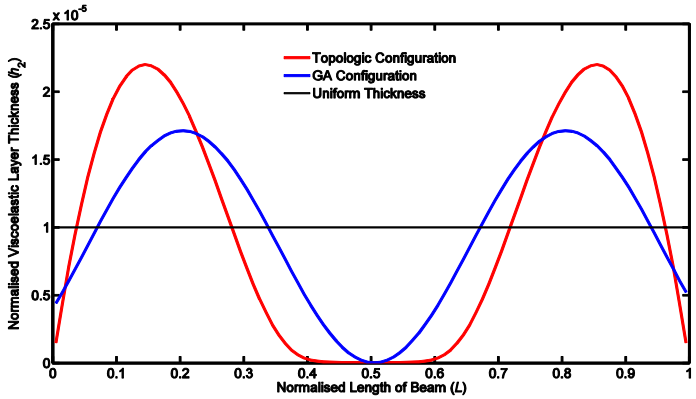

a) h_2 = 1E-5

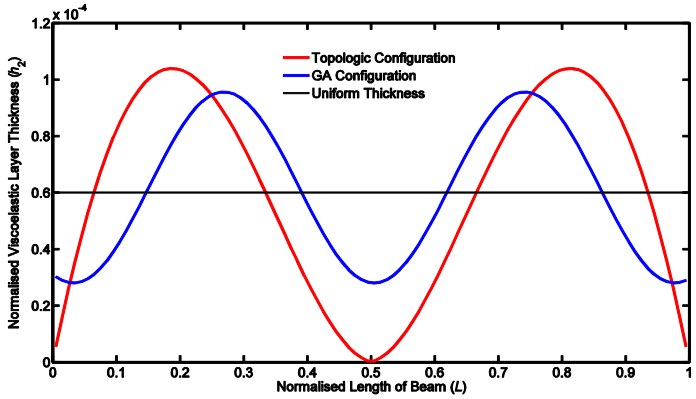

b) h_2 = 6E-5

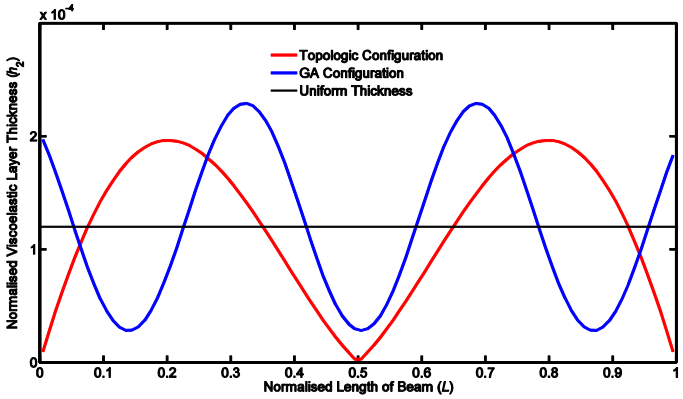

c) h_2 = 1.2E-4

Figure 8.53: Uniform thickness and variable configurations for h_1 = 0.006

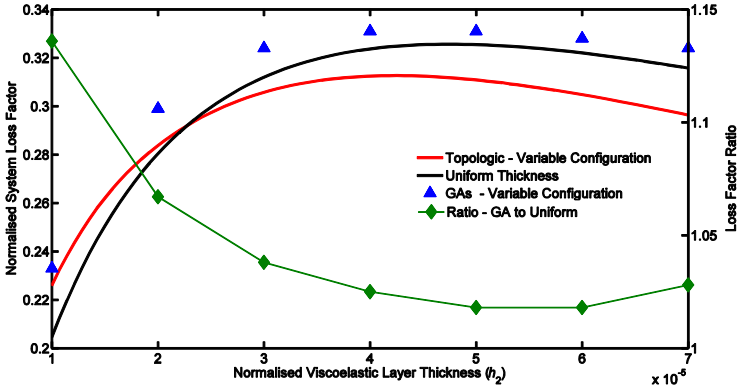

Figure 8.54: Loss factor vs. thickness of uniform and variable layers for h_1 = 0.01

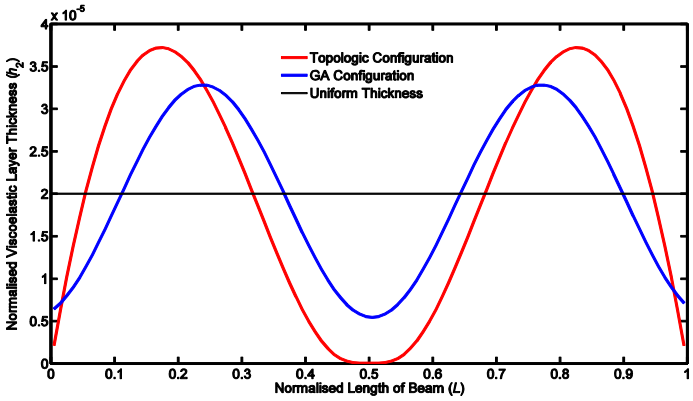

(a) h_2 = 2E-5

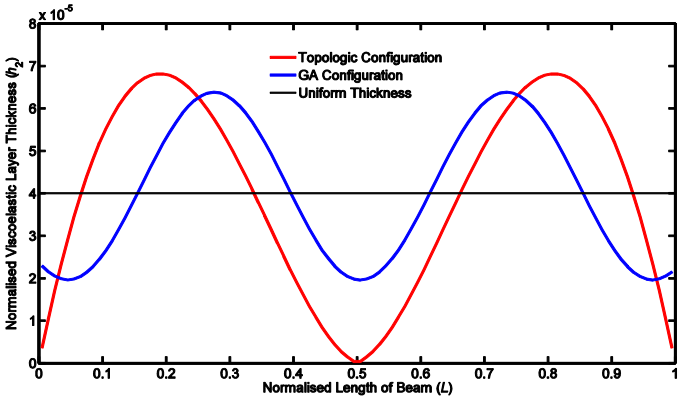

(b) h_2 = 4E-5

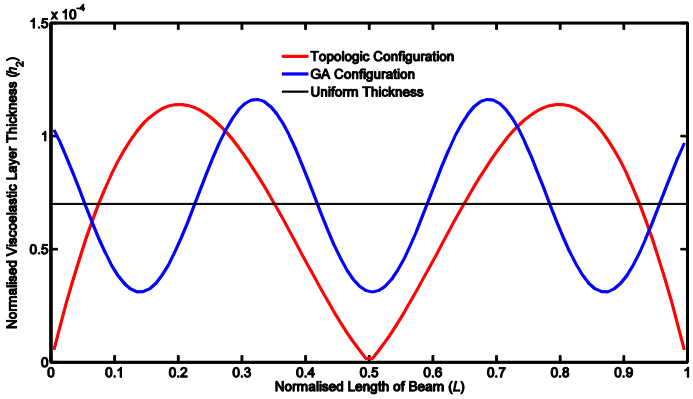

(c) h_2 = 7E-5

Figure 8.55: Uniform thickness and variable configurations for h_1 = 0.01

Volume and shape optimisation with GAs of a variable VEM layer

Table 8.8 presents the results and the confinements applied to the genetic algorithm for the four variables in (8.1) so that the shape, as well as the volume, could be optimised. Two h_1 ratios with loss factor peaks were chosen, a low ratio and a higher one.

Table 8.8: Constraint bounds and results for two h_1 ratios

Ratios	**h_1 = 0.004**				**h_1 = 0.01**			
Variables	x_1	x_2	x_3	x_4	x_1	x_2	x_3	x_4
GA Lower Bounds	0	1	1	0	0	1	1	0
GA Upper Bounds	10 E-4	6	4	1 E-4	5 E-4	6	4	2 E-5
GA Results	1.1 E-4	2.38	1.92	7 E-5	5.2 E-5	2.28	2.2	2 E-5

Figure 8.56 exhibits the shape that was obtained with the results from Table 8.8 and makes a comparison with the results from the previous shape optimisation. Once more, the general outline of the configuration is coherent with the distribution of the shear strain energy, except for the extremities of the beam.

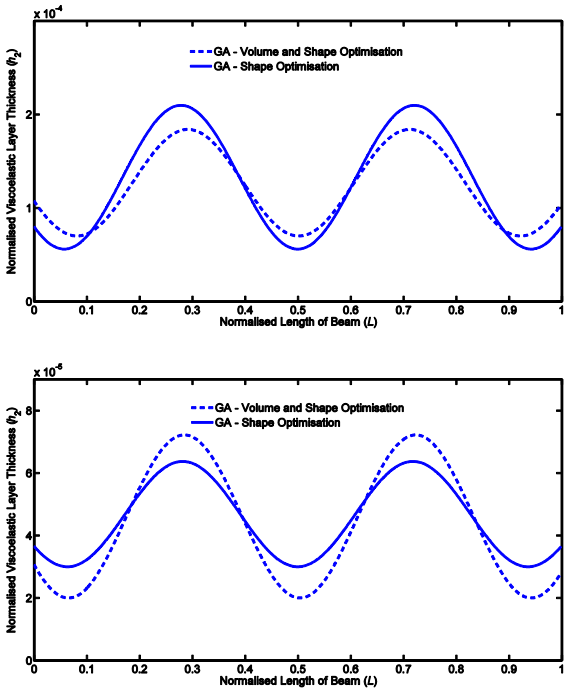

(a) h_1 = 0.004

(b) h_1 = 0.01

Figure 8.56: GA variable configurations for two h_1 ratios

Analysis of uniform versus variable configurations (two h_1 ratios)

With the results from the GA volume and shape optimisation (four variables) shown in Table 8.8, the average thickness of the variable core layer was determined and compared to a layer of homogeneous thickness (Table 7.1).

Table 8.9: Optimum VEM layer thickness for two h_1 ratios

Ratios	h_1 = 0.004	h_1 = 0.01
Average h_2 (4 var.)	1.202 E-4	4.33 E-5
Uniform thickness	1.28 E-4	4.7 E-5

Figure 8.57 is a graphical representation of the results shown in Table 8.9; in accordance with the values in the figure and in terms of percentage, the variable shapes for the two ratios analysed represent a reduction of viscoelastic material that is needed to obtain the highest loss factor peak.

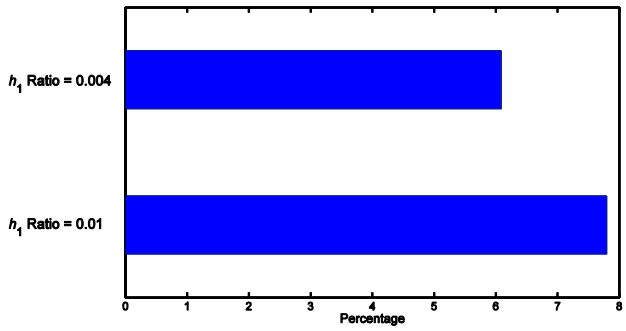

Figure 8.57: Percentage reduction of VEM

The loss factors corresponding to the optimum VEM layers shown in Table 8.9 are presented in Table 8.10.

Table 8.10: Optimum loss factors for two h_1 ratios

Ratios	h_1 = 0.004	h_1 = 0.01
Average h_2 (4 var.)	0.341	0.332
Uniform thickness	0.334	0.325

It can be seen from Figure 8.58 that the variable average thicknesses presented in Table 8.9 also generate a percentage increase relatively to a uniform outline, in terms of loss factors

(Table 8.10). In other words, the variable shape needs less material to reach the loss factor peak; even so, it obtains higher loss factors than the homogeneous layer.

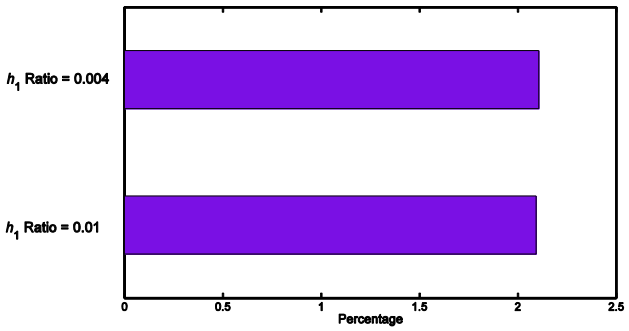

Figure 8.58: Percentage increase of loss factors

8.3.3 Second mode

Lengthwise distribution of the extensional strain energy in the base layer

The distribution of the extensional strain energy across the beam in the base layer (and also the constraining layer of a CLD symmetrical configuration) is presented in Figure 8.59.

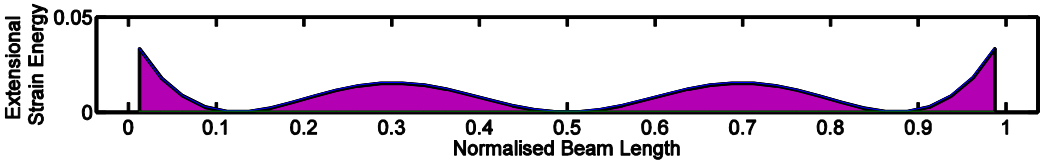

Figure 8.59: Extensional strain energy for h_1 = 0.01 and h_2 = 5E-5

Lengthwise distribution of the shear strain energy in a VEM uniform layer

Figure 8.60 and Figure 8.61 depict the distribution of the shear strain energy across the length of a built-in beam when vibrating in the second mode.

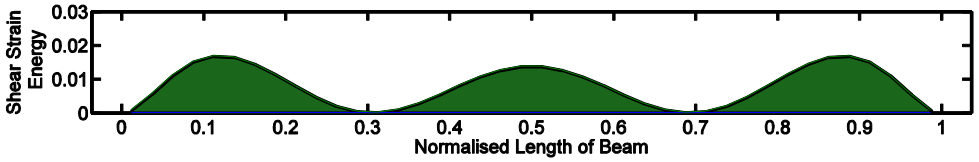

h_2 = 5E-5

Figure 8.60: VEM layer shear strain energy for h_1 = 0.01

Figure 8.61: Shear strain distribution: VEM layer top view (FEMAP)

Shape optimisation of a variable VEM layer

The GA optimised shape outperforms the topologic configuration and the uniform thickness layer, with respect to the damping effect, especially for thinner viscoelastic layers, as the ratio (GA to uniform) curve demonstrates in Figure 8.62.

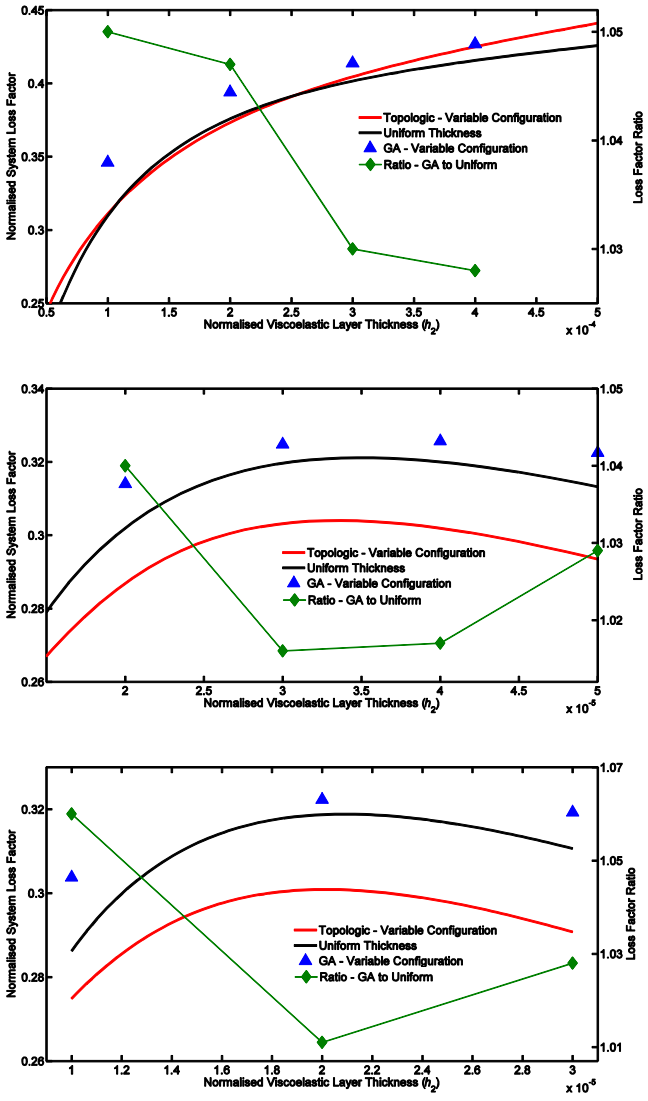

(a) $h_1 = 0.001$

(b) $h_1 = 0.006$

(c) $h_1 = 0.01$

Figure 8.62: Loss factor vs. thickness of uniform and variable layers for 3 h_1 ratios

Figure 8.63 shows the typical variable contours that the GA and topologic codes developed for the 2nd mode of vibration concerning the following ratios: h_1 = 0.001 and h_2 = 2E-4.

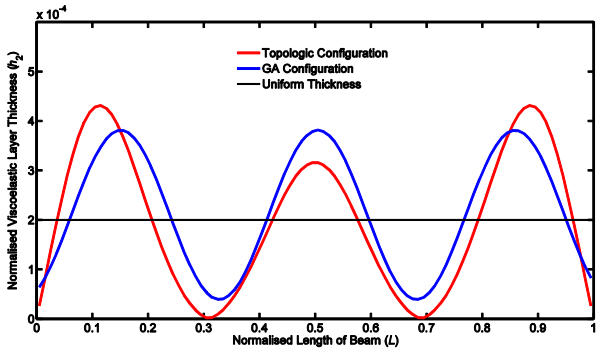

Figure 8.63: Uniform thickness and variable configurations

Volume and shape optimisation with GAs of a variable VEM layer

The volume and shape optimisation for the 2nd vibrational mode was done for one h_1 ratio (0.01). Firstly, Table 8.11 presents the results of the optimisation, which are then used to plot a variable configuration shown in Figure 8.64.

Table 8.11: Constraint bounds and results for h_1 = 0.01

Variables	GA Lower Bounds	GA Upper Bounds	GA Results
x_1	0	5 E-4	2.21 E-5
x_2	1	6	3.16
x_3	1	6	2.68
x_4	0	1 E-5	8.24 E-6

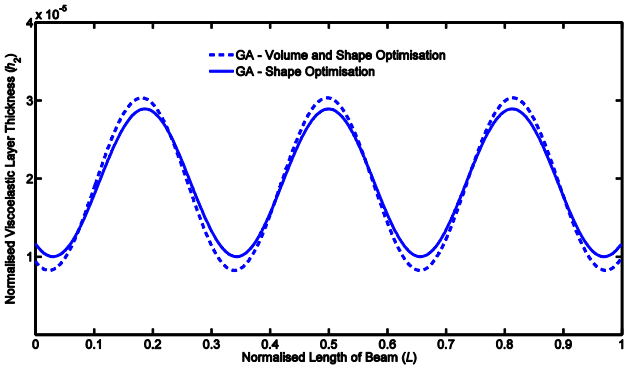

Figure 8.64: GA variable configuration for h_1 = 0.01

8.3.4 Third mode

Lengthwise distribution of the extensional strain energy in the base layer

The distribution of the extensional strain energy across the beam in the base layer (and also the constraining layer of a CLD symmetrical configuration) is presented in Figure 8.65.

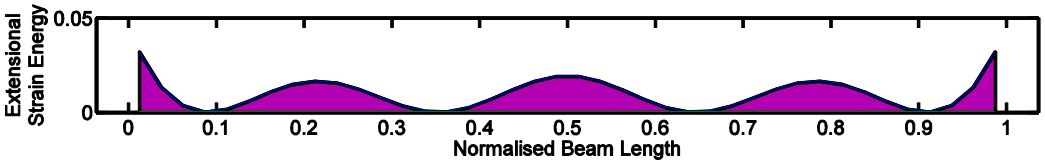

Figure 8.65: Extensional strain energy for h_1 = 0.01 and h_2 = 5E-5

Lengthwise distribution of the shear strain energy in a VEM uniform layer

Figures 8.66 and 8.67 depict the distribution of the shear strain energy across the length of a built-in beam when vibrating in the third mode. The h_1 and h_2 ratios being considered are shown in the figure.

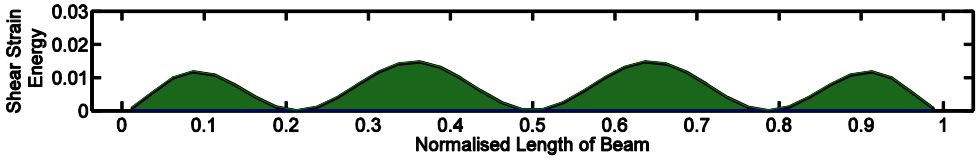

Figure 8.66: VEM layer shear strain energy for h_1 = 0.006

Figure 8.67: Shear strain distribution: VEM layer top view (FEMAP)

Shape optimisation of a variable VEM layer

The GA optimised shape is slightly better than the topologic configuration and the uniform thickness layer, as far as the loss factor is concerned, especially for very thin viscoelastic layers (Figure 8.68). At the peak, the loss factors of the GA shape and the homogeneous layer are practically identical. However, as far as the configuration itself is concerned

(Figure 8.69), the GA code has some difficulty in generating a shape that does not place some material at the extremities of the beam (h_1 = 0.006, h_2 = 2E-5).

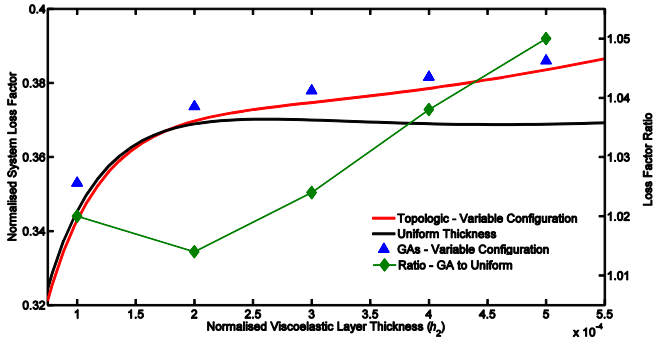

(a) h_1 = 0.001

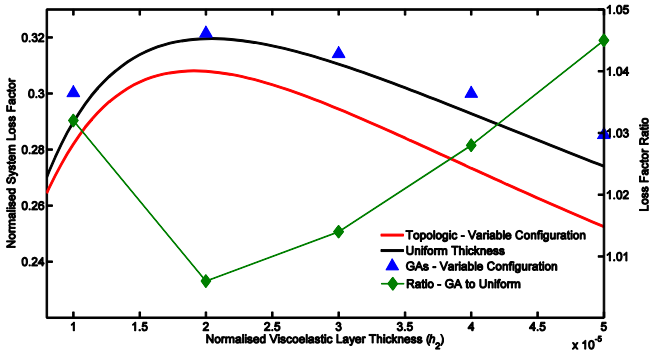

(b) h_1 = 0.006

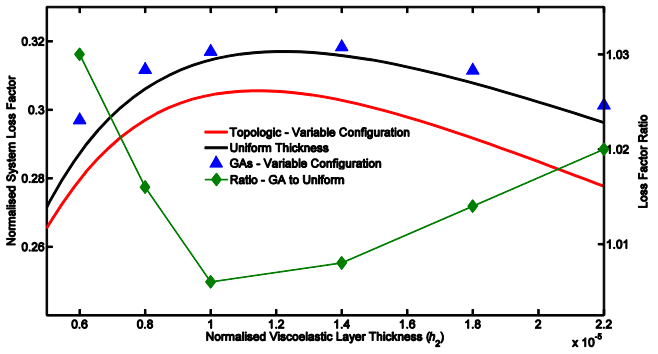

(c) h_1 = 0.01

Figure 8.68: Loss factor vs. thickness of uniform and variable layers for 3 h_1 ratios

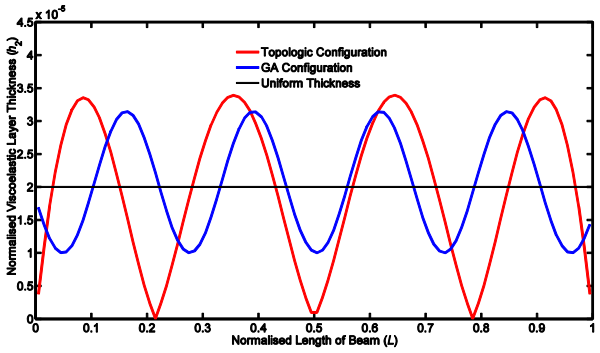

Figure 8.69: Uniform thickness and variable configurations

Volume and shape optimisation with GAs of a variable VEM layer

The results of the volume and shape optimisation for the 3rd vibrational mode of ratio h_1 = 0.01 is reflected in Table 8.12. They are used to plot the variable configuration in Figure 8.70.

Table 8.12: Constraint bounds and results for h_1 = 0.01

Variables	GA Lower Bounds	GA Upper Bounds	GA Results
x_1	0	5 E-4	9.27 E-6
x_2	3.5	4.5	4.43
x_3	1	6	1.77
x_4	0	1 E-5	7.74 E-6

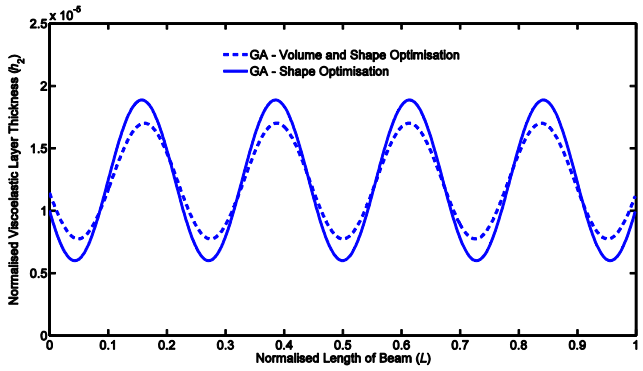

Figure 8.70: GA variable configuration for h_1 = 0.01

Analysis of uniform versus variable configurations (3 modes)

The average thicknesses and loss factors for h_1 = 0.01 were calculated based on the results in Tables 8.8 (h_1 = 0.01 only), 8.11 and 8.12 (1st, 2nd and 3rd modes, respectively) and they are shown in Table 8.13. Based on the values in Table 8.13, the percentage reduction of the variable VEM is shown in Figure 8.71. Similarly to the free-free beam, the lower amount of VEM used by the variable shape is accompanied by higher loss factors in the case of the first two modes. Concerning the 3rd mode, the advantage of a variable shape is negligible.

Table 8.13: Optimum VEM layer thickness for h_1 = 0.01

	Average h_2 (4 var.)	Uniform configuration
1st Mode	4.33 E-5	4.7 E-5
2nd Mode	1.875 E-5	2.1 E-5
3rd Mode	1.205 E-5	1.2 E-5

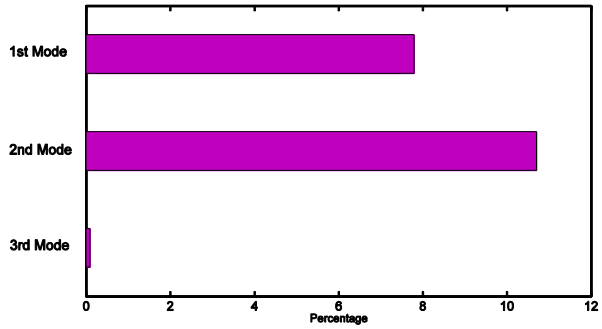

Figure 8.71: Percentage reduction of VEM

Also based on the results in Table 8.13, the loss factors are shown in Table 8.14. The percentage loss factor increase is shown in Figure 8.72.

Table 8.14: Optimum loss factors for h_1 = 0.01

	Average h_2 (4 var.)	Uniform configuration
1st Mode	0.332	0.325
2nd Mode	0.3225	0.3187
3rd Mode	0.3203	0.317

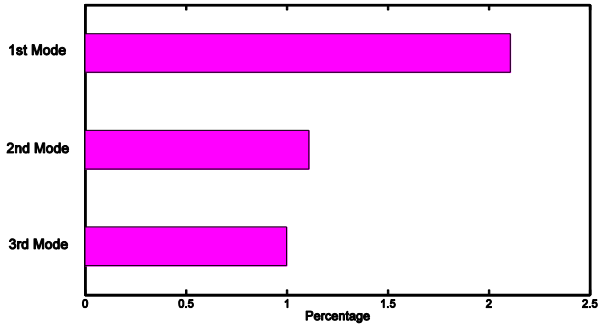

Figure 8.72: Percentage increase of loss factors

8.4 Summary

To achieve one of the main goals set out for this chapter, that is, to be able to find the optimum variable thickness of the VEM layer with the MATLAB genetic algorithm tool, a fitness function had to first be devised. Having formulated the fitness function, the genetic algorithm was able to produce a contour that could be compared to the outline developed by the topologic code and to a layer of uniform thickness.

The behaviour of the extensional strain energy in the outer layers and particularly the shear strain energy in the core layer for various h_1 and h_2 ratios was also investigated. This was an essential component of the work undertaken so that another main objective could be achieved, that is, to relate the variable configuration of the GA generated VEM layer to the distribution of the shear strain energy of a homogeneous layer.

The loss factors for variable shapes generated by the genetic algorithm and the topologic code were then compared to the loss factor obtained for a uniform thickness. The analysis of this ratio, associated with the percentage reduction of viscoelastic material used by a variable configuration provides sufficient information to accomplish the objective of determining the viability of the VEM variable shape.

Chapter 9

Final Conclusions and Future Work

In this chapter the concluding remarks are presented along with some suggestions of related topics that may be developed in the future.

According to one of the main objectives of this thesis, the dissertation addresses the optimisation of both homogeneous and variable thickness of viscoelastic material in CLD treatments for the passive damping of vibration.

Vibration is a problem that inevitably affects structures and machines and this aspect should be taken care of as an important specification during the designing stage. Very often this requirement is neglected but it can also happen that a good design, somehow, develops problems at a later stage. When the level of vibration becomes excessive, it becomes imperative to take action and, naturally, the most obvious step should be directed towards detecting its origin and solving it. When that is not sufficient, or simply impracticable, damping mechanisms are alternative methods of controlling vibrations. There are numerous solutions in both active and passive treatments but viscoelastic treatments are, nowadays, considered to be the most efficient method of restraining vibration.

However, before embarking on the application of VEM to solve vibration problems, engineers should have an adequate knowledge of the properties and the modelling of these materials. An important characteristic is that viscoelastic materials are much more sensitive to temperature than metal or composites and they exhibit three main temperature regions. Among these regions is the transition region where the material is the most effective. It is, therefore, crucial to take into consideration the operating temperature so that the correct viscoelastic material can be chosen, one whose transition region falls within the range of the operating temperature.

Frequency also has a great effect on the dynamic properties of the viscoelastic material, although comparatively to the temperature effect, the relationship is inverse; in other words, if the frequency is increased, the effect is the same as for low temperatures. Additionally, the frequency transition region is also the region where the loss factor is the highest. Similarly to the temperature effect, the frequency transition region of the selected material should coincide with the range of operating frequency.

As far as the viscoelastic treatments are concerned, they may be unconstrained or constrained (symmetrically or otherwise). The most efficient of these configurations is the symmetrical CLD treatment, which consists of a base and constraining layers of equal thickness; for this reason, most of the research involved in this study is associated with CLD treatments.

The behaviour of structures also deserves a careful analysis and the method of finite elements is the most widely used scheme. However, the success of its application depends on the models that are selected to represent the structure. Concerning CLD treatments, the three models requiring consideration in this study are: the spatial model, the constitutive model and the method of analysis.

When a structure in a CLD treatment undergoes vibration, high levels of shear strain energy are generated in the VEM core and the shear strain energy developed needs to be represented accurately by the spatial or discretisation method. The most adequate method is the layerwise model, which is based on a piecewise description of the displacement field.

This model has several advantages, the main one being the simplicity associated to the generation of the spatial model (finite element mesh).

Additionally, the behaviour of the viscoelastic material must also be described adequately and the complex modulus model is the constitutive model that best characterises it.

The effectiveness of VEM in dampening vibrations is due to the fact that, when subjected to vibration, these materials absorb the strain energy thus generated and then dissipate it to the ambient air in the form of heat. The evaluation of the energy dissipation is very complex and it is, therefore, usually evaluated in terms of damping level. One of the most simple and quick methods of determining the damping level (also known as loss factor) is the Modal Strain Energy, which is a method that can be used directly in a numeric analysis based on the F.E. method.

Having undertaken the study of the previously mentioned requirements, the focus was on an optimisation method that was able to meet the goals of this dissertation. The central objective of the study is to develop a VEM layer with a variable configuration that is able to achieve a higher damping effect, comparatively to a layer of homogeneous thickness. This involved the selection of an adequate optimisation process and the Genetic Algorithm was the method chosen for this purpose. However, its dynamics had to first be investigated to be able to draw the necessary conclusions.

9.1 Concluding remarks on Genetic Algorithms

To be able to optimise a design model, an optimisation procedure that is simple, efficient and computationally inexpensive needs to be chosen. Random search methods fulfil these requirements and one of the most popular in this category is the Genetic Algorithm.

For a successful search of solutions to be obtained with a Genetic Algorithm, a balance between a diverse population of solutions and the effectiveness of the selection process is essential. If the diversity of the population is high (brought about in the study in Chapter 5 by a high mutation rate), a more effective selective process must be chosen. On the other

hand, lower population diversity requires a less selective method. These conclusions are validated by the numerous runs that were performed within the scope of this work.

The analysis of the relationship between the convergence trend of the best solution and the mean function values proved to be a very useful in the evaluation and consequent control of the relative weight of the two opposing parameters: selection and diversity.

9.2 Concluding remarks on the parametric analysis of CLD treatments

Having chosen and investigated the genetic algorithm optimisation process, before applying it, it was necessary to make an analysis of the parameters that affect the behaviour of a CLD treatment. A dimensionless analysis was performed on sandwich beams with viscoelastic cores and an interesting feature was observed when dealing with relatively thin cores for thick beam structures.

The first and most important result evidences the capability of obtaining a peak in the efficiency curve for very thin damping layers, especially when dealing with symmetric sandwich beams with relatively high skin thickness-length ratios. This observation contradicts the usual monotonic shape of the efficiency curve of a CLD configuration.

Another interesting result from the study is related to the reduction of the optimal thickness of the damping core (the thickness corresponding to the efficiency peak) when the ratio between the thickness of the skin and the beam length increases. This interesting observation shows that, if the beam length is kept constant, in a sandwich configuration, thicker outer skins require thinner VEM layers to maintain the efficiency peak – an observation that contradicts the common design approach that tends to define the damping layer thickness according to and in balance with the thickness of the host structure.

The effects of other geometry parameters were explored, as well as the mode shape wave length, the material modulus ratio and applied boundary conditions. It was found that the

final outcome of such design variables on the efficiency curve can always be described from the direct effect produced on the sub-curves of the efficiency, especially the one related to the specific shear deformation produced in the dissipative core.

Furthermore, since a non-dimensional analysis is provided and the effects of the parameters investigated are implicit in the shape reconfiguration of the efficiency curve, those effects can be simply combined by superposition. These observations and the published results may provide some useful guidelines for the optimum design of passive damping treatments using viscoelastic materials. These guidelines can be briefly listed here following the main results obtained from the individual analysis of each design parameter:

- When dealing with beams with damping treatments, a proper selection of the viscoelastic layer thickness may provide a peak performance without the need of thick damping layers.
- The peak location in terms of the viscoelastic thickness ratio relatively to the length of the beam depends on the ratio between the host structure thickness and the length of the beam and this is an inverse relation, i.e. efficiency peak is observed for lower values of viscoelastic layer thickness when thicker host beams are used (Figure 6.3 illustrates this relation for the symmetric CLD configuration).
- When using a non-symmetric configuration, the reduction of the constraining layer thickness is responsible for the decrease of the efficiency peak value (Figure 6.7), its location is also dependent on this parameter and an inverse relation is again observed, i.e. when the constraining layer thickness increases towards the symmetric CLD configuration, the viscoelastic layer thickness ratio h_2 corresponding to the damping treatment efficiency peak is lower.
- Despite the usual interest to merely consider the fundamental natural mode in the analysis of a damping treatment, this parameter also plays a role in the definition of the optimum viscoelastic layer thickness ratio and, as observed in Figure 6.9, the higher the mode number, the lower this thickness ratio must be in order to follow the performance peak of the damping treatment.
- The boundary conditions have a direct effect on the optimum value of the viscoelastic thickness and it is observed that those boundary conditions providing

higher levels of the shear deformation pattern tend to lower the value of the optimum viscoelastic thickness ratio.

- The storage modulus of the viscoelastic material must be also considered in the definition of the best value for the thickness of the damping layer and a direct relation is observed (Figure 6.8), i.e. when the value of the storage modulus of the VEM decreases (higher e_1 ratios), as a result of the effect of frequency and temperature or simply because a different material is used, the optimum value for the thickness of the viscoelastic layer becomes smaller.
- The relation between the loss factor of the material and the damping treatment efficiency is direct and proportional when the material damping of the host structure and the constraining layer is or can be considered negligible in comparison to the loss factor of the damping material.
- All the above relations can be quantitatively defined through the use of the information depicted in the graphics of figures presented in Chapter 6 (Figure 6.3 to Figure 6.10). These graphics are defined by non-dimensional parameters that generalise the use of this information.

Finally, it is worth mentioning the significance of the results obtained for the design and investigation of multi-layer damping treatments. As demonstrated by numerous studies, including those from references [48, 49, 112], the application of multiple thin damping layers instead of a single thicker one provides a valuable solution for the stiffness decoupling of the skins, improves the efficiency of the damping treatment and permits a multi-material configuration. The results from this study confirm the potential superiority of relatively thin viscoelastic layers in comparison to thick cores and may provide some useful information towards the proper definition of the optimal thickness of the individual thin layers. In fact, despite the relative inferior damping effect of very thin VEM layers in comparison to thick ones, the specific efficiency – achieved damping per volume unit of added VEM – is increasingly higher for reduced thicknesses of the layer, especially when the composite design is able to take advantage of an efficiency maximum peak, as demonstrated in this study.

9.3 Concluding remarks on the optimisation of CLD treatments

The optimisation of damping treatments in a constrained configuration is performed on both homogeneous and variable shapes of the viscoelastic layer and the tool used for that purpose is the Genetic Algorithm.

9.3.1 Homogeneous thickness VEM layer

The most important conclusion drawn from the comparison of the results from the parametric study in Chapter 6 and the optimisation of a homogeneous VEM layer using the GA in Chapter 7 is that there are no evident discrepancies, i.e. the results obtained from the optimisation analysis of homogeneous CLD (Table 7.1) coincide with the observations of the parametric study. The values of the optimised VEM thickness obtained with GAs coincide with the respective curve peaks, as illustrated by the vertical lines in the various figures of Chapter 7. It is important to recall here that it is only possible to obtain optimum results with GAs for curves that display a peak in the efficiency curves since the objective function only accounts for the efficiency of the damping treatments and does not include any cost function related to the amount of VEM.

However, other conclusions include:

- Out of the three boundary conditions, the cantilever imposes the lowest deformation gradient and the clamped structure the highest. This is in accordance with the study of the influence of the boundary conditions on the VEM loss factor in Chapter 6. The conclusion is that boundary conditions that impose higher shear deformation, such as, the built-in condition, require lower optimum VEM thicknesses.
- The parametric study analysed the effect of the natural mode on the structure damping efficiency. Higher mode orders produce higher deformation gradients and move the curve peak to lower h_2 ratios. This observation is also confirmed with the Genetic Algorithms.

- The influence of the h_1 ratio (thickness/length) is also confirmed. The parametric study, as well as the GA optimisation, shows that higher ratios require thinner layers.
- The analysis of the effect of the constraining layer in the parametric study concludes that the thinner the constraining layer, the lower the shear strain energy generated. This means that thinner constraining layers require thicker VEM layers and that symmetrical structures produce the highest damping effect. This is confirmed in Chapter 7 (Table 7.2) by two observations: one is that the lower deformation gradients that are imposed by the thinner constraining layer are reflected in higher optimum h_2 ratios; the other is that there is an increase in monotonic curves.
- The material properties, namely the elastic modulus, also have an influence on the damping efficiency. The higher e_1 ratio is, the lower the optimum VEM thickness (higher e_1 ratios may be the result of higher E_1 or lower E_2).

As far as setting out the bounds in the Genetic Algorithm, particularly the upper bound, a certain degree of difficulty was initially experienced. This parameter strongly influences results and the search space needs to be kept within realistic boundaries. What constitutes a realistic boundary is somewhat intuitive, being the result of initial trial and error and subsequent endless algorithm runs.

Nonetheless, the results obtained with the Genetic Algorithm optimisation can be considered very satisfactory as they effectively corroborate the findings of the parametric analysis conducted previously. The comparison between the results obtained with this algorithm and the results from the parametric analysis validate and confirm the quality of the GA optimisation process.

9.3.2 Variable thickness VEM layer

One of the proposed aims of this dissertation is to verify if it is possible to establish a correlation between the distribution shape of the shear strain energy in a VEM homogeneous layer and the optimised variable core shape. The conclusion from this

investigation is that there is an evident similarity between the two cases, which is confirmed by the consistency of the results with different h_1 ratios (see Figures 8.4 and 8.10 as an example).

Another objective was to develop a non-uniform shape for the viscoelastic layer with an equivalent volume as a uniform one that will, in spite of that, be able to achieve higher loss factors. In the first part of the work, only the shape is optimised, the volume of the variable profile being the same as the volume of the homogeneous one; in the second part both the shape and the volume are optimised.

On the shape optimisation issue, the observation of the variable configuration superiority, as far as damping capability is concerned, is quite clear in the figures of the loss factor versus thickness of uniform and variable layers for the various h_1 ratios.

In the case of the monotonic curves, considering each value of the ratio h_2, the variable shape obtains higher loss factor values. As far as the non-monotonic curves are concerned, the peak of the variable configuration happens before and above the peak of the uniform thickness. The conclusion relatively to the one curve being above the other is rather obvious, i.e. with an equivalent amount of viscoelastic material the variable shape manages to achieve higher loss factor values. The fact that the peak of the variable shape also occurs to the left hand side of the homogeneous peak means that, with a variable configuration, less VEM is necessary to obtain higher damping.

The superiority of the variable contour is even more pronounced for thinner layers of VEM, as shown by the curves of the loss factor ratio (variable/homogeneous) that are shown in green with triangular markers. These findings are consistent in both the free-free and built-in boundary conditions for the first three modes of vibration.

With respect to the optimisation of both the shape and volume, the genetic algorithm is given the freedom to search for the best solution, not only as far as the contour is concerned, but also its dimensions. The shape generated by the GA in the two boundary conditions and first three modes are very close to the configuration obtained with the shape

optimisation. Furthermore, the dimensions and variable shape obtained show important advantages over the uniform outline. One is in the percentage increase of the loss factor and the other, the percentage reduction of viscoelastic material that is required, as shown by the graphs and quantified in the tables. These results are in accordance with the conclusions concerning the shape optimisation, where it was also observed that, comparatively to the homogeneous shape, the GA variable shape obtains higher loss factors with less VEM. This analysis was performed first on different h_1 ratios (in the 1st mode) and then on the three modes of vibration. It can be concluded that in most cases, the use of a variable configuration proves to be worthwhile, mostly so when considering structures with large dimensions.

9.4 General conclusions

The bibliographic review of the current state-of-the-art was an important first step towards the understanding of the problems encountered in obtaining viable damping solutions. The choice of the most appropriate constitutive and discritisation models, as well as, the method of analysis is also relevant. In addition, to be able to carry out the proposed optimisation process with Genetic Algorithms, its dynamics need to be properly understood.

The parametric study that was undertaken in Chapter 6 to investigate the influence of the parameters involved in viscoelastic treatments revealed an interesting feature. It was found that the shape of the efficiency curve is not always monotonic, contradicting the usual shape shown in most of the literature on this topic. In fact, depending on the dimensions of beam, the efficiency curve may display a peak. These results are significant, as it enables a designer to take advantage of the efficiency peak.

The conclusions that could be derived from the parametric analysis of CLD treatments were essential in the optimisation of both homogeneous and variable viscoelastic layers. As far as the homogeneous layer is concerned, Genetic Algorithms were used to determine and confirm the minimum VEM thickness that produce the highest loss factor and results are coincident with the parametric study.

With respect to the variable configuration, the two main assumptions concerning this topic were positively validated. Firstly, in most cases, the non-uniform contour needs less VEM to achieve higher loss factors. Secondly, it is amply demonstrated that the areas that need to be damped and, therefore, treated with VEM correspond to the areas where a homogeneous layer generates the highest levels of strain energy, thereby simplifying the design of partial treatments.

9.5 Contributions

The work developed in this thesis provides some important contributions to science, to the industry and also to society.

9.5.1 Contribution to science

The study developed in this thesis contributes to the clarification and better understanding of the influence of parameters on the performance of CLD treatments. It offers some guidelines and simplification of the process concerning their design, where the designer may take advantage of the dimensionless parametric analysis that was carried out. It also provides very useful conclusions on the design of partial coverage.

9.5.2 Contribution to the industry

The consideration of the results and conclusions from both the uniform and the variable configurations enables the designer to save viscoelastic material, thereby reducing costs.

9.5.3 Contribution to society

English written thesis provides wider dissemination of contents.

9.6 Suggestions for future work

Some research guidelines for future work are hereby presented:

1. The cosine wave configurations generated by the Genetic Algorithm are somewhat impracticable to be applied in real situations. However, other forms could be developed. Instead of a smooth curve, a step-like configuration could provide an interesting alternative, as this could be obtained by means of multiple layers of different lengths.

2. However, the theory involving multiple layers would also have to be investigated. In this thesis, it is amply demonstrated that certain h_1 ratios produce peak damping values. By having multiple layers of viscoelastic material, where the adjacent material to the intermediate VEM layers is also a viscoelastic material, deserves an analysis as to whether peak loss factor values would also occur.

3. The entire dissertation is based on the theory of beams and it would be interesting to expand this line of work for plates.

4. Furthermore, the topology optimisation to obtain a non-uniform configuration is based on the redistribution of a given amount of material, placing more material in the spots where the shear strain energy is the highest and less where the shear strain energy is lowest. Another perspective, could involve the numeric removal of VEM instead of redistribution.

5. The variable shape optimisation dealt with in this thesis involves only symmetrical shapes. The optimisation of non-symmetrical variable shapes regarding different boundary conditions at the extremities (e.g. the cantilever) can also be developed.

6. Finally, the validation process of the numeric results by means of experimental data would provide a valuable contribution to the reliability of the numerically obtained results.

Appendix A – Flowcharts

A.1 – MATLAB code "assembly.m"

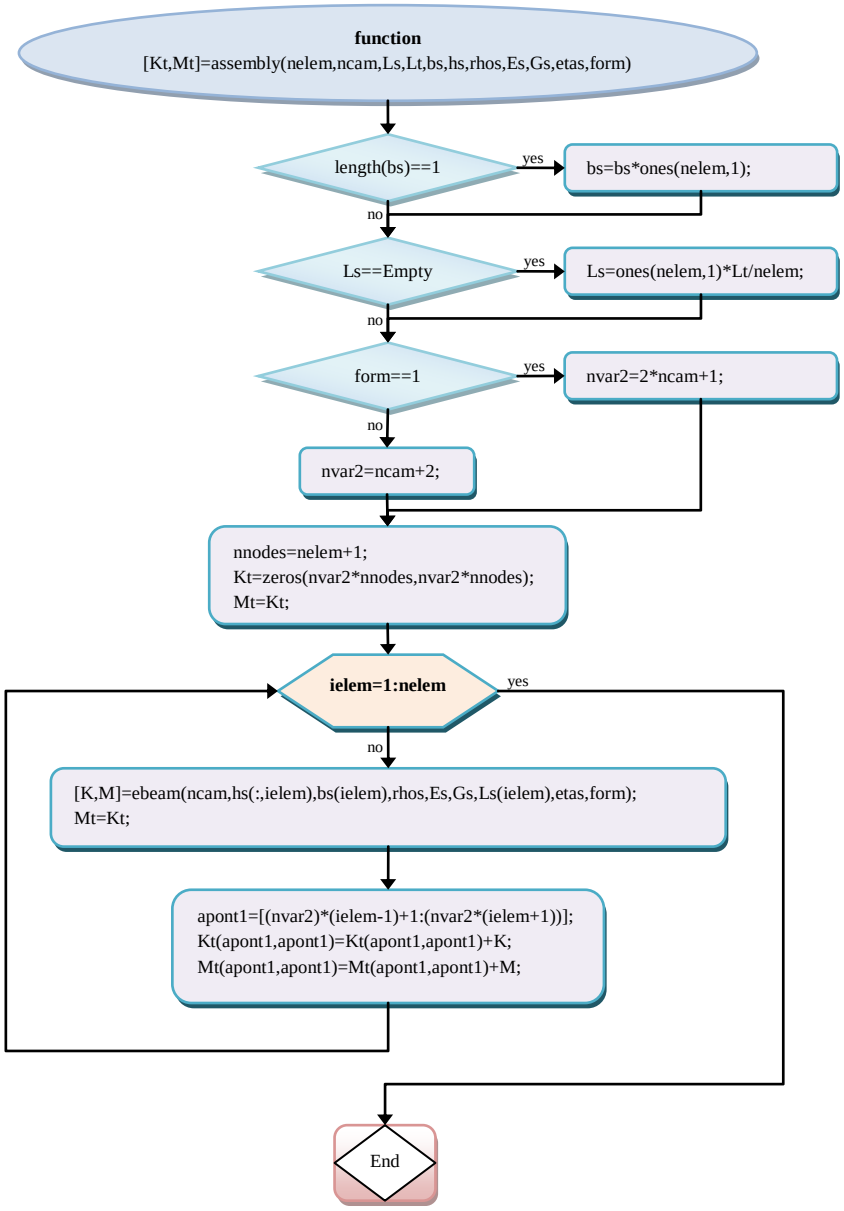

A.2 – MATLAB code “ebeam.m”

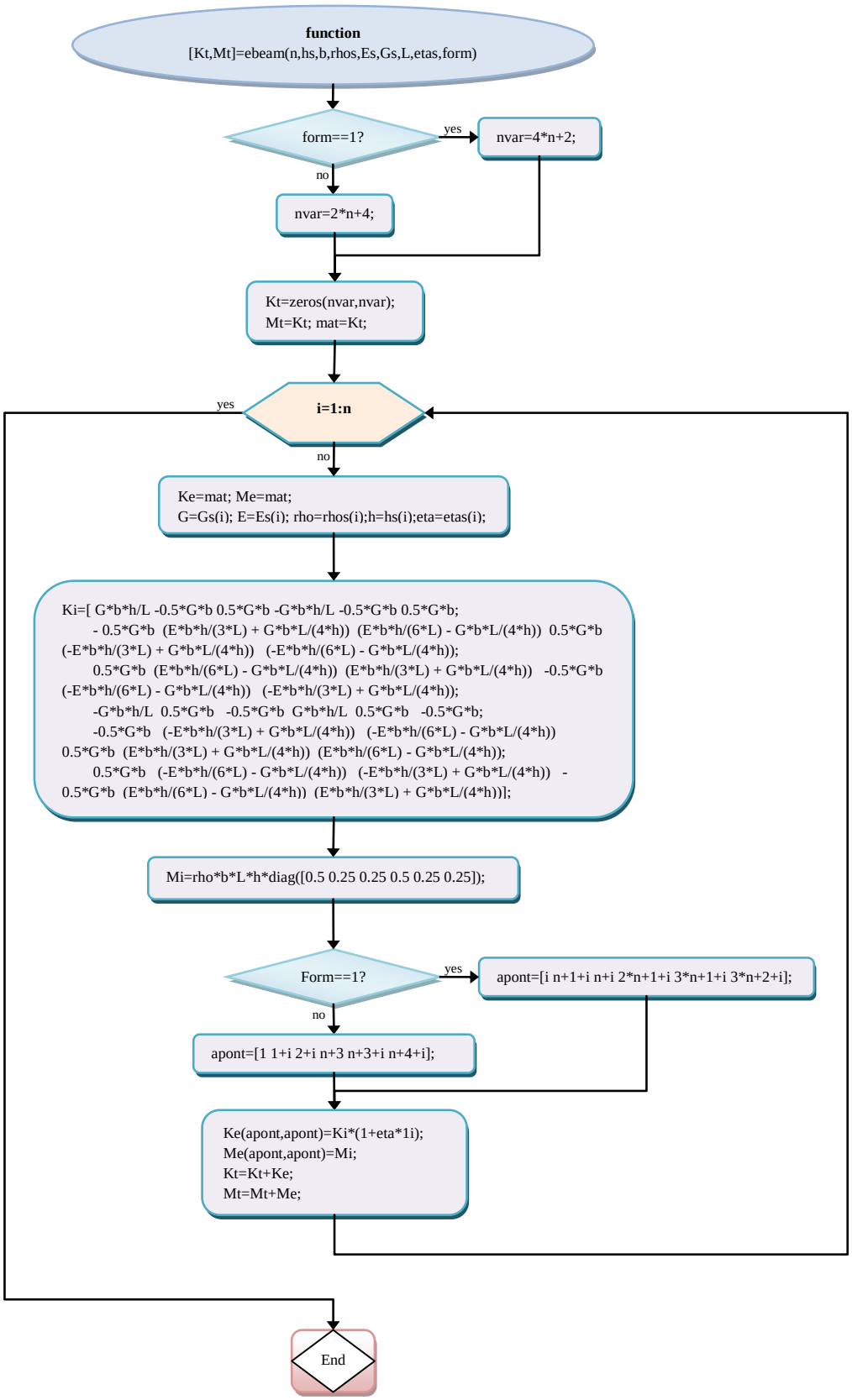

A.3 – MATLAB code “boundaryC.m”

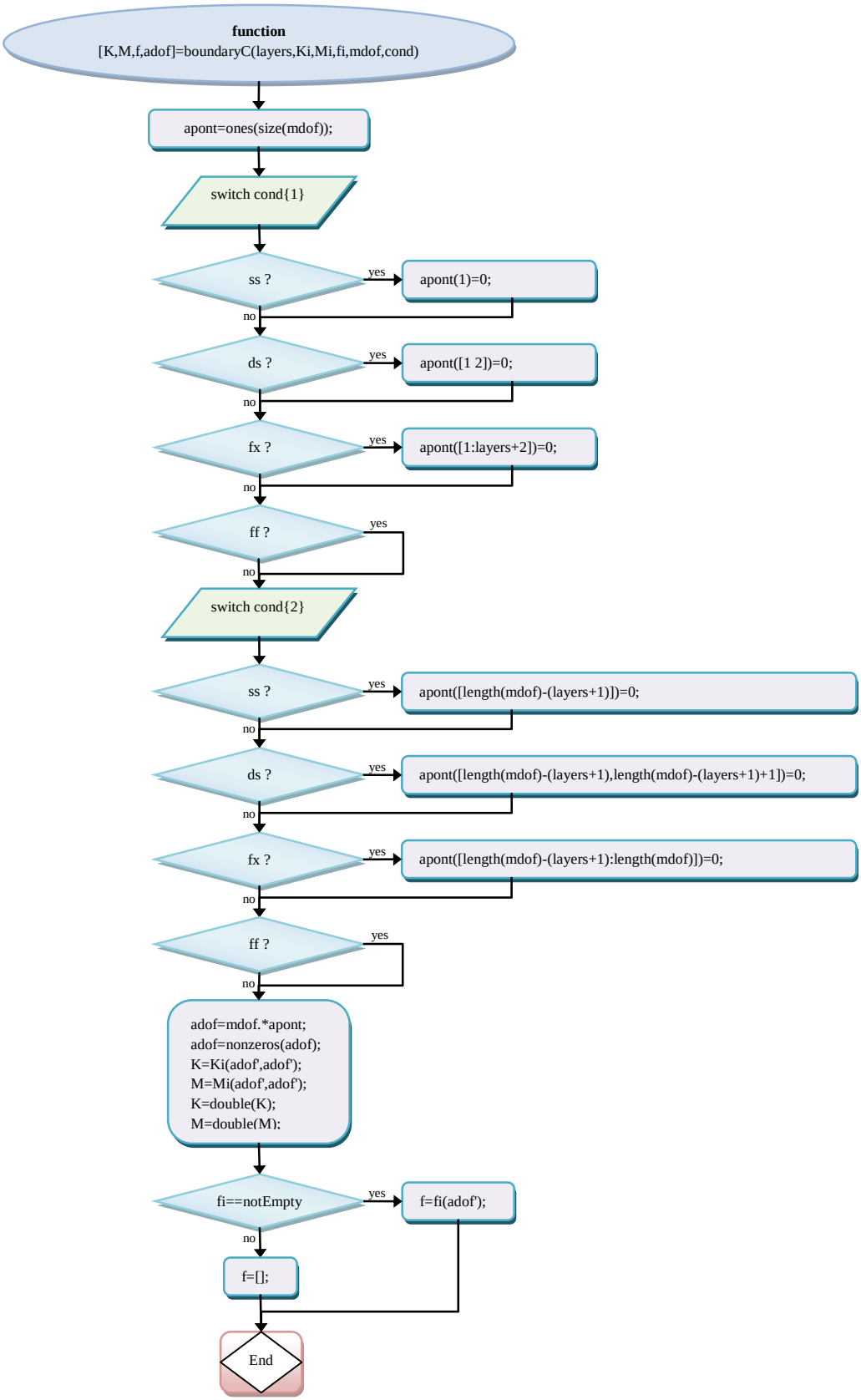

A.4 – MATLAB code “totalcld.m”

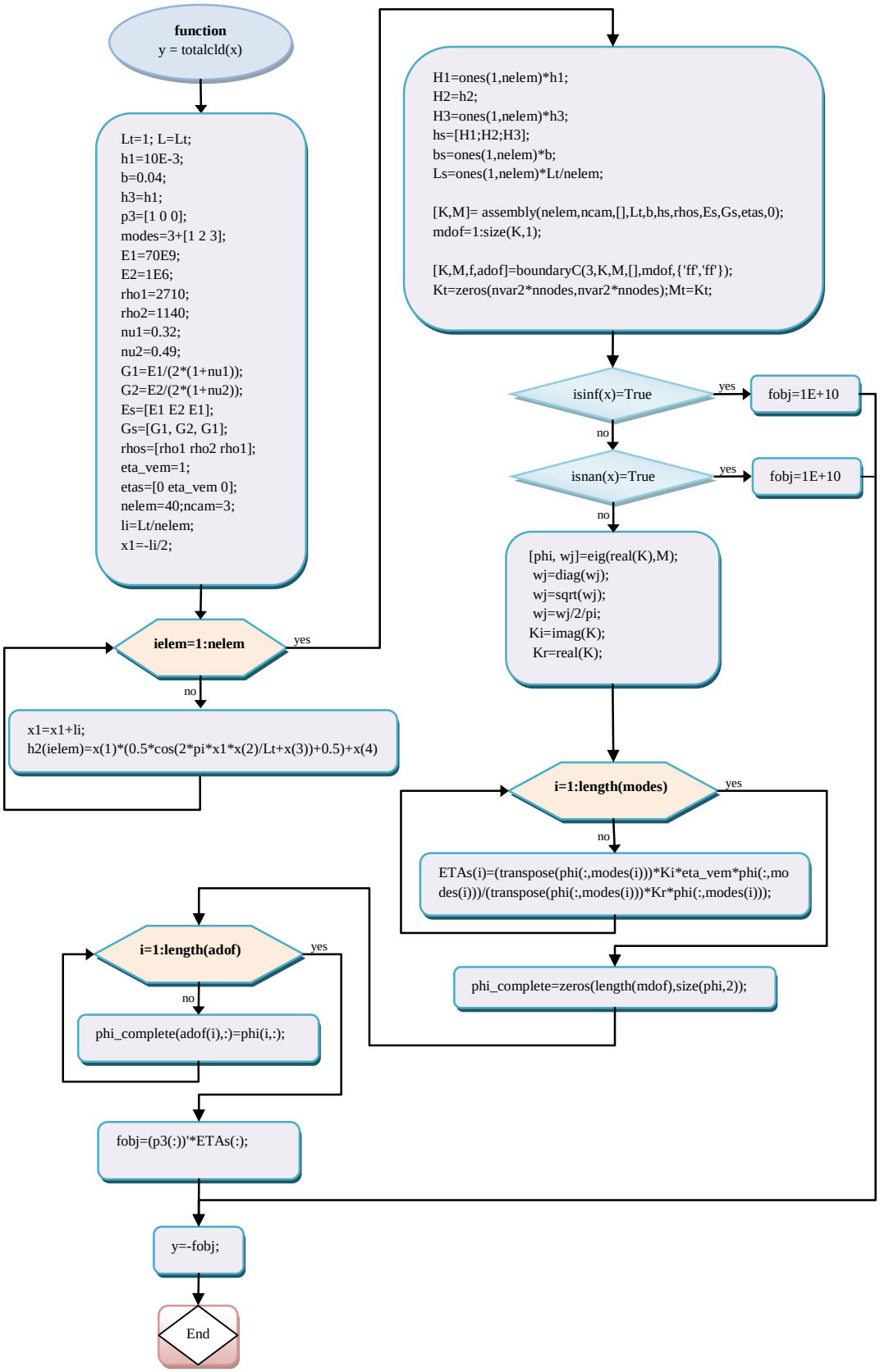

A.5 – MATLAB code "verif_strain_energy.m" – 1/2

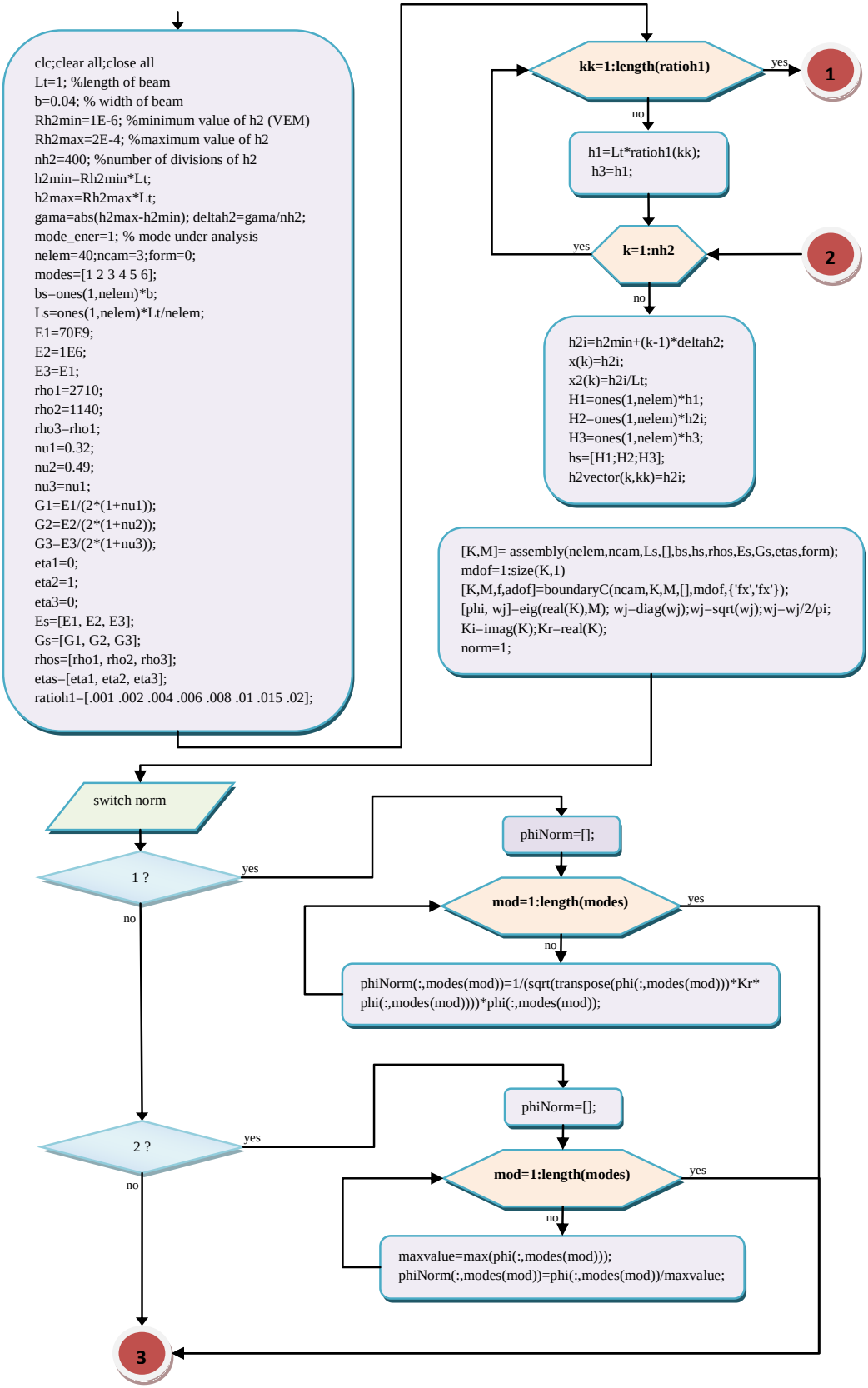

A.5 – MATLAB code “verif_strain_energy.m” – 2/2

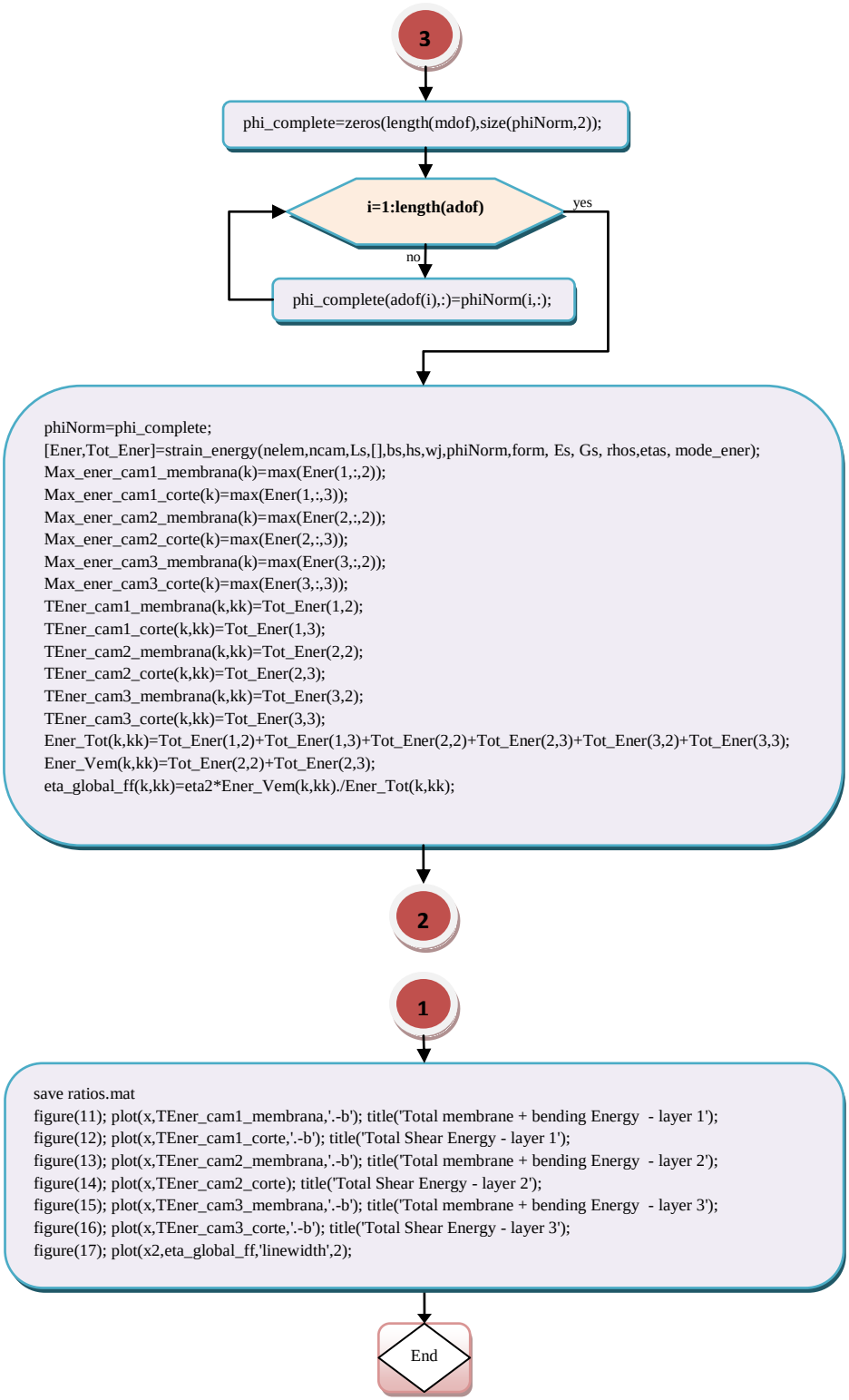

A.6 – MATLAB code “strain_energy.m” – 1/3

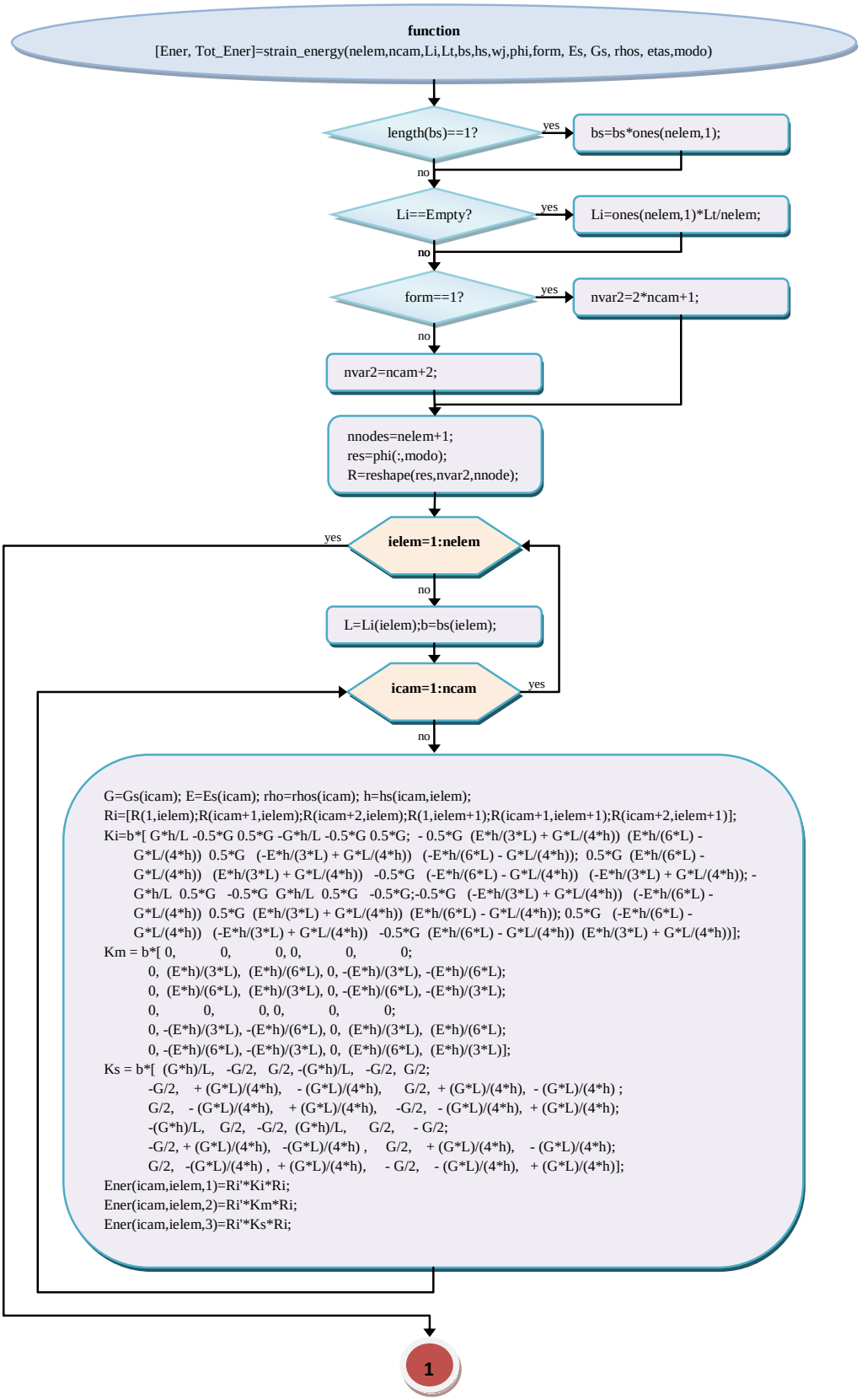

A.6 – MATLAB code “strain_energy.m” – 2/3

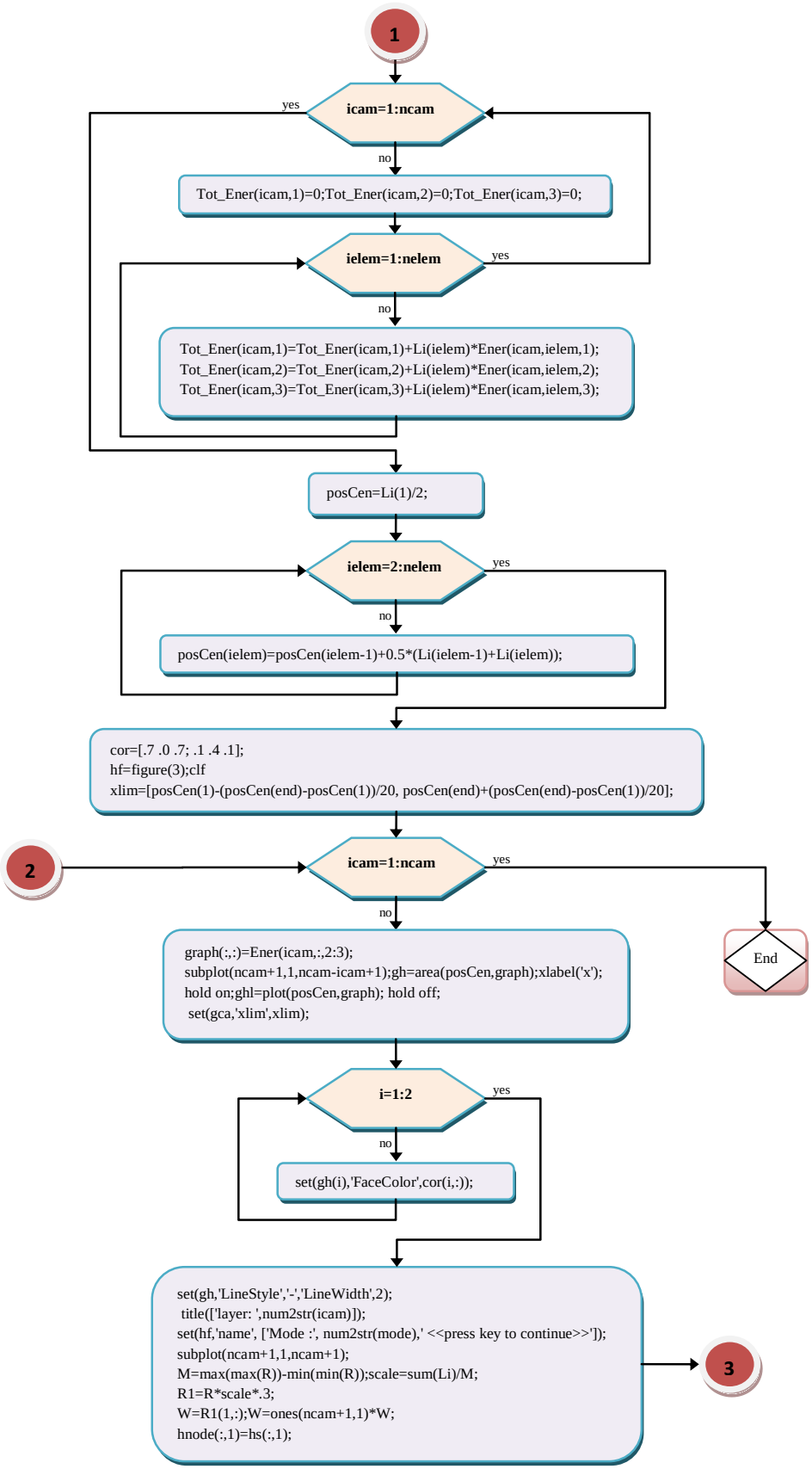

A.6 – MATLAB code “strain_energy.m” – 3/3

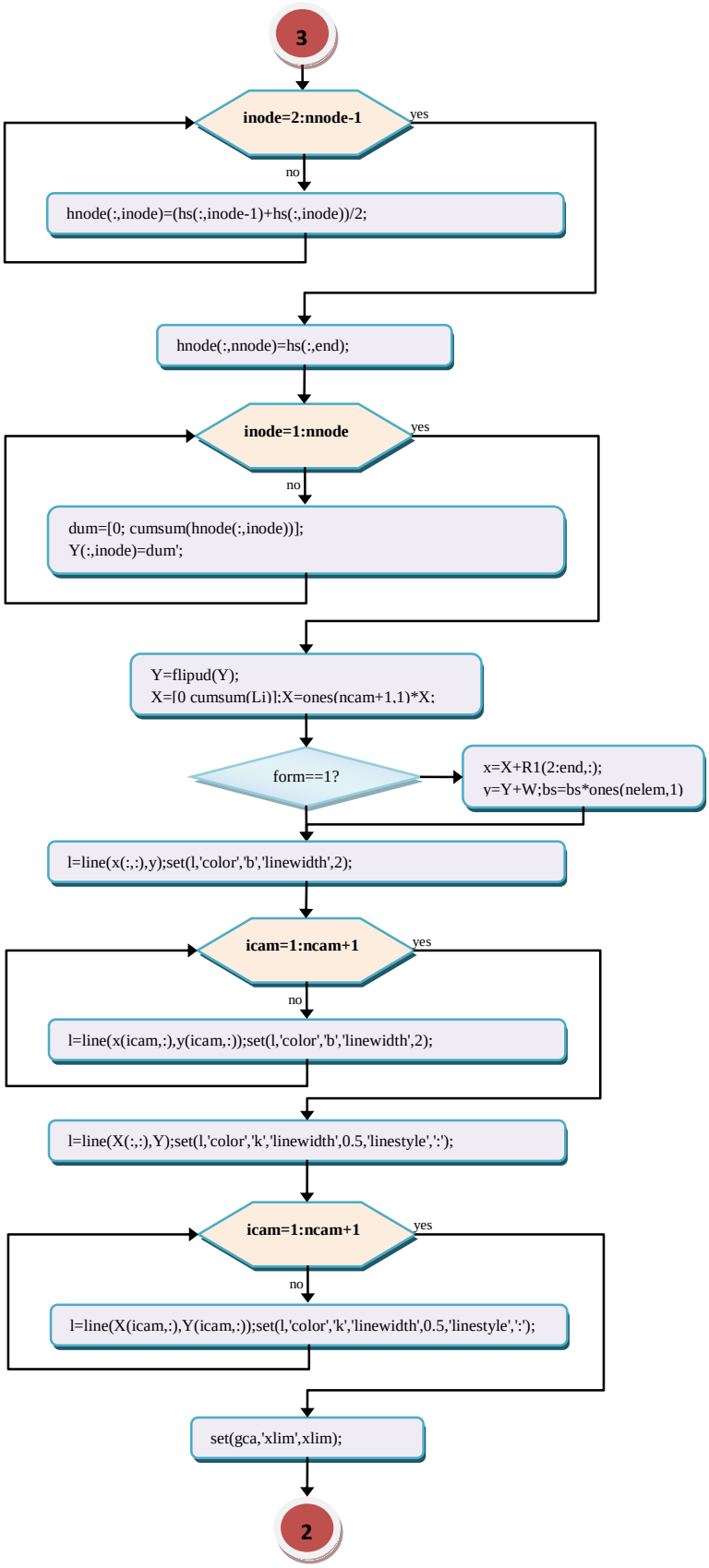

A.7 – MATLAB code “topology.m” – 1/3

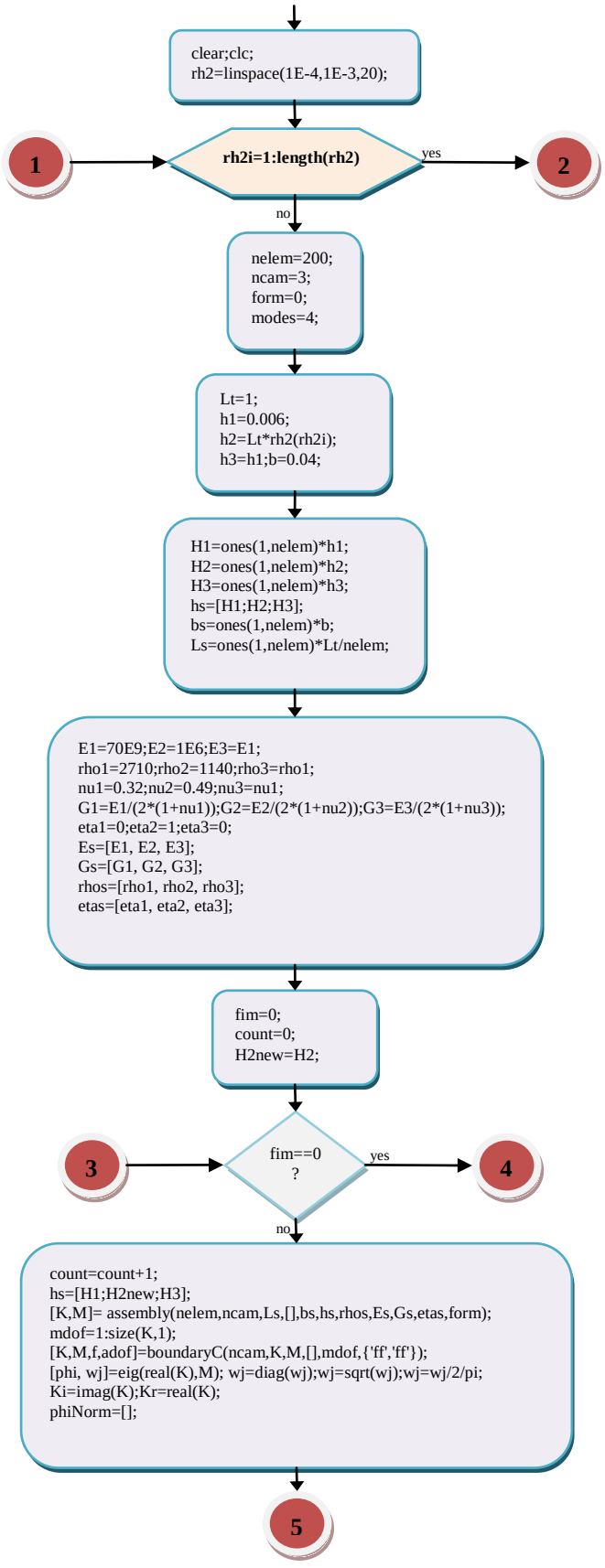

A.7 – MATLAB code “topology.m” – 2/3

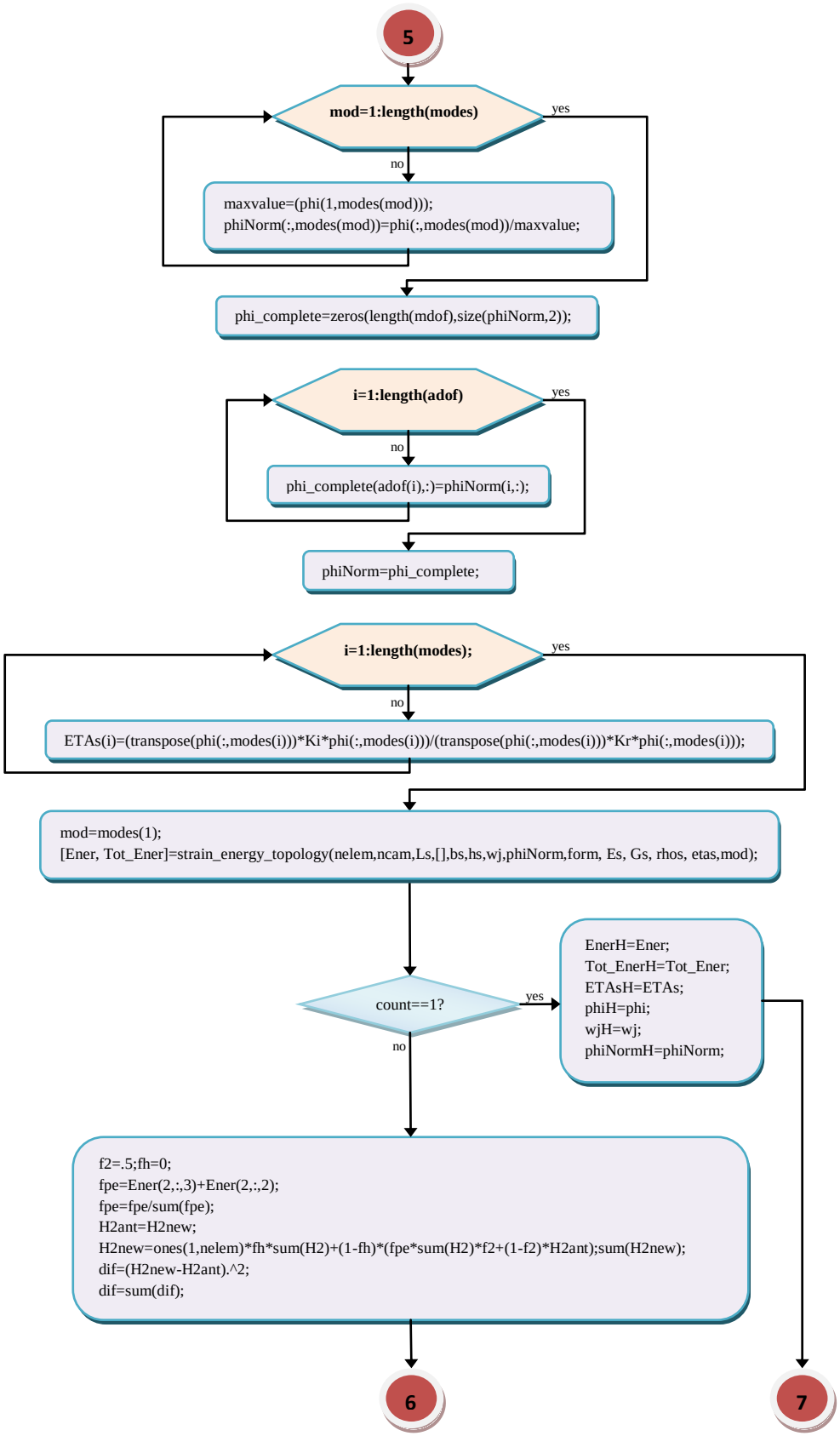

A.7 – MATLAB code “topology.m” – 3/3

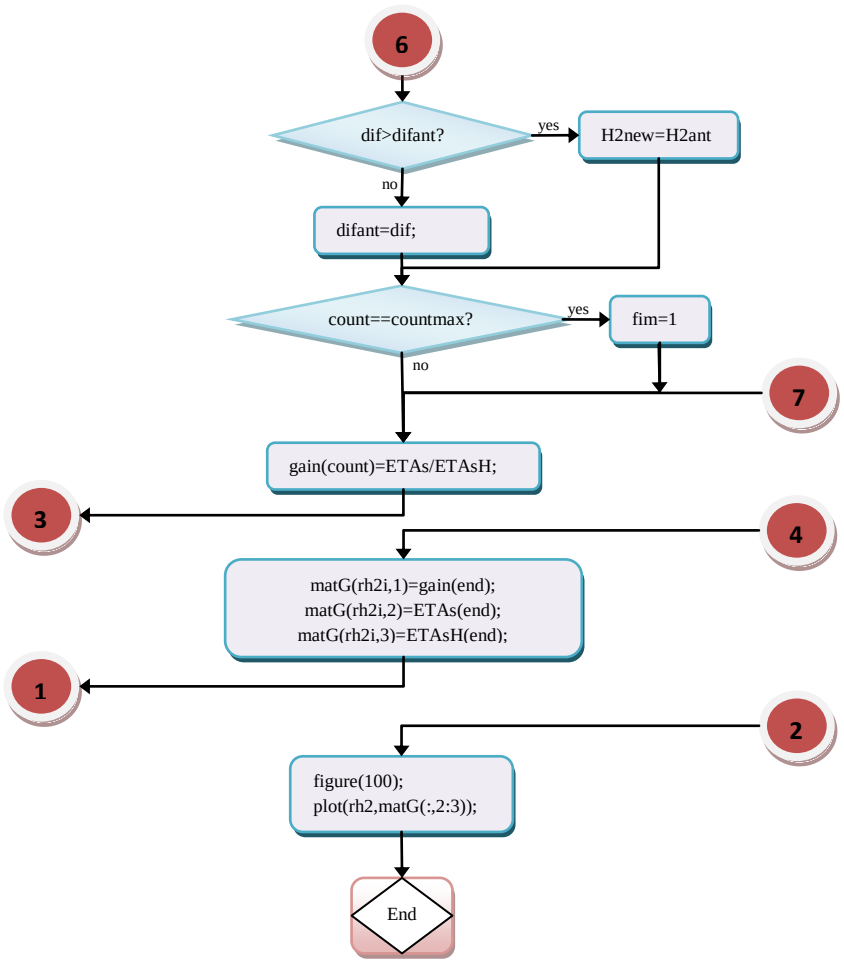

A.8 – MATLAB code “strain_energy_topology.m” – 1/2

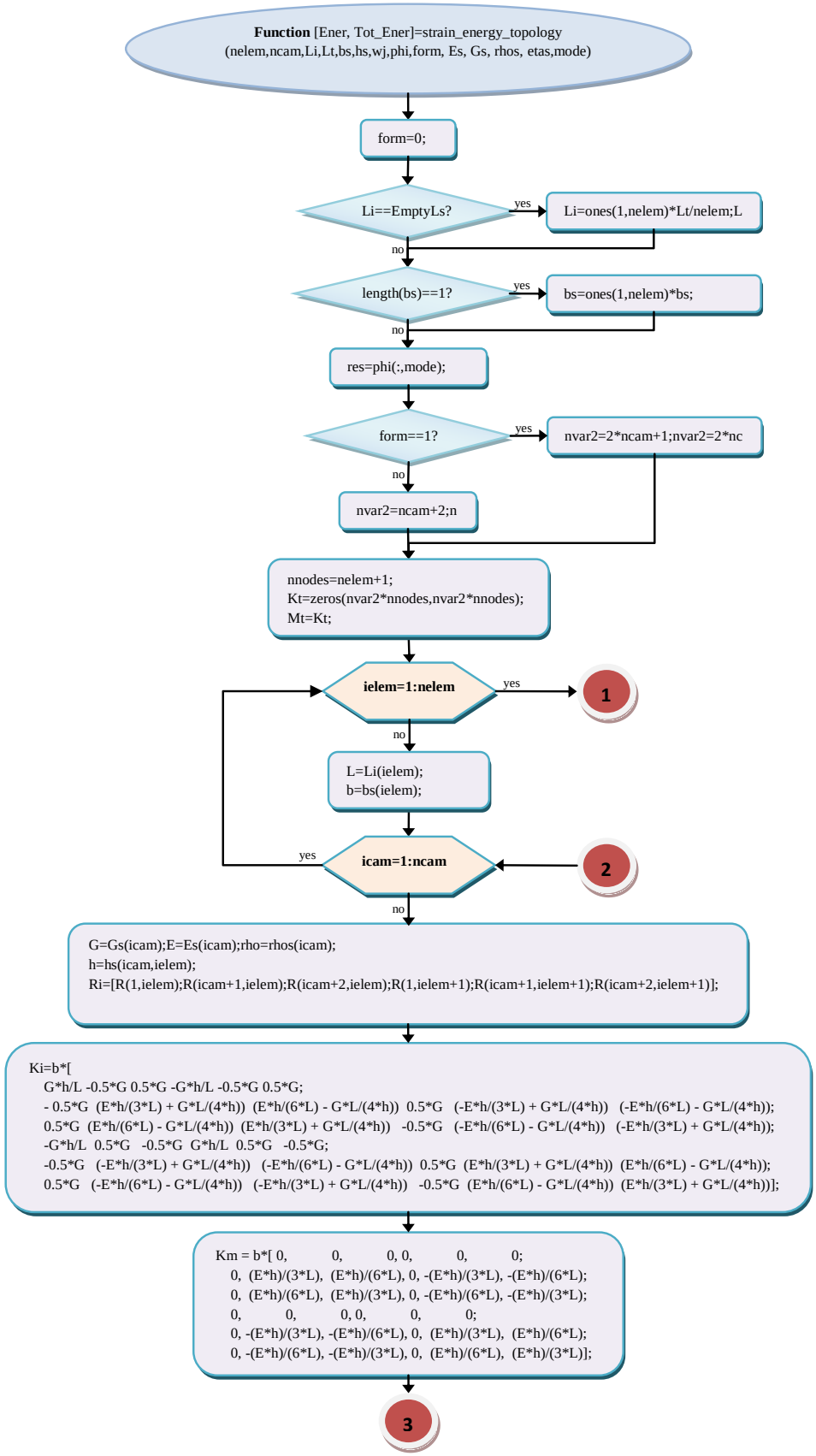

A.8 – MATLAB code “strain_energy_topology.m” – 2/2

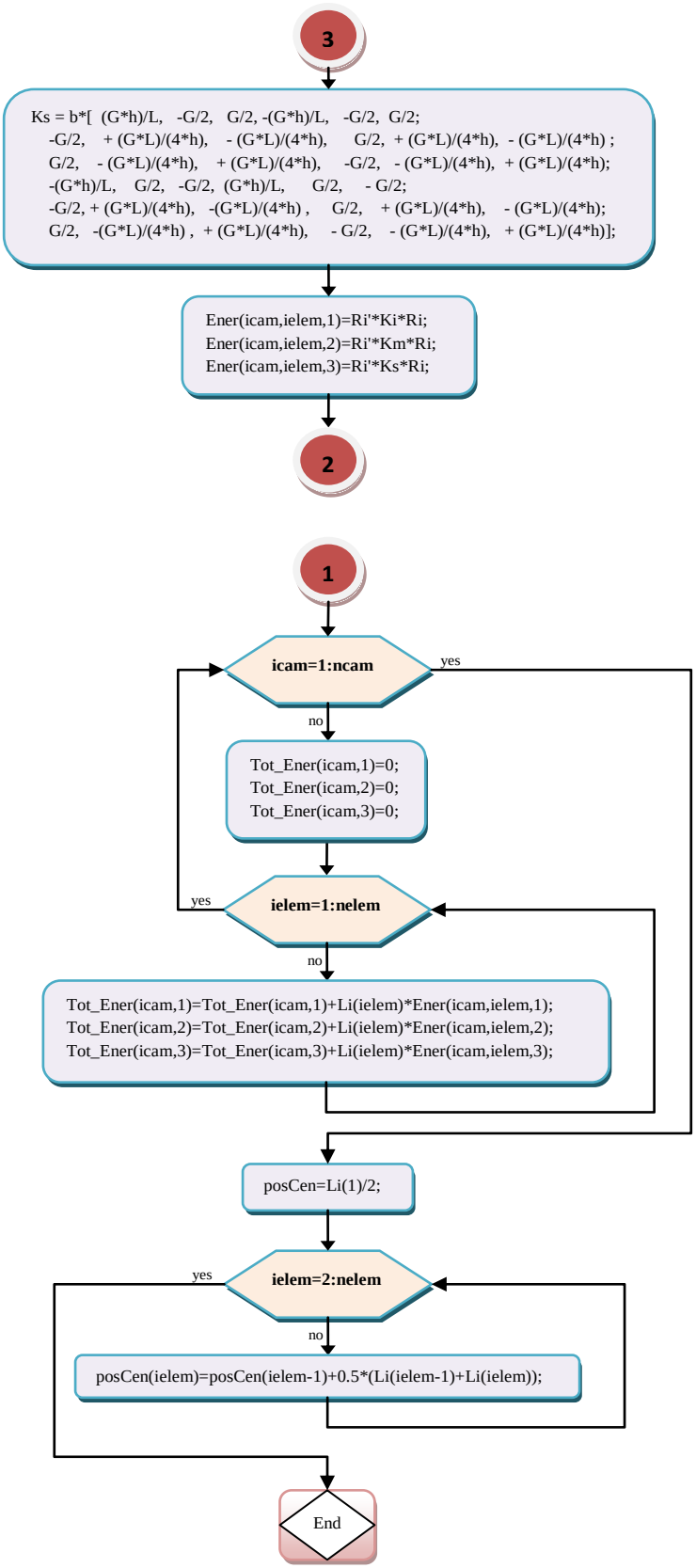

Appendix B - Algorithms

B.1 – MATLAB code "assembly.m"

```
function [Kt,Mt]=assembly(nelem,ncam,Ls,Lt,bs,hs,rhos,Es,Gs,etas,form)


if length(bs)==1
    bs=bs*ones(nelem,1);
end

if isempty(Ls)
    Ls=ones(nelem,1)*Lt/nelem;
end

if form==1;nvar2=2*ncam+1;

else;nvar2=ncam+2;

end

nnodes=nelem+1; %number of nodes

Kt=zeros(nvar2*nnodes,nvar2*nnodes);Mt=Kt;

for ielem=1:nelem

%calculates element individual matrix

[K,M]=ebeam(ncam,hs(:,ielem),bs(ielem),rhos,Es,Gs,Ls(ielem),etas,form);

    %assembles individual matrices in a global matrix

    apont1=[(nvar2)*(ielem-1)+1:(nvar2*(ielem+1))];
    Kt(apont1,apont1)=Kt(apont1,apont1)+K;
    Mt(apont1,apont1)=Mt(apont1,apont1)+M;

end

return
```

B.2 – MATLAB code “ebeam.m”

```
function [Kt,Mt]=ebeam(n,hs,b,rhos,Es,Gs,L,etas,form)

if form==1; nvar=4*n+2;
else nvar=2*n+4;
end

Kt=zeros(nvar,nvar);Mt=Kt;

mat=Kt;

for i=1:n

    Ke=mat;Me=mat;

    G=Gs(i);E=Es(i);rho=rhos(i);h=hs(i);eta=etas(i);

    Ki=[G*b*h/L -0.5*G*b 0.5*G*b -G*b*h/L -0.5*G*b 0.5*G*b;

        - 0.5*G*b  (E*b*h/(3*L) + G*b*L/(4*h))  (E*b*h/(6*L) -
        G*b*L/(4*h))  0.5*G*b   (-E*b*h/(3*L) + G*b*L/(4*h))
        (-E*b*h/(6*L) - G*b*L/(4*h));

        0.5*G*b  (E*b*h/(6*L) - G*b*L/(4*h))  (E*b*h/(3*L) +
        G*b*L/(4*h))   -0.5*G*b   (-E*b*h/(6*L) - G*b*L/(4*h))
        (-E*b*h/(3*L) + G*b*L/(4*h));

        -G*b*h/L  0.5*G*b   -0.5*G*b  G*b*h/L  0.5*G*b   -0.5*G*b;

        -0.5*G*b   (-E*b*h/(3*L) + G*b*L/(4*h))   (-E*b*h/(6*L) -
        G*b*L/(4*h))  0.5*G*b  (E*b*h/(3*L) + G*b*L/(4*h))  (E*b*h/(6*L)
        - G*b*L/(4*h));

        0.5*G*b   (-E*b*h/(6*L) - G*b*L/(4*h))   (-E*b*h/(3*L) +
        G*b*L/(4*h))   -0.5*G*b  (E*b*h/(6*L) - G*b*L/(4*h))
        (E*b*h/(3*L) + G*b*L/(4*h))];

    Mi=rho*b*L*h*diag([0.5 0.25 0.25 0.5 0.25 0.25]);

    if form==1; apont=[i n+1+i n+i 2*n+1+i 3*n+1+i 3*n+2+i];

    else apont=[1 1+i 2+i n+3 n+3+i n+4+i];

    end

    Ke(apont,apont)=Ki*(1+eta*1i);
    Me(apont,apont)=Mi;

    Kt=Kt+Ke;
    Mt=Mt+Me;

end
```

B.3 – MATLAB code “boundaryC.m”

```
function [K,M,f,adof]=boundaryC(layers,Ki,Mi,fi,mdof,cond)


% boundary conditions
% { extremity 1, extremity 2}
% 'ss' simply supported (w=0)
% 'ds' double support (u0=0,w=0)
% 'fx' built-in (ui=0,w=0 for any i)
% 'ff' free-free

apont=ones(size(mdof));


switch cond{1}
    case 'ss';  apont(1)=0;
    case 'ds';  apont([1 2])=0;
    case 'fx';  apont([1:layers+2])=0;
    case 'ff';
end

switch cond{2}
    case 'ss';  apont([length(mdof)-(layers+1)])=0;
    case 'ds';  apont([length(mdof)-(layers+1),length(mdof)-
                (layers+1)+1])=0;
    case 'fx';  apont([length(mdof)-(layers+1):length(mdof)])=0;
    case 'ff';
end


adof=mdof.*apont;

adof=nonzeros(adof);

K=Ki(adof',adof');
M=Mi(adof',adof');
K=double(K);
M=double(M);

if ~isempty(fi)
    f=fi(adof');
else
    f=[];
end

return
```

B.4 – MATLAB code “totalcld.m”

```
function y = totalcld(x)

% geometry variables

Lt=1; L=Lt; %length of beam
h1=10 E-3; %thickness of base layer
b=0.04; % width of beam

h3=h1;

p3=[1 0 0];

modes=3+[1 2 3];

% materials properties

E1=70 E9; % E - Young's modulus
E2=1 E6;
rho1=2710; % rho - Density
rho2=1142;
nu1=0.32; % nu - Poisson's ratio
nu2=0.49;%
G1=E1/(2*(1+nu1)); % G - shear modulus or modulus of rigidity
G2=E2/(2*(1+nu2));
Es=[E1 E2 E1];
Gs=[G1, G2, G1];
rhos=[rho1 rho2 rho1];
eta_vem=1; %viscoelastic damping ratio
etas=[0 eta_vem 0];

nelem=40;ncam=3;
li=Lt/nelem;
x1=-li/2;

for ielem=1:nelem
    x1=x1+li;

    h2(ielem)=x(1)*(0.5*cos(2*pi*x1*x(2)/Lt+x(3))+0.5)+x(4);

end

H1=ones(1,nelem)*h1;

H2=h2;

H3=ones(1,nelem)*h3;

hs=[H1;H2;H3];
bs=ones(1,nelem)*b;
Ls=ones(1,nelem)*Lt/nelem;
```

```
% calculates stiffness and mass matrices and vector of degrees of freedom


[K,M]= assembly(nelem,ncam,[],Lt,b,hs,rhos,Es,Gs,etas,0);
mdof=1:size(K,1);

[K,M,f,adof]=boundaryC(3,K,M,[],mdof,{'ff','ff'}); %applies boundary
conditions

if isinf(x)
    fobj=1E+10;

elseif isnan(x)
    fobj=1E+10;

else

    %calculates modes

    [phi, wj]=eig(real(K),M);
    wj=diag(wj);
    wj=sqrt(wj);
    wj=wj/2/pi;

    % calculates Modal Strain Energy - ETAs (MSE)

    Ki=imag(K);
    Kr=real(K);

    for i=1:length(modes);
        ETAs(i)=(transpose(phi(:,modes(i)))*Ki*eta_vem*phi(:,modes(i)))/
                (transpose(phi(:,modes(i)))*Kr*phi(:,modes(i)));
    End

     % where ETA is the system damping ratio or loss factor for the nth
     mode
    % phi is the mode shape for the nth mode
    % eta_vem is the viscoelastic damping ratio

    phi_complete=zeros(length(mdof),size(phi,2));

    for i=1:length(adof)
        phi_complete(adof(i),:)=phi(i,:);
    end

    fobj =(p3(:))'*ETAs(:);

    end

y=-fobj;

return
```

B.5 – MATLAB code “verif_strain_energy.m”

```
clc;clear all;close all

% geometry variables and analysis parameters

Lt=1; %length of beam
b=0.04; % width of beam
Rh2min=1E-6; %minimum value of h2 (VEM)
Rh2max=2E-4; %maximum value of h2
nh2=400; %number of divisions of h2
h2min=Rh2min*Lt;
h2max=Rh2max*Lt;
gama=abs(h2max-h2min); deltah2=gama/nh2;

mode_ener=1; % mode under analysis

%parameters of finite element

nelem=40;ncam=3;form=0;
modes=[1 2 3 4 5 6];

bs=ones(1,nelem)*b;
Ls=ones(1,nelem)*Lt/nelem;

%materials properies

E1=70E9;
E2=1E6;
E3=E1;
rho1=2710;
rho2=1140;
rho3=rho1;
nu1=0.32;
nu2=0.49;
nu3=nu1;
G1=E1/(2*(1+nu1));
G2=E2/(2*(1+nu2));
G3=E3/(2*(1+nu3));
eta1=0;
eta2=1;
eta3=0;
Es=[E1, E2, E3];
Gs=[G1, G2, G3];
rhos=[rho1, rho2, rho3];
etas=[eta1, eta2, eta3];


ratioh1=[.001 .002 .004 .006 .008 .01 .015 .02];


for kk=1:length(ratioh1)
    h1=Lt*ratioh1(kk);
    h3=h1;
```

```
for k=1:nh2
    h2i=h2min+(k-1)*deltah2;
    x(k)=h2i;
    x2(k)=h2i/Lt;
    H1=ones(1,nelem)*h1;
    H2=ones(1,nelem)*h2i;
    H3=ones(1,nelem)*h3;
    hs=[H1;H2;H3];
    h2vector(k,kk)=h2i;


    % calculates stiffness and mass matrices and vector of degrees
    of freedom

    [K,M]= assembly(nelem,ncam,Ls,[],bs,hs,rhos,Es,Gs,etas,form);
    mdof=1:size(K,1);

    % applies boundary conditions

    [K,M,f,adof]=boundaryC(ncam,K,M,[],mdof,{'fx','fx'});

    %calculates natural modes

    [phi, wj]=eig(real(K),M); wj=diag(wj);wj=sqrt(wj);wj=wj/2/pi;

    Ki=imag(K);Kr=real(K);


    norm=1; % normalisation of the natural modes based on the real
    component of stiffness matrix

    switch norm

        case 1

            phiNorm=[];

            for mod=1:length(modes)
                phiNorm(:,modes(mod))=1/(sqrt(transpose(phi(:,modes
                 (mod)))*Kr*phi(:,modes(mod))))*phi(:,modes(mod));
            end

        case 2
            % Normalisation based on displacement field

            phiNorm=[];

            for mod=1:length(modes)
                maxvalue=max(phi(:,modes(mod)));
                phiNorm(:,modes(mod))=phi(:,modes(mod))/maxvalue;
            end
    end


    phi_complete=zeros(length(mdof),size(phiNorm,2));
```

```
        for i=1:length(adof)
            phi_complete(adof(i),:)=phiNorm(i,:);
        end

        phiNorm=phi_complete;


        [Ener,Tot_Ener]=strain_energy(nelem,ncam,Ls,[],bs,hs,wj,phiNorm,
        form, Es, Gs, rhos,etas, mode_ener);

        Max_ener_cam1_membrana(k)=max(Ener(1,:,2));
        Max_ener_cam1_corte(k)=max(Ener(1,:,3));
        Max_ener_cam2_membrana(k)=max(Ener(2,:,2));
        Max_ener_cam2_corte(k)=max(Ener(2,:,3));
        Max_ener_cam3_membrana(k)=max(Ener(3,:,2));
        Max_ener_cam3_corte(k)=max(Ener(3,:,3));

        TEner_cam1_membrana(k,kk)=Tot_Ener(1,2);
        TEner_cam1_corte(k,kk)=Tot_Ener(1,3);
        TEner_cam2_membrana(k,kk)=Tot_Ener(2,2);
        TEner_cam2_corte(k,kk)=Tot_Ener(2,3);
        TEner_cam3_membrana(k,kk)=Tot_Ener(3,2);
        TEner_cam3_corte(k,kk)=Tot_Ener(3,3);


        Ener_Tot(k,kk)=Tot_Ener(1,2)+Tot_Ener(1,3)+Tot_Ener(2,2)
        +Tot_Ener(2,3)+ Tot_Ener(3,2)+Tot_Ener(3,3);
        Ener_Vem(k,kk)=Tot_Ener(2,2)+Tot_Ener(2,3);
        eta_global_ff(k,kk)=eta2*Ener_Vem(k,kk)./Ener_Tot(k,kk);

    end
end

save ratios.mat


figure(11); plot(x,TEner_cam1_membrana,'.-b'); title('Total membrane +
bending Energy  - layer 1');

figure(12); plot(x,TEner_cam1_corte,'.-b'); title('Total Shear Energy -
layer 1');

figure(13); plot(x,TEner_cam2_membrana,'.-b'); title('Total membrane +
bending Energy  - layer 2');

figure(14); plot(x,TEner_cam2_corte); title('Total Shear Energy - layer
2');

figure(15); plot(x,TEner_cam3_membrana,'.-b'); title('Total membrane +
bending Energy  - layer 3');

figure(16); plot(x,TEner_cam3_corte,'.-b'); title('Total Shear Energy -
layer 3');

figure(17); plot(x2,eta_global_ff,'linewidth',2);
```

B.6 – MATLAB code “strain_energy.m”

```
function[Ener,Tot_Ener]=strain_energy(nelem,ncam,Li,Lt,bs,hs,wj,phi,form,
Es,Gs,rhos,etas,mode)


form=0;

if isempty(Li); Li=ones(1,nelem)*Lt/nelem;end
if length(bs)==1;bs=ones(1,nelem)*bs;end

res=phi(:,mode);

if form==1;nvar2=2*ncam+1;else;nvar2=ncam+2;end

nnode=nelem+1;
R=reshape(res,nvar2,nnode);

for ielem=1:nelem
    L=Li(ielem);b=bs(ielem);

    for icam=1:ncam

        G=Gs(icam);E=Es(icam);rho=rhos(icam);
        h=hs(icam,ielem);

        Ri=[R(1,ielem);R(icam+1,ielem);R(icam+2,ielem);R(1,ielem+1);
        R(icam+1,ielem+1);R(icam+2,ielem+1)];


        Ki=b*[G*h/L -0.5*G 0.5*G -G*h/L -0.5*G 0.5*G;

           - 0.5*G  (E*h/(3*L) + G*L/(4*h))  (E*h/(6*L) - G*L/(4*h))
           0.5*G   (-E*h/(3*L) + G*L/(4*h))   (-E*h/(6*L) - G*L/(4*h));

           0.5*G  (E*h/(6*L) - G*L/(4*h))  (E*h/(3*L) + G*L/(4*h))   -
           0.5*G   (-E*h/(6*L) - G*L/(4*h))   (-E*h/(3*L) + G*L/(4*h));

            -G*h/L  0.5*G   -0.5*G  G*h/L  0.5*G   -0.5*G;

           -0.5*G   (-E*h/(3*L) + G*L/(4*h))   (-E*h/(6*L) - G*L/(4*h))
           0.5*G  (E*h/(3*L) + G*L/(4*h))  (E*h/(6*L) - G*L/(4*h));

            0.5*G   (-E*h/(6*L) - G*L/(4*h))   (-E*h/(3*L) + G*L/(4*h))
           -0.5*G  (E*h/(6*L) - G*L/(4*h))  (E*h/(3*L) + G*L/(4*h))];


        Km = b*[ 0,           0,           0, 0,           0,           0;
             0,  (E*h)/(3*L),  (E*h)/(6*L), 0, -(E*h)/(3*L), -(E*h)/(6*L);
             0,  (E*h)/(6*L),  (E*h)/(3*L), 0, -(E*h)/(6*L), -(E*h)/(3*L);
             0,           0,           0, 0,           0,           0;
             0, -(E*h)/(3*L), -(E*h)/(6*L), 0,  (E*h)/(3*L),  (E*h)/(6*L);
             0, -(E*h)/(6*L), -(E*h)/(3*L), 0,  (E*h)/(6*L), (E*h)/(3*L)];
```

```
        Ks = b*[  (G*h)/L,   -G/2,   G/2, -(G*h)/L,   -G/2,  G/2;

             -G/2,+(G*L)/(4*h),-(G*L)/(4*h),G/2,+(G*L)/(4*h),-G*L)/(4*h) ;

             G/2,-(G*L)/(4*h),+(G*L)/(4*h),-G/2,-(G*L)/(4*h),+(G*L)/(4*h);

             -(G*h)/L,    G/2,   -G/2,  (G*h)/L,      G/2,     - G/2;

             -G/2,+(G*L)/(4*h),-(G*L)/(4*h),G/2,+(G*L)/(4*h),-(G*L)/(4*h);

             G/2,-(G*L)/(4*h),+(G*L)/(4*h),-G/2,-G*L)/(4*h),+(G*L)/(4*h)];

        Ener(icam,ielem,1)=Ri'*Ki*Ri;
        Ener(icam,ielem,2)=Ri'*Km*Ri;
        Ener(icam,ielem,3)=Ri'*Ks*Ri;

    end
end

% to compute total energy

for icam=1:ncam

    Tot_Ener(icam,1)=0;Tot_Ener(icam,2)=0;Tot_Ener(icam,3)=0;

    for ielem=1:nelem
        Tot_Ener(icam,1)=Tot_Ener(icam,1)+Li(ielem)*Ener(icam,ielem,1);

        Tot_Ener(icam,2)=Tot_Ener(icam,2)+Li(ielem)*Ener(icam,ielem,2);

        Tot_Ener(icam,3)=Tot_Ener(icam,3)+Li(ielem)*Ener(icam,ielem,3);

    end
end
% return

posCen=Li(1)/2;

for ielem=2:nelem
    posCen(ielem)=posCen(ielem-1)+0.5*(Li(ielem-1)+Li(ielem));
end

cor=[.7 .0 .7; .1 .4 .1];

hf=figure(3);clf

xlim=[posCen(1)-(posCen(end)-posCen(1))/20, posCen(end)+(posCen(end)-
posCen(1))/20];

for icam=1:ncam

    graph(:,:)=Ener(icam,:,2:3);
    subplot(ncam+1,1,ncam-icam+1);gh=area(posCen,graph);xlabel('x');
    hold on;ghl=plot(posCen,graph); hold off;
    set(gca,'xlim',xlim);
```

```
    for i=1:2
        set(gh(i),'FaceColor',cor(i,:));end

    set(gh,'LineStyle','-','LineWidth',2);

    title(['layer: ',num2str(icam)]);

    set(hf,'name', ['Mode :', num2str(mode),' <<press key to
    continue>>']);
    subplot(ncam+1,1,ncam+1);

    %% to draw natural mode

    M=max(max(R))-min(min(R));scale=sum(Li)/M;
    R1=R*scale*.3;
    W=R1(1,:);W=ones(ncam+1,1)*W;

    hnode(:,1)=hs(:,1);

    for inode=2:nnode-1
        hnode(:,inode)=(hs(:,inode-1)+hs(:,inode))/2;
    end

    hnode(:,nnode)=hs(:,end);

    for inode=1:nnode
        dum=[0; cumsum(hnode(:,inode))];
        Y(:,inode)=dum';
    end

    Y=flipud(Y);
    X=[0 cumsum(Li)];X=ones(ncam+1,1)*X;

    if form==1
    else
        x=X+R1(2:end,:);
        y=Y+W;
    end

    l=line(x(:,:),y);set(l,'color','b','linewidth',2);

    for icam=1:ncam+1
        l=line(x(icam,:),y(icam,:));set(l,'color','b','linewidth',2);
    end

    l=line(X(:,:),Y);set(l,'color','k','linewidth',0.5,'linestyle',':');

    for icam=1:ncam+1
        l=line(X(icam,:),Y(icam,:));set(l,'color','k','linewidth',0.5,
        'linestyle',':');
    end

    set(gca,'xlim',xlim);

end
```

B.7 – MATLAB code “topology.m”

```
clear;clc;

rh2=linspace(1E-4,1E-3,20);

for rh2i=1:length(rh2)

    % FEM parameters

    nelem=200; ncam=3; form=0;

    modes=4;

    % geometry variables

    Lt=1; %length of beam
    h1=0.006; %thickness of base layer
    h2=Lt*rh2(rh2i);
    h3=h1;
    b=0.04; %thickness of base layer

    % geometry matrices

    H1=ones(1,nelem)*h1;
    H2=ones(1,nelem)*h2;
    H3=ones(1,nelem)*h3;
    hs=[H1;H2;H3];
    bs=ones(1,nelem)*b;
    Ls=ones(1,nelem)*Lt/nelem;


    % materials properties

    E1=70E9; E2=1E6; E3=E1;
    rho1=2710; rho2=1140; rho3=rho1;

    nu1=0.32; nu2=0.49; nu3=nu1;
    G1=E1/(2*(1+nu1));G2=E2/(2*(1+nu2));G3=E3/(2*(1+nu3));
    eta1=0; eta2=1; eta3=0;

    Es=[E1, E2, E3];
    Gs=[G1, G2, G3];
    rhos=[rho1, rho2, rho3];
    etas=[eta1, eta2, eta3];

    % beginning of iteration

    fim=0; %convergency variable
    count=0; %iteration counter

    H2new=H2; difant=100; countmax=10;

    % topology optimisation cycle
```

```
while fim==0

    count=count+1;

    hs=[H1;H2new;H3];

    %% FEM - calculates the stiffness and mass matrices and degrees
    of freedom

    [K,M]= assembly(nelem,ncam,Ls,[],bs,hs,rhos,Es,Gs,etas,form);
    mdof=1:size(K,1);

    %apllies boundary conditions

    [K,M,f,adof]=boundaryC(ncam,K,M,[],mdof,{'ff','ff'});

    %calculates natural modes

    [phi, wj]=eig(real(K),M); wj=diag(wj);wj=sqrt(wj);wj=wj/2/pi;

    %% calculates the efficiency (eta global) using MSE

    Ki=imag(K);Kr=real(K);

    % normalisation of the displacement field

    phiNorm=[];

    for mod=1:length(modes)
        maxvalue=(phi(1,modes(mod)));
        phiNorm(:,modes(mod))=phi(:,modes(mod))/maxvalue;
    end

    phi_complete=zeros(length(mdof),size(phiNorm,2));

    for i=1:length(adof)
        phi_complete(adof(i),:)=phiNorm(i,:);
    end

    phiNorm=phi_complete;


    for i=1:length(modes);
        ETAs(i)=(transpose(phi(:,modes(i)))*Ki*phi(:,modes(i)))/
       (transpose(phi(:,modes(i)))*Kr*phi(:,modes(i)));
    end

    %% calculates energy for each layer and element

    mod=modes(1);

   [Ener,Tot_Ener]=strain_energy_topology(nelem,ncam,Ls,[],bs,hs,wj,
   phiNorm,form,Es,Gs,rhos,etas,mod);
```

```
        %% saves first iteration (count=1) that represents the
        homogeneous configuration

        if count==1
            EnerH=Ener; Tot_EnerH=Tot_Ener;
            ETAsH=ETAs;
            phiH=phi;wjH=wj;
            phiNormH=phiNorm;
        else

            f2=.5;  fh=0; % percentage of the distribution of the current
            iteration
            % in the 2nd iteration and thereafter, compares solutions,
            % changes H2 and evaluates convergence

            fpe=Ener(2,:,3)+Ener(2,:,2); %shear energy vector for layer 2
            and all elements
            fpe=fpe/sum(fpe);

            H2ant=H2new;

            H2new=ones(1,nelem)*fh*sum(H2)+(1-fh)*(fpe*sum(H2)*f2+
           (1-f2)*H2ant);sum(H2new);

            dif=(H2new-H2ant).^2;dif=sum(dif);

            if dif>difant

                H2new=H2ant;
            else

                difant=dif;
            end

            if count==countmax fim=1;end

        end

        gain(count)=ETAs/ETAsH;

    end

    matG(rh2i,1)= gain (end);
    matG(rh2i,2)=ETAs(end);
    matG(rh2i,3)=ETAsH(end);

end

figure(100);plot(rh2,matG(:,2:3));% BLUE is VARIABLE;GREEN is HOMOGENEOUS
```

B.8 – MATLAB code “strain_energy_topology.m”

```
function[Ener,Tot_Ener]=strain_energy_topology(nelem,ncam,Li,Lt,bs,hs,wj,
phi,form, Es, Gs, rhos, etas,mode)


form=0;

if isempty(Li); Li=ones(1,nelem)*Lt/nelem;end
if length(bs)==1;bs=ones(1,nelem)*bs;end

res=phi(:,mode);

if form==1;nvar2=2*ncam+1;else;nvar2=ncam+2;end

nnode=nelem+1;
R=reshape(res,nvar2,nnode);

for ielem=1:nelem
    L=Li(ielem);b=bs(ielem);

    for icam=1:ncam
        G=Gs(icam);E=Es(icam);rho=rhos(icam);
        h=hs(icam,ielem);
        Ri=[R(1,ielem);R(icam+1,ielem);R(icam+2,ielem);R(1,ielem+1);
         R(icam+1,ielem+1);R(icam+2,ielem+1)];

        % element stiffness matrix (extensional and shear)

        Ki=b*[G*h/L -0.5*G 0.5*G -G*h/L -0.5*G 0.5*G;

            - 0.5*G  (E*h/(3*L) + G*L/(4*h))  (E*h/(6*L) - G*L/(4*h))
            0.5*G   (-E*h/(3*L) + G*L/(4*h))   (-E*h/(6*L) - G*L/(4*h));

            0.5*G  (E*h/(6*L) - G*L/(4*h))  (E*h/(3*L) + G*L/(4*h))   -
            0.5*G   (-E*h/(6*L) - G*L/(4*h))   (-E*h/(3*L) + G*L/(4*h));

            -G*h/L  0.5*G   -0.5*G  G*h/L  0.5*G   -0.5*G;

            -0.5*G   (-E*h/(3*L) + G*L/(4*h))   (-E*h/(6*L) - G*L/(4*h))
            0.5*G  (E*h/(3*L) + G*L/(4*h))  (E*h/(6*L) - G*L/(4*h));

            0.5*G   (-E*h/(6*L) - G*L/(4*h))   (-E*h/(3*L) + G*L/(4*h))
            -0.5*G  (E*h/(6*L) - G*L/(4*h))  (E*h/(3*L) + G*L/(4*h))];

        % element stiffness matrix (extensional)

        Km = b*[ 0,           0,           0, 0,           0,           0;
            0,  (E*h)/(3*L),  (E*h)/(6*L), 0, -(E*h)/(3*L), -(E*h)/(6*L);
            0,  (E*h)/(6*L),  (E*h)/(3*L), 0, -(E*h)/(6*L), -(E*h)/(3*L);
            0,            0,           0, 0,           0,           0;
            0, -(E*h)/(3*L), -(E*h)/(6*L), 0,  (E*h)/(3*L),  (E*h)/(6*L);
            0, -(E*h)/(6*L), -(E*h)/(3*L), 0,  (E*h)/(6*L), (E*h)/(3*L)];
```

```
        % element stiffness matrix (shear)

         Ks = b*[(G*h)/L,    -G/2,    G/2, -(G*h)/L,    -G/2,  G/2;

            -G/2,+(G*L)/(4*h),-(G*L)/(4*h),G/2,+(G*L)/(4*h),-(G*L)/(4*h);

            G/2,-(G*L)/(4*h),+(G*L)/(4*h),-G/2,-(G*L)/(4*h),+(G*L)/(4*h);

            -(G*h)/L,    G/2,    -G/2,   (G*h)/L,       G/2,      - G/2;

            -G/2,+(G*L)/(4*h),-(G*L)/(4*h),G/2,+(G*L)/(4*h),-(G*L)/(4*h);

            G/2,-(G*L)/(4*h),+(G*L)/(4*h),-G/2,(G*L)/(4*h),+(G*L)/(4*h)];

        %% energy per element and layer

        Ener(icam,ielem,1)=Ri'*Ki*Ri; % total energy (layer i, element i)
        Ener(icam,ielem,2)=Ri'*Km*Ri; % energy of extensional component
        Ener(icam,ielem,3)=Ri'*Ks*Ri; % energy of the shear component

    end
end

% to compute total energy

for icam=1:ncam

    Tot_Ener(icam,1)=0;Tot_Ener(icam,2)=0;Tot_Ener(icam,3)=0;

    for ielem=1:nelem

        Tot_Ener(icam,1)=Tot_Ener(icam,1)+Li(ielem)*Ener(icam,ielem,1);

        Tot_Ener(icam,2)=Tot_Ener(icam,2)+Li(ielem)*Ener(icam,ielem,2);

        Tot_Ener(icam,3)=Tot_Ener(icam,3)+Li(ielem)*Ener(icam,ielem,3);

    end
end

posCen=Li(1)/2;

for ielem=2:nelem
    posCen(ielem)=posCen(ielem-1)+0.5*(Li(ielem-1)+Li(ielem));
end


end
```

References

[1] H. Oberst, Material of high inner damping. Acustica: Journal international d'acoustique 6(1) (1956) 144-153.

[2] D. Ross, E.E. Ungar, E.M. Kerwin Jr., Damping of flexural vibrations by means of viscoelastic laminates, Structural Damping, ASME, New York, 1959.

[3] R.A. DiTaranto, Theory of vibratory bending for elastic and viscoelastic layered finite-length beams. ASME, Journal of Applied Mechanics (1965) 881-886.

[4] M.J. Yan, E.H. Dowell, Governing equations of vibrating constrained-layer damping sandwich plates and beams. ASME, Journal of Applied Mechanics (1972) 1041-1046.

[5] Y.V. Rao, B.C. Nakra, Vibrations of unsymmetrical sandwich beams and plates with viscoelastic cores. Journal of Sound and Vibration 34(3) (1974) 309-326.

[6] J.D. Ferry, Viscoelastic Properties of Polymers, John Wiley & Sons, New York, 1st edition, 1961.

[7] A.D. Nashif, D.I. Jones, J.P. Henderson, Vibration Damping, John Wiley & Sons, New York, 1985.

[8] P.K. Roy, N. Ganeson, Dynamic studies on plates with unconstrained layer treatment. Computers and Structures 49(3) (1993) 473-480.

[9] P.K. Roy, N. Ganeson, Dynamic studies on beams with unconstrained layer treatment. Journal of Sound and Vibration 195 (1996) 417-427.

[10] C.D. Johnson, Design of passive damping systems. ASME, Special 50th Anniversary Design Issue 117 (1995) 171-176.

[11] C.D. Johnson, D.A. Kienholz, J.P. Henderson, Finite element prediction of damping in structures with constrained viscoelastic layers. AIAA Journal 20 (1982) 1284-1290.

[12] D.J. Mead, Passive Vibration Control, John Wiley & Sons, 1998.

[13] D.I.G. Jones, Handbook of Viscoelastic Vibration Damping, John Wiley & Sons, 1st edition, 2001.

[14] W. Hufenbach, C. Holster, L. Kroll, Vibration and damping behavior of multi-layered composite cylindrical shells. Composite Structures 58 (2002) 165-174.

[15] S.H. Zhang, H.L. Chen, A study on the damping characteristics of laminated composites with integral viscoelastic layers. Composite Structures 74 (2006) 63-69.

[16] V. Pradeep, N. Ganeson, Vibration and thermal buckling of composite sandwich beams with viscoelastic core. Composite Structures 81 (2007) 60-69.

[17] R.A.S. Moreira, J.D. Rodrigues, Partial Constrained Viscoelastic Damping Treatment of Structures: a Modal Strain Energy Approach. International Journal of Structural Stability and Dynamics 6(3) (2006) 397-411.

[18] M.D. Rao, Recent applications of viscoelastic damping for noise control in automobiles and commercial airplanes. Journal of Sound and Vibration 262 (2003) 457-474.

[19] B.C. Nakra, Structural dynamic modification using additive damping. Sadhana (Academy Proceedings in Engineering Sciences) 25(3) (2000) 277-289.

[20] M.O.W. Richardson, Polymer Engineering Composites, Applied Science Publishers, 1977.

[21] T. Teng, N. Hu, Analysis of damping characteristics for viscoelastic laminated beams. Computer Methods in Applied Mechanics and Engineering 190 (2001) 3881-3892.

[22] http://www.aip.org/tip/INPHFA/vol-9/iss-6/p14.html (Accessed 6 January 2013).

[23] A. Preumont, Vibration Control of Active Structures - An Introduction, Kluwer Academic Publishers, 2nd edition, 1999.

[24] B.F. Spencer, S.J. Dyke, M.K. Sain, J.D. Carlston, Phenomenological model of a magnetorheological damper. Smart Material Structures 5 (1996) 272.

[25] B. Arzine, Vibration control of plates with active constrained layer damping. Smart Material Structures 4 (1995).

[26] J.D. Carlston, D.M. Catanzarite, K.A. St. Clair, Commercial magneto-rheological fluid devices. 5th International Conference on Electro-Rheological, Magnet-Rheological Suspensions and Associated Technology, Sheffield, 1995.

[27] W.D. Callister, Jr., Fundamentals of Materials Science and Engineering, John Wiley & Sons, 2nd edition, 2005.

[28] http://www.roush.com/Portals/1/Downloads/Articles/Insight.pdf (Accessed 6 January 2010).

[29] J.D. Ferry, E.R. Fitzgerald, L.D. Grandine, M.L. Williams, Temperature dependence of dynamic properties of elastomers, relaxation distributions. Industrial & Engineering Chemistry 44(4) (1952) 703-706.

[30] J.D. Ferry, L.D. Grandine, E.R. Fritzgerald, The relaxation distribution function of Polyisobutylene in the transition from rubber-like to glass-like behavior. Journal of Applied Physics 24(7) (1953) 911-916.

[31] B. Maxwell, An investigation of the dynamic mechanical properties of polymethyl methacrylate. Journal of Polymer Science 20(96) (1956) 551-566.

[32] R.L. Bagley, P.J. Torvik, Fractional calculus - A different approach to the analysis of viscoelastically damped structures. AIAA Journal 21(5) (1983) 741-748.

[33] R.L. Bagley, P.J. Torvik, Fractional calculus in the transient analysis of viscoelasticaly damped structures. AIAA Journal 23(6) (1985) 918-925.

[34] G.A. Lesieutre, E. Bianchini, Time domain modeling of linear viscoelastic using anelastic displacement fields. Journal of Vibration and Acoustics - Transactions of the ASME 117 (1995) 424-430.

[35] D.J. McTavish, P.C. Hughes, Modeling of linear viscoelastic space structures. Journal of Vibration and Acoustics 115 (1993) 103-110.

[36] M.T. Shaw, W.J. MacKnight, Introduction to Polymer Viscoelasticity, John Wiley & Sons, 3rd edition, 2005.

[37] ASTM. D4092-90 standard terminology relating to dynamic mechanical measurements on plastics. Annual Book of ASTM Standards 8(2) (1990) 345-347.

[38] T. Pritz, Loss factor peak of viscoelastic materials: magnitude to width relations. Journal of Sound and Vibration 246(2) (2001) 265-280.

[39] http://www.3m.com/product/information/viscoelastic-damper.html (Accessed 19 February 2013).

[40] http://www.sorbothane.com/material-properties.php (Accessed 26 February 2013).

[41] www.soundcoat.com (Accessed 21 February 2013).

[42] http://heathcotes.com/vibdamping.html (Accessed 21 February 2013).

[43] A. Lumsdaine, R.A. Scott, Shape optimization of unconstrained viscoelastic layers using continuum finite elements. Journal of Sound and Vibration 216(1) (1998) 29-52.

[44] K.K. Stevens, S. Shostein, Influence of partial viscoelastic damping treatments on the modal parameters of circular plates, Proceedings of 7th International Modal Analysis Conference (IMAC VII), Kissimmee, FL, USA, 1988, pp. 1616-1622.

[45] A. Akanda, T. Onsay, G.M. Goetchius, Perforated damping treatment: A novel approach to reduction of weight. SAE Noise & Vibration Conference, 1999, pp. 99-152.

[46] M.R. Garrison, R.N. Miles, J.Q. Sun, W. Bao, Random response of a plate partially covered by a constrained layer damper. Journal of Sound and Vibration 172(2) (1994) 231-245.

[47] A.W. Van Vuure, I. Verpoest, F.K. Ko, Sandwich-fabric panels as spacers in a constrained layer structural damping application. Composites: Part B 32 (2001) 11-19.

[48] D.I.G. Jones, Design of Constrained Layer Treatments for Broad Temperature. Damping, Shock & Vibration Bulletin 5 (1974) 1-12.

[49] D.I.G. Jones, Damping of Stiffened Plates by Multiple Layer Treatments. Journal of Sound and Vibration 35 (1974) 417-427.

[50] A. Baz, J. Ro, Optimum design and control of active constrained layer damping. Journal of Vibration and Acoustics (Special 50th Anniversary Design Issue) 117 (1995) 135-144.

[51] C. Chantalakhana, R. Stanway, Active constrained layer damping of clamped-clamped plate vibrations. Journal of Sound and Vibration 241(5) (2001) 755-777.

[52] T.E. Alberts, H. Xia, Design and analysis of fiber enhanced viscoelastic damping polymers. Journal of Vibration and Acoustics (Special 50th Anniversary Design Issue) 117 (1995) 398-404.

[53] E.E. Ungar, E.M. Kerwin Jr., Loss factors of viscoelastic systems in terms of energy concepts. Journal of Acoustical Society of America 34 (1962) 954-958.

[54] Y.S. Shin, G.J. Maurer, Vibration response of constrained viscoelastically damped plates: Analyses and experiments, Proceedings of 7th International Modal Analysis Conference (IMAC VII), Las Vegas, USA, 1989, pp. 1516-1520.

[55] D.K. Rao, Frequency and loss factors of sandwich beams under various boundary conditions. Journal of Mechanical Engineering Science 20(5) (1978) 271-282.

[56] C.M. Vasques, R.A.S. Moreira, J.D. Rodrigues, Viscoelastic damping technologies–Part I: Modeling and finite element implementation. Journal of Advanced Research in Mechanical Engineering 1 (2010) 76-95.

[57] R. Moreira, Modelação e análise de tratamentos viscoelásticos multi-camada para controlo passivo de vibrações, PhD Thesis, Faculdade de Engenharia da Universidade do Porto, 2004.

[58] R. Moreira, J.D. Rodrigues, Constrained damping layer treatments: Finite element modelling. Journal of Vibration and Control 10 (2004) 575-595.

[59] G.A. Lesieutre, D.L. Mingori, Finite element modelling of frequency-dependent material damping using augmenting thermodynamic fields. Journal of Guidance Control and Dynamics 13(6) (1990) 1040-1050.

[60] A. Schmidt, L. Gaul, FE implementation of viscoelastic constitutive stress-strain relations involving fractional time derivatives, Proceedings of the 2nd European Conference on Constitutive Models for Rubber (ECCMR), Hannover, September 2001, pp. 79-89.

[61] A. Schmidt, L. Gaul, Application of fractional calculus to viscoelastically damped structures in the finite element method, Proceedings of the International Conference on Structural Dynamics Modelling (SDM), Madeira, Portugal, June 2002, pp. 297-306.

[62] A. Schmidt, L. Gaul, Parameter identification and FE implementation of a viscoelastic constitutive equation using fractional derivatives, Proceedings in Applied Mathematics and Mechanics, Vol. 1(1), 2002, pp. 153-154.

[63] J.W. Killian, Y.P. Lu, A finite element modeling approximation for damping material used in constrained damped structures. Journal of Sound and Vibration 97(2) (1984) 352-354.

[64] D.A. Saravanos, Integrated damping mechanics for thick composite laminates and plates. Journal of Applied Mechanics 61 (1994) 375-383.

[65] D.A. Saravanos, J.M. Pereira, Dynamic characteristics of specialty composite structures with embedded damping layers. Journal of Vibration and Acoustics (Special 50th Anniversary Design Issue) 117 (1995) 62-69.

[66] D.H. Robbins Jr., J.N. Reddy, Modelling of thick composites using a layerwise laminate theory. International Journal for Numerical Methods in Engineering 36 (1993) 655-677.

[67] R.A.S. Moreira, J.D. Rodrigues, A.J.M. Ferreira, A generalized layerwise finite element for multi-layer damping. Computational Mechanics 37 (2006) 426-444.

[68] A.L. Araújo, C.M. Mota Soares, C.A. Mota Soares, Finite element model for hybrid active-passive damping analysis of anisotropic laminated sandwich structures. Journal of Sandwich Structures and Materials 12 (2010) 397-419.

[69] R.A.S. Moreira, F.J.Q. De Melo, J.D. Rodrigues, Static and dynamic characterization of composite cork for sandwich beam cores. Journal of Materials Science 45 (2010) 3350-3366.

[70] P.Y. Papalambros, D. J. Wilde, Principles of Optimal Design Modelling and Computation, Cambridge University Press, 2nd edition, 2000.

[71] D.E Goldberg, Genetic Algorithms in Search, Optimization, and Machine Learning, Addison-Wesley, 1989.

[72] M.P. Bendsϕe, N.Kikuchi, Generating optimal topologies in structural design using a homogenization method. Computational Mechanics 77 (1988) 197-224.

[73] K. Svanberg, The Method of Moving Asymptotes: a new method for structural optimization. International Journal for Numerical Method in Engineering 24 (1987) 359-373.

[74] K. Svanberg, A new globally convergent version of MMA. Technical report TRITA-MAT, Stockholm, 1999.

[75] J. H. Holland, Adaptation in Natural and Artificial Systems, MIT Press, Massachusetts, 1975.

[76] M. Mitchell, An Introduction to Genetic Algorithms, MIT Press, Massachusetts, 1996.

[77] D. Whitley, T. Starkweather, Genitor II: A distributed genetic algorithm. Journal of Experimental and Theoretical Artificial Intelligence 2 (1990) 189-214.

[78] J. Hesser, R. Manner, Towards an optimal mutation probability for Genetic Algorithms. Computer Science 496 (1991) 23-32.

[79] J. Smith, T.C. Fogarty, Self-adaptation of mutation rates in a steady state genetic algorithm, Proceedings of the IEEE Conference of Evolutionary Computation, 1996, pp. 318-323.

[80] G. Ochoa, I. Harvey, H. Buxton, On recombination and optimal mutation rates, Proceedings of the Genetic and Evolutionary Computation Conference, 1999.

[81] G. Harik, F. Lobo, A parameter-less genetic algorithm. IlliGAL Report 99009, 1999.

[82] A.E. Eiben, R. Hinterding, Z. Michalewicz, Parameter control in evolutionary algorithms. IEEE Transactions on Evolutionary Computation 3(2) (1999).

[83] H. Tzung-Pei, W. Hong-Shung, C. Wei-Chou, Simultaneously Applying Multiple Mutation Operators in Genetic Algorithms. J. Heuristics 6(4) (2000) 439-455.

[84] D. Thierens, Adaptive mutation rate control schemes in Genetic Algorithms, Proceedings of the IEEE World Congress on Computational Intelligence, 2002.

[85] I. Rechenberg, Evolutionsstrategie, Friedrich Frommann Verlag, 1973.

[86] M. Affenzeller, S. Wagner, SASEGASA: An evolutionary algorithm for retarding premature convergence by self-adaptive selection pressure steering. Computer Science 2686 (2003) 438-445.

[87] F. Sadjadi, Comparison of Fitness Scaling Functions in Genetic Algorithms with Applications to Optical Processing, Proceedings of SPIE Vol. 5557, 2004.

[88] F. Herrera, M. Lozano, J.L. Verdegay, Tackling real-coded Genetic Algorithms: operators and tools for behavioural analysis. Artificial Intelligence Review 12 (1998) 265-319.

[89] J.J. Grefenstette, Optimization of Control Parameters for Genetic Algorithms. IEEE T. Systems, Man and Cybernetics 16(1) (1986) 122-128.

[90] E. Falkenauer, Genetic Algorithms and Grouping Problems, John Wiley & Sons, West Sussex, 1998.

[91] Z. Michalewicz, Genetic Algorithms + Data Structures = Evolution Programs, Springer, Heidelberg, 1999.

[92] P.H. Chu, S.A. Dudley, The effect of population structure on the rate of convergence of Genetic Algorithms, Proceedings of the 1993 ACM/SIGAPP symposium on Applied computing: states of the art and practice, Indianapolis, USA, 1993, pp. 147-151.

[93] J.T. Alander, Population Size, Building Blocks, Fitness Landscape and GA Search Efficiency in Combinational Optimization - an Empirical Study, in: L.D. Chambers (Ed.), Practical Handbook of Genetic Algorithms, Complex Coding Systems, Boca Raton, Florida, 1998, pp. 459-482.

[94] S. Gupta, Relative Fitness Scaling for Improving Efficiency of Proportionate Selection in Genetic Algorithms. GECCO 09, Proceedings of the 11th Annual Conference, 2009.

[95] G. Winter, Genetic Algorithms in Engineering and Computer Science, John Wiley & Sons, New York, 1996.

[96] M. Gen, R. Cheng, Genetic Algorithms & Engineering Optimization, John Wiley & Sons, New York, 2000.

[97] A.M.S. Zalzala, P.J. Fleming, Genetic Algorithms in Engineering Systems, Institution of Engineering and Technology, London, 1997.

[98] M.D. Vose, The Simple Genetic Algorithm - Foundations and Theory, MIT Press, Massachusetts, 1999.

[99] W.M. Spears, Crossover or Mutation?, in: L.D. Whitley (Ed.), Foundations of Genetic Algorithms 2. Morgan Kaufmann, San Francisco, 1993.

[100] H. Mühlenbein, How Genetic Algorithms really work: Mutation and Hill Climbing, in: R. Männer, B. Manderick (Eds.), Parallel Problem solving from Nature 2, North-Holland, Netherlands, 1992.

[101] R.L. Haupt, S.E. Haupt, Practical Genetic Algorithms, John Wiley & Sons, New York, 1998.

[102] E. Cantú-Paz, Efficient and Accurate Parallel Genetic Algorithms, Kluwer, Massachusetts, 2000.

[103] S. Yu, S. Huang, Vibration of a three-layered viscoelastic sandwich circular plate. International Journal of Mechanical Sciences 43 (2001) 2215-2236.

[104] H. Arvin, M. Sadighi, A.R. Ohadi, A numerical study of free and forced vibration of composite sandwich beam with viscoelastic core. Composite Structures 92 (2010) 996-1008.

[105] X. Dechang, Y. Zuguang, Forced vibration of sandwich beam with segmented elastic-viscoelastic layers, Proceedings of 5th International Modal Analysis Conference (IMAC V), London, UK, 1987, pp. 1033-1040.

[106] C. Levy, Q. Chen, Vibration analysis of a partially covered, double sandwich-type, cantilever beam. International Journal of Solids and Structures, 31(17) (1994) 2377-2391.

[107] M.R. Garrison, R.N. Miles, J.Q. Sun, W. Bao, Random response of a plate partially covered by a constrained layer damper. Journal of Sound and Vibration 172(2) (1994).

[108] S. Assaf, M. Guerich, P. Cuvelier, Vibration and damping analysis of plates with partially covered damping layers. Acta Acustica united with Acustica 97 (2011) 553-568.

[109] D. Granger, A. Ross, Effects of partial constrained viscoelastic layer damping parameters on the initial transient response of impacted cantilever beams: experimental and numerical results. Journal of Sound and Vibration 321 (2009) 45-64.

[110] A. Lumsdaine, R. Pai, Design of Constrained Layer Damping Topologies, Proceedings of IMECE, ASME International Mechanical Engineering, Washington D.C., USA, 2003.

[111] 3M, Scotchdamp – Vibration control systems, 3M Product information and performance data, Engineered materials – 3M Industrial Specialties Division, St. Paul, M.N., 1993.

[112] R.A.S. Moreira, J.D. Rodrigues, Multilayer damping treatments: Modeling and experimental assessment. Journal of Sandwich Structures and Materials 12 (2010) 181-198.